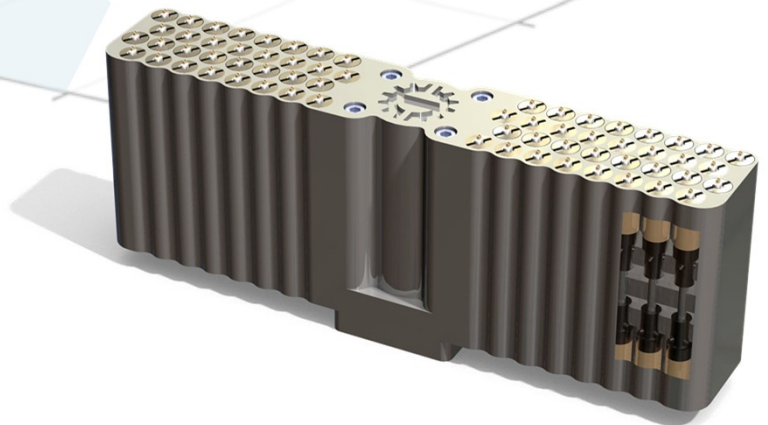


# DFP 12

## Proceedings of THE FIFTH WORKSHOP ON DIGITAL FLUID POWER

October 24-25, 2012, Tampere, Finland



TAMPERE UNIVERSITY OF TECHNOLOGY



**Rexroth**  
Bosch Group

Tampereen teknillinen yliopisto - Tampere University of Technology

Arto Laamanen & Matti Linjama (Eds.)

Proceedings of the Fifth Workshop on Digital Fluid Power  
October 24-25 2012, Tampere, Finland

Tampere University of Technology. Department of Intelligent Hydraulics and  
Automation  
Tampere 2012

Proceedings of the Fifth Workshop on Digital Fluid Power,  
October 24-25 2012, Tampere, Finland

Editors: Arto Laamanen and Matti Linjama

ISBN 978-952-15-2941-2 (printed)

ISBN 978-952-15-2942-9 (USB)

ISBN 978-952-15-3271-9 (PDF)

Tampere University of Technology  
Department of Intelligent Hydraulics and Automation  
Tampere 2012

© The Fifth Workshop on Digital Fluid Power (DFP12). All rights reserved. Republication or redistribution of DFP12 proceedings content is prohibited.

## PREFACE

The Digital Fluid Power workshops have been arranged annually since 2008 alternating between Linz and Tampere. This is the third time in Tampere and the number of participants is as high as 114 from 11 countries, 33 companies and 8 universities despite bad economic situation. It is my pleasure to welcome you all to Tampere.

The digital fluid power technology is developing rapidly and new principles still emerges. The component availability is better and several papers present research results with commercial digital valves. The good old days with self-wound coils and fuming power electronics seem to be ending. Other trends are sophisticated control methods, which consider digital nature of the systems, energy efficient fully digital solutions, and faster and more compact valves.

Organizing a workshop is not a trivial task at all. Sincere thanks are expressed to Dr. Arto Laamanen and Mrs. Virpi Multanen who have taken care of hundreds of big and smaller things so that the workshop is possible. Special thanks also to my research group in setting up innovative demonstrations and the spirit of this Tampere DFP.

Tampere, October 2012



Adj. Prof. Matti Linjama, Workshop Chairman



TAMPERE UNIVERSITY OF TECHNOLOGY



**Rexroth**  
Bosch Group



## CONTENTS

DIGITAL HYDRAULICS AT BOSCH REXROTH – A TREND EVOLVES TO REAL APPLICATIONS Markus Flor, Stefan Scheller and Rolf Heidenfelder.....	5
SLIDING MODE CONTROL FOR DIGITAL HYDRAULIC APPLICATIONS Arnold Hiebl, Andreas Plöckinger, Bernd Winkler and Rudolf Scheidl .....	15
LAMINATED MANIFOLD FOR DIGITAL HYDRAULICS – PRINCIPLES, CHALLENGES AND BENEFITS Miika Paloniitty, Matti Karvonen, Matti Linjama and Tuomo Tainen .....	27
OPTIMISATION OF WORKING AREAS IN DISCRETE HYDRAULIC POWER TAKE OFF-SYSTEM FOR WAVE ENERGY CONVERTERS Anders H. Hansen, Rico H. Hansen and Henrik C. Pedersen .....	43
ENERGY RECOVERY USING A DIGITAL PISTON-TYPE ACCUMULATOR C. Stauch, F. Schulz, P. Bruck and J. Rudolph .....	57
IMPROVING DAMPING CHARACTERISTICS OF DISPLACEMENT CONTROLLED DIGITAL HYDRAULIC SYSTEM Mikko Heikkilä and Matti Linjama .....	75
STABILIZING REST POSITIONS OF THE LINEAR DIGITAL HYDRAULIC AMPLIFIER Rudolf Scheidl, Ingo Biedermann and Andreas Plöckinger.....	89
COMPARISON AND EVALUATION OF DIGITAL CONTROL METHODS FOR ON/OFF VALVES Ingo Schepers, Daniel Weiler and Juergen Weber.....	103
HARDWARE IN THE LOOP MULTI OBJECTIVE GENETIC OPTIMIZATION FOR EFFICIENT VALVE CONTROL Paul Foschum, Andreas Plöckinger and Rudolf Scheidl .....	123
SIMULATION AND EXPERIMENTAL RESULTS OF PWM CONTROL FOR DIGITALHYDRAULICS Andreas Plöckinger, Mikko Huova and Rudolf Scheidl .....	133
THE PRODUCT CALLED NORRDIGI™ Ari Sipola, Jussi Mäkitalo and Jouni Hautamäki .....	153
IMPLEMENTATION OF A DIGITAL HYDRAULIC VALVE SYSTEM WITH BOSCH REXROTH SEC VALVES Miikka Ketonen .....	161

A HIGH FLOW FAST SWITCHING VALVE FOR DIGITAL HYDRAULIC SYSTEMS Sylwester Kudzma, Nigel Johnston, Andrew Plummer, Nathan Sell, Andy Hillis and Min Pan .....	175
COMMERCIAL HIGH FLOW ON/OFF-VALVES FOR DIGITAL HYDRAULICS Ilari Hyöty .....	189
MODELLING OF FLOW CHARACTERISTICS OF ON/OFF VALVES Matti Linjama, Mikko Huova and Matti Karvonen .....	209
SIMULATIONS WITH FAULT-TOLERANT CONTROLLER SOFTWARE OF A DIGITAL VALVE Mikko Huova, Miikka Ketonen, Petr Alexeev, Pontus Boström, Matti Linjama, Marina Waldén and Kaisa Sere .....	223
DIGITAL CONTROL OF PRESSURE IN A VESSEL P.I. Greshnyakov, A.F. Sinyakov, D.M. Stadnick, V.N. Ilyukhin, V.Y. Sverbilov ....	243

## DIGITAL HYDRAULICS AT BOSCH REXROTH – A TREND EVOLVES TO REAL APPLICATIONS

Markus Flor, Stefan Scheller, Rolf Heidenfelder  
Bosch Rexroth AG  
Zum Eisengießer 1  
97816 Lohr am Main, Germany  
Phone +49-9352-18-1032  
E-Mail: markus.flor@boschrexroth.de

### ABSTRACT

Digital hydraulics can provide numerous benefits in comparison to the state of the art analogue technology. Independent of the digital approach (e.g. switching technology or parallel connected systems), all concepts share the need for on/off valves that are fast, price-efficient, compact and durable. This paper describes how the advantages of digital hydraulics can be achieved in suitable applications without such valves being commercially available by using intelligent, “bit-split” control approaches.

**KEYWORDS:** digital hydraulics, bit-split method, ballistic mode, ballistic controlled pilot stage, ballistic controlled main stage, on/off valve, cylinder axis

### 1. INTRODUCTION

In comparison to the state of the art analogue technology, the concept of digital hydraulics offers a promising vision with numerous both proven and theoretical advantages like energy efficiency, robustness, variance reduction, flexibility, performance and fault tolerance. These benefits have already been described in detail by several sources during the last years, e.g. by [1, 2]. Independent of their classification in “parallel connected systems” or “switching technologies”, all digital hydraulic systems rely on on/off valves as the crucial system component [2, 3]. In order to achieve the mentioned system advantages, these on/off valves need to fulfil multiple challenging requirements with regard to physical size, response times, robustness, durability and especially costs. As per mid-2012, none of the commercially available on/off valves can meet these demands satisfactory. In order to realize a parallel connected system that is able to compete performance-wise with state of the art proportional valves, at least five valves per control edge are needed [2]. Based on four control edges (P, A, B, T), a digital fluid control unit (DFCU) will at least consist of 20 valves and a suitable manifold. Considering the criteria installation space and cost, such a DFCU (made of commercially available on/off valves) currently can not compete with the available



highly optimized servo- or proportional valves, especially when higher volume flows are needed.

Taking these current constraints into account, the following question arises: How can digital hydraulics achieve a positive cost-benefit ratio already today / how can one exploit the benefits digital hydraulics promises without having to buy the currently unsolved challenges? With regard to the use of digital hydraulics, Bosch Rexroth's current strategy can be described as a combined two-factor approach:

1. Selecting specific applications that benefit most from the (possible) advantages digital hydraulics offers
2. Reduction of the effort needed to realize a digital system by using and combining intelligent architecture concepts and suitable control methods

In 2011, Heino Försterling et al. presented a paper at DFP11 [4] and provided approaches on how to reduce the efforts needed for digital hydraulic systems, focussing especially on suitable control methods and the resulting improvements. Here, "bit-split" methods like ballistic mode (BaM) or meter-in / meter-out (MiMo) and their specific advantages were presented.

This paper focuses on the ballistic mode approach and how it is successfully being used in industrial hydraulic applications.

## 2. BALLISTIC MODE

The number of parallel connected valves of a DFCU directly influences the achievable volume flow resolution and thus the control quality of a hydraulic axis. Presuming that a high volume flow resolution is desirable in order to obtain precise position, speed or pressure control, a conflict between the criteria "high resolution" and "installation space / costs and complexity" emerges. The ballistic mode resolves this conflict by increasing the achievable volume flow resolution while maintaining the number of parallel connected valves. As described in [5] by Mehling et al., the concept of the BaM approach is to use one of the parallel connected valves of one DFCU and control it with a time switching pattern in such a way, that it will provide a partial opening cross-section flow area smaller than the valve's nominal opening cross-section flow area. As a result, the ballistic controlled on/off valve no longer only has two discrete states (valve opened, valve closed) but is able to provide a "digital-proportional" volume flow characteristic.

The different operation modes of an on/off valve with regard to different time switching pattern characteristics have been analyzed by Schepers et al. in 2011 [6]. Figure 1 illustrates the five different valve modes by showing the dependency between pulse duty factor of the digital control signal and the resulting valve stroke (the following explanations are based on a normally-closed valve).

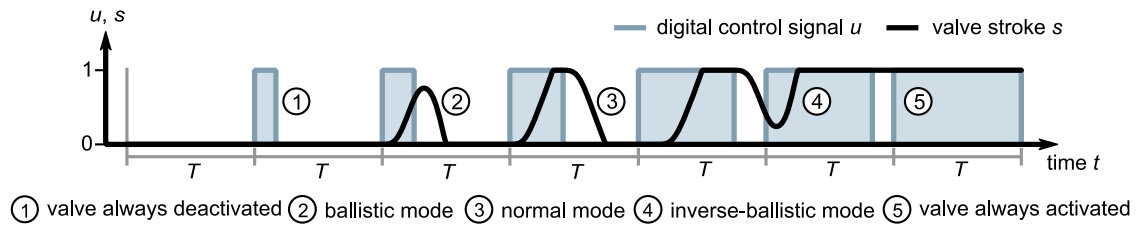


Figure 1. Modes of an on/off valve controlled by a digital command signal [6]

1. Valve always deactivated: The duration of the digital control signal is too short to create a valve stroke. The on/off valve therefore remains in its closed state.
2. Ballistic mode: In comparison to 1. “Valve always deactivated”, the control signal duration has been increased. The activation time is still shorter than the valve switching time. As a result, the spool now starts to move but does not reach its upper end position (= opened valve state) since the energy provided to the magnetic actuator is not sufficient. Instead, the spool returns to the lower end position (= closed valve state) in a ballistic motion sequence. The valve only opened partially.
3. Normal mode: The control signal duration now is equal or longer than the valve switching time, the spool therefore reaches the upper end position – the valve now is in the opened state.
4. Inverse-ballistic mode: Based on the constant frequency of the control signal, an increasing pulse time results in a reduced pause time. At a certain level, the pause time is too small for the valve spool to reach the lower end position – the valve no longer can reach its closed state and remains open to a certain degree. This mode is called inverse-ballistic.
5. Valve always activated: Reducing the pause time even further (in comparison to 4. “Inverse-ballistic mode”) results in the valve spool remaining in the upper position and the valve therefore being continuously in its opened state.

Given that a valve provides a repeatable correlation between the length of the digital control signal and its resulting (partial) spool stroke, the use of the ballistic mode can transform an on/off valve with previously only two states (opened, closed) into a 1-bit digital-proportional control valve. The benefits of such a solution have already been demonstrated at the Hannover Messe (trade show) in 2011 by Bosch Rexroth [7] and were evaluated in [4].

The following section of this paper will take a closer look on an application example that has successfully and beneficially been solved with a digital hydraulics control approach.

### 3. BALLISTIC MODE APPLICATION EXAMPLE CYLINDER AXIS

The application example to be presented is the cylinder axis “SYEHL”, an electro-hydraulic system used to realize the tool motions of punching, cutting and forming machines. Typical application areas for such a cylinder axis are inter alia:

- Nibbling machines
- Notching and perforating machines

- Cutting presses
- Hole punching machines
- Copy punching machines
- Automatic punching machines
- Slot punching machines
- Turret punching machines
- Embossing machines

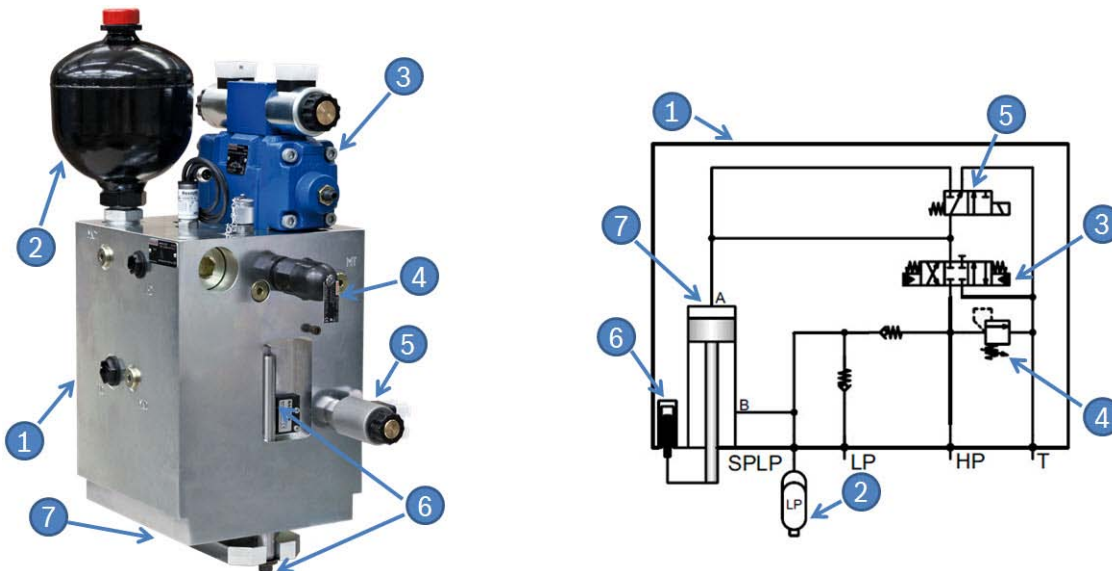


Figure 2. Cylinder axis system structure

The cylinder axis consists of the following main elements:

- |                                  |                        |
|----------------------------------|------------------------|
| 1. Manifold and cylinder housing | 5. Safety valve        |
| 2. Accumulator                   | 6. Position transducer |
| 3. Control valve                 | 7. Cylinder            |
| 4. Pressure relief valve         |                        |

Bosch Rexroth has developed a punching axis model range consisting three different performance categories in order to satisfy the diverse market requirements with regard to the criteria dynamics, precision and cost. The distinction therefore is made between standard, advanced and high performance cylinder axes.

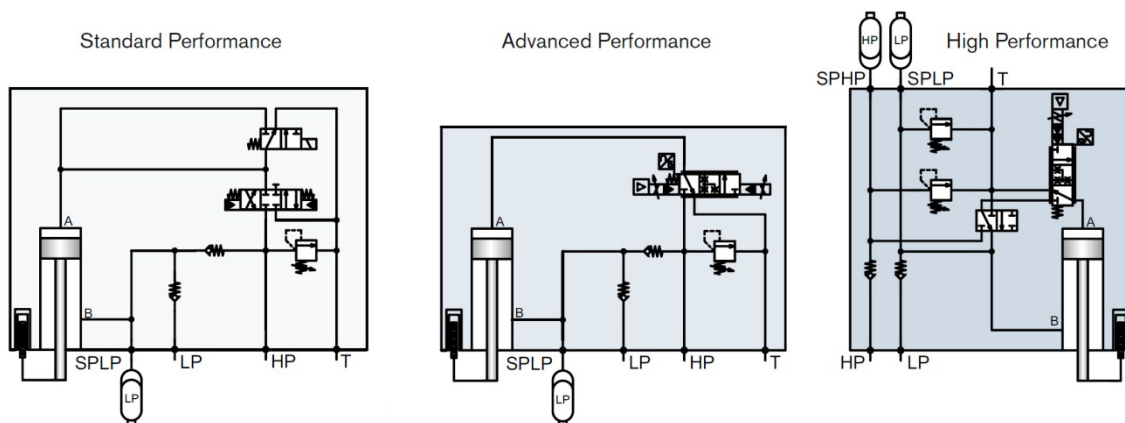


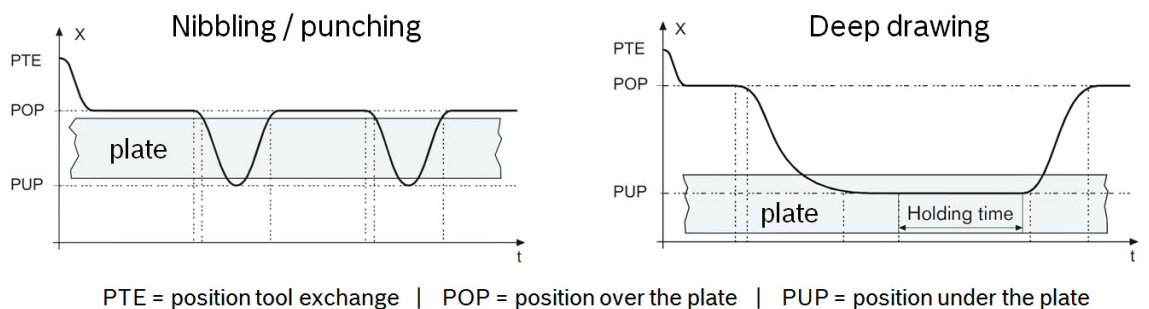
Figure 3. Cylinder axis model range: standard, advanced and high performance [8]

		200kN punching force					300kN punching force				
		Standard		Advanced	High		Standard		Advanced	High	
		Type 600	Type 750	Type 900	type 1200	type 1600	Type 600	Type 750	Type 900	type 1200	type 1600
punch stroke time [ms]	4mm	48	38	28	24	18	50	40	34	28	22
	6mm	54	44	34	30	24	65	55	40	34	28
	10mm	80	70	50	40	32	90	80	56	44	38
Possible stroke frequency [1/min] of punching machine at 4 mm stroke		600	750	900	1200	1600	600	750	900	1200	1600

Figure 4. Performance data of the three different performance categories [8]

The main distinction between the different performance types is the used control valve. While both, advanced and high performance axis are equipped with pilot-operated high-performance proportional cartridge valves, the standard performance axis is only equipped with a pilot-operated directional valve (= on/off valve).

The use of directional valves in standard performance axes can be considered as state of the art technology since it is well-established and widely used in the market. The main drivers for their application are price-efficiency and availability of the hydraulic system. Directional valves are considered to be more robust in comparison to high-performance control valves since they are insensitive to shock and fluid contamination due to the absence of on-board electronics (OBE) and higher fitting tolerances of the components. The limitations of this solution though are the dynamic behaviour and especially the achievable position accuracy of the cylinder axis. As a result, a state of the art standard performance cylinder axis is only able to perform cutting processes like nibbling or punching. Here, the ram tool only has to completely penetrate the work piece while occurring position inaccuracy simply results in additional cylinder stroke but not in quality defects of the product. Forming processes like deep drawing on the other hand require high position accuracy since position inaccuracies would create scrap. Thus, these forming processes are not feasible with a state of the art standard performance axis.



PTE = position tool exchange | POP = position over the plate | PUP = position under the plate  
Figure 5. Manufacturing processes nibbling / punching and deep drawing [8]

In order to create unique selling propositions, Bosch Rexroth decided to evaluate how the standard performance cylinder axis could be improved and focussed on the criteria dynamics and position accuracy. Given the constraint that the directional valve must not be exchanged due to cost and availability issues, the optimisation of the control strategy was regarded as a promising potential. Based on the excellent results that had been achieved with a ballistic controlled 4SEC6 valve [4, 7], a test setup with a ballistic controlled standard performance cylinder axis was created. The basic setup structure is shown in Figure 6 and consists of:

1. Digital motion and logic controller HNC100
2. Booster amplifier VT-MSFA1
3. Directional valve 4WEH, nominal size 10

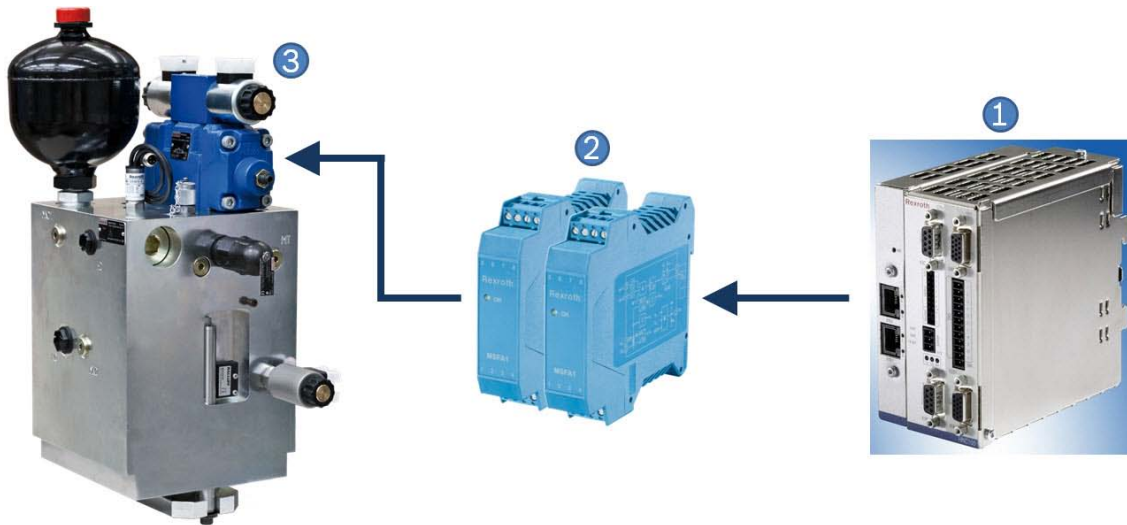


Figure 6. Digital hydraulics (ballistic mode) cylinder axis setup

The main difference between the 4SEC6 and the 4WEH10 valve is the hydraulic design. While the 4SEC6 is a direct operated directional poppet valve, the 4WEH10 is a pilot operated directional spool valve as shown in Figure 7. It is equipped with a 4WE6 directional valve as internal pilot stage.

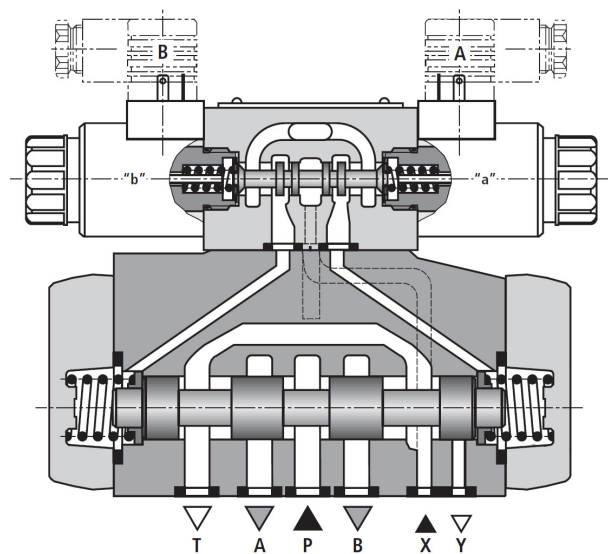


Figure 7. Cross-sectional view directional valve 4WEH10 [9]

Since low valve response times have proven to be beneficial for the control quality of the cylinder axis, the pilot stage solenoids are actuated by booster amplifiers. These amplifiers overexcite the solenoids for a short time period in order to energize them more quickly and thus shorten the pilot stage response time. The motion controller HNC100 uses a PWM-signal to control the booster amplifier output and therefore the valve stroke of the pilot stage. In this application, both pilot stage and main stage of the 4WEH10 valve can be ballistic operated as described in chapter 2 of this paper. Unlike the standard 4WEH10, the test setup valve had been equipped with position transducers

for the pilot stage spool and the main stage spool. Therefore, the spool strokes and the according cylinder axis stroke could be recorded for a typical tool positioning process.

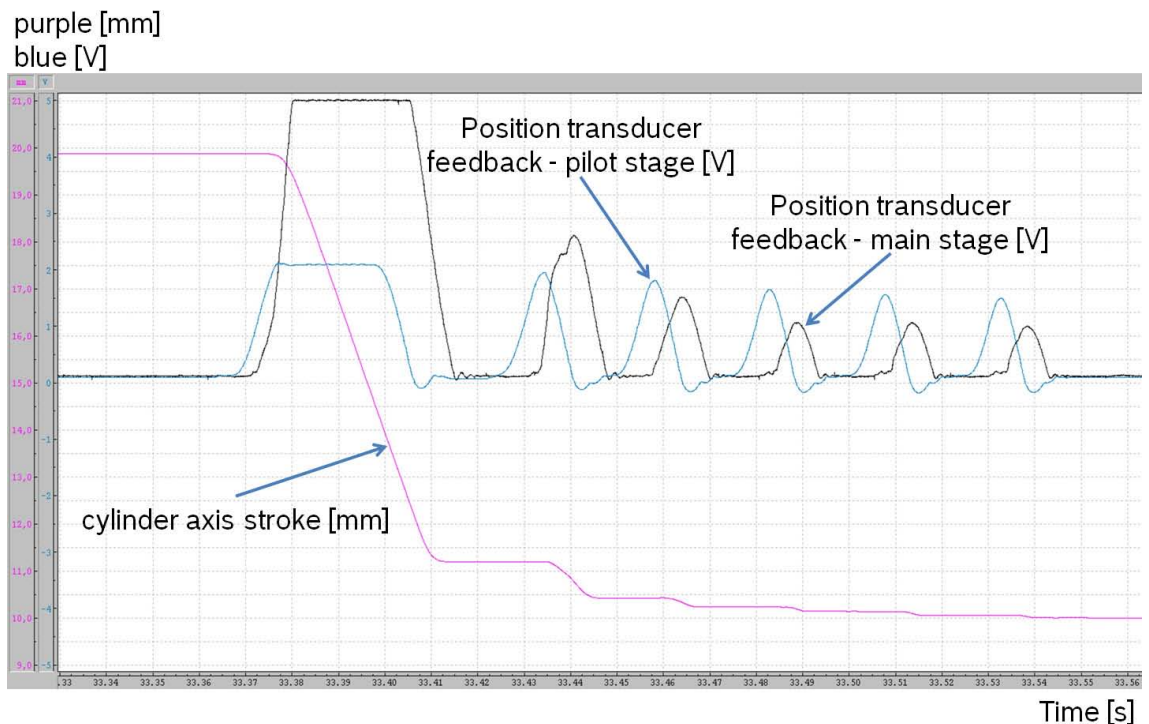


Figure 8. Trace of a cylinder axis motion and the according spool strokes

Figure 8 illustrates a positioning process of the cylinder axis with a starting position of approx. 20mm and a target position of 10mm. For a large part of the stroke, both the pilot stage and the main stage remain fully opened in order to allow for maximum volume flow and thus maximum cylinder movement speed. Shortly before reaching the final target position, the HNC100-controller switches to closed-loop ballistic mode control in order to achieve accurate positioning of the cylinder axis. In the given trace, five ballistic strokes are needed to traverse the cylinder axis to the final target position. Figure 8 shows that both pilot stage spool and main stage spool are performing ballistic movements.

A comparison between a state of the art standard performance cylinder axis (using a directional valve) and a digital hydraulics (ballistic mode) controlled standard performance axis shows that the chosen approach provides multiple benefits. First of all, the ballistic control results in a significant improvement of the achievable cylinder axis position accuracy. Without ballistic control, the setup was able to achieve a position accuracy of approximately  $\pm 0.3\text{mm}$  while now the position error could be reduced to less than  $\pm 50\mu\text{m}$  providing an improvement by a factor of 6. This raise in accuracy comes even close to the performance of the advanced and high performance cylinder axes with achievable position errors of  $< \pm 20\mu\text{m}$ . Due to this improvement, a ballistic controlled standard performance axis is now able to perform deep drawing processes instead of only being capable of performing cutting processes like nibbling or punching (see Figure 5). The use of the booster amplifiers shortens the pilot stage response time and therefore also improves the response time of the 4WEH10 directional valve main stage from approx. 65ms to approx. 15ms (measurement according ISO 6403 for 95% spool stroke). This gain in dynamics increases the possible stroke frequency of a standard performance axis from 150-200 1/min to 600-750 1/min

(assuming a 4mm stroke). Figure 4 provides a comparison chart of the different performance categories with regard to stroke time and stroke frequency.

Based on the fact that the ballistic control test set-up provided very satisfactory results, Bosch Rexroth decided to upgrade its standard performance cylinder axis to digital hydraulics and introduced them on the market accordingly.

#### 4. CONCLUSION AND OUTLOOK

This paper shows that even without the “right” on/off valves being commercially available (fast, price-efficient, compact and durable), the benefits of digital hydraulics can already be exploited today. The application example cylinder axis demonstrated that applying a ballistic control approach to an otherwise unchanged system was able to create significant benefits which also resulted in unique selling propositions and therefore in customer satisfaction.

In consideration of the current constraints, this paper proposes the following rules of thumb in order to gain user acceptance and bringing digital hydraulics onto the market step-by-step:

- Applying digital hydraulics does not mean a 1:1 substitution of existing control valves. In fact, the core function of the application and the potential benefits digital hydraulics might provide should be the decisive factor.
- The obstacle “lack of the right on/off valves” will most likely not be solved in near future. Therefore, the reduction of complexity and needed effort is crucial - the presented bit-split control approach is one potential solution.
- Hybrid solutions combining the advantages of digital hydraulics and the strengths of the conventional and well-engineered analogue technology should be regarded as a promising research and development domain.

#### REFERENCES

- [1] Scheidl, R., Linjama, M. and Schmidt, S. Is the future of fluid power digital? Proc IMechE, Part I: J Systems and Control Engineering. 226(6) 721–723. 2012
- [2] Linjama, M., 2011. Digital fluid power – state of the art. The Twelfth Scandinavian International Conference on Fluid Power, May 18–20, 2011, Tampere, Finland.
- [3] Achten, P. Discussion: Is the future of fluid power digital? Proc IMechE, Part I: J Systems and Control Engineering. 226(6) 724–727. 2012
- [4] Försterling, H., Stamm, E. and Roth, P. Tailored solutions limit complexity. The Fourth Workshop on Digital Fluid Power, 21st – 22nd September, 2011, Linz, Austria
- [5] Mehling, H. and Weiler, D. Digital hydraulics valve stage. Patent application, publication number WO 2011/054518, 12.05.2011

- [6] Schepers, I., Schmitz, D., Weiler, D., Cochoy, O. and Neumann, U. 2011. A novel model for optimized development and application of switching valves in closed loop control. *International Journal of Fluid Power (IJFP)*, Vol. 12, No. 3 pp. 31-40.
- [7] Bosch Rexroth AG. 2011. Hannover Messe. Digital hydraulics for leak-free proportional function - booth presentation.
- [8] Bosch Rexroth AG. 2012. Punching, Cutting, Forming – Standardized, optimal Drive & Control-Solutions. Technical information. RE 08101-02/03.12
- [9] Bosch Rexroth AG. 2008. 3/2, 4/2 and 4/3 directional valves, internally pilot operated, externally pilot operated. Data sheet. RE 24751/08.08





## SLIDING MODE CONTROL FOR DIGITAL HYDRAULIC APPLICATIONS

Arnold Hießl, Andreas Plöckinger, Bernd Winkler, Prof. Rudolf Scheidl\*  
Linz Center of Mechatronics, Hydraulic Drives and Actuation Systems  
\* Johannes Kepler University, Institute of Machine Design and Hydraulic Drives  
Altenbergerstraße 69, 4040 Linz, Austria  
E-Mail: [arnold.hiessl@lcm.at](mailto:arnold.hiessl@lcm.at)  
Phone: +43 732 2468 6057, Fax: +43 732 2468 6005

### ABSTRACT

The digitalisation of hydraulic drives leads to a simpler hardware, but asks for novel and sometimes even complex control strategies. This paper deals with the application of sliding mode control to a digital hydraulic drive. The sliding mode control is an approach for nonlinear systems with a discontinuous actuating variable, which makes it a favourable controller particularly for hydraulic switching control. An additional advantage is the robustness compared to the variation of system parameters.

A linear hydraulic drive with a specific digital circuit for which an experimental setup, called “Digi Actuator” exists, is used as example for this case study. The mathematical system model is transformed to Byrnes-Isidori normal form, for which a derivation of the sliding mode controller can be performed in a systematic way. The simulation results confirm the known advantages of this control concept, robustness even for quite nonlinear systems.

**KEYWORDS:** sliding mode control (SMC), discontinuous actuating variable, robustness due to parameter variation, digital hydraulics

## 1. INTRODUCTION

The sliding mode control (SMC) approach appeared in the Soviet Union, but was not published outside until 1975 by Itkis and 1976 by Utkin. Inspired by these publications many others followed. Hence the SMC community grew very fast and SMC became a non-yielding approach in linear and nonlinear control theory. The big advantage is the robustness compared to system parameter variation. This is a major reason for the fast dispersal of this theory. Another advantage is that the system can be used for nonlinear systems, which is the normal case in hydraulics.

The algorithm is tested on the model of the so called “Digi Actuator”. The Digi Actuator is a test bench, where the motion of a hydraulic cylinder is realised. The hydraulic circuit is shown in Figure 1. As control element fast switching valves developed by the Linz Center of Mechatronics are applied [6]. The valves are controlled via Pulse Width Modulation at a frequency of 70Hz.

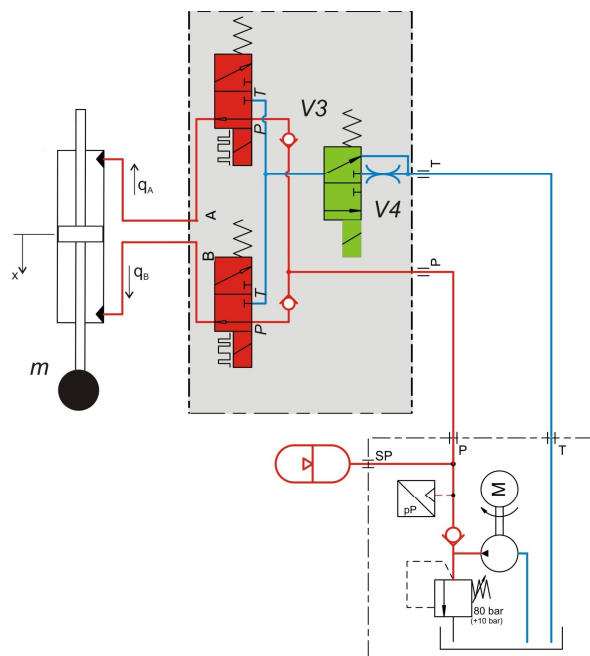


Figure 1. Hydraulic circuit of the “Digi Actuator”

To derive a SMC-concept the mathematic model of the system has to be built up. It is essential for applying this control scheme to the system. At the moment a third order system is considered. This implicates the equations of motion and the pressure built up equations. The throttle valve V4 has been neglected in this approach. This valve is just used to realise different operation points at one duty cycle in order to cope with the strong nonlinearities for small valve openings.

In a further step, simulations with the new control approach were made and compared to the measurements taken on the real system, where the duty cycle is proportional to the position error and the integral of the position error.

## 2. MODELLING

As mentioned above, the equations of motion and the pressure built up equation were built. A friction term is also considered. The friction term is approximated by the hyperbolic tangent, in order to guarantee the differentiability.

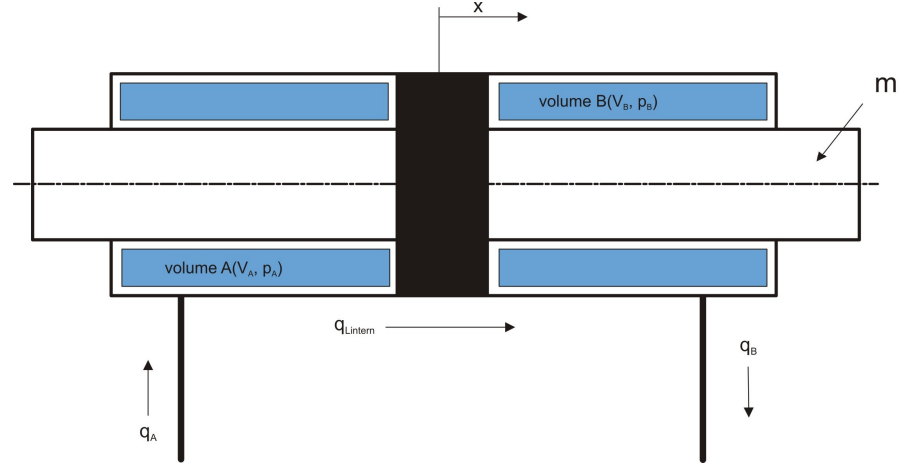


Figure 2. Hydraulic model of the cylinder

We consider the pressure built up equations as follows:

$$\dot{p}_A \cdot \frac{A}{E} \cdot (l_{A0} + x) + A \cdot \dot{x} = q_A - q_{Lintern} \quad (1)$$

$$\dot{p}_B \cdot \frac{A}{E} \cdot (l_{B0} + x) - A \cdot \dot{x} = q_B + q_{Lintern} \quad (2)$$

with

$$l_{A0} = \frac{1}{A} \cdot (V_{A0} - V_{LA}) \quad (3)$$

$$l_{B0} = \frac{1}{A} \cdot (V_{B0} - V_{LB}) \quad (4)$$

where  $V_{LA}, V_{LB}$  are the pipe volumes. Modelling a laminar flow for the intern leakage, the differential equation for the pressure reads:

$$\dot{p}_A = \frac{E}{A \cdot (l_{A0} + x)} \cdot \left[ q_A - \underbrace{K_{intern} \cdot (p_A - p_B)}_{q_{Lintern}} \right] \quad (5)$$

$$\dot{p}_B = \frac{E}{A \cdot (l_{A0} - x)} \cdot \left[ -q_B + \underbrace{K_{int\,ern} \cdot (p_A - p_B)}_{q_{L\,int\,ern}} \right] \quad (6)$$

The actuating variable is the flow rate. Interacting with the mass  $m$  of the system and the friction force  $F_F$ , the equations of motion is:

$$m \cdot \ddot{x} = (p_A - p_B) \cdot A - F_F \quad (7)$$

The friction term is given by:

$$F_F = F_{Stick} \cdot \tanh(\tau \cdot \dot{x}) + d \cdot \dot{x} \quad (8)$$

In order to get a system without internal dynamics, some assumptions are made. This is essential for an accurate linearization of the system.

With  $q_A = q_B = q$ ,  $\dot{p}_A + \dot{p}_B = 0$ ,  $p_A - p_B = p_D$ ,  $\dot{p}_A - \dot{p}_B = \dot{p}_D$  and  $l_{A0} = l_{B0} = L$  the differential equation for the pressure difference is received:

$$\dot{p}_D = [2 \cdot q - 2 \cdot K_{int\,ern} \cdot p_D - 2 \cdot A \cdot \dot{x}] \cdot \underbrace{\frac{E}{A \cdot L}}_{\frac{1}{C_H}} \quad (9)$$

### 3. SLIDING MODE CONTROL DESIGN

The idea behind this control scheme is a discontinuous acting variable, which forces the system to reach the so called sliding surface and remain in second consequence on it [1], [2], [5]. In order to derive the control design the system must be available in normal form.

#### 3.1. Transformation to Byrnes-Isidori normal form

The SISO system

$$\begin{aligned} \dot{\mathbf{x}} &= f(\mathbf{x}) + g(\mathbf{x}) \cdot u & \mathbf{x} \in \mathfrak{R}^n; u, y \in \mathfrak{R} \\ y &= h(\mathbf{x}) \end{aligned} \quad (10)$$

has to fulfil according to [3] the following criteria for system linearization

- $L_g L_f^k h(\mathbf{x}) = 0$ ,  $k = 0, \dots, r - 2$
- $L_g L_f^{r-1} h(\mathbf{x}) \neq 0$

where  $r$  is the relative degree of the system.

The system satisfies the conditions above and the relative degree of the system is equal to the system order, the coordinate transformation

$$\mathbf{z} = \begin{bmatrix} z_1 \\ z_2 \\ \vdots \\ z_n \end{bmatrix} = \Phi(\mathbf{x}) = \begin{bmatrix} h(\mathbf{x}) \\ L_f h(\mathbf{x}) \\ \vdots \\ L_f^{n-1} h(\mathbf{x}) \end{bmatrix} \quad (11)$$

can be applied to the nonlinear system. So the Byrnes-Isidori normal form

$$\dot{\mathbf{z}} = \begin{bmatrix} \dot{z}_1 \\ \dot{z}_2 \\ \vdots \\ \dot{z}_{n-1} \\ \dot{z}_n \end{bmatrix} = \begin{bmatrix} z_2 \\ z_3 \\ \vdots \\ z_n \\ \alpha(\mathbf{x}) + \beta(\mathbf{x}) \cdot u \end{bmatrix} \quad (12)$$

where

$$\alpha(\mathbf{x}) = L_f^n h(\mathbf{x})$$

$$\beta(\mathbf{x}) = L_g L_f^{n-1} h(\mathbf{x})$$

is received. In a next step the sliding mode control design can be applied on this transformed system.

### 3.2. Control Design

To cope with the tracking problem a sliding surface  $S = \mathbf{c} \cdot \mathbf{e}$  is defined. Where  $\mathbf{c} = [c_1 \ c_2 \ \dots \ c_{n-1} \ 1]$  is a constant vector and

$$\mathbf{e} = \begin{bmatrix} e_1 \\ e_2 \\ \vdots \\ e_n \end{bmatrix} = \mathbf{z} - \mathbf{r} = \begin{bmatrix} z_1 \\ z_2 \\ \vdots \\ z_n \end{bmatrix} - \begin{bmatrix} \xi_1 \\ \xi_2 \\ \vdots \\ \xi_n \end{bmatrix} \quad (13)$$

is the error vector. The sliding surface can be interpreted as collective variable, which guaranties perfect tracking in finite time T under following condition:

$$\lim_{t \rightarrow T} S(t) = 0 \quad (14)$$

The tracking problem is transformed to a stability problem. This can be solved via the Lyapunov approach [2]

$$V(S) = \frac{1}{2} \cdot S^2 \quad (15)$$

In order to fulfil the conditions of  $V(s)$  being a Lyapunov function, the following condition

$$\frac{dV}{dt} = S \cdot \frac{dS}{dt} \leq -\eta \cdot |S| \quad \eta > 0 \quad (16)$$

must be satisfied. This implicates  $\frac{dS}{dt} = -\mu \cdot \text{sign}(S)$  under the restriction  $\mu \geq \eta$ . The acting variable is gained from

$$\dot{S} = c_1 \cdot \dot{e}_1 + c_2 \cdot \dot{e}_2 + \dots + c_{n-1} \cdot \dot{e}_{n-1} + \dot{e}_n = -\mu \cdot \text{sign}(S)$$

$$\dot{e}_n = \dot{z}_n - \frac{d^n \xi}{dt^n}$$

$$\dot{z}_n = \alpha(x) + \beta(x) \cdot u$$

and results in

$$u = \frac{1}{\beta(\mathbf{x})} \cdot \left[ -\alpha(\mathbf{x}) + \frac{d^n \xi}{dt^n} - c_1 \cdot \dot{e}_1 - c_2 \cdot \dot{e}_2 - \dots - c_{n-1} \cdot \dot{e}_{n-1} \right] - \frac{\mu}{\beta(\mathbf{x})} \cdot \text{sign}(S) \quad (17)$$

as the control law.

### 3.3. Controller Design neglecting the friction term

According to chapter 2 the system reads:

$$\mathbf{x} = \begin{bmatrix} x \\ v \\ p_D \end{bmatrix} = \begin{bmatrix} x_1 \\ x_2 \\ x_3 \end{bmatrix} \rightarrow \dot{\mathbf{x}} = \begin{bmatrix} \dot{x}_1 \\ \dot{x}_2 \\ \dot{x}_3 \end{bmatrix} = \begin{bmatrix} f_1(\mathbf{x}) \\ f_2(\mathbf{x}) \\ f_3(\mathbf{x}) \end{bmatrix} + \begin{bmatrix} g_1(\mathbf{x}) \\ g_2(\mathbf{x}) \\ g_3(\mathbf{x}) \end{bmatrix} \cdot u \quad (18)$$

In order to transform the system to normal form the Lie derivatives have to be calculated.

$$L_f^0 h(\mathbf{x}) = h(\mathbf{x}) = x_1 \quad (19)$$

$$L_f^1 h(\mathbf{x}) = (\nabla h(\mathbf{x})) \cdot f(\mathbf{x}) = [1 \quad 0 \quad 0] \cdot \begin{bmatrix} f_1(\mathbf{x}) \\ f_2(\mathbf{x}) \\ f_3(\mathbf{x}) \end{bmatrix} = x_2 \quad (20)$$

$$L_g L_f^0 h(\mathbf{x}) = (\nabla h(\mathbf{x})) \cdot g(\mathbf{x}) = [1 \ 0 \ 0] \cdot \begin{bmatrix} g_1(\mathbf{x}) \\ g_2(\mathbf{x}) \\ g_3(\mathbf{x}) \end{bmatrix} = 0 \quad (21)$$

$$L_f^2 h(\mathbf{x}) = (\nabla L_f^1 h(\mathbf{x})) \cdot f(\mathbf{x}) = [0 \ 1 \ 0] \cdot \begin{bmatrix} f_1(\mathbf{x}) \\ f_2(\mathbf{x}) \\ f_3(\mathbf{x}) \end{bmatrix} = -\frac{d}{m} \cdot x_2 + \frac{A}{m} \cdot x_3 \quad (22)$$

$$L_g L_f^1 h(\mathbf{x}) = (\nabla L_f^1 h(\mathbf{x})) \cdot g(\mathbf{x}) = [0 \ 1 \ 0] \cdot \begin{bmatrix} g_1(\mathbf{x}) \\ g_2(\mathbf{x}) \\ g_3(\mathbf{x}) \end{bmatrix} = 0 \quad (23)$$

$$L_f^3 h(\mathbf{x}) = (\nabla L_f^2 h(\mathbf{x})) \cdot f(\mathbf{x}) = \left( \frac{d^2}{m^2} - \frac{2 \cdot A^2}{m \cdot C_H} \right) \cdot x_2 - \left( \frac{A \cdot d}{m^2} + \frac{2 \cdot A \cdot K}{m \cdot C_H} \right) \cdot x_3 \quad (24)$$

$$L_g L_f^2 h(\mathbf{x}) = (\nabla L_f^2 h(\mathbf{x})) \cdot g(\mathbf{x}) = \frac{2 \cdot A}{m \cdot C_H} \quad (25)$$

As we can see the relative degree of the system is equal the system order. Hence, the system can be transformed via

$$\Phi(\mathbf{x}) = \begin{bmatrix} h(\mathbf{x}) \\ L_f^1 h(\mathbf{x}) \\ L_f^2 h(\mathbf{x}) \end{bmatrix} \quad (26)$$

without any internal dynamics.



#### 4. RESULTS AND DISCUSSION

The basic control structure is indicated by Fig. 3. This means an additional mapping between the desired output of the controller and the input of the system.

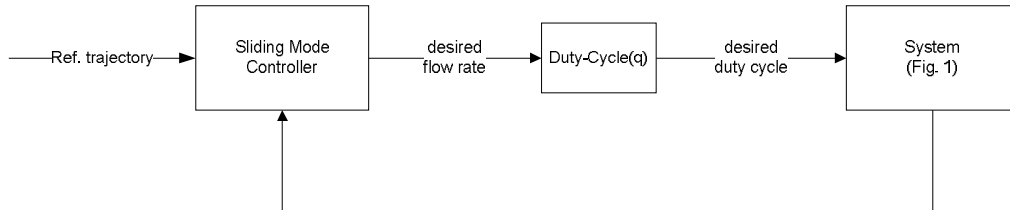


Figure 3. control structure

As shown in Fig. 3 the output of the sliding mode controller is the flow rate. To map this flow rate to the duty cycle of the switching valves, a characteristic curve was measured and inverted.

Simulations were made for a sinusoidal movement and a ramp with steady-state position. To show the robustness compared to the system parameter variation, an additional simulation was done.

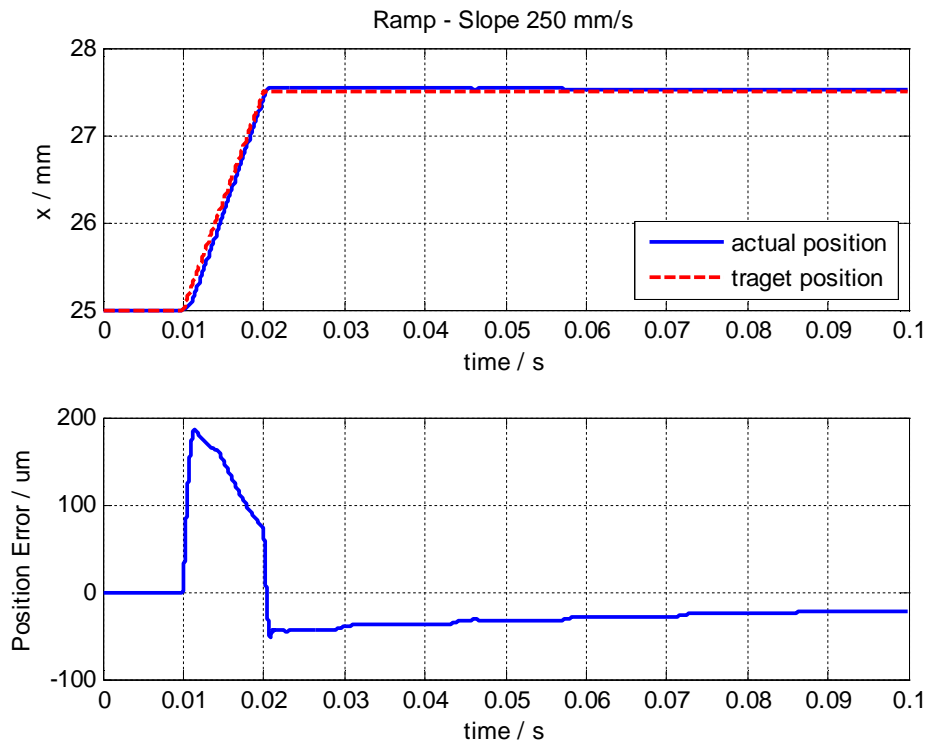


Figure 4. Position  $x$  and position error for a ramp type reference position with a slope of 250 mm/s

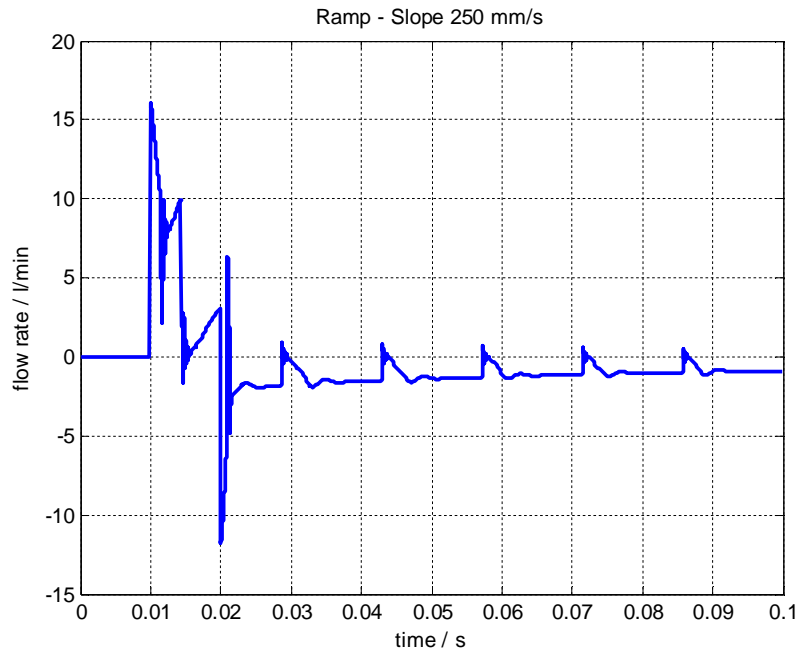


Figure 5. Flow rate for a ramp type reference position with a slope of 250 mm/s

Fig. 4 shows the actual position due to a ramp with a slope of 250mm/s whereas the theoretical maximum speed is 540 mm/s. The position error during the motion is limited to the maximum of 180 $\mu$ m. Compared to the simulations and measurements of the actual test bench during this movement, a five times higher accuracy can be achieved. The steady-state positional deviation is about 30 $\mu$ m. The spikes which can be observed in Fig. 5 are a result of the discontinuous actuating variable.

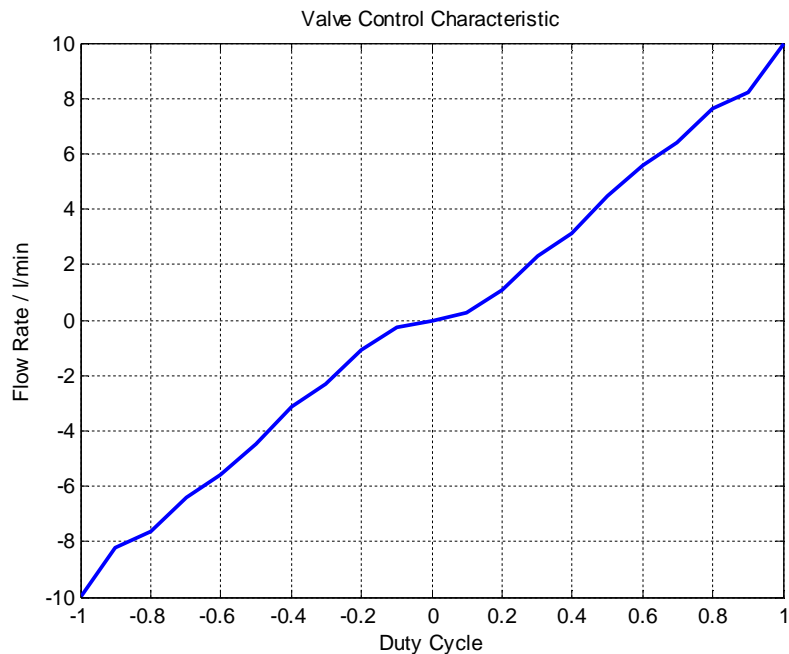


Figure 6. Valve Control Characteristic

The behaviour between flow rate and duty cycle can be considered in Fig. 6. This characteristic maps the output of the control algorithm to the system input.

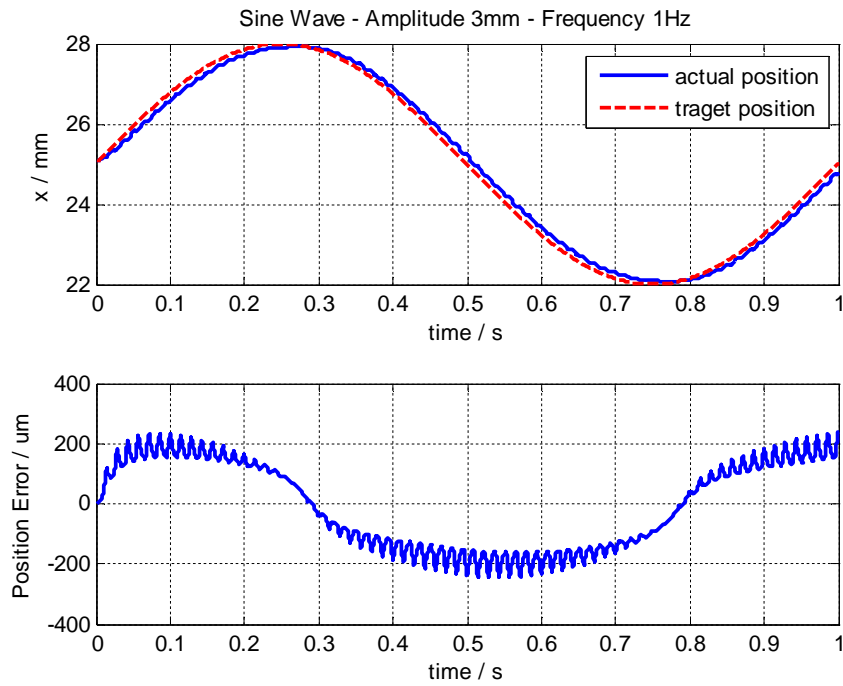


Figure 7. Position  $x$  and position error for a sinusoidal reference position with an amplitude of 3mm at frequency of 1Hz

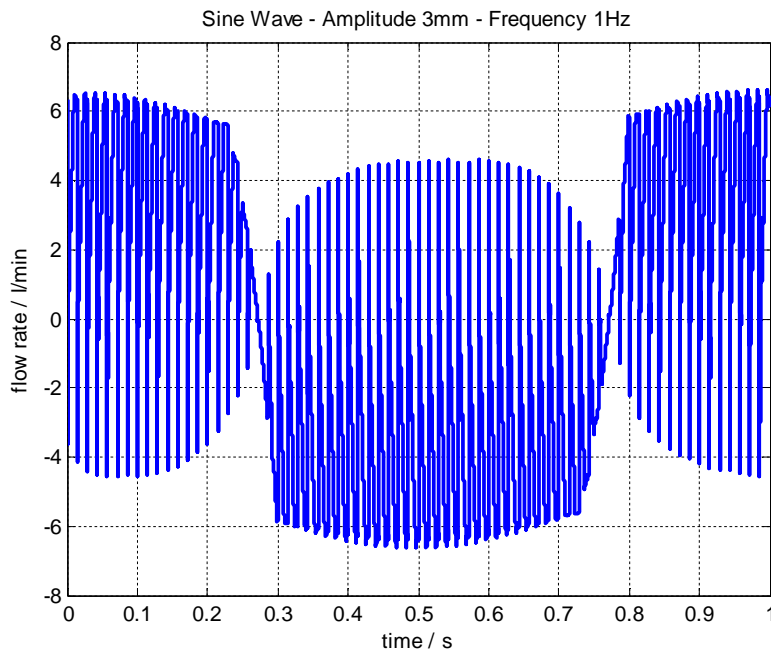


Figure 8. Flow rate for a sinusoidal reference position with an amplitude of 3mm at frequency of 1Hz

The sinusoidal movement was carried out with an amplitude of 3mm at a frequency of 1Hz. In addition, a constant lag in position can be seen. Fig. 8 shows the robustness of the controller. This simulation was done once with the initial system and once using the system with 3x the mass without changing the controller parameters. As one can see, the position error is limited to 350 $\mu$ m during the movement with constant speed and to 60 $\mu$ m in the steady-state case.

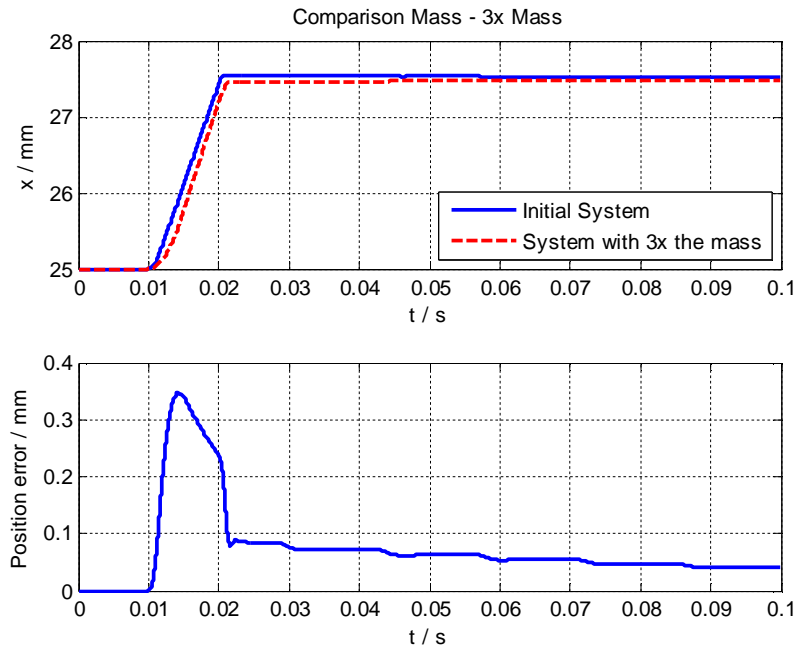


Figure 9. Position  $x$  and position error for a ramp type reference position, comparing the initial system to the system with 3x the mass

The simulations show that the sliding mode approach leads to better results compared to those implemented in the application right now. In order to verify the results, measurements on the test set up have to be done in the near future.

Simulations have also shown that the tracking error can be reduced by increasing the switching frequency of the valves without improving the model. The model uncertainties are playing a minor role due to the robustness of the proposed controller.

#### ACKNOWLEDGEMENT

The authors gratefully acknowledge the sponsoring of this work by the “Austrian Center of Competence in Mechatronics (ACCM)” in the framework of the COMET program. This work was sponsored by the Austrian government, the federal state Upper Austria and the Johannes Kepler University.

#### REFERENCES

- [1] Utkin V.I.: Variable Structure Systems with Sliding Modes, IEEE Trans. Automat. Control, Vol. 22, No. 2, April 1977, pp 212-222.
- [2] Khalil H.K.: Nonlinear Systems, Prentice Hall, 2002.
- [3] Kugi A.: Regelsysteme, Lecture Notes, Vienna Univericity of Technology, 2011.
- [4] Scheidl R.: Ölhydraulik, Lecture Notes, Johannes Kepler University Linz, 2010.

- [5] Hung J.Y., Gao W., Hung J.C.: Variable Structure Control: A Survey, IEEE Trans. Industrial Electronics, Vol. 40, No. 1, February 1993, pp 2-22.
- [6] Plöckinger A., Winkler B., Scheidl R.: Development and Prototyping of a Compact, Fast 3/2 Way Switching Valve with Integrated Onboard Electronics, The 11<sup>th</sup> Scandinavian International Conference on Fluid Power, June 2009.

## LAMINATED MANIFOLD FOR DIGITAL HYDRAULICS – PRINCIPLES, CHALLENGES AND BENEFITS

M.Sc. Miika Paloniitty, M.Sc. Matti Karvonen, Adj. Prof. Matti Linjama, Prof. Tuomo Tiainen\*

Tampere University of Technology  
Department of Intelligent Hydraulics and Automation

\* Department of Materials Science

[miika.paloniitty@tut.fi](mailto:miika.paloniitty@tut.fi)

### ABSTRACT

The path to digital hydraulic valve package, consisting dozens or even hundreds of similar small valves, is having wide gorges on the way. To build bridges over them, untypical technologies must be used. The hydraulic valve package consisting of a manifold and valves is a multidisciplinary design problem needing design skills from, e.g., fluid dynamics and electromagnetics but also from materials science and manufacturing engineering. In this paper the last mentioned areas are studied in order to find a path for an economical way to produce a hydraulic manifold for dozens of miniature valves. In this paper, lamination technology and its suitability for hydraulic manifold design are studied. The main principles are presented and the challenges and benefits are discussed.

**KEYWORDS:** Lamination, brazing, hydraulic manifold, digital hydraulics

### 1. INTRODUCTION

In previously published papers it has been suggested that a “perfect valve” could be obtained by using Pulse Number Modulated digital valve system, which contains a large number of similar small on/off-valves [1]. A theoretical background for this can be found in scaling laws; while the valve size and power consumption decrease, the operation frequency increases [2]. The effect of scaling a simple miniature needle valve is presented in [3]. On the other hand, the plurality of needed on/off-valves increases and the smaller size tends to lead to tightened machining tolerances. R&D has been done for fast, small and simple on/off-valves to be used as parts of a larger valve package. Prototypes have been built: the earlier ones were fast, low power consuming, bistable on/off-valves [4] [5] but their production costs were estimated to be too high for PNM-coded valve packages. Therefore more simple spring return miniature needle

valves have been designed and the first one was published in [6]. The latest version of the miniature needle valve are not yet published, but it can be stated that the manufacturing point of view is now taken into account much more than in the first version. The performance should be on the same scale.

Assuming that we have good miniature on/off-valves to use as parallel connected series to form a digital valve, we still face the challenge with the valve manifold where the on/off-valves should be installed. Due to the great number of those, the manifold would require a lot of time consuming machining, which is quite expensive. It is also likely that the manifold would require quite a large number of auxiliary flow channels, which may require plugs and which for high pressure are also a major cost, both by parts and also by installation work. If the valve can be freely designed, the compact manifold design should be possible with conventional machining, but if a CETOP-subplate is required things get much more complicated, as presented later. Subplate installation capability is essential, if economical retrofits are to be achieved. Clear benefits of lamination technology will be shown in this paper.

The “magic-tool” which would solve many of the manifold manufacturing problems would be some kind of a “wormlike drill”, with which one could make bending bores, not just straight lines. Yet a drill like this is an engineer’s dream, but fortunately other fabrication methods for almost freely shaped flow channels are available. Casting gives some and sintering almost full freedom for designers. Because our design is likely to include narrow shapes, casting is not likely to be possible. Sintering is better for rapid prototyping than for mass production; therefore that alternative was dismissed. Building a manifold by laminating it from precut sheets is an interesting alternative. Sheets can be mechanically pierced or thermally cut to proper shape. The channels in a laminated manifold can be freely designed but of course the thickness of the sheets influences the obtainable resolution. Solid block from various sheets can be produced by adding brazing filler between the sheets and brazing them together by properly heating them in a furnace. Figure 1 illustrates how a bending flow path could be achieved with conventional machining and with lamination technology.

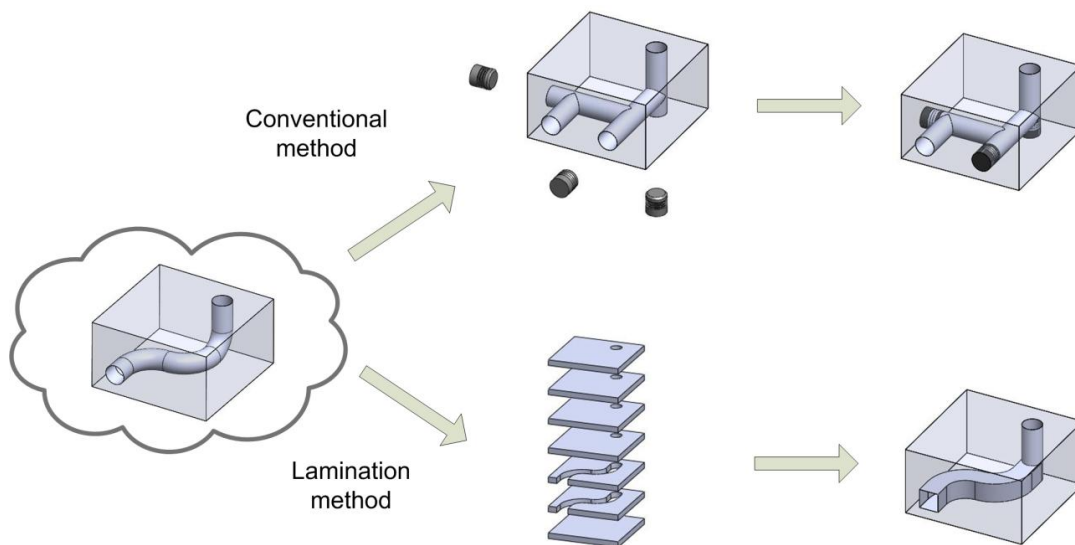


Figure 1. A simplified example of producing an imaginary block by two alternative production methods. Upper: standard way; straight drillings and plugs. Lower: Laminated block.

In this paper the basic principles, challenges and benefits of making a hydraulic valve manifold by lamination method is described. The produced test piece, is a part with which the lamination method was at first studied and the pressure tests were carried out. Encouraged by the results future plans were made and they are also presented and discussed.

## 2. LAMINATION AND BRAZING

### 2.1. Lamination technology

Lamination is not a new technology in the field of fluid power. Laminated manifolds are mentioned in a patent [7] and a patent application [8]. Linde Hydraulics presented beneficial aspects of lamination method for mobile hydraulic manifolds in [9]. In a staff report in the journal of Hydraulics & Pneumatics [10] single-piece manifolds are divided to laminated and drilled ones. Anyway, laminated manifolds are not common on the market.

Modern brazed plate heat exchangers utilize manufacturing technology, which is quite close to the technology needed with laminated manifolds. In these heat exchangers the steel sheets are not flat and they are not joined together by whole area, but the joining technology is equivalent and the internal cavities have to be leakage tight. By brazing, the rubber seals can be avoided and the structure withstands higher pressures without external plate frames.

The manufacturing process of laminated manifolds utilizes modern sheet metal processing methods. Every internal shape including flow channels and valve cavities can be produced by piercing or cutting sheets. In the optimal case the production of mounting threads is the only operation which has to be carried out to finish the manifold after the sheets have pierced, stacked and brazed together.

Lamination technology has also challenges. There is a need for accurate dimensions in the manifold. The accuracy of dimensions on the sheet plane comes from piercing or cutting machine, but the control of thickness dimensions is more complicated. It is still needed, especially in the case where the valve cavities are made without post-brazing machining. From the manufacturing point of view the alignment of the sheets was proven to be challenging.

### 2.2. Brazing in general

Brazing is a general joining process in industry. In brazing the filler alloy melts and fills the clearance between closely assembled surfaces to be joined. The material of the components to be joined must have a higher melting range than the filler alloy. Typical brazing filler alloys in conventional brazing are silver- or copper-based. Soldering is an equivalent joining process operating at lower temperatures typically with tin-based fillers, but the joint strength is typically lower. Welding is carried out at higher temperatures and unlike in soldering or brazing, also the base metal melts in the welding process, not just the filler.



To obtain a good joint by brazing, many things have to be taken into account. Essential physical phenomena for enabling good joints by brazing are capillary flow and wetting. The molten filler alloy has to wet the surfaces to be joined. There are many things influencing the filler ability to wet the surfaces. One of the key issues is the cleanliness of the surfaces without any contamination especially oxides. Metallurgical properties influence also the wetting phenomenon and define which filler alloys can be used with a particular base metal. [11]

Fluxing is mostly used in brazing to dissolve any oxide films from joining surfaces and to protect the surfaces and the filler from re-oxidation during brazing. Another function of the flux is to enhance the wetting and flow characteristics of the molten filler. Filler has to displace the flux while spreading in the clearance. When the joint is cooled the extruded and solidified flux has to be completely removed before the use of the component due to the possible corrosive properties of the flux. This could be tricky with complex-shaped manifolds. [12]

### 2.3. Special brazing processes

Using a furnace as a heat source, controlled atmosphere can be used and a sufficient protection against oxidation can be achieved without flux. Furnace atmospheres used in brazing can be divided into three categories: neutral, reducing and vacuum. Neutral atmospheres like argon can protect components and filler against oxidation. Reducing atmospheres like hydrogen provide also the oxidation protection but in addition, they have an ability to remove existing oxides. Vacuum is in a way a neutral atmosphere because there is almost nothing left in the atmosphere but it also acts like active gases and has an ability to remove oxides. Both reducing and vacuum atmospheres have a positive influence on wetting. [13]

One of the fluxless brazing processes used in the industry is the CuproBraz® process, which is developed especially for manufacturing efficient heavy-duty mobile and industrial heat exchangers [14]. This process is only suitable for brazing copper and copper alloys, because the filler alloy used in this process contains high amount of phosphorus, which forms extremely brittle compounds with iron.

Vacuum brazing is typically a high temperature fluxless brazing process where the typical fillers are nickel-based alloys or pure copper. The advantages of using vacuum as an atmosphere are that the purity level of the atmosphere can be precisely controlled and, as already mentioned, the ability to remove oxide layers at high temperature. [15] Plate heat exchangers are typically composed of stainless steel plates which are brazed together with pure copper in a vacuum furnace.

Nickel-based brazing alloys which are developed for use in fluxless brazing process contain additives like silicon, boron and phosphorus which lower the melting range and enhance the wetting and flow characteristics of the filler alloy. Those additives make these alloys inherently brittle when they have the conventional crystalline structure but with rapid solidification technology, ductile amorphous foils can be produced [16]. Otherwise these brittle alloys are available in powder form. The use of filler metal foils is superior as compared to the gas-atomized filler powder, because films contain much less harmful oxides than powders. These oxides influence the flow characteristics of the molten filler [16]. Poor flow of filler may lead to a non-homogenous brazing joint, if the

filler will not flow over the entire connection surface area. From the manufacturing point of view, foils can be stacked between sheets and powder paste can be applied, e.g., by screen printing. Both methods are possible.

### 3. BENEFICIAL ASPECTS OF LAMINATION TECHNOLOGY FOR DIGITAL HYDRAULIC RETROFITS

One of the benefits of lamination method is that the flow channels can be not only straight bores but they can also be bending. In order to make economical digital hydraulic retrofits for replacing existing proportional valves, the valve package should be mountable to a standard subplate like CETOP 3. However the subplate is not designed for this kind of purpose, and challenges occur when attempting to install dozens of on/off-valves in the single CETOP 3-mountable manifold.

The flow channels of a CETOP 3-subplate fitting valve package are outlined in Figure 2. Taking into account the allowed dimensions of CETOP 3-mountable valve [17] and dimensions of the miniature valve prototype [6], four valves could be assembled parallel in the manifold. The draft in Figure 2 reveals difficulty in getting the flow paths to the valve rows which are behind the fastening screw holes. It is not a problem to get the flow paths to the two rows near the centerline of the manifold, but with dozens of valves to be installed, all available space is needed. If only the two easily reachable rows were used, the manifold would become too long which would also make it difficult to drill. The main advantage of the lamination technology in PNM-coded CETOP 3-mountable digital valve manifold is that the on/off-valves can be assembled with higher density and still get proper flow paths for all of them. Also flow channels are wider and more valves can be mounted without any auxiliary drillings and plugs. Figure 3 illustrates these benefits.

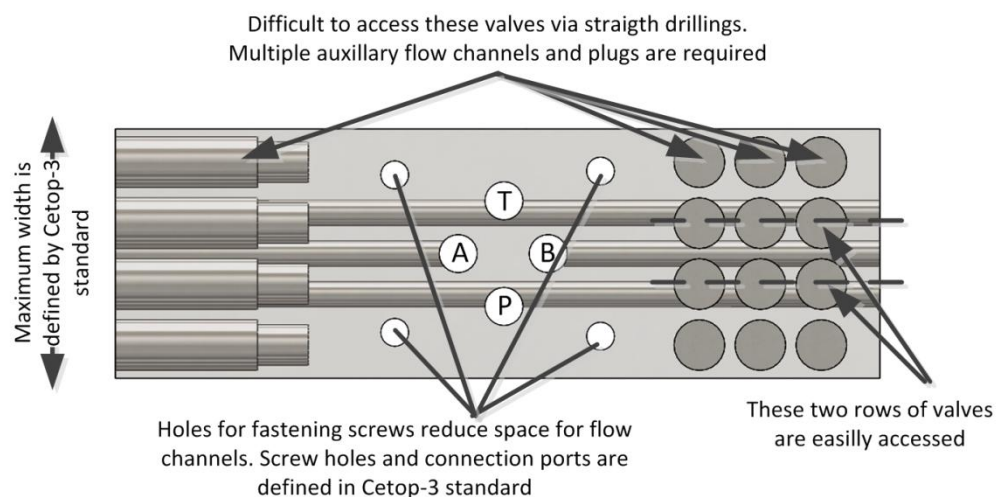


Figure 2. A graphical explanation of difficulties with CETOP 3-mountable PNM-coded digital valve manifold

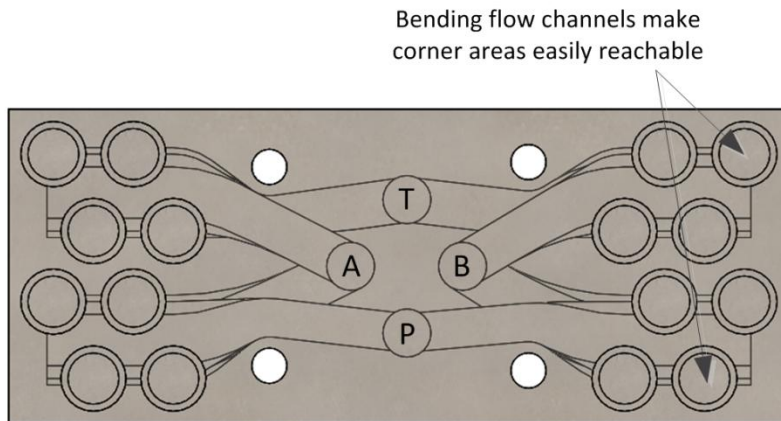


Figure 3. The benefits of freely designable flow channels in a laminated CETOP 3-mountable digital valve.

#### 4. TEST SETUP

To verify the applicability for high pressures and to study the practical issues of the lamination technology, a test block was produced. The block was composed of 30 steel sheets and its outer dimensions were 50x50x60mm. The block is presented in Figure 4 and the pile of sheets is in Figure 5. There were four different chambers in the block and each of them was designed to reveal specific issues on the pressure-enduring characteristics of the brazed structure.

- Chamber one was right-angled volume having 1.5mm wall thickness.
- Chamber two was with the same minimum wall thickness as chamber one but it was profiled to endure higher pressure.
- Chamber three had equal dimensions with chamber one but its longest dimension was in different direction as compared to the direction of the sheets. In chamber one, the stress concentration due to the pressure is attempting to break a brazed joint while in chamber three it is attempting to break the corners of the sheets
- Chamber four was planned to be more durable than the other chambers but it had three holes being one millimeter away from the chamber to reveal possible leakages through the narrow brazement.

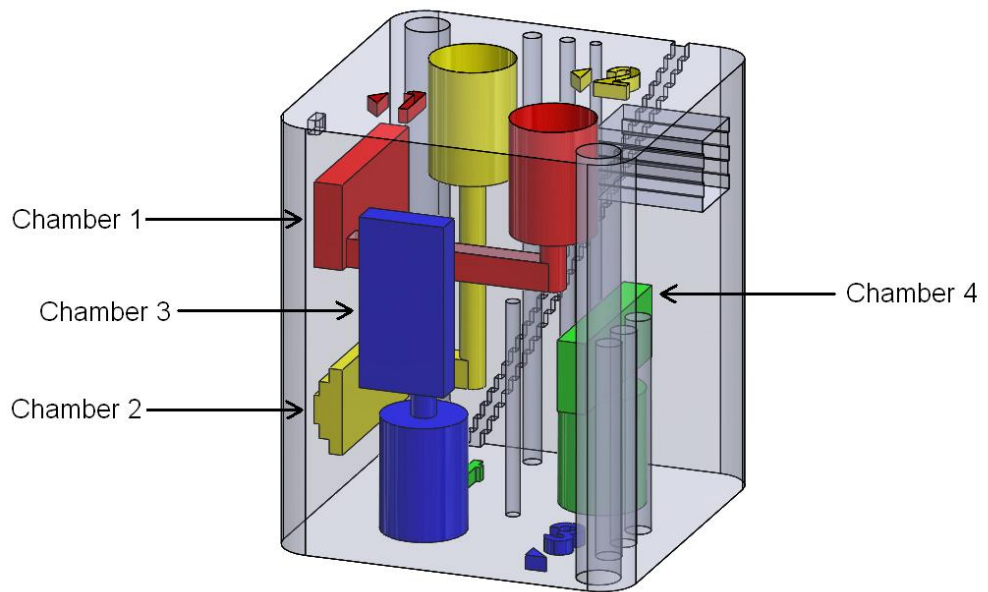


Figure 4. The test block. The four test chambers are presented in different colours.

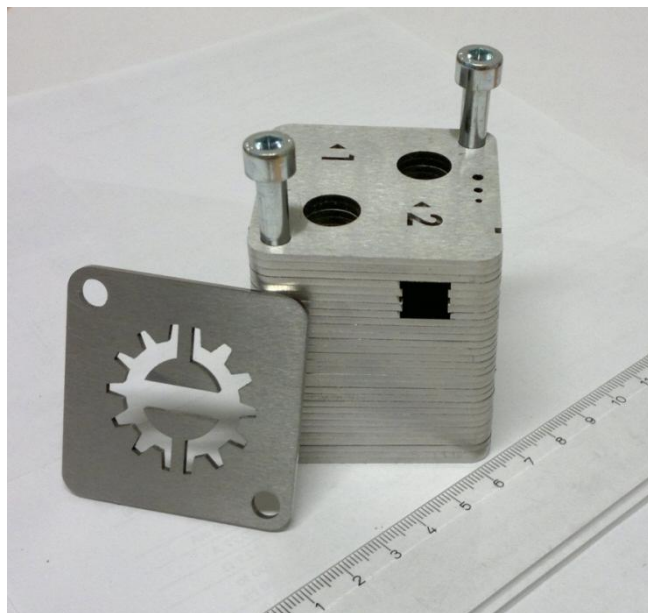


Figure 5. The test block sheets as stacked but not yet brazed.

The sheet and brazing materials used in the test block were selected so that the digital valve manifold can be made with the same materials. Mild structural steel was selected because of its sufficient strength properties without any special heat treatment cycles which could be affected by the brazing cycle. The magnetic properties of mild steel are also sufficient for the solenoid valve assembled wholly inside the block in a way where the block itself works as a part of the magnetic circuit. Therefore it is important that both the sheet material and brazing material are ferromagnetic. From brazing fillers used in fluxless brazing processes nickel-based fillers form the only filler group which is ferromagnetic. In addition to that, high joint strength can be obtained with

nickel-based fillers. The amorphous nickel-based foil, Vacuumschmelze VZ2120, was selected as filler material. The thickness of the foil was 40 $\mu$ m. Holes for the alignment pins were cut to the filler foils, but any other holes were not pre-cut. Stack was brazed together in a vacuum furnace with a hydrogen partial pressure of 2 mbar. Hydrogen was decided to be used to confirm the adequate reducing behavior of the atmosphere. The temperature during the brazing process reached 1070 °C and the temperature profile as a function of time was controlled during heating. The cooling was carried out as rapid as possible, which however, means quite slow rates in vacuum atmosphere.

## 5. STRUCTURAL ANALYSIS

To gain information on the pressure endurance limit of chamber 1 without brazed joints, structural FEM-analysis was carried out. Initial studies revealed that a 2D-analysis with cross-sectional geometry of the chamber is a sufficient method in this case [18]. Due to the expected plastic deformation especially in chamber corners, the elastoplastic material model was used. Analysis was carried out with constant pressure in the chamber. The pressure level at which corner stresses reaches the ultimate strength of the material was determined by driving calculations with various pressure levels. The ultimate tensile strength of the steel was estimated to be 500 N/mm<sup>2</sup>. The corner fillet radius in simulations was 0.04mm corresponding to the filler foil thickness. The density of the calculation elements was strongly increased near corners to get proper stresses.

The relative principal stresses at the pressure level of 29MPa are presented in Figure 6. At that pressure level the stress of the corners reaches the ultimate tensile strength. Displacements in the figure are scaled to be tenfold, so it is shown that there is no visible deformations until the corners begin to fracture. At higher pressure levels the used physical model is not valid because the fracture phenomenon was not modeled. However, it can be assumed that visible deformation follows the fracture of the corners in short order when the pressure level is further increased.

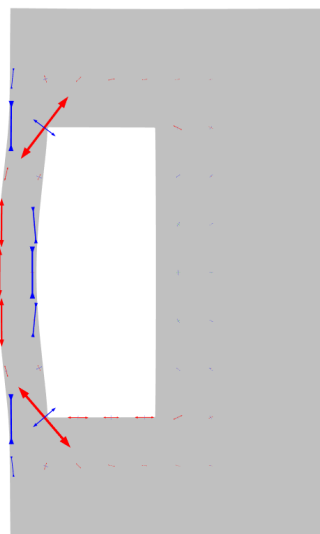


Figure 6. FEM analysis show that the highest stresses occur at the corners of the chamber.

## 6. MEASUREMENTS

### 6.1. Pressure tests and valve response test

The pressure tests were carried out with pneumatic/water hydraulic pressure intensifier (Figure 7). Daisy Lab was used as a measuring software. The pressure transducer for measuring chambers 1-3 was Trafag NAH with the measuring range of 40 MPa and for chamber 4 the transducer was Trafag EPN with the measuring range of 200 MPa. Measuring frequency was 1 kHz. Pressure was increased until external leakage occurred. The measurements were also recorded on video.

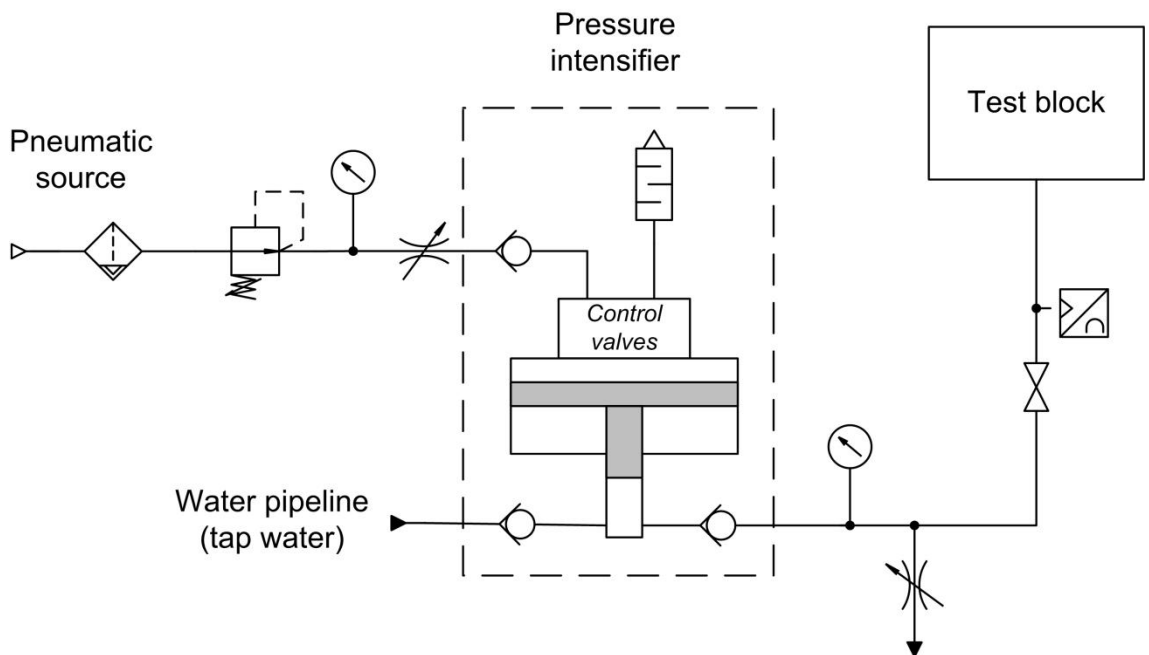


Figure 7. Schematic diagram of the pressure test assembly

### 6.2. Results

During the pressure test the pressure was measured as a function of time. The results are shown in Figure 9. Explanations of the individual tests are given below. After pressure tests the block was sawed so that the chambers could be analyzed. In Figure 8 a microscope image of chamber 1 is shown. The layers of the sheets are clearly visible.

When the pressure in chamber 1 was raised, visible deformation occurred at the level around 28 MPa. It is worth noting that in structural analysis a similar fracture pressure was estimated. Also it can be seen from Figure 8 that plastic deformation has occurred in base metal while there is no fracture at the joint. Based on this result it can be stated that the brazed joints had higher strength than the base material yield strength is. When the chamber pressure was further increased, the chamber continued to deform, until it broke at the pressure level of 37,5MPa.

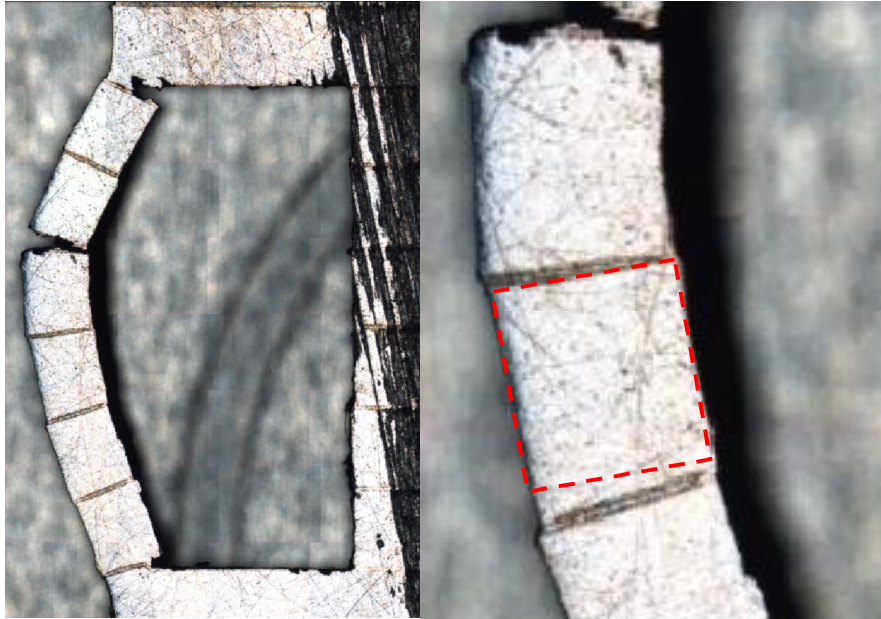


Figure 8. Left: Chamber 1 was deformed from the corners until it tore open from the middle. The thickness of the wall was 1.5 mm. Right: Plastic strain is clearly visible on the cross-section of the wall

Chamber 2 had a small external leakage already at low pressure levels. This indicates that the brazed joint had a flaw. The leak was, however minor, so that the pressure could be increased. Increasing was stopped at the pressure level of 44 MPa because of the measuring range of the pressure transducer. Steep pressure drop occurred when the test was stopped. There were not any visible deformations in that chamber despite of higher pressure level than the chamber 1 was able to sustain.

Chamber 3 had an external leakage on small pressure levels but it was minor enough so that the pressurization was possible. During pressurization the chamber wall deformed and its leakage increased at the pressure of 40 MPa. After a short thinking, chamber re-pressurization was carried out and then the chamber rupture spread wide open at 44 MPa.

Chamber 4 was not leaking and the pressure rose up to over 100 MPa but then a nipple connecting the high pressure line to the pressure intensifier was torn apart from the intensifier so that the measurements had to be stopped. However, the achieved pressure level is sufficiently high so that there was no need to continue the measurements anymore.

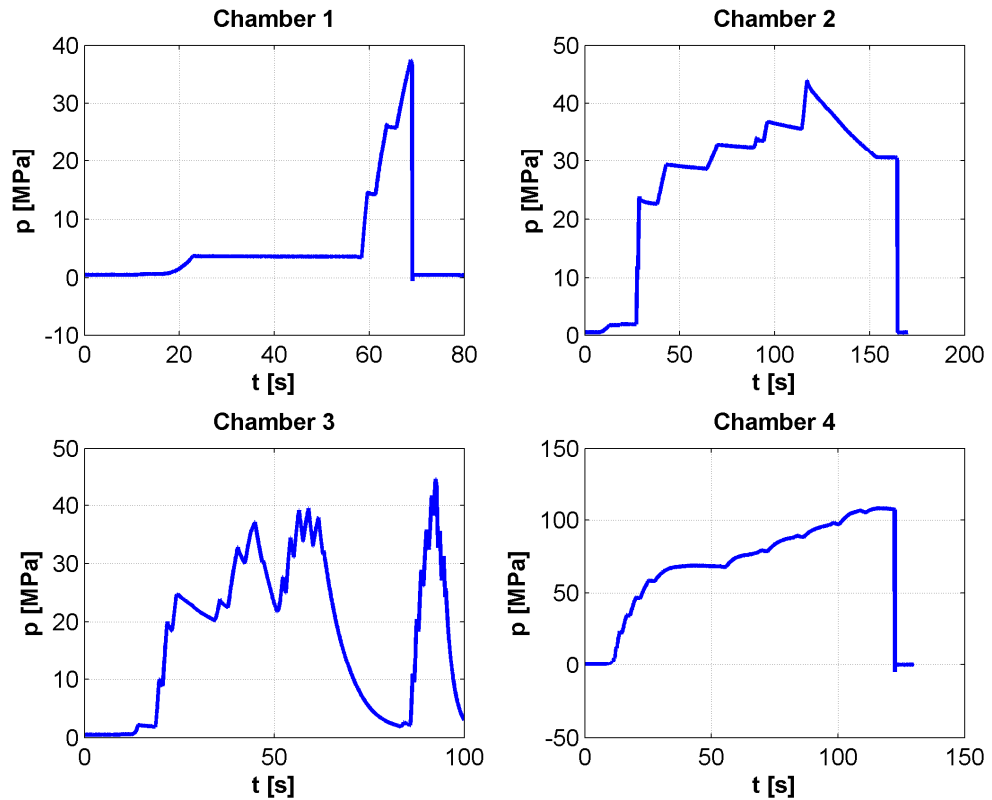


Figure 9. The measured pressure signals from the pressure tests of different chambers of the test block.

### 6.3. Magnetic properties of the laminated block

After the pressure tests a cavity for a single prototype valve was machined to the laminated test block. The influence of the brazing layers to the magnetic circuit of the solenoid actuator was studied. Valve response times and hold current were measured and there was no difference between the results of laminated and normal steel block. This was an expected result because the filler sheets were made of a ferromagnetic nickel alloy. The performance would have been lower if copper, or other non-ferromagnetic filler metal were used. This was, however, not tested.

## 7. FUTURE MANIFOLD DESIGN

Because the lamination method seems to be promising, a manifold for PNM-coded valve package was designed by utilizing the lamination technology. The target values were as follows:

- CETOP 3-mounting
- 4 control notches
- 32 on/off-valves per control notch
- Valve prototypes designed at IHA should be used. If necessary, the valve should be modified for easier manufacture and installation.



Initial studies suggested that vertically assembled valves and horizontal slices would lead to an efficient use of sheet metal processing and minimal post-processing after brazing [18]. The maximum width of CETOP 3-mounting valve is 50mm [17] and the diameter of the valve prototypes is circa 10 mm. Consequently four valve rows can be assembled side by side. To avoid too long manifold, two valve layers are used (bottom and top).

Horizontal flow paths could not be round-shaped due to the direction of laminates, but curves and cross-sectional changes can be designed smooth, as seen in Figure 10. Valve cavities could be made to final dimensions by piercing sheets. An accurate control of the thickness of the sheets as well as of the brazing layer is definitely needed. A foil-type brazing filler is better than powder paste in that sense.

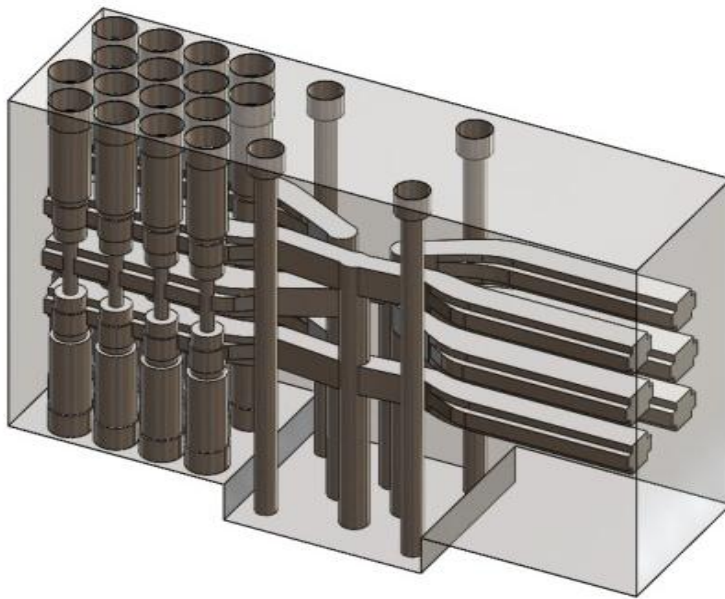


Figure 10. A 3D illustration of the flow paths inside the valve manifold. Valve cavities are shown only on the other side for the sake of clarity

The manifold is designed to be composed of 2 mm thick structural steel sheets. The bottom elevation is needed in order to offer space for the electric connections at the bottom layer of valves. Laser cutting of the sheets provides high freedom to shape the manifold, so industrial design could be exploited in manifold appearance, e.g., for fulfilling the eventual commercial demands. The complete manifold for a digital 4x32 valve is shown in Figure 11. Examples of a few sheets needed in the construction are shown in Figure 12.



Figure 11. The author's suggestion for a 4x32 bit CETOP 3-mountable valve package. Individual valves can be seen from the "window" on the model. University logo can be cut to the topmost sheet to increase marketing value

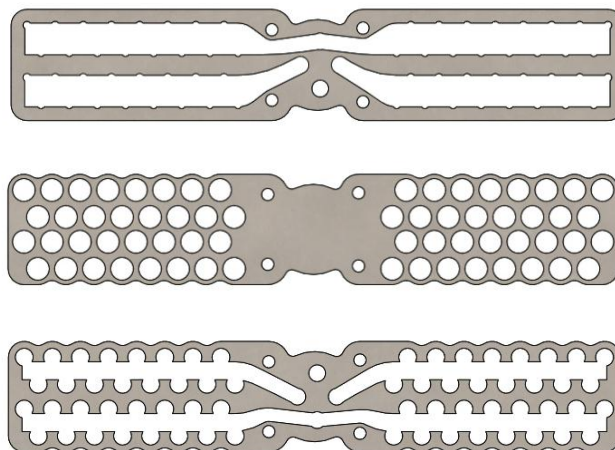

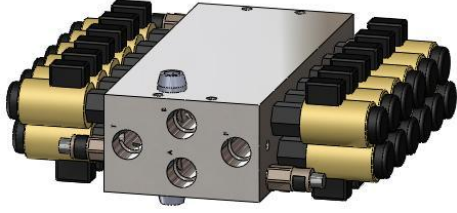


Figure 12. Examples of the sheets to be stacked and brazed to create a manifold for 4x32 bit valve package

When comparing the designed PNM-coded digital hydraulic valve package with the PCM-coded valve package utilizing commercial on/off-valves, the benefits are evident. To make these packages suitable for comparison, both should be feasible with the same pressure differential, should have the same resolution and should have the same step sizes. This requires appropriate sizing of serial orifices in the PCM-coded package. The PCM-coded package utilizes manifold design which has been used in prototypes. Calculated characteristics of the two valve packages are presented in Table 1. According to the manufacturer of the KSDEU valve, maximum flow is limited to 20 l/min. Anyway, with the series design described in the Table 1, the maximum flow is 24,5 l/min with the maximum pressure differential. According to the authors' experience, the valve is still feasible with that volume flow.

Table 1. Comparison of planned PNM-coded and PCM-coded digital hydraulic valve packages

	
<p><b>PNM design</b></p> <p><b>Manifold:</b> Laminated</p> <p><b>Valves:</b> 128 x IHA prototype</p> <p><b>Mounting:</b> CETOP 3</p> <p><b>Dimensions(mm):</b> 272x49x102*</p> <p><b>Weight:</b> 8,5kg</p> <p><b>Series:</b> 1,25 l/min * [1 1 1 ... 1] @ 3,5 MPa</p> <p><b>Q<sub>N</sub>:</b> 40 l/min @ 3,5MPa</p> <p><b>Theoretical resolution:</b> 32</p> <p><b>p<sub>max</sub>:</b> 21 MPa</p> <p><b>Δp<sub>max</sub>:</b> 21 MPa</p> <p><b>Response time:</b> 2–6 ms</p>	<p><b>PCM design</b></p> <p><b>Manifold:</b> Machined</p> <p><b>Valves:</b> 24 x Bosch Rexroth KSDEU</p> <p><b>Mounting:</b> Custom piping</p> <p><b>Dimensions(mm):</b> 310x290x80*</p> <p><b>Weight:</b> 31kg</p> <p><b>Series:</b> 1,25 l/min * [1 2 4 8 8 8] @ 3,5 MPa</p> <p><b>Q<sub>N</sub>:</b> 39 l/min @ 3,5MPa</p> <p><b>Theoretical resolution:</b> 31</p> <p><b>p<sub>max</sub>:</b> 50 MPa</p> <p><b>Δp<sub>max</sub>:</b> 21 MPa</p> <p><b>Response time:</b> 10–15 ms</p>

\*Without electric connectors

## 8. CONCLUSIONS

In this paper, suitability of the lamination technology for manufacturing the manifold for PNM-coded digital hydraulic valve package is studied. Laminated test block was produced and pressure test were carried out. Based on FEM-analysis, laminated structure seems to have corresponding pressure capability with similar block without brazed joints. Strength of the joint was found to be higher than yield strength of the base metal, so in a design procedure where target is to maintain under yield strength, same design rules that are used with solid manifolds can be utilized. However geometrical aspects, like sharp corners which are natural to laminated structures, must be carefully inspected. Based on the special features of the lamination technology, a CETOP 3-mountable hydraulic manifold for 4x32 bit PNM-coded digital hydraulic valve was designed and compared to the PCM-coded digital hydraulic valve.

The studied technology:

- is available on the market
- is suitable for high pressures, because the well brazed joint can be as strong as the pure base material
- increases the packing density of the individual on/off-valves in the digital hydraulic valve package
- does not necessarily require any plugs or auxiliary flow channels.
- possible for mass production (cf. heat exchangers)
- requires good knowledge on materials science and manufacturing engineering as well as skills to design sophisticated hydraulic manifolds.

According to the results of the study presented in this paper, it seems to be possible to produce compact PNM-coded valve-package which is suitable for the CETOP 3-subplate. This may require a new generation of miniature valve prototypes.

## 9. ACKNOWLEDGEMENTS

This research is funded by the DiHy-project which is part of EFFIMA-program of the Finnish Metals and Engineering Competence Cluster, FIMECC Ltd.

The authors are indebted to Antti Piensoho from Sten Oy and Thomas Hartmann from Vacuumschmelze.

## 10. REFERENCES

- [1] Linjama M, Vilenius M. Digital Hydraulics - Towards Perfect Valve Technology. In: Proceedings of the Tenth Scandinavian International Conference on Fluid Power; 2007; Tampere, Finland.
- [2] Wautelet M. Scaling laws in the Macro- Micro- and Nanoworlds. European Journal of Physics. 2001 601-611.
- [3] Linjama M. Fundamentals of Digital Microhydraulics. In: 8th International Fluid Power Conference; 2012; Dresden, Germany.
- [4] Uusitalo JP, Lauttamus T, Linjama M, Söderlund L, Vilenius M, Kettunen L. Miniaturized Bistable Seat Valve. In: Proceedings of The Tenth Scandinavian International Conference on Fluid Power; 2007; Tampere, Finland.
- [5] Uusitalo JP, Söderlund L, Kettunen L, Ahola V, Linjama M. Novel Bistable Hammer Valve for Digital Hydraulics. In: Proceedings of The Second Workshop on Digital Fluid Power; 2009; Linz, Austria. p. 33-48.

- [6] Karvonen M, Juhola M, Ahola V, Söderlund L, Linjama M. A Miniature Needle Valve. In: Proceedings of The Third Workshop on Digital Fluid Power; 2010; Tampere, Finland. p. 61-78.
- [7] Courson RB, inventor. Hydraulic manifold system. 1971 June 30. US 3,763,889.
- [8] Krause B, inventor. Laminated block with segment sheets connected by high-temperature soldering. 2005 April 20. US 2005/0244669 A1.
- [9] Lasaar R, Stoll A. New Innovative Components for Energy Efficient Working Hydraulics in Mobile Machines. In: Conference Proceedings of The 7.th International Conference on Fluid Power; 2010; Aachen, Germany. p. 37-52.
- [10] Hydraulics & Pneumatics Corporate. The center of it all. 2006.
- [11] Schwartz M,M. Welding, Brazing and Soldering. In: Olson DL, Siewert TA, Liu S, Edwards GR, editors. ASM Handbook. Vol 6. ASM International; 1993. p. 114-125.
- [12] Brandon D, Kaplan WD. Joining processes: An introduction. John Wiley & Sons Ltd.; 1997.
- [13] Andersson R, Holm T, Wiberg S, Åstrom A. [Internet]. [cited 2012 August 15]. Available from:  
[http://heattreatment.linde.com/International/Web/LG/HT/like351ght.nsf/repositorybyalias/wp\\_brzg\\_9/\\$file/9.pdf](http://heattreatment.linde.com/International/Web/LG/HT/like351ght.nsf/repositorybyalias/wp_brzg_9/$file/9.pdf).
- [14] Luvata. CuproBraze Handbook. 9th ed. Luvata; 2009.
- [15] Kowalewski J, Szczurek J. Issues in vacuum brazing. 2006;6(3).
- [16] Rabinkin A. Brazing with amorphous foil preforms. 2001;159(6).
- [17] ISO 4401. 2005.
- [18] Paloniitty M. Lamino-intimenetelmän soveltaminen digitaalihuhtiliikan venttiililohkoihin. Tampere 2012.
- [19] Sakamoto A, Fujiwara C, Hattori T, Sakai S. Optimizing processing variables in high temperature brazing with nickel-based filler metals. 1989;68(3).

## OPTIMISATION OF WORKING AREAS IN DISCRETE HYDRAULIC POWER TAKE OFF-SYSTEM FOR WAVE ENERGY CONVERTERS

Ph.D. Fellow Anders H. Hansen, Ph.D. Fellow Rico H. Hansen,  
Asc. Prof. Henrik C. Pedersen  
Aalborg University  
Department of Energy Technology  
Pontoppidanstræde 101, 9220 Aalborg East  
E-mail: ahh@et.aau.dk, rhh@et.aau.dk, hcp@et.aau.dk

### ABSTRACT

Fluid power is the leading technology in Power Take Off(PTO) systems in Wave Energy Converters(WEC's), due to the capability of generating high force at low velocity. However, as hydraulic force controlling system may suffer from large energy losses the efficiency of the hydraulic PTO systems may be a limiting factor for wave energy. Therefore, a secondary controlled force system has been proposed as PTO element for WEC's. This paper investigates the configuration of a multi-chamber cylinder utilising two common pressure lines. By usage of model based optimisation an optimal number and size of working areas is proposed. This area encoding strategy is investigated and compared to two standard binary encodings, finding that the optimised area coding yields significantly higher energy output.

**KEYWORDS:** Digital hydraulics, Discrete force system, Wave Energy, Power Take Off system

### 1. INTRODUCTION

Wave energy converters are designed to harvest energy from ocean waves in terms of mechanical movement which is converted to electricity. Numerous concepts for exploiting ocean waves as an energy source are under development. In [1] Drew et al. gives a review of wave energy converter concepts, including various topologies, as e.g. oscillation water column, attenuation, point absorbers etc. However, so far none of the concepts have proven commercially feasible. For wave energy converters to get a commercial breakthrough they need to prove a higher reliability and lower cost of energy, such the price of energy, [€/kWh], will match the price of energy from e.g. wind turbines.

The Wavestar WEC is a multiple point absorber type, with 20 floats moving with the ocean waves relative to a bottom fixed structure, see figure 1 [2].

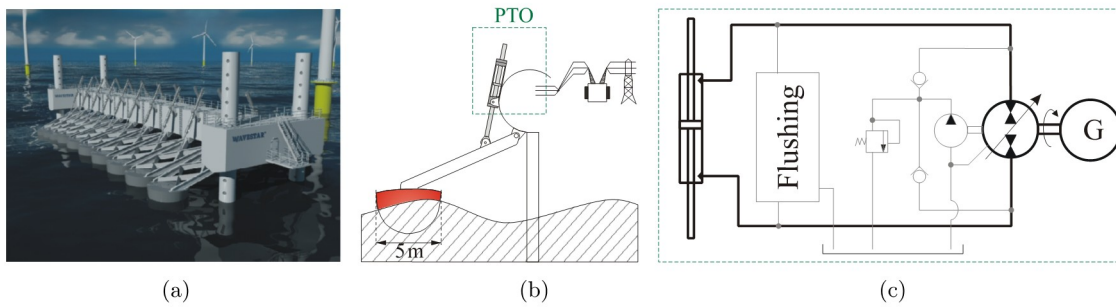


Figure 1. a) Sketch of the Wavestar WEC, b) general power absorption principle and c) overview of current PTO hydraulic system

With the Wavestar WEC, energy is harvested as a force is applied to oppose the natural movement of the float due to the ocean waves. The PTO force is applied by a hydraulic cylinder, which in this system mainly works as a pumping unit. The hydraulic energy harvested by the cylinder is converted to electricity by a hydraulic motor powering a generator. In [3] the current PTO-system, cf. figure 1(c), of the Wavestar WEC is modelled for efficiency analysis, showing that the current PTO-system utilising direct motor-cylinder force control suffers from poor and insufficient efficiency, as the hydraulic motor/pump most of the time is operating far outside the optimal region.

In [4] a discrete hydraulic force system is proposed as an element for a novel PTO-system for the Wavestar WEC. Two systems were modelled; one using four pressure lines and a symmetric cylinder and one utilising two pressure lines and two differential cylinders. In both systems each cylinder chamber may be connected to each of the common pressure lines to generate various force combinations. Both systems benefit from 16 discrete force combinations. As shown in [5] the Pelamis WEC utilises two differential cylinders connected to two common pressure lines to generate a similar type of discrete PTO torque.

One reason for using a discrete force system is to avoid the throttle loss induced in a traditional valve controlled force systems. By proper design of a discrete force system the throttle loss across the control valves may be minimised. More importantly a discrete force system benefits from having common pressure lines in contradiction to a direct cylinder pump/motor force system as used currently in the Wavestar WEC test machine. Hereby power smoothing between the 20 floats may be obtained. In [6] the authors investigated a discrete force system utilising a symmetric cylinder and a fixed number of common pressure lines, where it was shown, under the assumptions made, how much the power production increases when increasing the number of pressure lines. The current work focus on a system utilising a secondary control system like the one proposed in [7], hence a system with two common pressure lines and a multi-chamber cylinder. A sketch of such a system is given in figure 2.

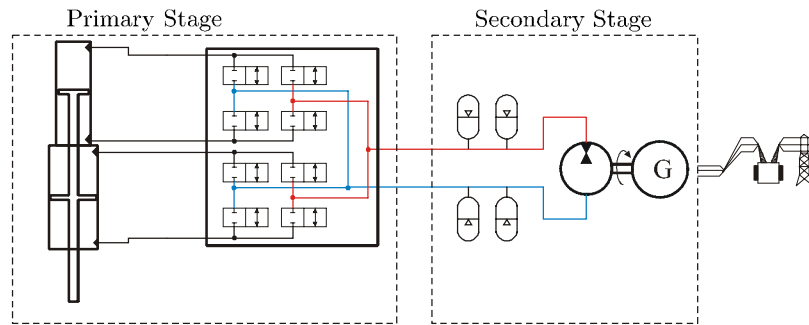


Figure 2. Schematic of discrete PTO system.

The aim for this work is to discuss the optimal configuration of the multi-chamber cylinder in terms of the number and sizes of the working areas. Here the optimal system will be the one leading to the highest energy production. To accomplish this, the paper initiates with a description of the system configurations tested in section 2. Section 3 gives an overview of the simulation model utilised in the optimisation. The simulation results are given in section 4 followed by a discussion in section 5.

## 2. SYSTEM CONFIGURATION

The configuration of the discrete force system covers how the working areas and pressure lines are outlined. Hence, how the multi-chamber cylinder is designed along with the pressure levels of the common pressure lines. In this work three area coding strategies are discussed, including two binary strategies and one, where the areas are optimised based on the operating conditions for the WEC. The system is here restricted to two pressure lines with 20bar and 250bar respectively. The physical construction of the multi-chamber cylinders is beyond the scope of this work; however, some of focus points for the cylinder constructors may be to design a multi-camber cylinder with common centreline for the forces of the various working areas and to keep friction force low. A presentation of the various area coding strategies is given next.

### 2.1. Area coding; Binary 1

The first area coding strategy has one working area applying force in positive direction,  $A_1$ . The areas in the negative direction are binary half's of the area in positive direction. Hence, each time an extra area is introduced its size is half of the smallest in the negative direction. This is illustrated in figure 3. The basic area  $A_1$  is similar to the area found on the symmetric cylinder used by Wavestar WEC today and corresponds to a  $190 \text{ cm}^2$  cylinder, generating a PTO torque of 1MNm around the float arm hinge. An overview of the first two systems using area coding Binary 1 are seen in figure 3



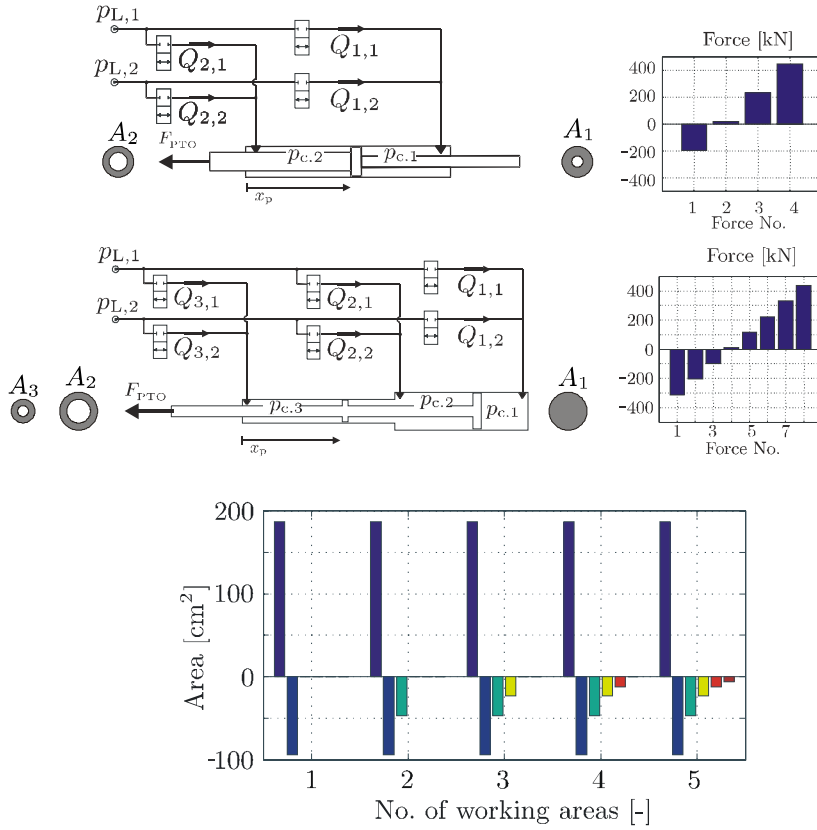


Figure 3. Overview of the discrete hydraulic force system and the force combinations when utilising area coding Binary 1. Each bar in the right plot illustrates a working area.

From the force illustrations in figure 3 it is seen that the maximum negative force is much smaller than the maximum positive force for the first and second system configuration. However, the difference is decreasing as the numbers of working areas are increased. Hence the force combinations will be more equally distributed around zero as the number of working areas are increasing.

## 2.2. Area coding; Binary 2

The second coding strategy follows the area distribution utilized by Linjama et. al in [7]. This encoding is describe as; the first area is in positive direction, the second area is in negative direction and is half in size of the first, the third area is in positive direction and is half in size of the second, the fourth area is in negative direction and is half in size of the third. This is illustrated in figure 4, together with an overview of the third system using area coding Binary 2.

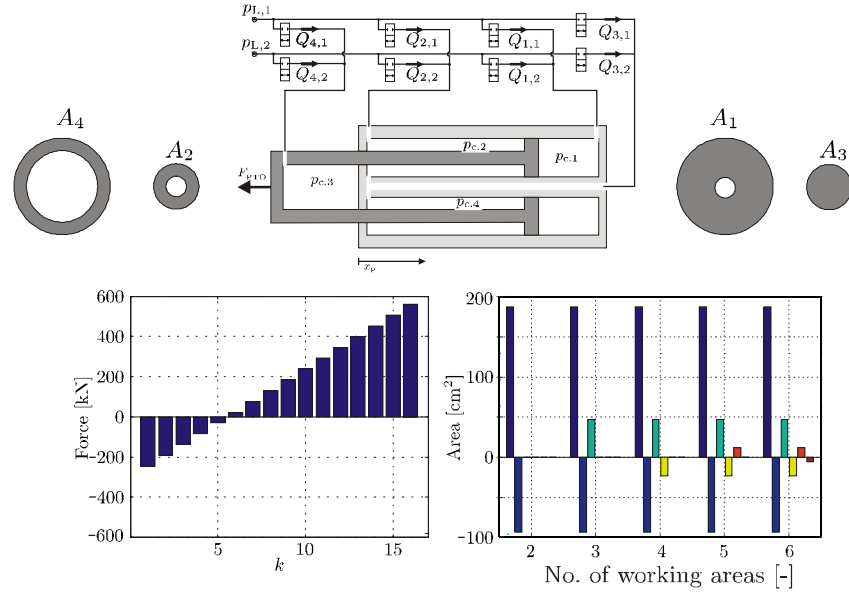


Figure 4. Overview of the discrete hydraulic force system utilising area coding Binary 2 and the force combination.

When using this area encoding, the force combination will be unevenly distributed around zero force. Hence, the system has high positive and low negative force capabilities. Note however, that the differences in force between adjacent forces are equal.

### 2.3. Area coding 3 – Optimised

The third encoding strategy is based on a model based optimisation, i.e. the area coding for the system does not follow a predefined encoding layout but is fitted to the conditions in which the system is used. Hence, the third area in system 2 and 3 do not have to be equal as were the case for the binary coding strategies. The areas are optimised such that the power output to the common pressure line is maximised. During the optimisation constraints are implemented to bound the areas. The constraints ensure that the force is zero when all working areas are applied same pressure and that the size of the areas follows the numbering;

$$A_{p,i} \leq A_{p,i+1} \quad (2)$$

Hence, the sum of all areas working in positive direction is equal to the sum of all area working in negative direction. Furthermore the maximum area of a single working area is constrained by:

$$0 \leq A_{p,i} \leq A_{p,max} \quad (3)$$

### 3. MODELLING

The simulation model utilised for the model based optimisation is constructed in Matlab Simulink. The model includes wave generation, wave float interaction, float dynamics and a hydraulic model of the primary stage of PTO-system. The wave data utilised represents waves similar to typical data from the Wavestar test facility. An overview of the simulation model is given in figure 5

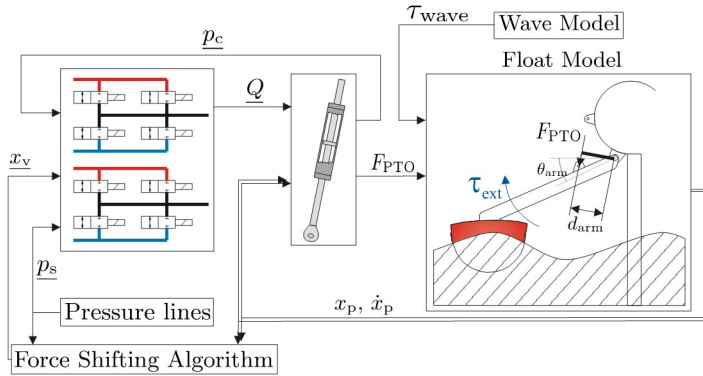


Figure 5. Overview of simulation model

#### 3.1. Wave Model

The wave model illustrated in figure 6 takes a wave spectrum characterised by a wave height and a wave period and gives out a torque around the float hinge. However, in an intermediate state an actual wave height,  $\eta_w$ , is given.

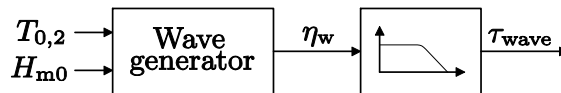


Figure 6. Illustration of wave model.

The filter converting an irregular wave time series,  $\eta_w(t)$ , to an applied torque time series  $\tau_w(t)$  is based on float dimension and shape and is constructed using WAMIT and linear wave theory. An elaboration on the derivation is given in [8]. The filter gain plot resembles a first order filter. In the current paper three sea states are utilised, represented by the density spectrum's shown to the right in figure 7.

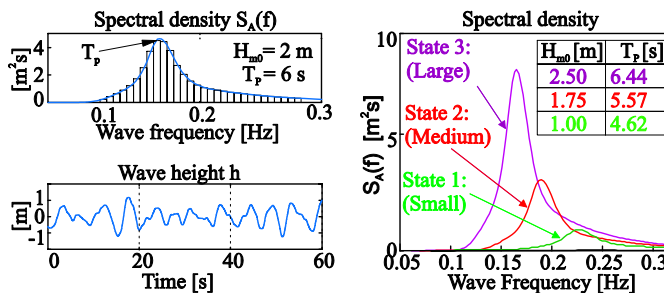


Figure 7. To the right wave data for the utilised sea states are given. Upper left an example of a density spectrum is given for the time series wave shown in the lower left part.

### 3.2. Float Model

The float model utilised is described in [8], however a brief introduction is provided next. The float dynamics may be modelled as shown in figure 8. The wave and PTO torque are inputs and the float arm angle and angular velocity are outputs. The model is seen to be similar to a second order ordinary differential equation describing a mass-spring-damper system. However, due to the nature of partly submerged bodies the damping term becomes frequency dependent. i.e., for the model employed the damping term  $K_r(s)$  is a fifth order transfer function.

For the float model the spring term,  $k_{res}$ , is associated with gravity and buoyancy (Archimedes force), the damping term,  $K_r(s)$ , represents the power dissipation due to wave radiation by float oscillation. The inertia term  $\frac{1}{J_{arm} + J_{add,\infty}}$  gives the acceleration of the float based on a given torque. Here the arm inertia,  $J_{arm}$ , is the inertia of the arm and float and the added inertia,  $J_{add,\infty}$ , is a term introduced due to the nature of partly submerged bodies implying that the surrounding water is accelerated as well. The latter is frequency dependent, but may be approximated by a constant term.

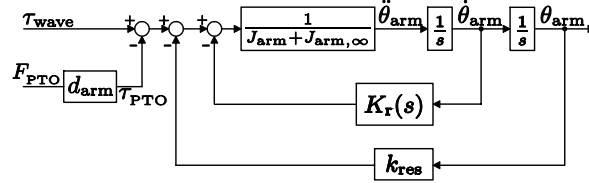


Figure 8. Block diagram of the float model.

### 3.3. Hydraulic Model

A generic model of the discrete hydraulic force system is utilised. The model is constructed where the number of working areas are easily changed; hence the model may represent various system designs. The number of working areas and pressure lines are in the following denoted by  $n$  and  $m$  respectively, whereas  $i$  and  $j$  are used as counters for summation over the working chambers and the pressure lines respectively.

#### 3.3.1. PTO Force

The PTO force generated by the PTO cylinder is defined as the combined force generated by the fluid pressure in the cylinder chambers.

$$F_{PTO}(t) = \sum_{i=1}^n D_i A_{p,i} p_{c,i}(t) \quad (4)$$

Here  $D_i$  indicates the direction of the force generated by the fluid pressure in the  $i$ 'th chamber, by taking the value of either 1 or -1. In this simulation study no friction force has been included for the cylinder.

### 3.3.2. Flow

The flow through the control valves are modelled with the orifice equation, each flow through the valves are modelled positive into the cylinder chambers;

$$Q_{i,j}(t) = k_{v,i} \bar{x}_{v,i,j} \sqrt{|p_{l,j}(t) - p_{c,i}(t)|} \text{sign}(p_{l,j}(t) - p_{c,i}(t)) \quad (5)$$

Where  $k_{v,i}$  is the valve coefficient given as:

$$k_{v,i} = \frac{A_{p,i} \dot{x}_{p,nom}}{\sqrt{p_{nom}}} \quad (6)$$

With a nominal piston velocity of 0.5m/s and a pressure drop of 5bar.  $\bar{x}_{v,i,j}$  is the normalised spool position for the valve connecting the  $i$ 'th cylinder chamber and the  $j$ 'th pressure line.  $p_{l,j}$  and  $p_{c,i}$  are the pressure in the  $j$ 'th line and the  $i$ 'th cylinder chamber respectively. Hence the flow into the  $i$ 'th chamber is defined as:

$$Q_{c,i}(t) = \sum_{j=1}^m Q_{i,j}(t) \quad (7)$$

Whereas the flow out of the  $j$ 'th pressure line is defined as:

$$Q_{l,j}(t) = \sum_{i=1}^n Q_{i,j}(t) \quad (8)$$

### 3.3.3. Pressure Dynamics

The pressure dynamics in each cylinder chamber is modelled with the flow continuity equation, which for the  $i$ 'th cylinder chamber yield;

$$\dot{p}_{c,i}(t) = \frac{\beta(p_{c,i}(t))}{V_i(t)} (Q_{c,i}(t) - \dot{x}_p(t) A_{p,i}) \quad (10)$$

The pressure in the common pressure lines are assumed constant.

### 3.3.4. Bulk Modulus

The bulk modulus model utilised incorporates pressure dependency and air content in the oil, assuming adiabatic behaviour of the air:

$$\beta(p) = \frac{1}{\frac{1}{\beta_{oil}} + \frac{\varepsilon_{air}(p)}{\beta_{air}}}, \quad \varepsilon_{air}(p) = \left( \frac{p_0 \varepsilon_{air,0}}{p} \right)^{\frac{1}{\kappa}} \quad (11)$$

Where  $\varepsilon_{air,0}$  is the air content at atmospheric pressure  $p_0$ . The volumetric air content is set to 1% at atmospheric pressure, and the adiabatic air constant is  $\kappa = 1.4$ .

### 3.3.5. Valve Dynamics

The On/Off valves are modelled with a rate limit such that:

$$\dot{x}_v = \begin{cases} \dot{x}_{v,\max} & \text{for } x_v < x_{v,\text{ref}} \\ 0 & \text{for } x_v = x_{v,\text{ref}} \\ -\dot{x}_{v,\max} & \text{for } x_v > x_{v,\text{ref}} \end{cases} \quad (12)$$

Where

$$\dot{x}_{v,\max} = \frac{1}{t_{\text{valve}}} \quad (13)$$

Here  $t_{\text{valve}}$  is the valve opening and closing time which are both set to 16[ms], as this is an obtainable valve speed and [9] showed that increasing the valve speed further do not given significant lower shifting losses.

## 3.4. Energy

The purpose of the wave energy converter is to produce electric energy to the grid. Meanwhile this work is also concerned with the intermediate stages, to be able to maximize the total energy output. For the discrete system considered here the considered energy stages are; energy contents in the incoming waves, the energy harvested by the PTO cylinder, the energy supplied to the common pressure line and the electric energy output. With an objective of investigating the primary stage of the PTO system the energy stages that are treated are the harvested energy and the energy output to the common pressure lines. A definition of these energy stages are given next.

### 3.4.1. Harvested energy

The energy harvested is defined as the energy which is extracted by the cylinder from the ocean waves. The energy harvested is here defined as;

$$E_{\text{har}}(t_{\text{end}}) = \int_0^{t_{\text{end}}} F_{\text{PTO}}(t) \dot{x}_p(t) dt \quad (14)$$

### 3.4.2. Output energy

The energy flow to the common pressure lines are found as;

$$E_{\text{out}}(t_{\text{end}}) = - \int_0^{t_{\text{end}}} \sum_{i=1}^n \sum_{j=1}^m [Q_{i,j}(t) p_{l,j}(t)] dt \quad (15)$$

This calculation gives the net energy supplied to the common pressure lines. Hence the energy input to the chambers when oil flows in is withdrawn from the energy output. The minus sign is due to the sign convention used for the flow.

### 3.4.3. Efficiency of primary stage

In wave energy efficiency is used in various ways. The current paper utilises the efficiency of the primary PTO stage which is define as the ratio between the mean output power to the common pressure line and the mean power harvested by the PTO cylinder.

$$\eta = \frac{P_{\text{out}}}{P_{\text{har}}} \quad (16)$$

### 3.5. Control of primary PTO stage

The control of the primary PTO stage consists of controlling the valve manifold. The control is based on the float arm velocity and the float arm position. A force reference is continuously calculated based on a reactive control scheme as given in Eq. (17)

$$F_{\text{PTO.ref}}(t) = \frac{1}{d_{\text{arm}}} (B_{\text{PTO}} \dot{\theta}_{\text{arm}} + K_{\text{PTO}} \theta_{\text{arm}}) \quad (17)$$

The discrete force combination applied by the valve manifold is decided by a Force Shifting Algorithm choosing the force leading to the highest power output to the common pressure lines. An elaboration on the FSA's is given in [4] and [6].

## 4. SIMULATION RESULTS

The mean harvested power and the mean power delivered to the common pressure lines are plotted in figure 9 for the three sea states and the three area encoding strategies, Binary 1, Binary 2 and Optimised. Furthermore the efficiencies of the primary PTO stage are given. By conducting the optimisation analysis for each sea state it can be investigated how the wave condition effects the optimal system configuration by detecting the change. Additionally the maximum obtainable performance in each sea state is found and can be utilised as a baseline.

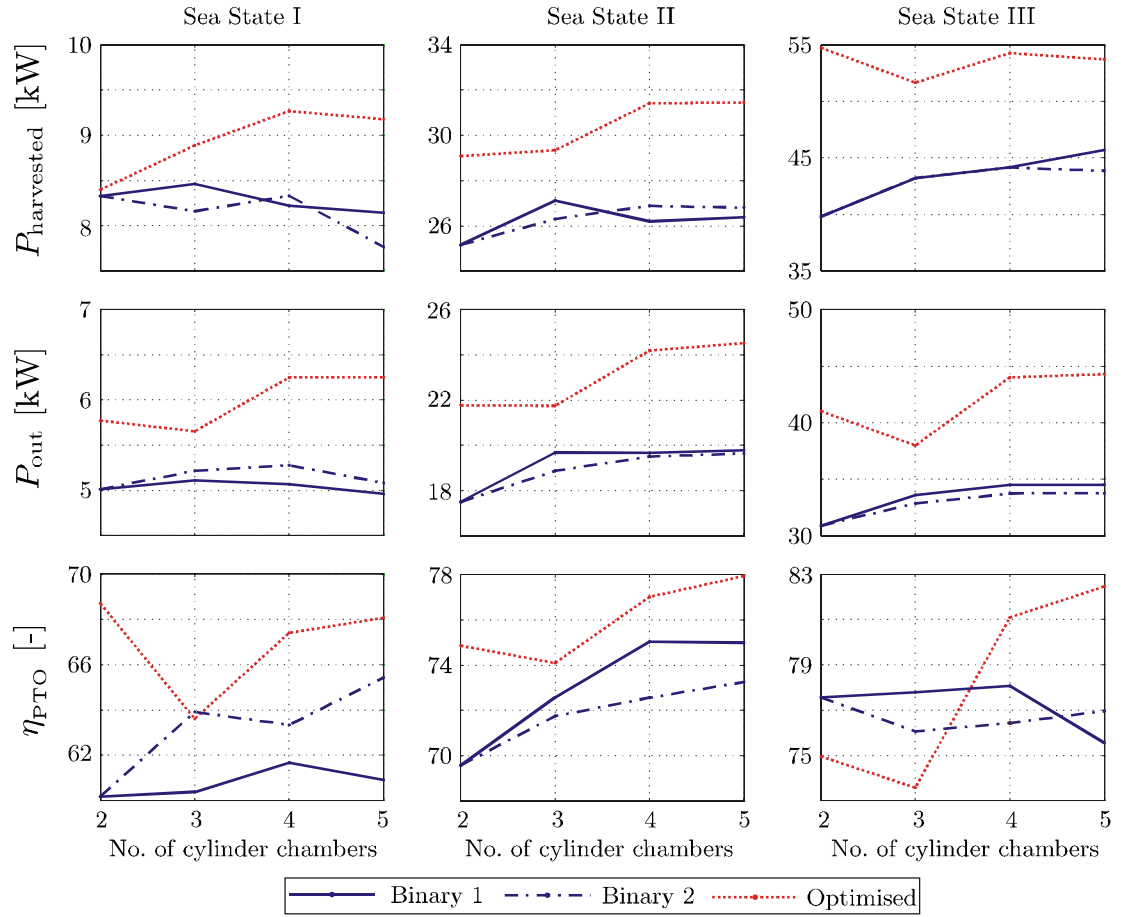


Figure 9. Simulation results, each column represents a sea state. The upper row is the harvested power, middle row is the output power to the pressure line, and lower row is the efficiency of the primary PTO stage.

The numbers of valve actuations during usage of the various system configurations are given in table 1.

Table 1. Number of valve actuations pr. second for the various configurations and sea states

		Sea State		
Configuration	n	I	II	III
Binary 1	2	1.37	2.22	2.47
Binary 2	2	1.37	2.22	2.47
Optimised	2	1.23	1.11	1.49
Binary 1	3	1.78	3.08	3.53
Binary 2	3	1.58	2.88	3.87
Optimised	3	1.45	1.94	3.18
Binary 1	4	2.15	2.97	4.52
Binary 2	4	2.07	3.48	4.53
Optimised	4	2.33	2.55	3.13
Binary 1	5	2.60	3.64	7.16
Binary 2	5	2.17	4.00	5.19
Optimised	5	2.50	3.00	3.03



The sizes of the working areas are unchanged for the binary strategies whereas the working areas for the optimised strategy are changed accordingly to the sea condition. In figure 10 the working areas for the optimised configurations are given. The binary areas were given in figure 3 and 4.

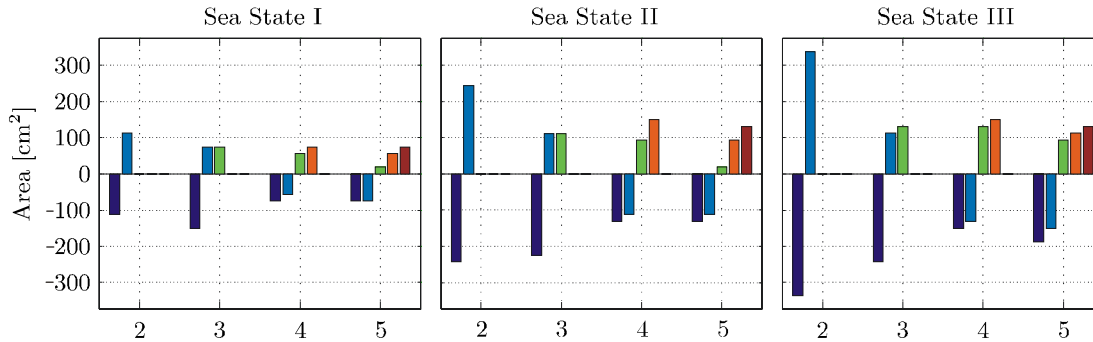


Figure 10. Optimised areas for the three sea states.

## 5. DISCUSSION

From the simulation results it is seen that the optimised area encoding strategy is the one leading to the highest harvested power and power output for all sea states. The higher harvested power may be due to the obtainable force combinations been optimised for the sea conditions. Besides the higher harvested power it is seen that the efficiency is higher and that the number of valve actuations are lower for the optimised area encoding compared to the two binary encoding strategies in most situations. Hence the optimised system configuration leads to fewer force shifts and thereby often lower shifting losses. Hence, it seems that the optimised area distributions will perform better than the binary. Over all the optimised configuration with four working areas may be preferred as increasing to five do not imply significant improvements.

However it should be noted that the system configurations for the binary strategies are unchanged over the sea states contrary to the optimised strategy. Hence, for a more realistic comparison a single optimised area distribution should be chosen for all sea states, as the multi-chamber cylinder is not changed for various sea conditions. Future work may therefore include calculating the area encoding leading to the highest power production as the time distribution of the various sea states are accounted for. This production value may hereafter be compared to a similar value for the binary encoding strategies. This time distribution of the sea conditions is however highly dependent on the specific site for installation of the wave energy converter. Furthermore it is seen that the change in size of working area between sea states is greater for a low number of working areas. Hence, one may argue that a configuration with more than three working areas performs better in all sea states than one with three or less.

Additionally neither valve actuation energy nor the friction loss in the cylinder is accounted for. One may argue that the cylinder friction will increase as the number of working areas increases, due to expected larger contact surfaces when a larger number of working areas are introduced. Hence, an increase in valve actuation energy and friction loss may be experienced when increasing the number of working areas.

## REFERENCES

- [1] B. Drew, A. Plummer, and M.N. Sahinkaya. A review of wave energy converter technology. *Proceedings of the Institution of Mechanical Engineers, Part A: Journal of Power and Energy*, 223, 8:pp. 887–902, 2009.
- [2] Morten M. Kramer, Laurent Marquis, and Peter Frigraad. Performance evaluation of the wavestar prototype. In *The 9th European Wave and Tidal Energy Conference : EWTEC*, 2011.
- [3] Rico H. Hansen, Torben O. Andersen, and Henrik C. Pedersen. Model based design of efficient power take-off systems for wave energy converters. In *Proc. The Twelfth Scandinavian International Conference on Fluid Power, SICFP'11*, Tampere, Finland, May 18-20 2011
- [4] Rico H. Hansen, Torben O. Andersen, and Henrik C. Pedersen. Analysis of discrete pressure level systems for wave energy converters. In *International Conference On Fluid Power And Mechatronics*, 2011.
- [5] Ross Henderson. Design, simulation, and testing of a novel hydraulic power take-off system for the pelamis wave energy converter. *Renewable Energy*, 31(2):271 – 283, 2006. ISSN 0960-1481.
- [6] Hansen, A. Hedegaard, Hansen, R. Hjerm & Pedersen, H.C. Optimal number of pressure lines in a discrete hydraulic force system for the PTO-system in wave energy converters. *Proceedings of the 7th FPNI PhD Symposium on Fluid Power*, 2012
- [7] Linjama, M.; Vihtanen, H.-P.; Sipola, A. & Vilenius, M. Secondary controlled multi-chamber hydraulic cylinder. *The 11th Scandinavian International Conference on Fluid Power, SICFP'09*, June 2-4, 2009, Linköping, Sweden, 2009
- [8] Rico H. Hansen and Morten M. Kramer. Modelling and control of the wavestar prototype. In *EWTEC 2011*, 2011.
- [9] Rico H. Hansen, Torben O. Andersen, and Henrik C. Pedersen. Determining Required Valve Performance for Discrete Control of PTO Cylinders for Wave Energy. In *Proceeding of the Fluid Power and Motion Control (FPMC'12)*. Bath University



## ENERGY RECOVERY USING A DIGITAL PISTON-TYPE ACCUMULATOR

C. Stauch\*, F. Schulz\*\*, P. Bruck\*\*, and J. Rudolph\*\*\*

\*\*HYDAC Fluidtechnik GmbH, Sulzbach, Germany

\*\*\*Chair of Systems Theory and Control Engineering,  
Saarland University, Saarbrücken, Germany,

\*Zentrum für Mechatronik und Automatisierungstechnik ZeMA gGmbH,  
Gewerbepark Eschberger Weg,  
66121 Saarbrücken, Germany

Phone +49 681 8578745

E-mail : christian.stauch@mechatronikzentrum.de

### ABSTRACT

In numerous technical applications, new challenges for energy storage and recovery arise from efficiency requirements. The main advantage of hydropneumatic accumulators is a large power-to-weight ratio in comparison to other types of energy storage devices. However, they show an important drawback concerning applications with limited ranges of load pressure. This is due to the fact that the relation between the stored energy and the accumulator pressure is strongly nonlinear as a result of the nonlinear gas dynamics.

In the present contribution, a new type of gas charged multi-area accumulator is introduced. The accumulator considered utilizes digital fluid power principles by allowing for a stepwise variation of the actual pressurized area in the section facing the load connection. This is realized by means of several binary coded fluid chambers in parallel, connected to a switching valve manifold. Accordingly, it is more suitable for energy storage in applications with narrow ranges of load pressure variations than conventional accumulators. An approach for system dimensioning as well as actuation is discussed. Finally, an exemplary simulation study involving a simple lift system with recovery of the potential energy is presented.

**KEYWORDS:** hydropneumatic piston-type accumulator, energy recovery, energy efficiency, digital fluid power

### 1 INTRODUCTION

As Linjama stated in [1], one of the most important trends in digital fluid power is the development of energy efficient solutions. A survey of such digital fluid power solutions concerning energy efficiency was given by the same author in [2]. In many applications,

energy efficiency can be increased significantly by using the concepts of energy storage and recovery. Recent examples for digital solutions addressing energy recovery are a multi chamber cylinder capable of feeding back hydraulic energy to the power supply (cf. [3]) or the digital hydraulic power management system in [4].

Energy recovery is a matter of particular interest in mobile hydraulic systems. Moreover, in engineering mobile systems, special requirements concerning the available space as well as the overall weight have to be met. Most of the energy recovery systems embracing digital fluid power principles known to the authors are a combination of a digital hydraulic system and a conventional energy storage facility. In this contribution, an integrated digital hydropneumatic piston-type accumulator is presented. The oil side of the considered system is subdivided into separate annular fluid chambers each of which can be switched either to the load port or to the low pressure port. The generation of variable piston forces using fixed pressure levels and an adjustable pressure-active area are utilized in the digital hydraulic transformer presented by Bishop in [5] and in the linear digital hydraulic amplifier introduced by Scheidl et al. in [6]. Here, only the low pressure level is considered constant whereas the high pressure port is connected to the load and therefore, the related pressure is manipulated in a targeted manner.

This paper is organized as follows. In section 2, the energy recovery challenge and the digital hydropneumatic accumulator are introduced. A mathematical model of the system considered is derived in section 3. Section 4 involves the development of a rudimentary control strategy. In section 5, an approach for system dimensioning based on this control strategy is presented and compared to the dimensioning of conventional hydropneumatic accumulators. Some results of a numerical simulation study with the purpose of validating both the accumulator principle and the dimensioning approach are provided in section 6. Finally, section 7 gives a conclusion and an outlook for future work.

## 2 CHALLENGE AND CONCEPT

### 2.1 Energy recovery challenge

As mentioned before, especially in mobile hydraulic systems, there is an urgent need for energy efficiency which first and foremost can be met by finding solutions for energy storage and energy recovery. A simple example is given in terms of a mobile hydraulic lifting system such as a forklift or a high-bay warehouse system. In such applications, a significant amount of potential energy is released on a regular basis when a load mass or at least the curb weight of the mast is lowered. The storage and recovery of this potential energy could increase the efficiency of the lifting system substantially. The fact that such a lifting facility is generally realized in terms of linear hydraulic actuators as well as the high power-to-weight ratio of conventional hydropneumatic accumulators suggest the implementation of a hydraulic storage solution.

Notwithstanding these advantages, there is a major drawback resulting from the nonlinear dynamics of the accumulator gas. Whereas the lifting force, and with it the load pressure required to accelerate the load, deviate only slightly from their steady-state values, the

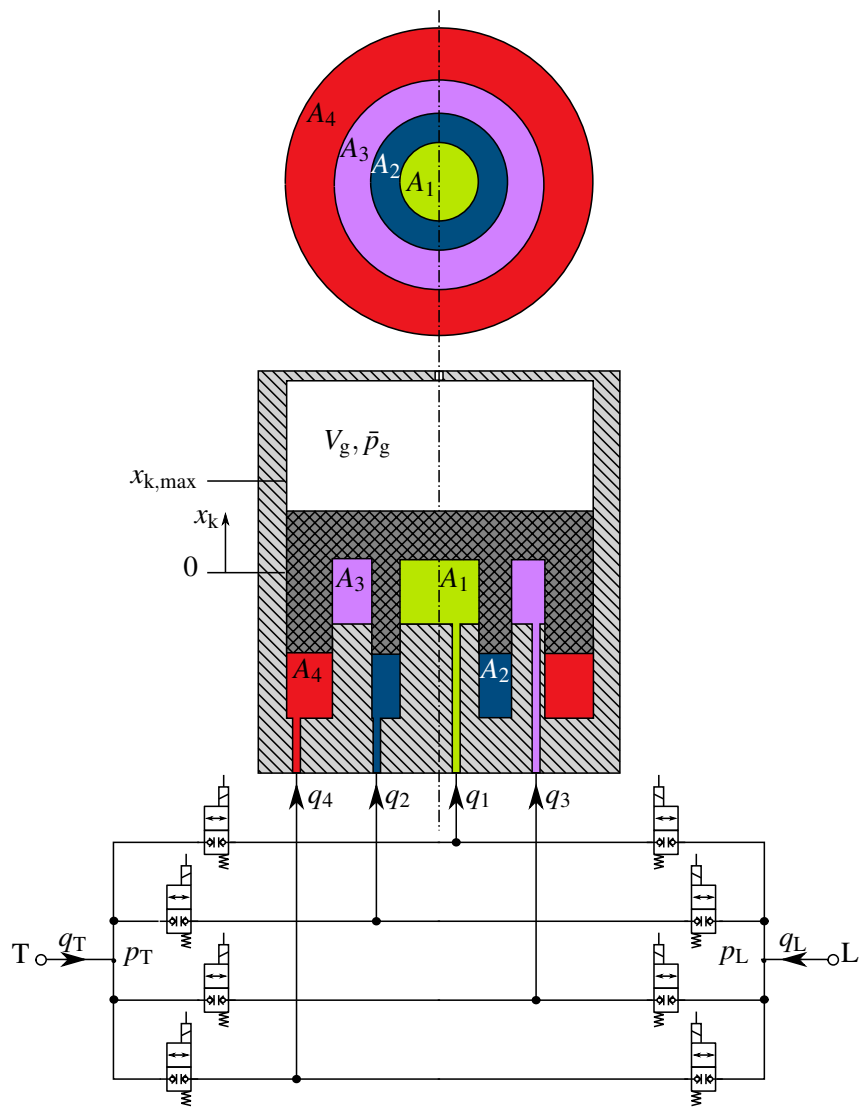


Figure 1. Sketch of the digital accumulator.

gas pressure of the accumulator largely depends on the stored energy. Consequently, the application of conventional hydropneumatic accumulators requires strong throttling of the flow between the accumulator and the load cylinder in order to adjust the pressures.

The main challenge, therefore, is to design a storage solution which operates within a narrow pressure range to minimize the throttling losses. Furthermore, it should also be capable of handling different sizes of load masses, i.e., the position of the operating pressure range should be variable. Above all, the system should account for the restrictions of mobile applications.

## 2.2 Digital accumulator concept

In order to meet the precedingly defined criteria, a novel multi-area piston-type accumulator is introduced. Instead of a single fluid chamber, it contains  $n$  separate concentric annular fluid chambers. Each of these chambers can be switched between a load port L and a low

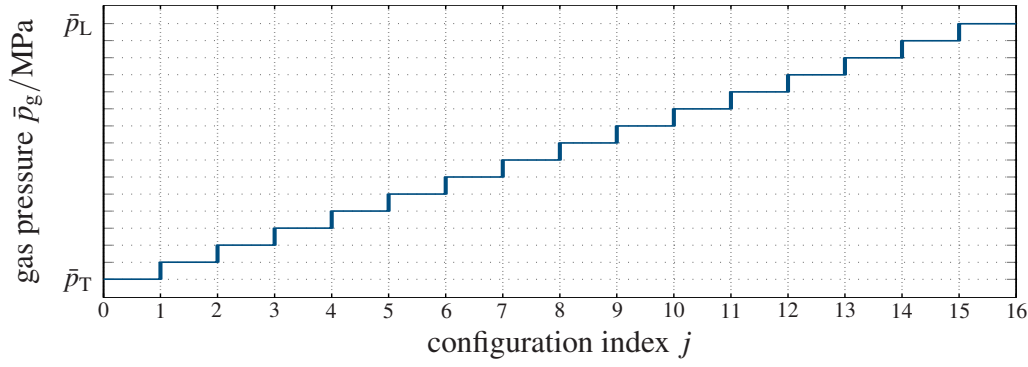


Figure 2. Steady-state gas pressure characteristic ( $n = 4$ ).

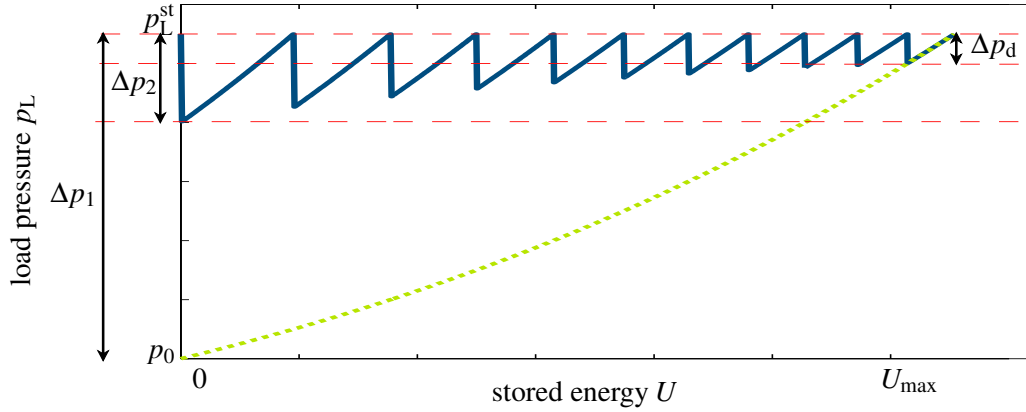


Figure 3. Load pressure of conventional (dashed) and digital (solid) accumulator.

pressure port T via an integrated valve manifold. Thus, it embraces digital fluid power principles by allowing for the quantized variation of the force applied to the piston from the oil side. A sketch of the considered accumulator system is provided in Fig. 1, where  $n = 4$ .

Given a binary coding of the oil side pressure-active areas

$$A_i = \frac{2^{n-i}}{2^n - 1} A_g = \frac{2^{n-i}}{l} A_g, \quad i \in \{1, \dots, n\} \quad (1)$$

there are  $l + 1 = 2^n$  possible configurations characterized by the index  $j$  and the corresponding area ratio

$$f_j = \frac{A_{L,j}}{A_g} = \frac{j}{l}, \quad j \in \{0, \dots, l\} \quad (2)$$

of the actual area  $A_{L,j}$  connected to the load port L and the gas side pressure-active area  $A_g$ . The theoretic characteristic line of the gas pressure for steady states is depicted in Fig. 2. Obviously, there are  $l$  steady-state levels of the gas pressure<sup>1</sup>  $\bar{p}_g$  distributed equidistantly between the load pressure  $\bar{p}_L$  and the low pressure level  $\bar{p}_T$ .

The main advantage of the digital accumulator is the capability of reducing the width of the pressure range at the load port. An exemplary comparison of the load pressures

<sup>1</sup>Since there has to be made a difference between gauge pressures and absolute pressures, the latter ones are denoted by overlined pressure symbols  $\bar{p}$ , whereas gauge pressures are denoted simply by  $p$ .

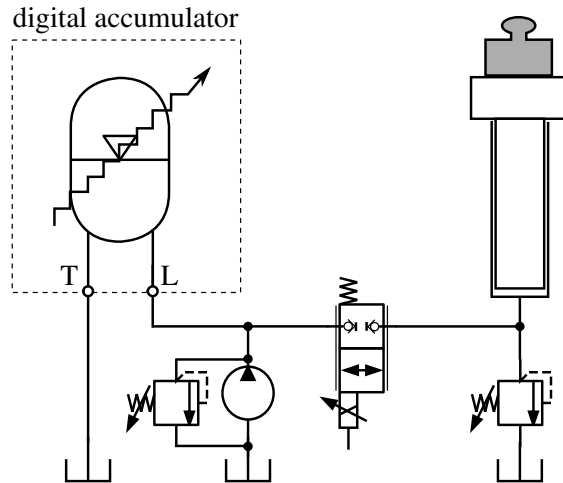


Figure 4. Exemplary circuit.

of the digital accumulator considered (solid line) and a conventional hydropneumatic accumulator (dotted line) dependent on the state of charge is illustrated in Fig. 3. Regarding the fully uncharged accumulator, the maximum difference  $\Delta p_1$  between the steady-state load pressure  $p_L^{st}$  and the actual pressure of the conventional accumulator can be reduced significantly to  $\Delta p_2$  by choosing an appropriate switching configuration of the digital accumulator. Since the pressure difference  $\Delta p_d$  is sufficient to cause a movement of the load, the surplus pressure difference is compensated for by throttling. Accordingly, the energy losses due to throttling can be reduced almost over the whole range of operation using the digital accumulator concept.

An exemplary circuit where the digital accumulator is used in a lifting system is depicted in Fig. 4. A throttling valve situated between the accumulator load port and the load cylinder can be used either for controlling the load velocity or to disconnect the load from the accumulator for charging. In the same manner, the integrated valve manifold can be used to disconnect the accumulator for pump driven operation.

### 3 MATHEMATICAL MODEL

The mathematical model of the system serves as a basis for the subsequent control design and the dimensioning approach. For the sake of brevity, this section provides only model equations which are most essential in the following sections.

#### 3.1 Gas dynamics

A comprehensive study on modeling hydropneumatic accumulators was given by Rott-häuser in [7]. In the following, the derivation of the differential equation governing the gas dynamics is briefly revisited. Starting from the first law of thermodynamics

$$dU - dQ + \bar{p}_g dV_g = 0, \quad (3)$$



the internal energy change is substituted by  $dU = m_g c_v dT_g$  where  $c_v$  is the specific heat at constant volume,  $m_g$  is the total mass of the accumulator gas, and  $T_g$  is the gas temperature. The absolute gas pressure is denoted by  $\bar{p}_g$ , the heat exchange by  $dQ$ , and the gas volume by  $V_g$ . Dividing the resulting equation by  $dt$  gives

$$m_g c_v \dot{T}_g - \dot{Q} + \bar{p}_g \dot{V}_g = 0. \quad (4)$$

The heat flow  $\dot{Q}$  across the wall of the vessel is modeled by means of an integral form of Fourier's law

$$\dot{Q} = \frac{T_{\text{env}} - T_g}{R_{\text{th}}}, \quad (5)$$

where  $T_{\text{env}}$  is the environmental temperature. The overall thermal resistance  $R_{\text{th}}$  depends on geometrical and physical system parameters. Introducing the thermal characteristic time  $\tau_{\text{th}} = R_{\text{th}} C_{\text{th}}$  as a product of the thermal resistance  $R_{\text{th}}$  and the heat capacity  $C_{\text{th}} = m_g c_v$ , equation (4) can be written as

$$\dot{T}_g + \frac{1}{\tau_{\text{th}}} (T_g - T_{\text{env}}) + \frac{\bar{p}_g \dot{V}_g}{C_{\text{th}}} = 0. \quad (6)$$

Additionally, there exists a thermal equation of state

$$S(\bar{p}_g, V_g, T_g) = 0 \quad (7)$$

which relates  $\bar{p}_g$ ,  $V_g$ , and  $T_g$ , the thermal variables of state. In the present context, only the state equation for ideal gases

$$S_{\text{ideal}}(\bar{p}_g, V_g, T_g) = \bar{p}_g V_g - m_g R_g T_g = 0 \quad (8)$$

is made use of, since it facilitates the system dimensioning. Nevertheless, in section 6, it is compared to a more sophisticated gas model using numerical simulations.

### 3.2 Accumulator piston

Considering the accumulator piston as a rigid body, the momentum balance can be written in terms of

$$m_k (\ddot{x}_k + c_g g) + d_{r,k} \dot{x}_k + p_g A_g - \sum_{i=1}^n p_i A_i = 0, \quad (9)$$

where  $x_k$  and  $m_k$  denote the position and the mass of the piston, respectively. The friction force is modeled as a viscous friction with coefficient  $d_{r,k}$ . The gravitational acceleration  $g$  is scaled by  $c_g$ , the cosine of the mounting angle. The driving force divides into a part resulting from the gas pressure  $p_g$  acting on the total piston area  $A_g$  and one resulting from the individual pressures  $p_i$  of the fluid chambers acting on the areas  $A_i$  in each case.

### 3.3 Load cylinder

The lifting facility is modeled as a simple plunger moving a load mass (cf. Fig. 4). Accordingly, the momentum balance reads

$$m_p (\ddot{x}_p + g) + d_{r,p} \dot{x}_p - p_p A_p = 0 \quad (10)$$

Here,  $m_p$  is the total mass of the lifting facility and the attached load,  $x_p$  is the lifting height, and  $d_{r,p}$  is the coefficient of the viscous friction. The load pressure  $p_p$  acts on the plunger area  $A_p$ .

## 4 SYSTEM ACTUATION

In this section, a simple control concept is presented which primarily serves as a basis for system dimensioning. Within this concept, there are three operating modes: lifting mode, lowering mode, and hold mode. The latter one is achieved simply by keeping the appropriate valves shut and, therefore, does not deserve further discussion. Both the lifting mode and the lowering mode are based on stepwise variation of the area ratio  $f_j$ . The main idea is to provide a load pressure level that is situated slightly above (in lifting mode) or below (in lowering mode) the steady-state load level. The resulting pressure difference causes the driving force which accelerates the load.

The design of the control concept involves defining when to switch between two configurations. It seems to be evident to define switching points dependent on a load pressure feedback since the objective is to set that latter pressure. Here, however, the switching points will be defined dependent on the gas pressure feedback as there is a simple steady-state relationship between those pressures. This choice facilitates the dimensioning approach presented in section 5.

### 4.1 Steady state gas pressure levels

First, the steady-state gas pressure levels are determined. From the momentum balance (10) of the load, the steady-state load pressure

$$p_L^{\text{st}} = p_p^{\text{st}} = \frac{m_p g}{A_p} \quad (11)$$

can be found. For each configuration  $j$ , the corresponding steady-state gas pressure level<sup>2</sup>  $p_{g,j}^{\text{st}}$  is calculated by replacing the chamber pressures  $p_{i,j}$  in (9) by the constant low pressure  $p_T$  and the steady-state value  $p_L^{\text{st}}$  of the load pressure, and zeroing the time derivatives:

$$p_{g,j}^{\text{st}} = \sum_{i=1}^n p_{i,j}^{\text{st}} \frac{A_i}{A_g} - \underbrace{\frac{m_k}{A_g} c_g g}_{\ll p_L^{\text{st}}} \approx f_j p_L^{\text{st}} + (1 - f_j) p_T. \quad (12)$$

The impact of the gravitational force due to the mass of the accumulator piston may be neglected here. Obviously, the steady-state gas pressure level  $p_{g,j}^{\text{st}}$  is bounded from above by the steady-state load pressure  $p_L^{\text{st}}$ . Simultaneously, it is bounded from below by the precharge pressure  $p_0$ . As a consequence of this lower boundary, not all configurations are usable. This is due to the fact that in configurations with small index  $j$ , the force applied to the piston from the oil side does not overcome the force due to the precharge pressure. Hence, the accumulator piston will rest at the lower end stop. Therefore, the index  $k$  of the smallest usable configuration is subject to the restriction

$$k > l \frac{p_0 - p_T}{p_L^{\text{st}} - p_T}, \quad k \in \mathbb{N}, \quad (13)$$

i.e., the choice of the precharge pressure has a significant impact on the number of usable configurations.

---

<sup>2</sup>Steady state pressure levels are denoted by a superscript index "st".

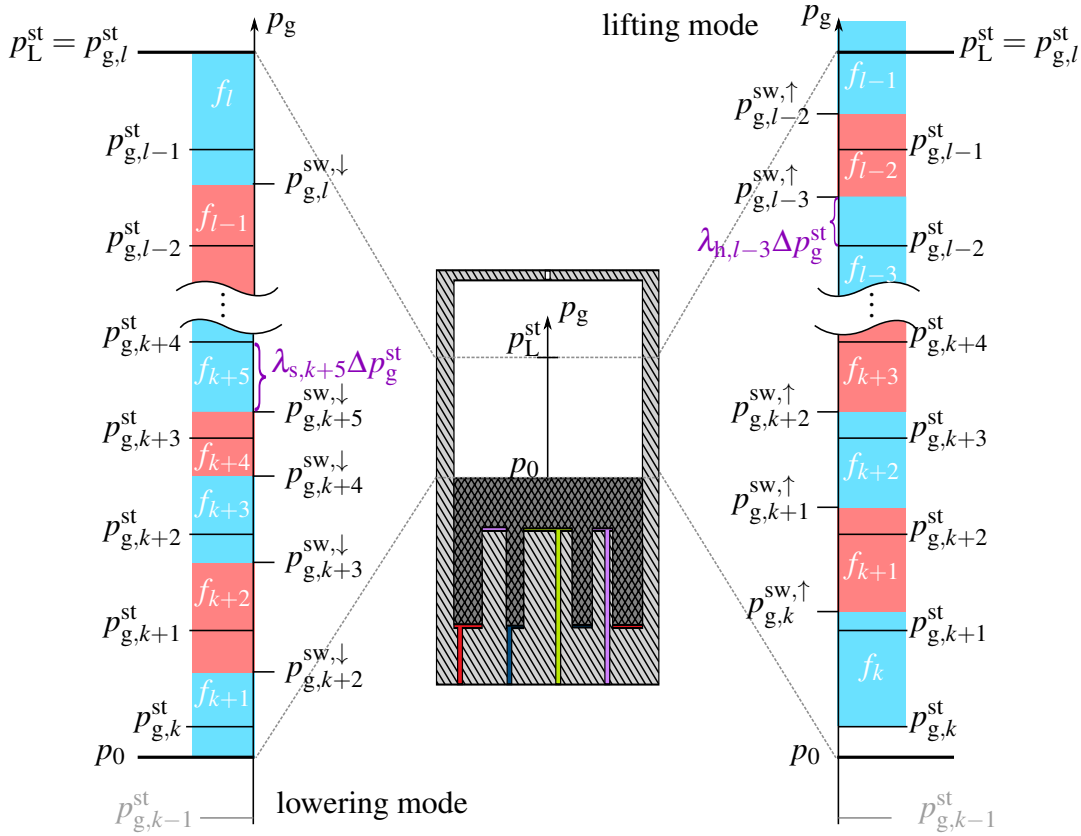


Figure 5. Switching pattern.

## 4.2 Switching points

In order to ensure that the load will not rest in steady state in either lifting or lowering mode, the switching points have to be chosen sufficiently distant<sup>3</sup> from the steady-state pressure levels. The actual difference between the switching point to the  $j$ -th configuration and the associated steady-state level is a design parameter for control design. Accordingly, the switching points for lifting and lowering mode are chosen as

$$p_{g,j}^{sw,\uparrow} = p_{g,j+1}^{st} + \lambda_j^{\uparrow} \Delta p_g^{st} = p_T + \frac{j+1 + \lambda_j^{\uparrow}}{l} (p_L^{st} - p_T), \quad j \in \{k, k+1, \dots, l-2\}, \quad (14)$$

$$p_{g,j}^{sw,\downarrow} = p_{g,j-1}^{st} - \lambda_j^{\downarrow} \Delta p_g^{st} = p_T + \frac{j-1 - \lambda_j^{\downarrow}}{l} (p_L^{st} - p_T), \quad j \in \{k+2, k+3, \dots, l\}, \quad (15)$$

where  $\Delta p_g^{st}$  denotes the difference of adjacent steady-state pressure levels. The relative switching distances

$$\lambda_j^{\uparrow/\downarrow} = \pm \frac{p_{g,j}^{sw,\uparrow/\downarrow} - p_{g,j\pm 1}^{st}}{\Delta p_g^{st}} \quad (16)$$

<sup>3</sup>In this context, sufficiently distant means that there should be a cushion due to model uncertainties and simplifications (such as in (12)).

are design parameters. The resulting switching pattern (see Fig. 5) reads

$$\begin{aligned}
\textbf{Lifting mode:} \quad & f_{l-1}, \text{ if } p_g \geq p_{g,l-2}^{\text{sw},\uparrow}, \\
& f_j, \text{ if } p_{g,j-1}^{\text{sw},\uparrow} \leq p_g < p_{g,j}^{\text{sw},\uparrow}, \quad j \in \{k+1, \dots, l-2\} \\
& f_k, \text{ if } p_g < p_{g,k}^{\text{sw},\uparrow}, \\
\textbf{Lowering mode:} \quad & f_{k+1}, \text{ if } p_g \leq p_{g,k+2}^{\text{sw},\downarrow}, \\
& f_j, \text{ if } p_{g,j}^{\text{sw},\downarrow} \leq p_g < p_{g,j+1}^{\text{sw},\downarrow}, \quad j \in \{k+2, \dots, l-1\} \\
& f_l, \text{ if } p_g > p_{g,l}^{\text{sw},\downarrow}.
\end{aligned}$$

At the valve level, measures have to be taken to prevent the short circuit flows that can occur in the switching stage. If there is a temporal overlap of the switching operations of two valves belonging to the same chamber, a cross flow forms between the load port and the low pressure port. The easiest way to avoid such a flow is to implement an artificial delay of the opening operations which is based on the valve switching time. However, the impact of the resulting pressure peaks due to the inertia of the moving masses has to be analyzed separately.

## 5 DIMENSIONING

The dimensioning of the gas chamber involves the choice of a pair  $p_0$  and  $V_0$  for the precharge pressure and the total accumulator gas volume. To this end, the extreme case of lifting the maximum load to maximum height using a fully charged accumulator is considered. First, the conventional way of dimensioning hydropneumatic accumulators is briefly discussed. After that, a second approach to dimensioning the digital accumulator is presented which takes into account that only some of the fluid chambers are connected to the load in each step. Both dimensioning procedures are based on an ideal gas model assuming an adiabatic process.

### 5.1 Conventional dimensioning approach

Combining the equation of state (8) for ideal gases and the differential equation (6) governing the gas dynamics yields

$$\dot{p}_g V_g + \left(1 + \frac{R_g}{c_v}\right) \bar{p}_g \dot{V}_g + \frac{1}{\tau_{\text{th}}} (\bar{p}_g V_g - m_g R_g T_{\text{env}}) = 0. \quad (17)$$

Assuming an adiabatic process, i.e., there is no heat exchange between the accumulator and its environment ( $\tau_{\text{th}} \rightarrow \infty$ ), the previous equation reduces to

$$\dot{p}_g V_g + \kappa \bar{p}_g \dot{V}_g = 0 \quad (18)$$

where  $\kappa = 1 + R_g/c_v$  is the specific heat ratio. Integrating (18) by separating the variables relates the current variables of state to their precharge values:

$$\bar{p}_0 V_0^\kappa = \bar{p}_g V_g^\kappa. \quad (19)$$

Conventional dimensioning is based on the comparison of the internal energy change of the accumulator gas and the exchanged energy. In the present case, the latter one corresponds to the change of the potential energy

$$\Delta \mathcal{V} = \int_0^{x_{\max}} g m_{p,\max} d\xi \quad (20)$$

of the maximum load  $m_{p,\max}$  when lifted from zero to maximum height  $x_{\max}$ . The internal energy change is obtained by integrating the first law of thermodynamics (3) using (19):

$$U_2 - U_1 = -\bar{p}_0 V_0^\kappa \int_{V_1}^{V_2} V^{-\kappa} dV = \frac{\bar{p}_0^{\frac{1}{\kappa}} V_0}{\kappa - 1} \left( \bar{p}_2^{1-\frac{1}{\kappa}} - \bar{p}_1^{1-\frac{1}{\kappa}} \right). \quad (21)$$

This approach does not take into account the energy exchange which takes place at the low pressure port of the accumulator considered. Consequently, it underestimates the required total gas volume.

## 5.2 Alternative dimensioning approach

Instead of comparing exchanged energies, the dimensioning is carried out by balancing the exchange volume at the load port. Since the lifting mode of the proposed control algorithm involves a sequential pass through each configuration from  $f_l = 1$  to the smallest possible ratio  $f_k = k/l$ , the exchange volume of each step is calculated separately. Summing these volumes finally yields the total exchange volume.

Given (19), the gas volume associated with a switching point is

$$V_{g,j}^{\text{sw}} = \left( \frac{\bar{p}_0}{\bar{p}_{g,j}^{\text{sw}}} \right)^{\frac{1}{\kappa}} V_0. \quad (22)$$

In the lifting mode, the volume  $\Delta V_{L,j}$  displaced across the load port within one stage corresponds to the product of the change in gas volume and the area ratio  $f_j$ . This yields

$$\Delta V_{L,j} = f_j \left( V_{g,j-1}^{\text{sw}} - V_{g,j}^{\text{sw}} \right) = \bar{p}_0^{\frac{1}{\kappa}} V_0 f_j \left( \left( \bar{p}_{g,j-1}^{\text{sw}} \right)^{-\frac{1}{\kappa}} - \left( \bar{p}_{g,j}^{\text{sw}} \right)^{-\frac{1}{\kappa}} \right). \quad (23)$$

Accordingly, the total volume exchanged at the load port while unloading the accumulator is computed by summing the discrete displacement volumes. The result of this computation,

$$\Delta V_L^\uparrow = \sum_{j=k}^{l-1} \Delta V_{L,j} = V_0 \bar{p}_0^{\frac{1}{\kappa}} \left( f_k \left( \bar{p}_{g,k}^{\text{st}} \right)^{-\frac{1}{\kappa}} + \frac{1}{l} \sum_{j=k+1}^{l-1} \left( \bar{p}_{g,j}^{\text{sw},\uparrow} \right)^{-\frac{1}{\kappa}} - f_{l-1} \left( \bar{p}_L^{\text{st}} \right)^{-\frac{1}{\kappa}} \right), \quad (24)$$

is compared to the maximum load displacement volume  $V_{p,\max} = A_p x_{p,\max}$ . Finally, the total accumulator volume can be determined via

$$V_0 = A_p x_{p,\max} \bar{p}_0^{-\frac{1}{\kappa}} \left( f_k \left( \bar{p}_{g,k}^{\text{st}} \right)^{-\frac{1}{\kappa}} + \frac{1}{l} \sum_{j=k+1}^{l-1} \left( \bar{p}_{g,j}^{\text{sw},\uparrow} \right)^{-\frac{1}{\kappa}} - f_{l-1} \left( \bar{p}_L^{\text{st}} \right)^{-\frac{1}{\kappa}} \right)^{-1}. \quad (25)$$

An exemplary comparison of the dimensioning approaches considered is depicted in Fig. 6. Here, the ratio  $V_0/V_x$  of the required accumulator volume and the maximum displacement

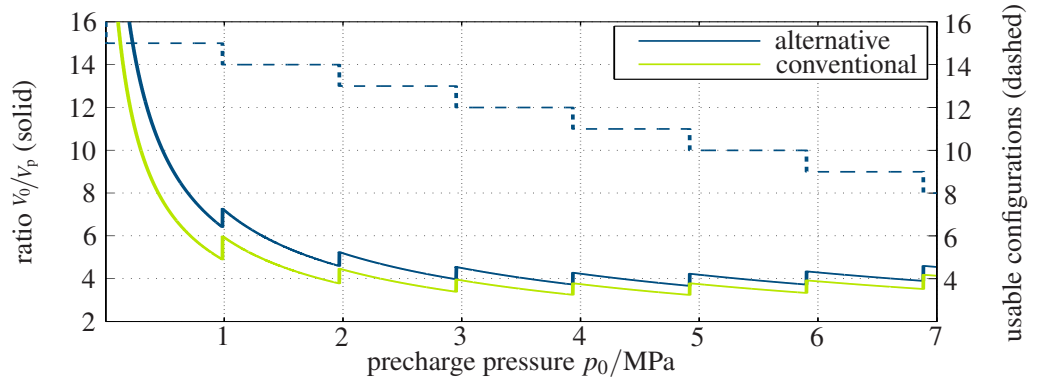


Figure 6. Comparison of the dimensioning approaches.

parameter	symbol	value	unit
low pressure	$p_{\tau}$	0.2	MPa
precharge pressure	$p_0$	4	MPa
total accumulator gas volume	$V_0$	27	l
thermal time constant	$\tau_{th}$	$\rightarrow \infty$	s
total load mass	$m_p$	2500	kg
maximum lifting height	$x_{p,max}$	4	m
relative switching distances	$\lambda_j^{\uparrow/\downarrow}$	$\frac{1}{4}$	1

Table 1. System parameters.

volume is plotted against the precharge pressure  $p_0$ . As expected, the conventional approach underestimates the required total gas volume. Furthermore, there are discontinuities in the results of both approaches. The cause of this can be found in the additional implicit dependence of the total accumulator volume on the precharge pressure. Since the number of usable configurations is bounded from below by the choice of the precharge pressure, as is apparent in (25), a discontinuity appears at each point where this boundary changes. The dashed line in Fig. 6 depicts the number of usable configurations.

## 6 NUMERICAL SIMULATIONS

The proposed dimensioning approach and the underlying control strategy are validated by numerical simulations. Furthermore, the influence of the relative switching distances and the valve switching times are illustrated and an assessment of the impact of the gas model and the heat exchange is made. To this end, a simulation model of the accumulator connected directly to a plunger cylinder (cf. Fig. 7) was implemented in AMESim. Unless stated otherwise, the parameters provided in Table 1 were used in simulation. A selection of simulation results is presented and discussed in the sequel.

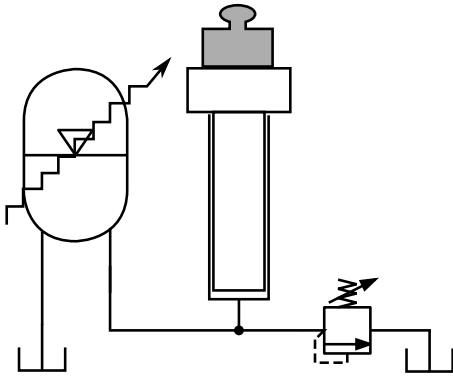


Figure 7. Simulated circuit.

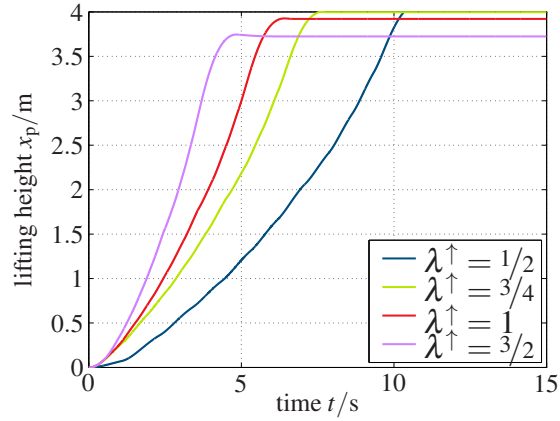


Figure 8. Lifting operation.

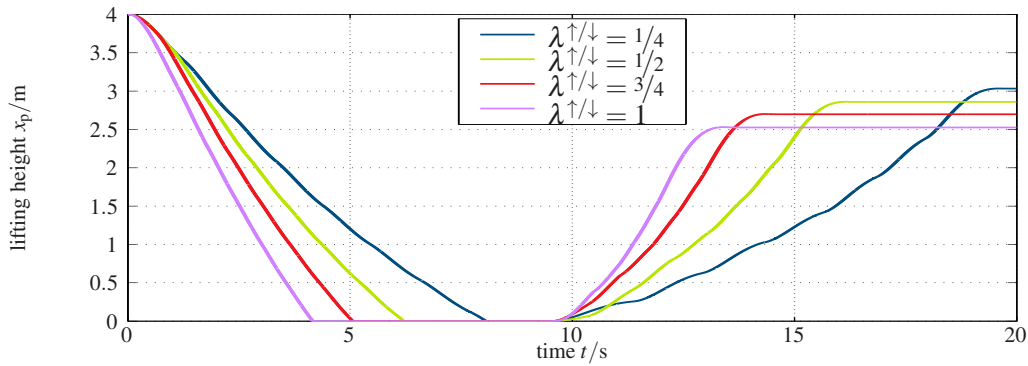


Figure 9. Reference cycle with variation of relative switching distances.

### 6.1 Relative switching distances

In Fig. 8, the lifting trajectory is plotted for a lifting operation using a fully charged accumulator. The switching points have been chosen to be equidistant, i.e.,  $\lambda_j^\uparrow = \lambda^\uparrow$ . The relative switching distance  $\lambda^\uparrow$  has been varied in comparative simulation runs. Obviously, an increasing relative switching distance causes a faster lifting operation, since the load pressure also increases. Apart from this, for relative switching distances significantly higher than the one used for dimensioning, the maximum height is not reached.

The results of a simulation of energy recovery are depicted in Fig. 9 and Fig. 10. Here, the maximum load was first lowered from maximum height to zero and lifted again without the use of any auxiliary energy source apart from the accumulator. In this case, there are more significant differences regarding the final lifting height than in the case of lifting from a fully charged accumulator. This is due to the fact that the dimensioning approach was targeted to provide enough volume for a full height lift whereas energy losses due to friction and throttling play a significant role when recovering the potential energy in the lowering stage. From Fig. 10b, it can be seen that the maximum gas pressure, which is a measure for the stored energy, reduces with increasing velocities due to the aforementioned energy losses.

Another observation that can be made is, that the velocity ripple increases as the gas pressure approaches the steady-state pressure levels. This of course is an undesirable effect. Regarding the relative switching distances, there is a necessity to find a trade off between

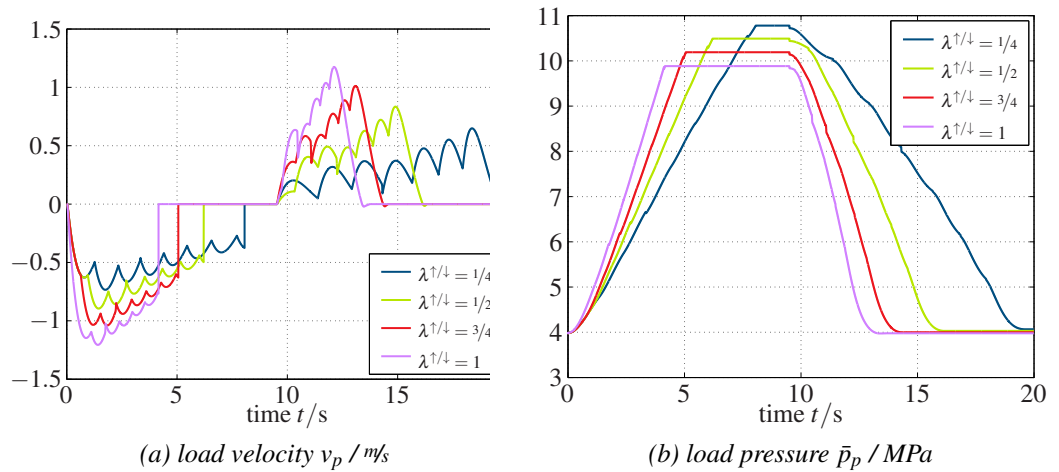


Figure 10. Variation of the relative switching distances.

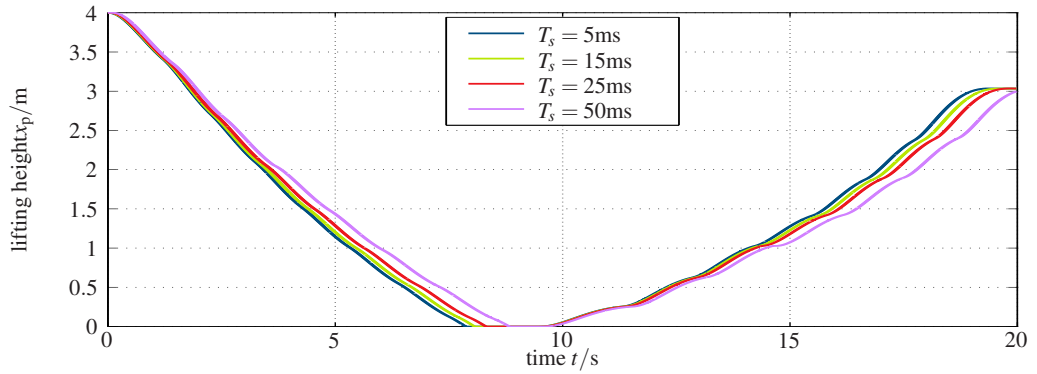


Figure 11. Variation of the valve switching time.

traverse rate, ripple, and energy losses, since both the throttling losses and the friction losses depend on and actually determine the traverse rate.

## 6.2 Switching sequences

When it comes to digital fluid power, the valve switching time often is a crucial factor. In the present case, there is only a minor impact, since the work cycle considered does not reach the dynamic limits of the system. As it can be seen in Fig. 11, there is a slight delay accumulating during the test cycle, whereas the maximum reachable lifting height is barely influenced. This is due to the artificial switching delays introduced in section 4.2, which while slightly prolonging the overall movement duration avoid short circuit flows and the associated loss of energy.

The load pressure of the same work cycles is depicted in Fig. 12. Obviously, there is one certain switching operation in both lifting mode and lowering mode where pressure peaks are significantly higher than elsewhere. A closer look reveals that these maximum peaks occur when switching from  $j = 7$  to  $j = 8$  and vice versa. These are the points where the maximum volume in the oil chambers has to be compressed at once in each mode, respectively. Similar observations were made by Laamanen et al. in [8], where pressure peaks due to binary coding in digital flow control units were discussed. In the



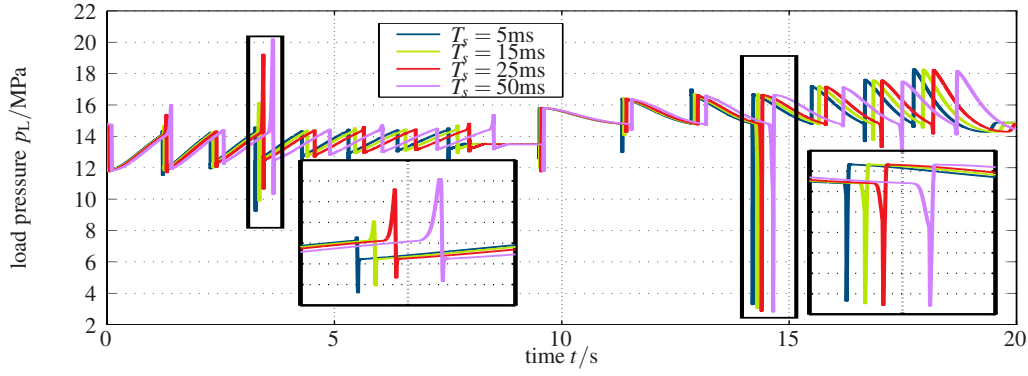


Figure 12. Load pressure peaks.

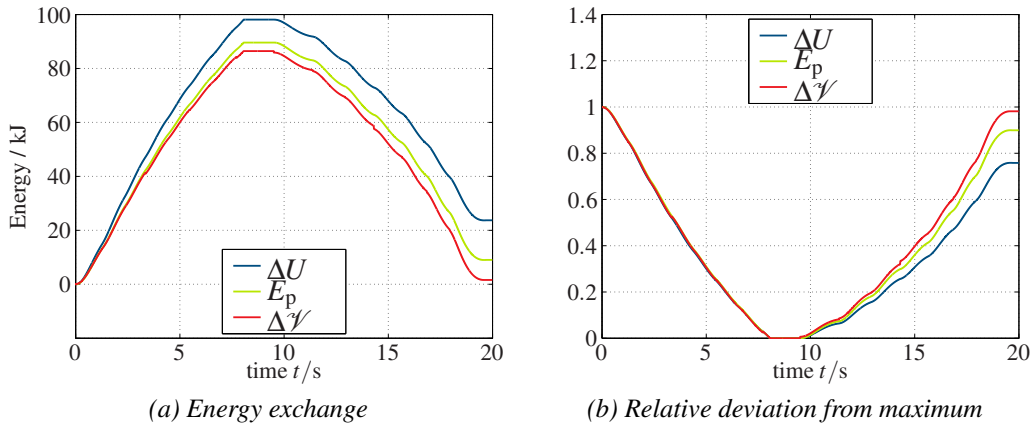


Figure 13. Comparison of selected energy balances.

present contribution, the occurring pressure peaks are analyzed qualitatively with regard to the switching sequences. Whereas the height of these peaks is determined mainly by the oil volume to be compressed, the valve switching times have an impact on the width of the peaks since the flow due to compression is throttled by the partially opened valves. However, an influence of the switching delays can be observed when comparing the peaks in the lifting mode to the ones in the lowering mode. In the latter mode, the inertia of the load mass causes an increase of the load pressure while the valves are closed. In the lifting mode by contrast, the inertia causes an additional decrease of the load pressure.

### 6.3 Energy losses

A distinction of the sources of energy loss is achieved by balancing the energy exchanged at selected points of the system. The cumulative potential energy change of the load mass

$$\Delta \mathcal{V}(t) = \int_0^{x(t)} g m_{p,\max} d\xi \quad (26)$$

is compared to the cumulative hydraulic exchange energy at the load cylinder

$$E_p(t) = - \int_0^t p_p q_p d\tau \quad (27)$$

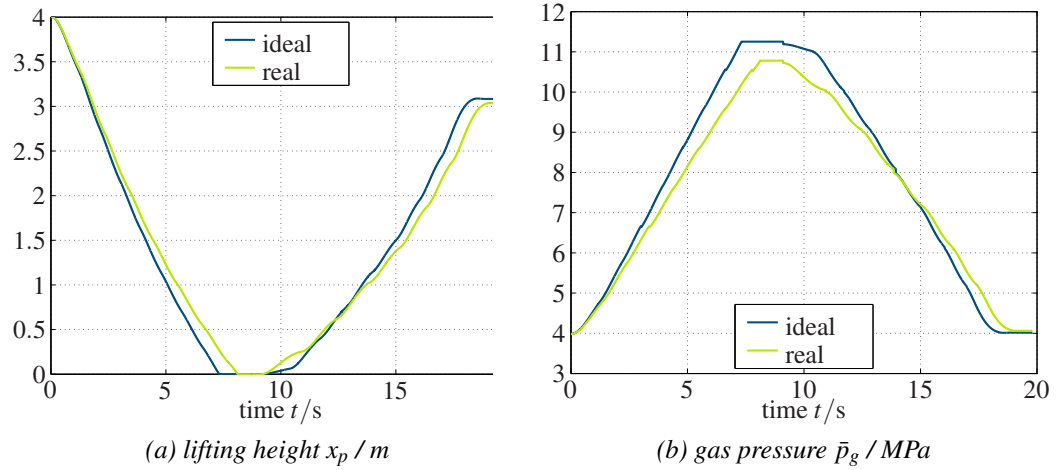


Figure 14. Comparison of ideal and real gas models.

and the stored energy

$$\Delta U(t) = - \int_{V_g(0)}^{V_g(t)} \bar{p}_g dV. \quad (28)$$

The evolution of these integrals during the work cycle is plotted in Fig. 13a. Their relative deviation from their maximal values is depicted in Fig. 13b. The difference between  $E_p$  and  $\Delta \mathcal{V}$  can be regarded as a measure for the friction losses in the load cylinder whereas a measure for the hydraulic losses due to throttling and (de-)compression is provided by the difference between  $\Delta U$  and  $E_p$ .

#### 6.4 Gas dynamics

In this section, a prudent assessment of the impact of the real gas behaviour is made. To this end, a comparison of the ideal gas model with the Peng-Robinson model (see [9]) using the work cycle from the preceding simulations is made. In Fig. 14, results for the lifting height and the gas pressure are depicted. Although there are significant differences concerning the gas pressure, the maximum reachable height is almost identical in both cases. This suggests that the impact of the gas model on the system dynamics must indeed not be neglected. However, the qualification of the system for energy recovery is not questioned.

In order to get a rough estimate for the impact of the heat exchange, the same work cycle was simulated using a finite thermal time constant  $\tau_{th}$ . In the absence of experience concerning the novel digital accumulator, the approximation

$$\frac{\tau_{th}}{1s} \approx 0.3 \frac{p_0}{1MPa} \left( \frac{V_0}{1m^3} \right)^{0.22} + 86.2 \left( \frac{V_0}{1m^3} \right)^{0.49} \quad (29)$$

for conventional piston-type accumulators (see [7]) is used as an estimate for the thermal time constant. The comparison of two work cycles with and without heat exchange is to be found in Fig. 15. As might be expected, there is a decrease in the maximum reachable height due to the energy losses. However, a quantitative assessment requires experimental validation of the accumulator model.

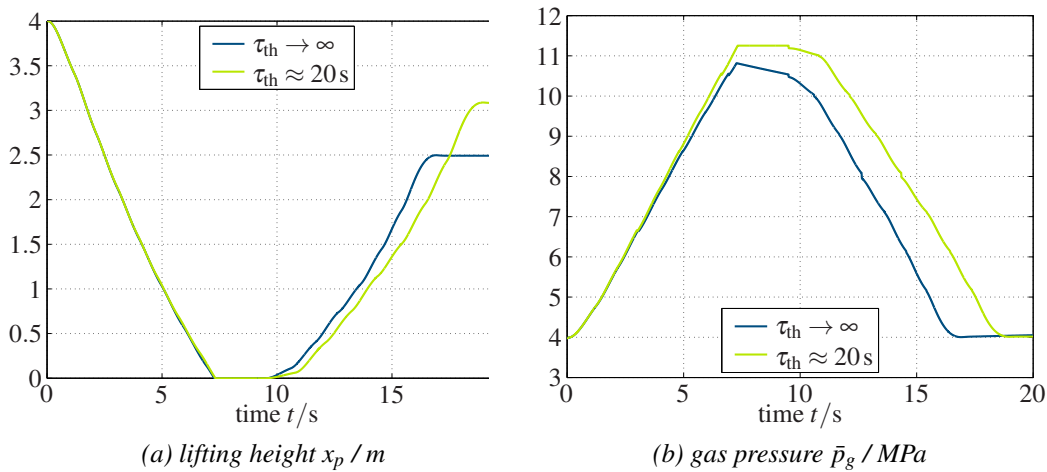


Figure 15. Approximation for the impact of heat exchange.

## 7 CONCLUSION AND FUTURE WORK

A novel digital piston-type accumulator is presented. The system under consideration embraces digital fluid power principles in terms of binary coded annular oil chambers which allow for a discrete variation of the transformation ratio between gas pressure and load pressure. A rudimentary control strategy is developed whose foremost purpose is to validate the qualification of the accumulator concept for energy recovery. Based on this control algorithm, an approach for system dimensioning is presented and compared to a conventional method. In numerical simulations, the control strategy and the dimensioning approach are validated. Furthermore, the results of these simulations provide evidence of the suitability of the digital accumulator concept presented for energy recovery tasks at least in a certain class of applications.

As a corollary of the results presented in this paper, future work will involve experimental investigation of the digital accumulator concept. Such investigations support the derivation of a more accurate system model and allow for the identification of both model structures and physical parameters. The simulation results show that there is a need for experimental model verification and refinement since essential factors such as the gas dynamics, the heat transfer or the friction losses can have significant influence on the overall system behavior. Simultaneously, these factors are a source of uncertainty in the assessment of the simulation results.

The system model verified by experimental results will be the basis for the design of more sophisticated control strategies. A model-based analysis and optimization can be used to improve the existing system and explore or even extend the range of usability. Additionally, the insights gained from experiments are valuable for further development. They can point out new challenges that were not predicted by model analysis and simulation so far.

In conclusion, it can be stated that the presented digital accumulator concept is qualified for energy recovery. First investigations involving model analysis and simulation show promising results. However, ongoing research is necessary, particularly in the field of experiments.

## ACKNOWLEDGMENT

Financial support by the European Union by means of the European Regional Development Fund is gratefully acknowledged.

## REFERENCES

- [1] M. Linjama, "Digital fluid power – state of the art," in *Proc. 12th Scandinavian Int. Conf. on Fluid Power*, pp. 331–353, 2011.
- [2] M. Linjama, "Energy saving digital hydraulics," in *Proc. 2nd Workshop on Digital Fluid Power*, pp. 5–20, 2009.
- [3] M. Linjama, H.-P. Vihtanen, A. Sipola, and M. Vilenius, "Secondary controlled multi chamber cylinder," in *Proc. 11th Scandinavian Int. Conf. on Fluid Power*, 2009.
- [4] M. Linjama, "Digital hydraulic power management system — towards lossless hydraulics," in *Proc. 3rd Workshop on Digital Fluid Power*, pp. 5–22, 2010.
- [5] E. D. Bishop, "Digital hydraulic transformer - for energy efficient hydraulic drives," in *Proc. 2nd Workshop on Digital Fluid Power*, pp. 72–84, 2009.
- [6] R. Scheidl, I. Biedermann, and A. Plöckinger, "A linear digital hydraulic amplifier," in *Proc. 4th Workshop on Digital Fluid Power*, pp. 75–89, 2011.
- [7] S. Rotthäuser, *Verfahren zur Berechnung und Untersuchung hydropneumatischer Speicher*. PhD thesis, Rhein.-Westf. Techn. Hochschule Aachen, 1993.
- [8] A. Laamanen, M. Linjama, and M. Vilenius, "On the pressure peak minimization in digital hydraulics," in *Proc. 10th Scandinavian Int. Conf. on Fluid Power*, pp. 107–122, 2007.
- [9] D. Peng and D. Robinson, "A new two-constant equation of state," *Industrial & Engineering Chemistry Fundamentals*, vol. 15, no. 1, pp. 59–64, 1976.



## IMPROVING DAMPING CHARACTERISTICS OF DISPLACEMENT CONTROLLED DIGITAL HYDRAULIC SYSTEM

M. Sc. Mikko Heikkilä and Adj. Prof. Matti Linjama  
Tampere University of Technology  
Department of Intelligent Hydraulics and Automation  
P.O. BOX 589  
FI-33101 Tampere, Finland

### ABSTRACT

Digital hydraulic power management system (DHPMS) is a solution for more efficient, energy recuperative hydraulic systems. One of the most promising system approaches is the direct connection of the DHPMS and an actuator. The displacement controlled digital system has no directional flow control valves, thus flow throttling losses are eliminated and pressure levels are always optimized. However, a challenge is low natural damping characteristics of the displacement controlled system. In this paper, different damping methods for direct connection are discussed and the system is analyzed by simulations. The results show that the system performance can be improved by using active pressure control together with displacement control when the flows are adequate. At low velocities slight throttling should be considered to avoid jerky motion.

**KEYWORDS:** Active damping, digital hydraulic power management system, direct connection, displacement control

### 1. INTRODUCTION

#### 1.1. Displacement controlled systems

Displacement control is one solution to improve energy efficiency of hydraulic systems. The idea is to control an actuator directly without using energy wasting flow throttling. Inderelst et al. [1] have studied different system layouts to reduce losses in mobile machines. The best results were achieved when actuators were controlled by using variable displacement pumps. Primary energy of the studied system was reduced down to 70 % compared to a conventional system with LS-hydraulics.

Zimmerman and Ivantysynova [2] have presented two hydraulic hybrid architectures for displacement controlled multi-actuator systems. Both parallel hybrid and series-parallel hybrid enabled energy storing into hydraulic accumulators and made active engine load

control possible. Their simulations showed that the hybrid systems could reduce the rated engine power up to 50 % compared to non-hybrid displacement controlled systems. Reduction in fuel consumption was also significant when the hybrids were used.

Rahmfeld and Ivantysynova [3] have studied active damping control of displacement controlled actuators. The proposed method utilized a filtered actuator acceleration signal alongside a position feedback in control of a servo pump. Simulation results showed an average reduction of about 30 % in boom oscillations compared to the system without active damping control. Utilization of a pressure feedback signal for stabilizing displacement controlled systems has been studied in [4].

## 1.2. Digital hydraulic power management system

Digital hydraulic power management system (DHPMS) is based on digital pump-motor technology but has arbitrary number of independent outlets [5]. Possibility for several outlets increases versatility of the machine. Figure 1 shows a drawing of a 3-piston DHPMS with two independent outlets. Each piston can be individually controlled by choosing different opening and closing cycles for the on/off control valves. Hence, fluid can be pumped to or sucked from the tank T or each outlet A and B. Pressure pre-compression and pressure release can be optimized for each pressure level, thus pressures of the outlets are independent of each other. The DHPMS can operate both as a pump and as a motor. In addition, power can be transferred between the outlets.

Measured characteristics of a 6-piston DHPMS were introduced in [6]. The first prototype showed the potential of the technology – power transfer between the outlets is possible and, moreover, can be very efficient. There are also several applications where the DHPMS can be used. Individual control of supply line pressures of a mobile crane was studied in [7]. In addition, a direct connection of the DHPMS and an actuator was presented in [8]. Both studies showed that significant energy saving can be achieved by using the DHPMS technology compared to traditional systems.

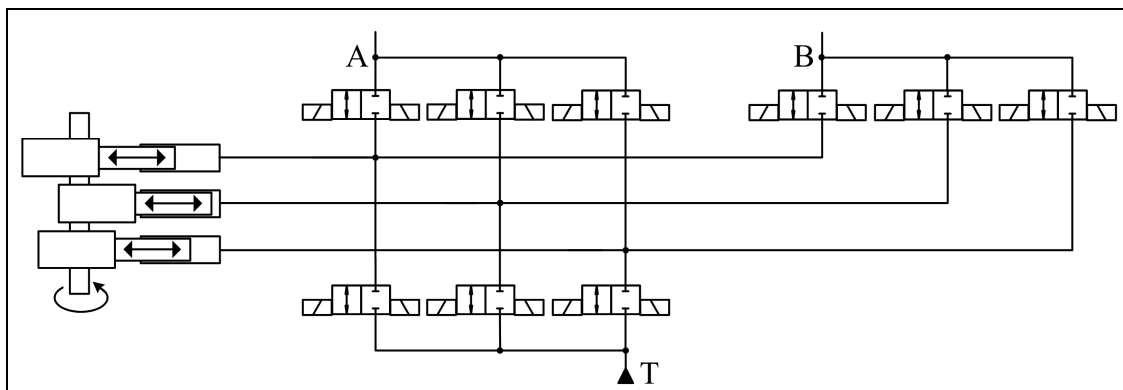


Figure 1. Schematic of a 3-piston DHPMS with two independent outlets

## 2. SYSTEM OVERVIEW

### 2.1. Simulation model of hydraulic boom mock-up

A simulation model used in the study is similar to the one presented in [8], with an exception of larger damping volumes which equal  $5 \text{ dm}^3$  in both supply lines. Larger volumes are applied to increase hydraulic capacitance and to make pressure fluctuation smaller. In addition, size of the damping orifices and cylinder port orifices varies in simulated cases depending on a studied damping method (Figure 2). A studied DHPMS has six pistons and the total displacement of about  $30 \text{ cm}^3$  while the rotational speed is 1500 rpm. The model does not consider internal leaks and only pressure losses are observed.

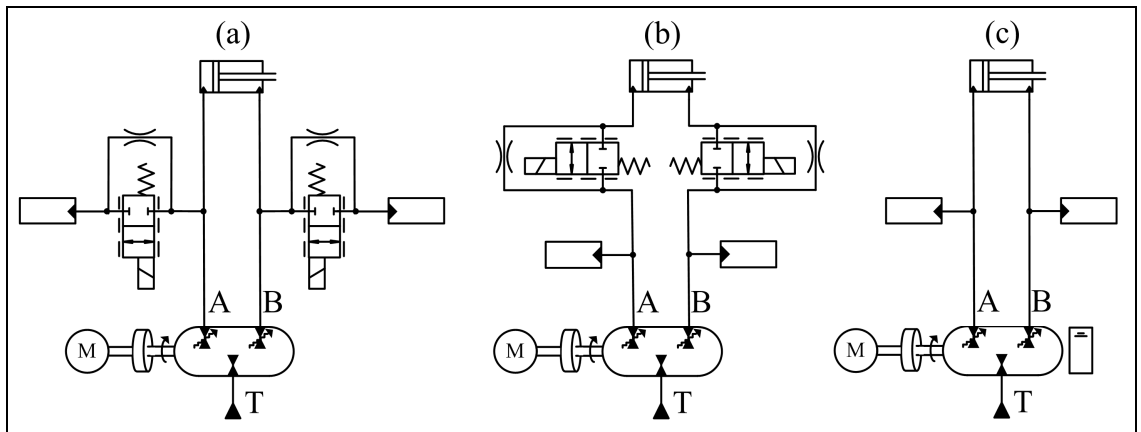


Figure 2. Direct connection with different damping methods: semi-active damping volume orifices (a), semi-active cylinder port orifices (b) and active pressure control (c)

### 2.2. Fluid volume control in the direct connection

A principle of the fluid volume control in a direct connection was introduced in [8]. Velocity reference of the piston is first converted into desired flows in supply lines considering cylinder areas. Volume targets are further calculated from the flow rates and the error is minimized by choosing the best pumping and suction modes at every mode selection instant. In this study, a theoretical piston displacement is used to estimate the change in fluid volumes i.e. no compressibility is considered. Thus, the simulations with different damping characteristics are more comparable when position feedback is not applied.



### 2.3. Combined volume-pressure control in the direct connection

In combined volume-pressure control, fluid volume control is utilized for one supply line and pressure control for another. Direction of the cylinder load force defines the controllable variable such that volume control is applied to the chamber working against the force. Back-pressure is sustained in the other cylinder chamber to avoid cavitation and to maintain stiffness of the system. A benefit of the method is that pressures do not drop even if there were internal leaks in the system.

The volume controller selects a mode primarily by using the logic explained in the previous chapter. Next, the pressure controller chooses a mode that does not conflict the formerly selected mode by using the following principles (conditions to control B-side pressure - A-side goes similarly):

- IF  $v_{\text{ref}} < 0$  AND  $p_{\text{target}} - p_{\text{B}} > 0$  THEN **Pump to B**
- IF  $v_{\text{ref}} > 0$  AND  $p_{\text{target}} - p_{\text{B}} < 0$  THEN **Suck from B**
- IF  $v_{\text{ref}} = 0$  AND  $p_{\text{target}} - p_{\text{B}} - p_{\text{tol}} > 0$  THEN **Pump to B**
- IF  $v_{\text{ref}} = 0$  AND  $p_{\text{target}} - p_{\text{B}} + p_{\text{tol}} < 0$  THEN **Suck from B**

Where  $p_{\text{B}}$  is pressure to be controlled,  $p_{\text{target}}$  user defined target pressure and  $p_{\text{tol}}$  pressure tolerance. If all conditions are false the idling mode is selected. In addition, sequential pumping or suction strokes are blocked if the pressure is between tolerance values.

## 3. METHODS FOR BETTER SYSTEM DAMPING

### 3.1. Passive damping volume orifices

Passive damping orifices are used to throttle the flows of the damping volumes. The orifices are fixed and they are sized considering the cylinder area ratio such that damping characteristics are good at relatively high velocity. The method was utilized in [8] and the results showed its feasibility. However, low velocities are challenging due to a bigger flow ripple.

In this study, passive damping orifices of the simulated system are sized by finding the best damping for the velocity step of  $\pm 0.07$  m/s when the load is resistive. Figure 3 shows the response when the orifice sizes are 3 l/min (A-side) and 2 l/min (B-side) at a pressure difference of 0.5 MPa. It can be seen that overshoot in the velocity is moderate both in the beginning and at the end of the movement. Oscillation in the velocity dies out almost completely, though the pressure ripple is quite significant during the motion.

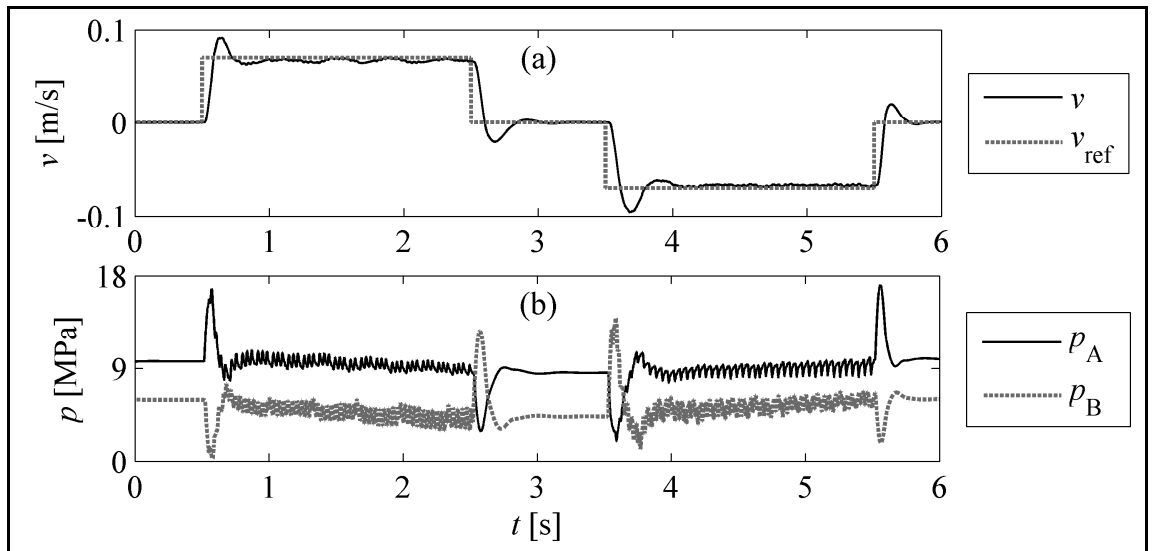


Figure 3. Damping characteristics of the system with passive orifices at the velocity of  $\pm 0.07$  m/s

Figure 4 shows a velocity step of  $\pm 0.01$  m/s with the same damping orifices. Velocity ripple is significantly higher in this case. Small orifices cannot dampen the pulsating pressure caused by sparse pumping and suction. In the simulations (Figures 3 and 4), velocity control is used while cylinder port orifice sizes are 100 l/min at 0.5 MPa pressure difference.

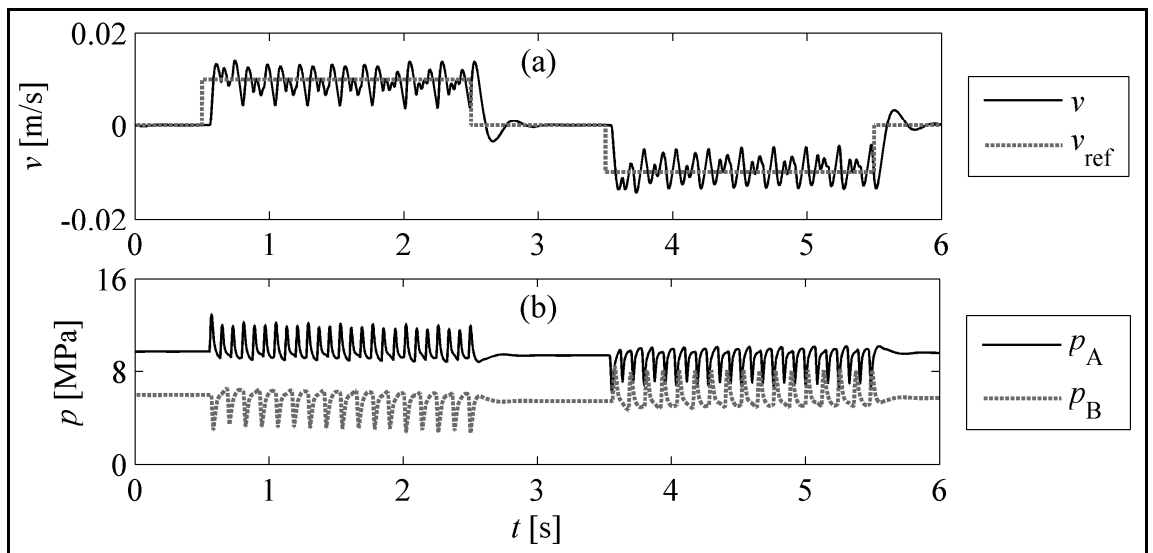


Figure 4. Damping characteristics of the system with passive orifices at the velocity of  $\pm 0.01$  m/s

### 3.2. Semi-active damping volume orifices

Semi-active damping orifices are established when a set of on/off control valves are connected parallel with a fixed orifice as shown in drawing (a) of Figure 2. The

principle is to adjust the size of the damping orifice according to a velocity reference of the actuator. The fixed orifices are sized to be the smallest ones and the throttled valves are opened to increase the flow of the damping volumes.

Table 1 shows optimal orifice sizes at different velocities. A principle of the dimensioning is the cylinder area ratio and the sizes of the orifices have been iterated by simulations to achieve acceptable damping characteristics with resistive cylinder load. It can be seen that only at the smallest simulated velocity the orifice sizes have to be increased. Hence, in this case only one active on/off valve is needed alongside the fixed orifice to realize semi-active damping.

*Table 1. Optimal sizing of semi-active damping volume orifices at different velocities*

<i>Velocity reference</i>	$\pm 0.01$		$\pm 0.02$		$\pm 0.03$		$\pm 0.05$		$\pm 0.07$		m/s
<i>Supply line</i>	A	B	A	B	A	B	A	B	A	B	
Orifice nominal flow @ 0.5 MPa	5.9	4.0	3.0	2.0	3.0	2.0	3.0	2.0	3.0	2.0	l/min

### 3.3. Semi-active cylinder port orifices

Figure 2 (b) shows a schematic of the displacement controlled system with semi-active cylinder port orifices. Throttling is applied in means of low-pass filtering of cylinder flows while damping volumes are connected straight to the supply lines. Sizing of the orifices for different velocities is a compromise between good damping characteristics and energy losses produced by throttling the flows.

Table 2 shows a dimensioning that provides reasonable system performance according to simulations when resistive cylinder load is applied. The area ratio is also taken into account due to different size flow rates. However, the valve set should be selected with a minimum number of components which mean compromises if a real system is considered.

*Table 2. Optimal sizing of semi-active cylinder port orifices at different velocities*

<i>Velocity reference</i>	$\pm 0.01$		$\pm 0.02$		$\pm 0.03$		$\pm 0.05$		$\pm 0.07$		m/s
<i>Supply line</i>	A	B	A	B	A	B	A	B	A	B	
Orifice nominal flow @ 0.5 MPa	3.7	2.5	6.0	4.0	9.0	6.0	11.2	7.6	11.2	7.6	l/min

### 3.4. Active pressure control

Active pressure control is realized by adding a derivative term into back pressure control explained in Chapter 2.3. Figure 2 (c) shows that no throttling components are used, but a bit more complex control algorithm. If pressure in the B-chamber is controlled, differential of the A-chamber pressure is observed and vice versa (Figure 5). In this study, the parameter  $K_d = 1500$  and is determined by simulations such that the system is stable at every operating point.

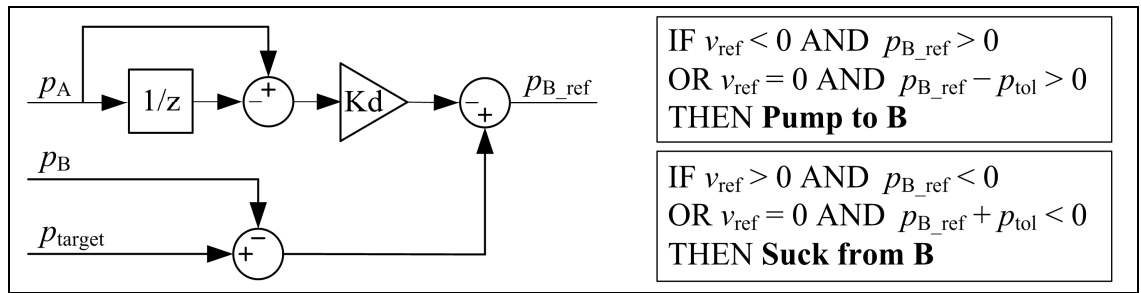


Figure 5. Principle of active pressure control

Figure 6 shows an effect of active pressure control to the system damping. It can be seen that oscillation in piston velocity damps in a second when a velocity step of  $\pm 0.02$  m/s is excited (graph (a) of figure 6). At small velocities pressure control is challenging because of small number of DHPMS pistons with relatively large displacement. At higher velocities damping characteristics are better: the oscillation dies out in about 0.05 seconds as seen in graphs (b) and (c) of Figure 6 where the velocity steps are  $\pm 0.03$  and  $\pm 0.5$  m/s correspondingly.

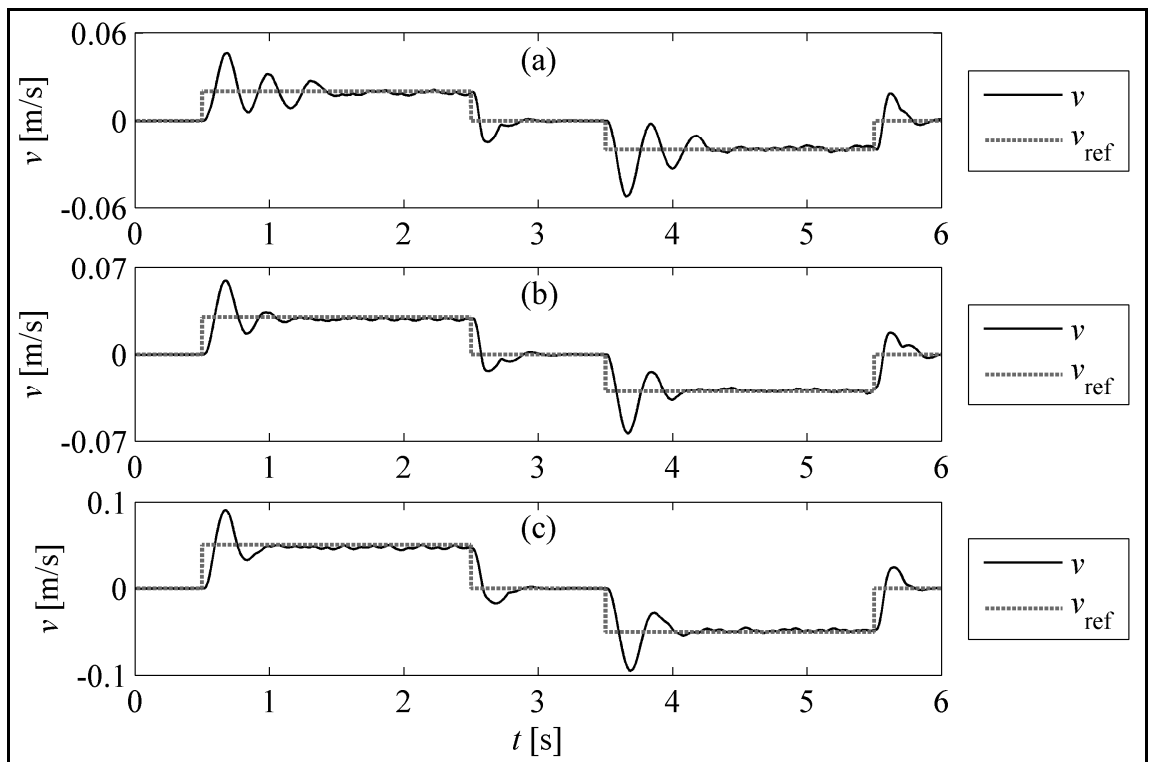


Figure 6. Damping characteristics of the system with active pressure control at the velocities of  $\pm 0.02$  m/s,  $\pm 0.03$  m/s and  $\pm 0.05$  m/s

## 4. COMPARISON OF THE DAMPING METHODS

### 4.1. Reference simulation – no added damping

Figure 7 shows a simulation of the system without added damping. The open-loop volume control of chambers is used for tracking the velocity step of  $\pm 0.07$  m/s. Oscillation in the velocity hardly damps at all during the motion and the cylinder piston temporarily moves against desired direction (graph (a) of Figure 7). In addition, both cylinder chambers cavitate during the movement as seen in graph (b) of Figure 7. The system seems to be uncontrollable if there is no extra damping.

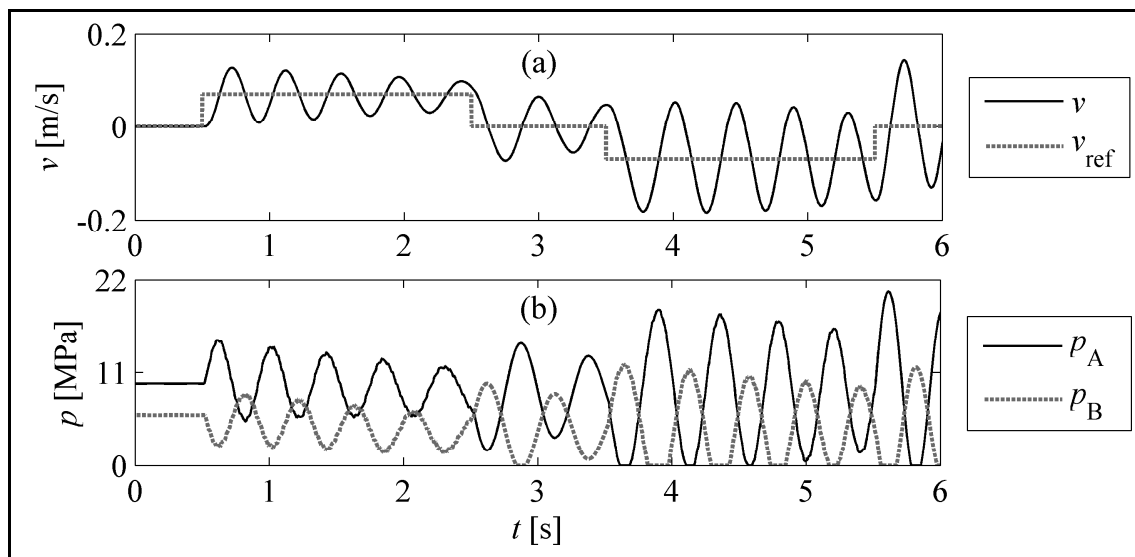


Figure 7. Velocity step of  $\pm 0.07$  m/s when no added damping

### 4.2. Piston velocity

Figure 8 compares simulated cylinder piston velocities when different damping methods are used in the displacement controlled digital hydraulic system. At slow velocity  $\pm 0.01$  m/s, the system with semi-active port orifices has the smallest ripple: only about 15 % of the target velocity (graph (b1) of Figure 8). The ripple is about 40 % when semi-active damping volume orifices are used as shown in graph (a1) of Figure 8. Graph (c1) of Figure 8 instead shows that active pressure control cannot handle this small velocity if the DHPMS has only six pistons.

At the velocity of  $\pm 0.07$  m/s all three damping methods are valid. Slight oscillation in the velocity can be noticed in case of the semi-active damping volumes orifice but the starting and the stopping are smooth (graph (a2) of Figure 8). When the semi-active cylinder port orifices are used, the oscillation damps slowly at the end of the movement (graph (b2) of Figure 8). Graph (c2) of Figure 8 shows that active pressure control performs also well despite of quite large overshoot in the beginning of the movement.

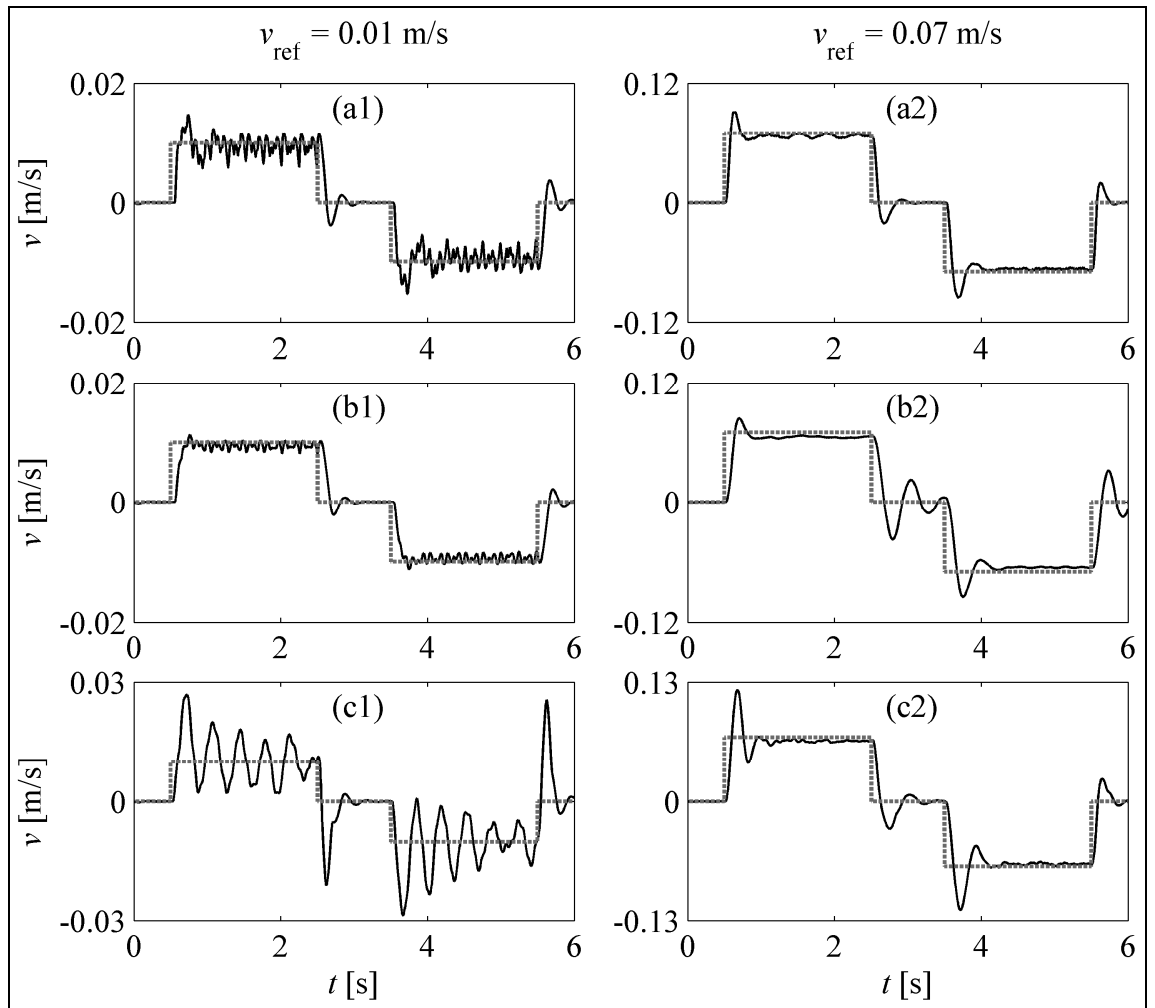


Figure 8. Cylinder piston velocities ( $-v - v_{ref}$ ): semi-active damping volume orifices (a), semi-active cylinder port orifices (b) and active pressure control (c)

#### 4.3. Cylinder pressures

Figure 9 compares simulated cylinder pressures. At slow velocity  $\pm 0.01$  m/s, the system with the semi-active port orifices has the smoothest pressure curves (graph (b1) of Figure 9). The ripple is about 0.7 MPa in both cylinder chambers. Graph (a1) of Figure 9 shows that pressure ripple can be as much as 2.5 MPa when the semi-active damping volume orifices are used. Poor damping capability of active pressure control at low velocity can be also seen from the system pressures (graph (c1) of Figure 9).

At the velocity of  $\pm 0.07$  m/s the pressure behaviour is quite similar regardless of the damping method. Pressure ripple is the highest when the semi-active damping volume orifices are used (graph (a2) of Figure 9) while in case of the semi-active cylinder port orifices the ripple is negligible (graph (b2) of Figure 9). Graph (c2) of Figure 9 shows that active pressure control enables smooth pressure curves when the velocity target is high enough.

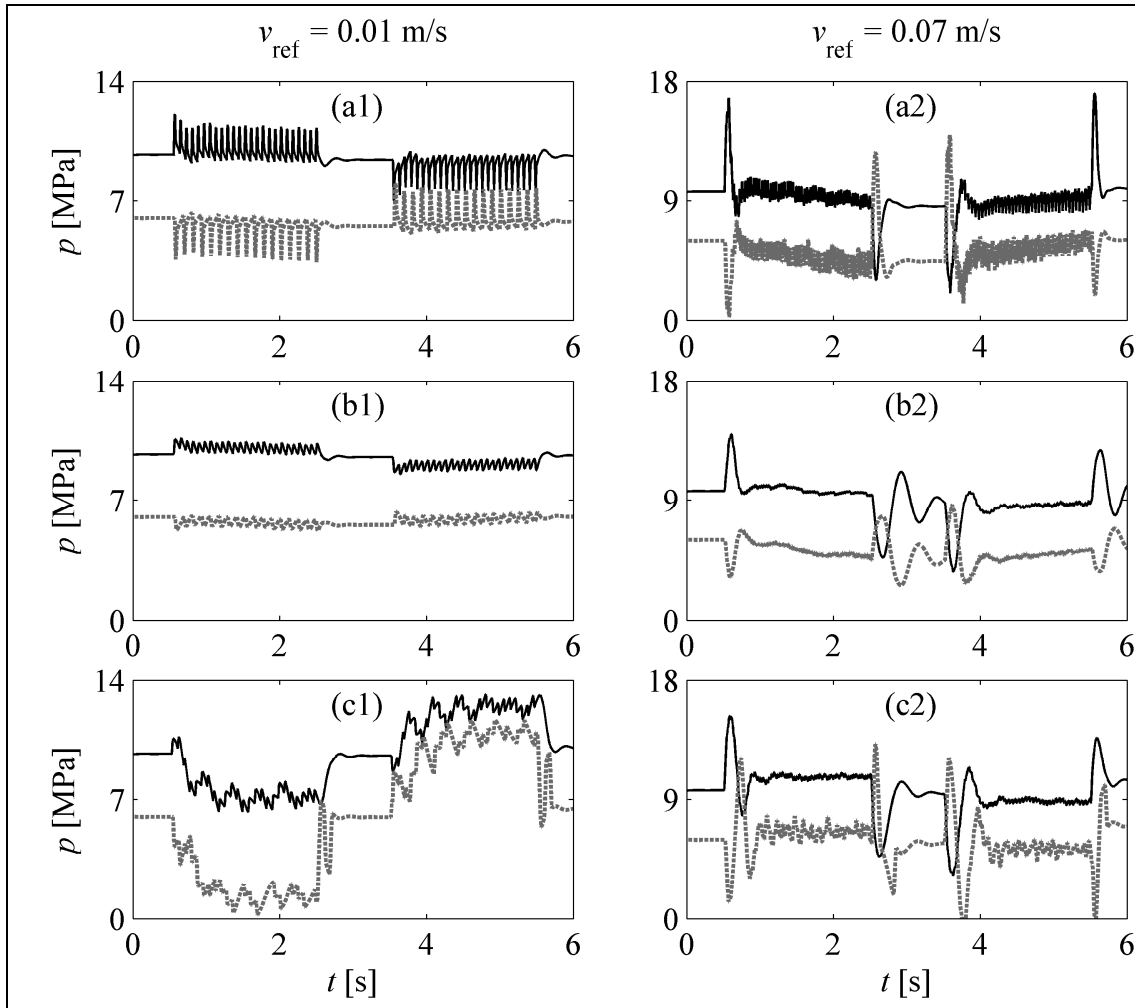


Figure 9. Cylinder chamber pressures ( $-p_A$   $-p_B$ ): semi-active damping volume orifices (a), semi-active cylinder port orifices (b) and active pressure control (c)

#### 4.4. Power and energy consumption

Figure 10 shows input and output powers during the movements. At lower velocity the power curves are quite similar with all three damping methods (graphs (a1), (b1) and (c1) of Figure 10). A simulation when the semi-active cylinder port orifices are used stands out from the rest at higher velocity as seen in graph (b2) of Figure 10. Difference between the input and output power levels is significant during the motion. Throttling the cylinder flows cause big losses. Active pressure control (graph (c2) of Figure 10) seems to be slightly more energy efficient method compared to the use of semi-active damping volume orifices (graph (a2) Figure 10).

Table 3 shows energy losses of the up-down movements at five different velocities. The best efficiency is achieved by using active pressure control when the losses are practically the same at every studied velocity. When the semi-active damping volume orifices are used the losses are 0.3 kJ bigger on average but they are still somewhat independent of the velocity. Instead, the amount of the losses is clearly velocity dependable in case of the semi-active cylinder port orifices. The losses are approximately the same than in two other cases if the velocity is small. At higher velocities the losses increase significantly.

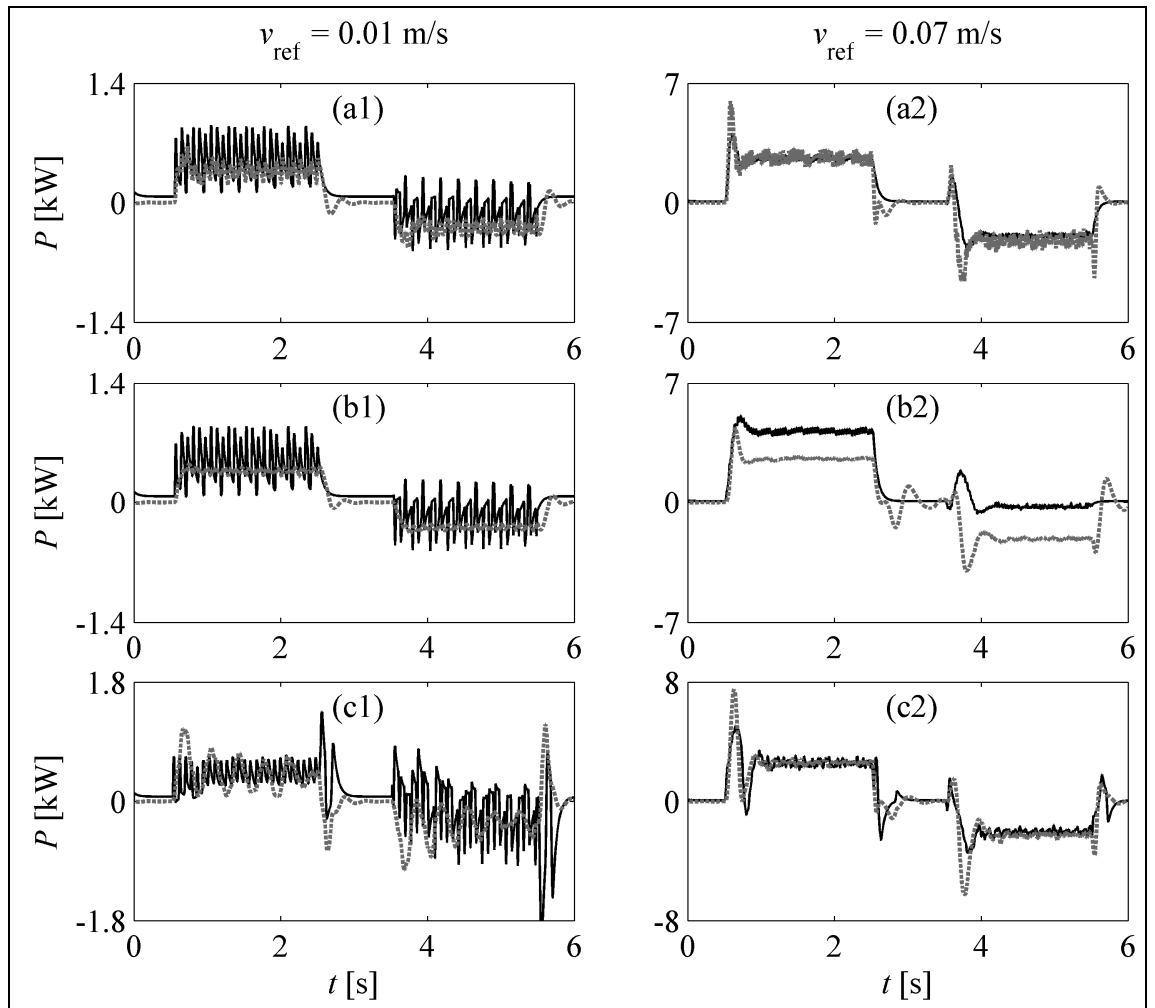


Figure 10. Input and output powers ( $-P_{in}$   $--P_{out}$ ): semi-active damping volume orifices (a), semi-active cylinder port orifices (b) and active pressure control (c)

Table 3. Energy losses during the movements

Velocity reference	$\pm 0.01$	$\pm 0.02$	$\pm 0.03$	$\pm 0.05$	$\pm 0.07$	m/s
Semi-active damping volume orifices	0.8	0.9	0.8	0.9	1.2	kJ
Semi-active cylinder port orifices	0.7	1.2	1.4	3.2	7.6	kJ
Active pressure control	0.6	0.6	0.6	0.6	0.7	kJ



## 5. DISCUSSION AND CONCLUSION

In this study, different methods for better system damping in a digital displacement controlled system were analysed. The use of passive damping volume orifices in the direct connection is a good solution due to simplicity and adequate damping characteristics. Furthermore, energy losses are reasonably low when the passive method is used. Semi-active damping volume orifices slightly improves the lowest simulated velocity, hence one extra on/off valve would be needed in addition to fixed orifices.

Semi-active cylinder port orifices effectively damp oscillations despite of the cylinder piston velocity as long as the flows are throttled sufficiently. A downside is that several on/off valves are needed to control the whole velocity range. The losses are moderate if the piston velocity is low, but the losses increase profusely when the flow rates rise. Hence, throttling of the cylinder flows is reasonable only at low velocities. In that case the ripple in the velocity and pressures can be considerably reduced without wasting excessive energy.

Combined volume-pressure control of DHPMS enables active damping control without any extra components. The method is the most energy efficient because the flows are not throttled by any means. However, small velocities are difficult to control if the DHPMS has only six pistons. At larger velocities the damping characteristics are very good.

In conclusion, all studied manners have their advantages and disadvantages. Hence the best solution to increase system damping in the direct connection would be a combination of two methods. Semi-active cylinder port orifices could be used together with passive damping volume orifices or with active pressure control. In both cases, only small velocities would be controlled by throttling the cylinder flows in order to smooth the motion and keep the losses tolerable. This means that one or two extra on/off valves would be needed per cylinder port, thus the system stays simple. Good properties of the passive damping volume orifices or active pressure control could be utilized at higher velocities instead.

## ACKNOWLEDGEMENT

The research was funded by the Academy of Finland (Grant No. 139540).

## REFERENCES

- [1] Inderelst, M., Losse, S., Sgro, S. and Murrenhoff, H. 2011. Energy Efficient System Layout for Work Hydraulics of Excavators. The Twelfth Scandinavian International Conference on Fluid Power, SICFP'11, Tampere, Finland, 2011.

- [2] Zimmerman, J., and Ivantysynova, M. 2011. Hybrid Displacement Controlled Multi-Actuator Hydraulic Systems. The Twelfth Scandinavian International Conference on Fluid Power, SICFP'11, Tampere, Finland, 2011.
- [3] Rahmfeld, R., and Ivantysynova, M. 2003. New Displacement Controlled Linear Actuator Technology – A Suitable Control Element for Active Oscillation Damping The Eighth Scandinavian International Conference on Fluid Power, SICFP'03, Tampere, Finland, 2003.
- [4] Williamson, C., and Ivantysynova, M. 2010. Stability and Motion Control of Inertial Loads with Displacement Controlled Hydraulic Actuators. The sixth FPNI PhD Symposium, West Lafayette, USA, 2010.
- [5] Linjama, M., Huhtala, K. 2009. Digital Pump-Motor with Independent Outlets. The 11th Scandinavian International Conference on Fluid Power, SICFP'09, Linköping, Sweden, 2009.
- [6] Heikkilä, M., Tammisto, J., Huova, M., Huhtala, K., Linjama, M. 2010. Experimental Evaluation of a Piston-Type Digital Pump-Motor-Transformer with Two Independent Outlets. Bath/ASME Symposium on Fluid Power and Motion Control (FPMC 2010), Bath, UK, 2010.
- [7] Karvonen, M., Heikkilä, M., Huova, M., Linjama, M., Huhtala, K. 2011. Simulation study - Improving Efficiency in Mobile Boom Using Digital Hydraulic Power Management System. The Twelfth Scandinavian International Conference on Fluid Power, SICFP'11, Tampere, Finland, 2011.
- [8] Heikkilä, M., Linjama, M. 2011. Direct Connection of Digital Hydraulic Power Management System and Double Acting Cylinder – A Simulation Study. The Fourth Workshop on Digital Fluid Power (DFP'11), Linz, Austria, 2011.



## STABILIZING REST POSITIONS OF THE LINEAR DIGITAL HYDRAULIC AMPLIFIER

Rudolf Scheidl\*, Ingo Biedermann\*\* and Andreas Plöckinger\*\*\*

\* Institute of Machine Design and Hydraulic Drives  
Johannes Kepler University Linz

\*\* Austrian Center of Competence in Mechatronics

\*\*\* Linz Center of Mechatronics

Altenbergerstraße 69, 4040 Linz, Austria

E-mail: rudolf.scheidl@jku.at

Phone: +43 732 2468 6521, Fax: +43 732 2468 6522

### ABSTRACT

The Linear Digital Hydraulic Amplifier is a modification of the classical linear hydraulic amplifier. It employs a finite number of hydraulic cylinders which are connected to high or low pressure depending on the force requirements. The control is accomplished only by mechanical and hydraulic components. Since a digital cylinder drive without closed centre valves can only realize discrete force values, a load force between these discrete force levels cannot be compensated statically but requires a periodic switching of the system leading to oscillations around the intended rest position and permanent energetic losses. In this paper two concepts for stabilizing the rest position employing check valves are studied. With these a rest position can be held stably in principle. In combination with position control, however, a complex stability problem occurs with complex stability boundaries in the parameter space.

**KEYWORDS:** Digital hydraulics, digital cylinder, linear amplifier, stability.

### 1. 1 INTRODUCTION

In [1] authors presented the so called Linear Digital Hydraulic Amplifier (LDHA), which is a modification of the classical linear hydraulic amplifier aiming at much better energy efficiency. Like the conventional linear hydraulic amplifier, the digital version is a position controlled system employing only mechanical control input and feedback. The basic means for this efficiency gain is the employment of a digital hydraulic cylinder concept (N cylinders of equal or different size) in combination with a hydraulic circuit which switches an appropriate portion of these cylinders to the pressure line to generate a proper force for the intended motion whereas the remaining cylinders are connected to tank line. One concept is shown in Figure 1 (taken from [1]). The N cylinders have a dual stepping of their active areas allowing for  $2^N - 1$  different force

levels. The hydraulic control is accomplished by the proportional valve  $V_x$ . It converts the control error  $x_d - x_a$  into a flow rate  $Q_l$  which raises or lowers the control pressure  $p_x$  in the pilot system. The 3/2 way switching valves  $S_1$  to  $S_N$  have different switching pressure levels for switching on ( $p_{x,i,on}$ ) and off ( $p_{x,i,off}$ ). The valve  $V_x$  generates integral control and the cylinder  $A_p$  proportional control properties.

This concept is not performing resistance control and thus produces no intrinsic losses.

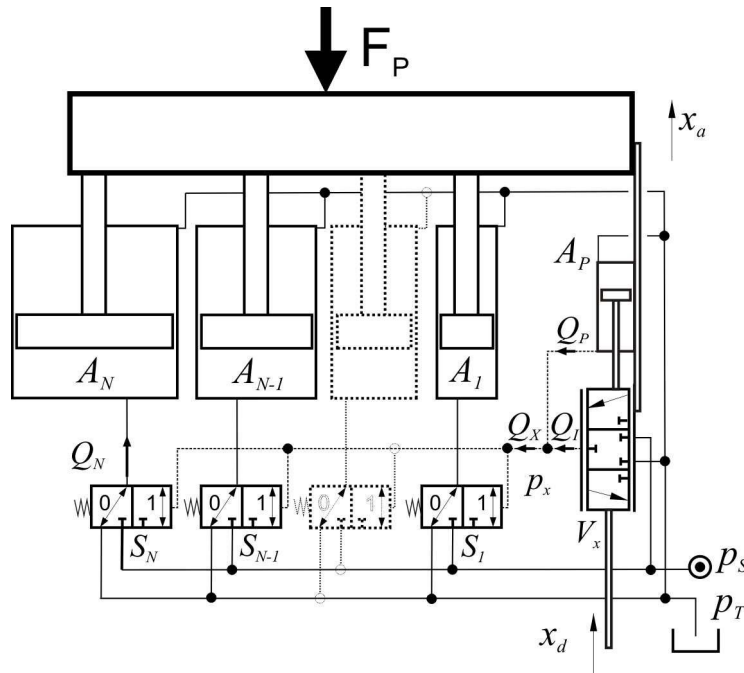


Figure 1. One realization of the LDHA according to [1]; at standstill periodic switching occurs and, in turn, mechanical oscillations (see Figure 2) and permanent energy consumption.

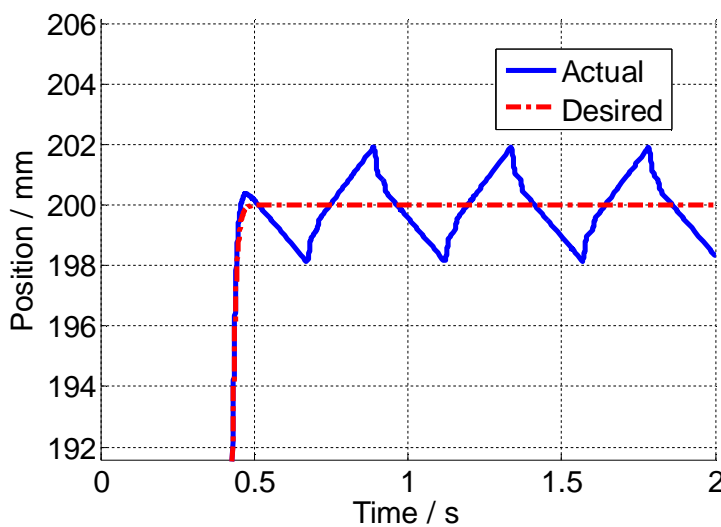


Figure 2. Periodic switching of a LDHA at standstill leading to mechanical oscillation; LDHA system according to Figure 1.

Since without any throttling  $N$  cylinders can only generate a finite set of hydraulic forces there is nearly always a slight mismatch between the required and the hydraulically feasible force. Particularly if a rest position is intended, this mismatch is crucial. It leads to periodic switching which is unwanted for two reasons:

- It possibly causes harmful vibrations of the whole technical system and
- a permanent energy consumption occurs which might even devour the energy saved by the efficiency advantage of the LDHA.

A strict avoidance of such permanent switching at intended rest positions requires a modification of the main hydraulic circuit. Basically, there are two options

1. **“Throttling concept”**: Allow for a certain oil flow over some of the valves  $S_i$  such that pressure values between tank ( $p_T$ ) and system pressure ( $p_S$ ) are generated in the corresponding cylinders by throttling losses. This, however, means a permanent flow from the system pressure line to the tank line and, hence, energy losses. A further drawback is the fact that some of the valves must be either continuously adjustable valves – this is a violation of the simple concept – or additional valves have to be spent, which complicates the system.
2. **“Closing concept”**: If at rest some of the many cylinder chambers are closed, hence disconnected from tank and pressure line, pressures in these cylinders as required for equilibrium establish automatically. There is no oil flow at rest and no losses. This concept employs a basic advantage of hydraulic drives over electrical drives, the ability to hold forces without permanent losses.

Basically, the problem of force mismatch does also concern the motion phases, meaning that the actually required acceleration to follow a certain trajectory, in particular to move the load at a specific constant speed, can only be approximated by selecting a force step  $F_i$  out of all digitally feasible hydraulic forces which is closest to the required force  $F_R$ . Of course, a switching between the two neighbouring forces  $F_i$  and  $F_{i+1}$  can provide an approximation which is identical to  $F_R$  in some average sense. In the case studies so far performed by the authors [1, 2] the problem of force mismatch in motion was much less significant than the equilibrium in the rest phase.

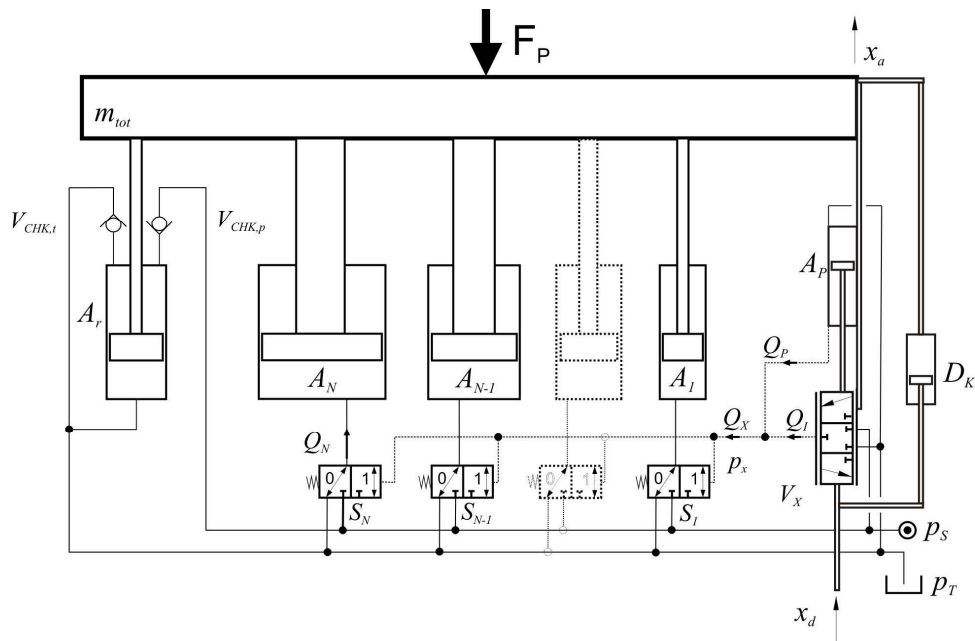
In this paper a concept to realize a “closing concept” by means of check valves is presented and investigated by some case studies. The study is limited to systems with a binary cylinder stepping, since this poses the highest difficulties.

## 2. HYDRAULIC CLOSING CONCEPT FOR THE LDHA

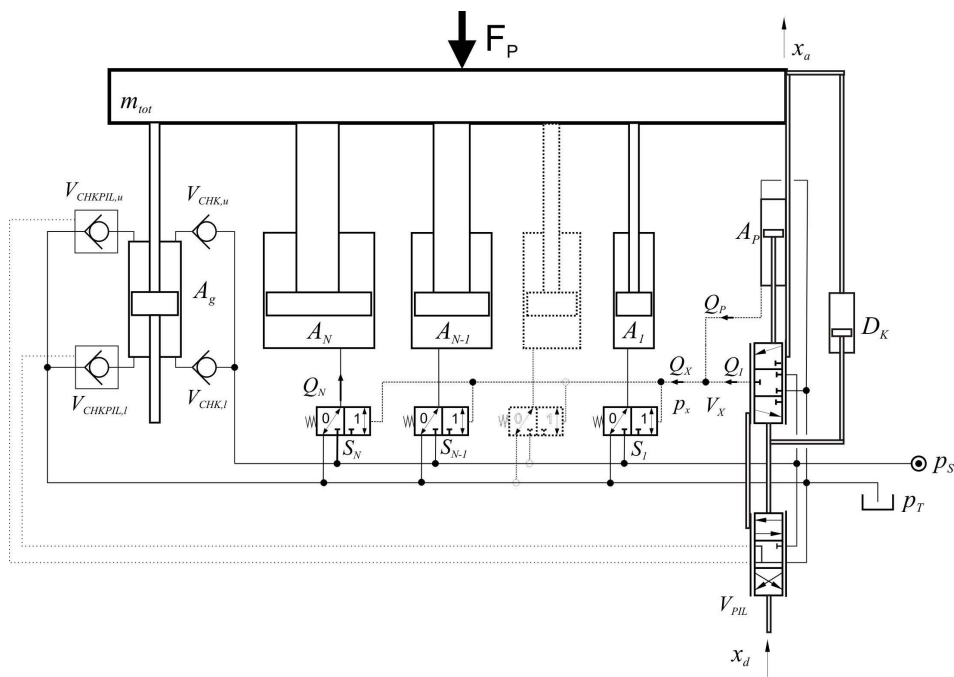
Basically, a closing concept could be realised by employing closed centre 3/3- way valves instead of the 3/2- way valves for  $S_1$  to  $S_N$  (see Fig. 1). This, however, conflicts with the dual switching concept in case of a binary stepping of the cylinders ( $A_i = A_1 \cdot 2^{i-1}$ ,  $i = 2 \dots N$ ), which requires a fast transition between the two switching states – the connection with tank or with pressure line.

The concept studied in this paper employs check valves which are placed either on one (the rod) side of an additional differential cylinder or on both sides of an additional double rod cylinder. The schematics of both variants are shown in Fig. 3. It has to be pointed out that the first variant with the differential cylinder can equivalently be

realized by placing the check valves in a similar fashion on the rod sides of one or more of the digital cylinders (those with piston areas  $A_1, \dots, A_N$  in Fig. 1).



(a)



(b)

Figure 3. Two variants of realizing a holding function for a LDHA; (a) check valves in a differential cylinder; (b) check valves in a double rod cylinder; check valves to tank line are piloted; pilot pressures and flow rates, respectively, are controlled by an additional proportional valve  $V_{PIL}$ .

The functioning principle is to provide a force dead band  $\Delta F_L$  which bridges the gap between two consecutive force steps of the digital cylinder system (see Fig. 4).

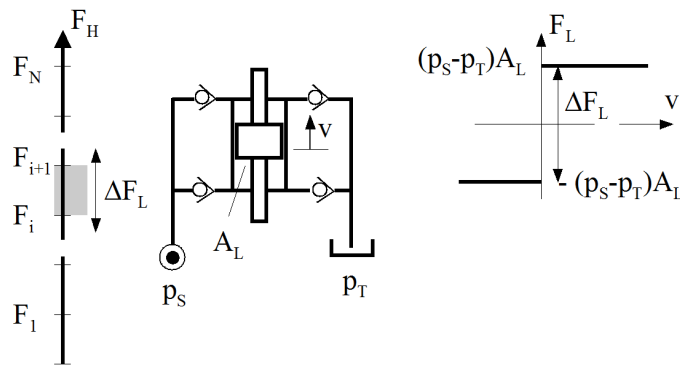


Figure 4. Function and realization of a holding element by a cylinder and by check valves; the force span  $\Delta F_L$  can be controlled by the system pressure and the cylinder area.

The double rod cylinder version as shown in Fig. 4 behaves symmetrically with respect to motions (velocity  $v$ ) up- and downwards. The differential cylinder version of the holding element according to Fig. 3 (a) provides only a holding force in one direction. From a static viewpoint  $\Delta F_L$  must be larger than the force step  $F_{i+1} - F_i$ . This element has the same characteristic as a dry friction element but without an intrinsic energetic loss. Of course, it limits the realizable maximum force of the digital drive by  $\Delta F_L / 2$ .

The holding force concept of Fig. 3 (b) employs an additional valve  $V_{PIL}$  and the check valves to the tank line are piloted.  $V_{PIL}$  is a valve with some overlap ( $x_{V,ov}$ ) and is controlled by the position control error  $x_d - x_a$ . This measure serves two purposes:

1. The holding force shall exist only in standstill around the desired position in order not to impair the force capacity of the digital cylinder arrangement. The span of the control error where  $V_{PIL}$  is active is controlled by the valve overlap value  $x_{V,ov}$ .
2. As a means to reduce the problem of oscillations which result from the dynamics of the whole system close to a rest position.

### 3. DYNAMIC BEHAVIOUR OF THE LDHA WITH THE HOLDING ELEMENT

The dynamic behaviour of a LDHA drive equipped with such a holding element is quite complex, since the system is hybrid with several continuous and discrete states. In the sequel a simulation study is presented for the two concepts shown in Fig. 3. For this purpose Matlab/Simulink models were established. They comprise

1. the linear equation of motion of the load (total mass of all moved parts  $m_{tot}$ ) driven by the hydraulic forces of all cylinders against a constant process force  $F_P$ ; the holding force is resulting from pressures in the holding cylinder;
2. pressure build up equations in all hydraulic cylinders and in the control line (pressure  $p_x$ );
3. the hydraulic displacements of all cylinders and of the valves  $S_1$  to  $S_N$ ;



4. the characteristic of the special valves  $S_1$  to  $S_N$  which employ an internal position feedback (see [1] and Fig. 5, respectively); each valve's position is derived from its spool's equation of motion;
5. the piloted check valves' ( $V_{CHKPIL,u,o}$ ) dynamical behaviour, guided by equations of motion of their poppets and by the pressure build-up equation in the pilot line as well as the dynamical behaviour of the check valves of the differential cylinder system ( $V_{CHKt,s}$ ) and their equations of motion; the normal check valves ( $V_{CHK,u,l}$ ) have been treated as having immediate response but with some pressure loss according to their nominal flow rate values;
6. the action of the control valves  $V_x$  and  $V_{PIL}$ , guided by the orifice equation;  $V_x$  and  $V_{PIL}$  are overlap valves.

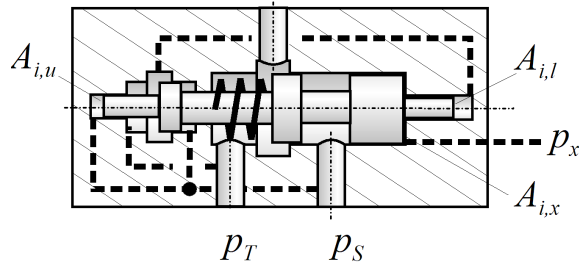


Figure 5. Switching valve with hysteretic behaviour employing position feed-back

The test case is a ramp like motion, the key figures of which are shown in Fig. 6 and in Table 1, respectively. Fig. 6 sketches also the values for quantifying the final position error. The system's final state may be actually a rest position  $x_{a,end}$  with some deviation  $e$  from the desired end position  $x_{d,end}$  or, due to instabilities, an oscillatory motion around some average position  $\bar{x}_{a,end}$ , defined as follows

$$\bar{x}_{a,end} = \frac{1}{0,3 s} \int_{T_{end}-0,3s}^{T_{end}} x_a(t) dt . \quad (1)$$

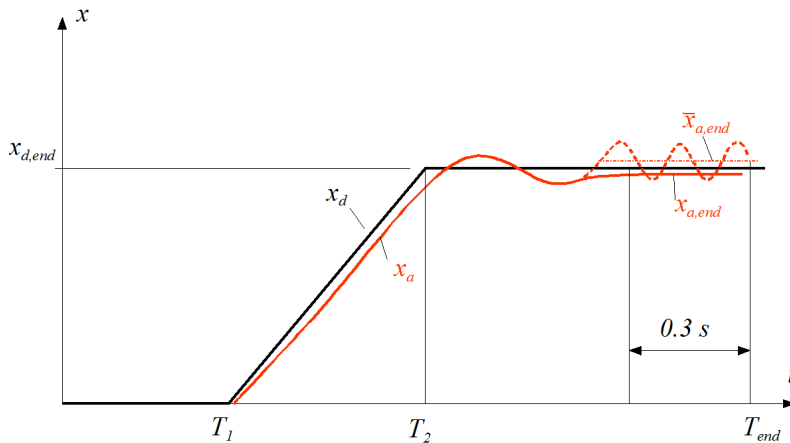


Figure 6. Test case is a ramp motion; definition of error

The error  $e$  is defined as follows.

$$\begin{aligned}
\text{In case of a non oscillating final position:} \quad e &= +|x_{d,end} - x_{a,end}|, \\
\text{In case of an oscillating behaviour:} \quad e &= -|x_{d,end} - \bar{x}_{a,end}|.
\end{aligned} \tag{2}$$

The system parameters used in this simulation study are listed in Tab. 1.

*Table 1. List of system parameter values of the simulation study*

Tank pressure	$p_T$	1 bar
System pressure	$p_S$	300 bar
Ramp start time	$T_1$	0.1 s
Ramp end time	$T_2$	0.43 s
Simulation end time	$T_{end}$	5 s
Ramp stroke	$x_{d,end}$	0.2 m
Proportional control flow	$Q_P$	0.12 l/min @ $ \dot{x}_a - \dot{x}_d  = 0.1$ m/s
Integral control flow	$Q_I$	0.05 l/min @ $ x_a - x_d  = 0.01$ m with $\Delta p = 5$ bar
Total mass	$m_{tot}$	100 kg
Damping constant	$D_K$	200 kNs/m (damper force limited to 4.6 kN)
Cylinder areas	$A_1 \dots A_4$	1 cm <sup>2</sup> , 2 cm <sup>2</sup> , 4 cm <sup>2</sup> , 8 cm <sup>2</sup>
Nominal flow rates of switching valves	$Q_1 \dots Q_4$	12, 24, 48, 96 l/min @ $\Delta p = 5$ bar
Cracking pressure for check valves $V_{CHKPILu,o}$ and $V_{CHKt,s}$	$p_{crack}$	5 bar

This error was evaluated for various combinations of the system parameters valve overlap  $x_{V,ov}$ , the process force  $F_p$ , the holding cylinder areas  $A_r$  and  $A_g$  and the nominal flow rate  $Q_{NOM,CHK}$  of the check valves  $V_{CHKt,s}$ ,  $V_{CHKl,u}$  and  $V_{CHKPILu,o}$ . Fig. 7 shows these error values for several parameter combinations and for the holding concept with the differential cylinder (Fig. 3 (a)) represented by plots over  $F_p$  and  $x_{V,ov}$ . The shaded surface in the plots is the zero error plane. Values below mean an oscillatory behaviour, above a stable rest position. Fig. 8 shows the same for the extended holding system with the double rod cylinder and the piloted check valves (Fig. 3 (b)).

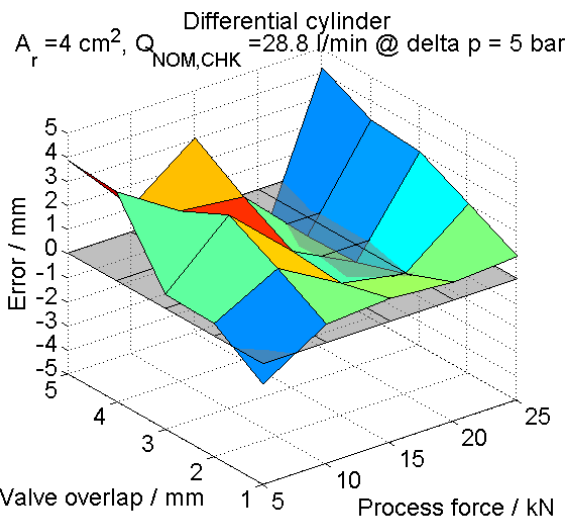
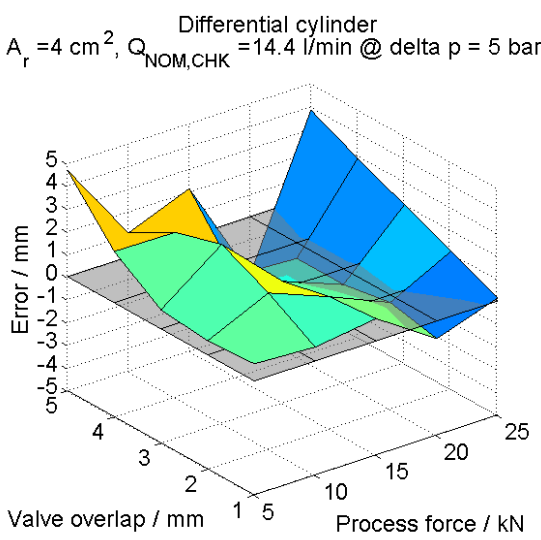
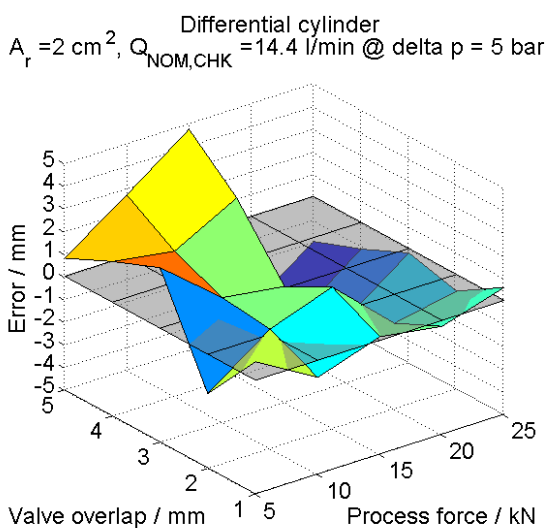
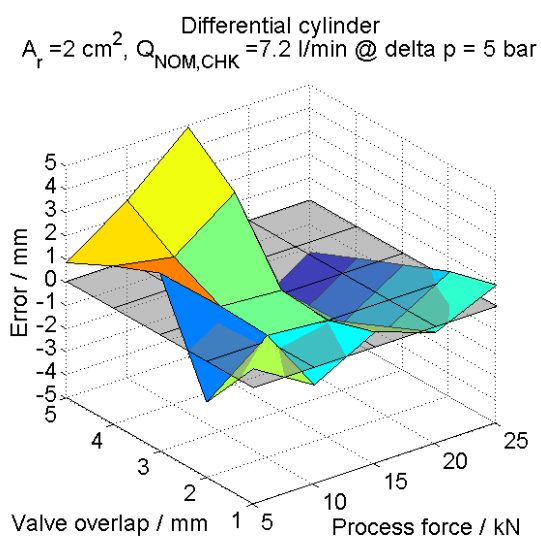
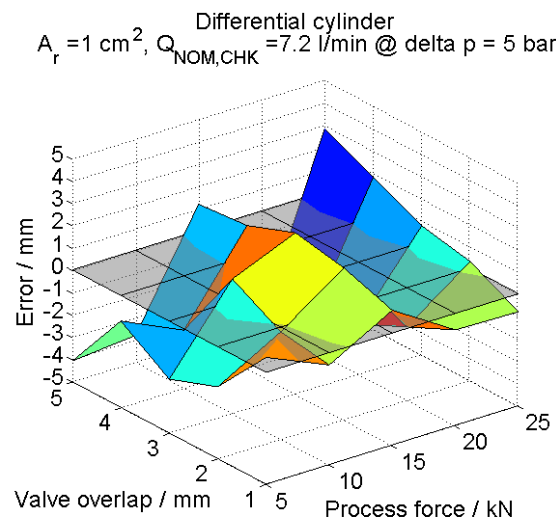
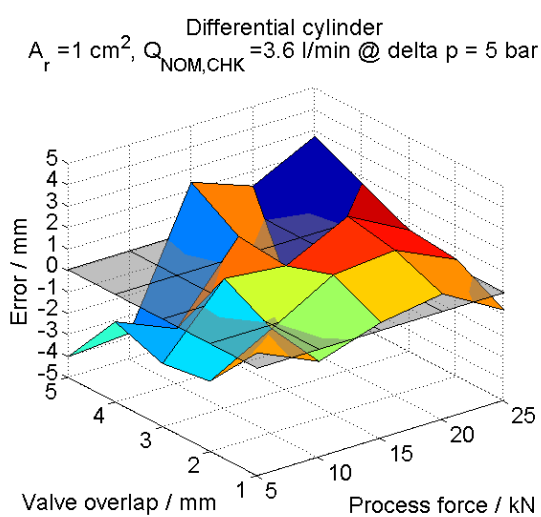


Figure 7. Steady state error  $e$  as defined in Eq. (2) for various parameter combinations for the holding concept differential cylinder (Fig. 3 (a)).

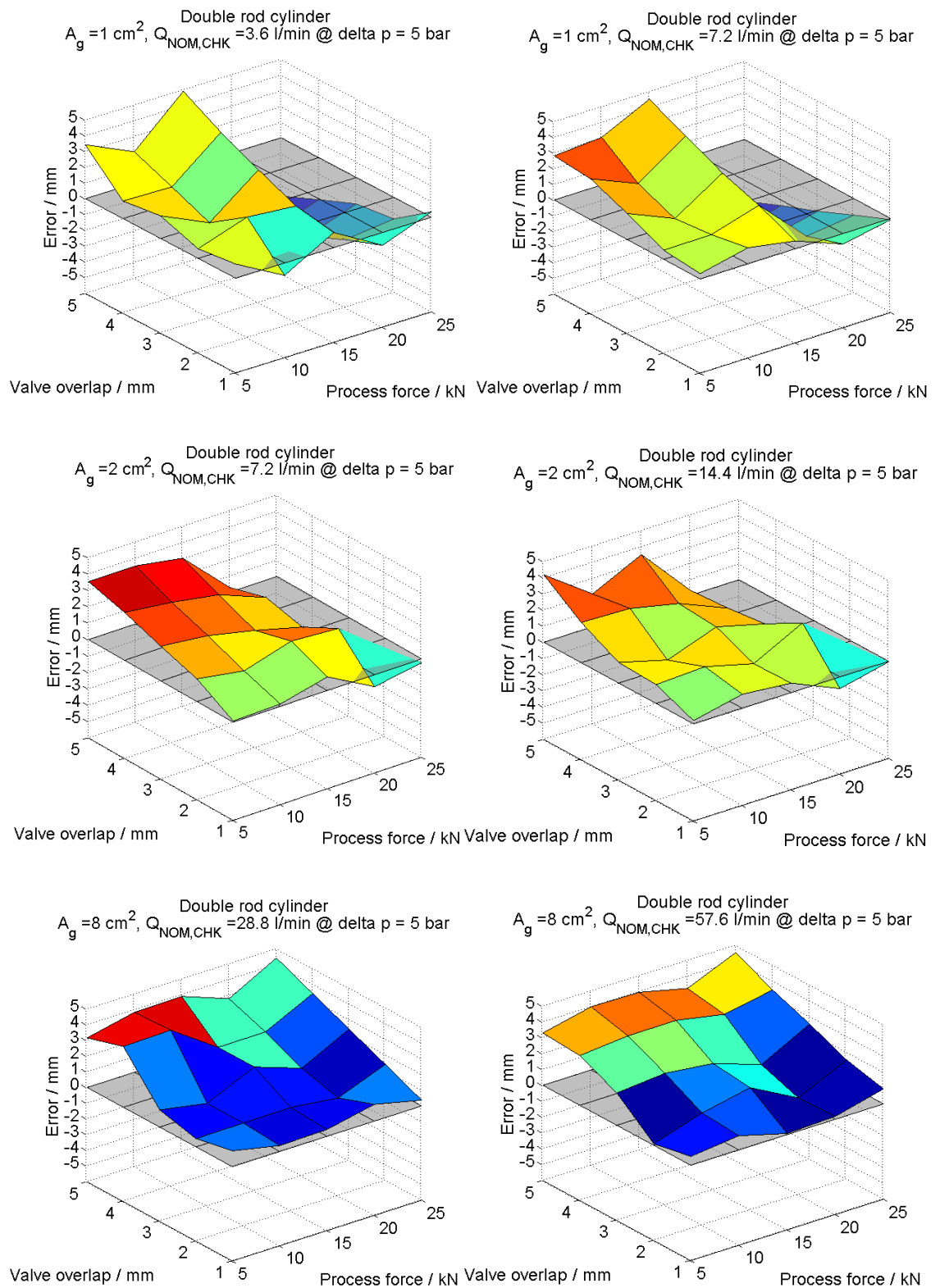
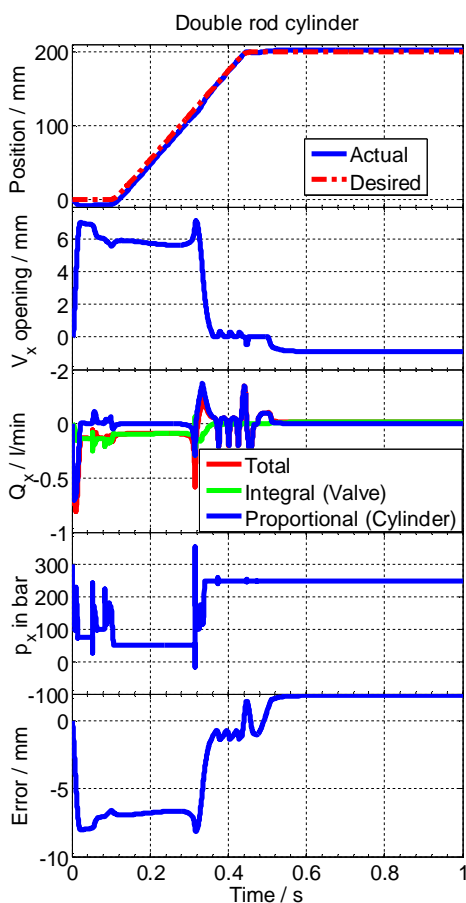


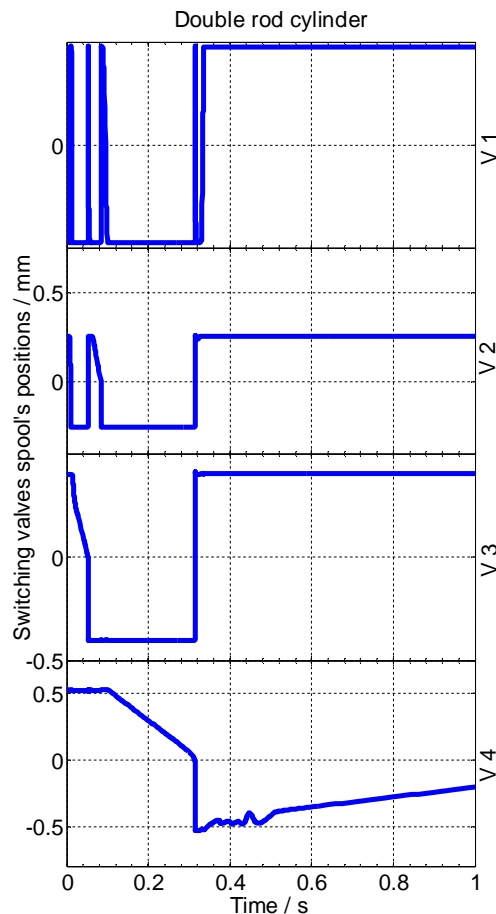
Figure 8. Steady state error  $e$  as defined in Eq. (2) for various parameter combinations for the holding concept with a double rod cylinder and piloted check valves (Fig. 3 (b)).

The conclusions from these results are:

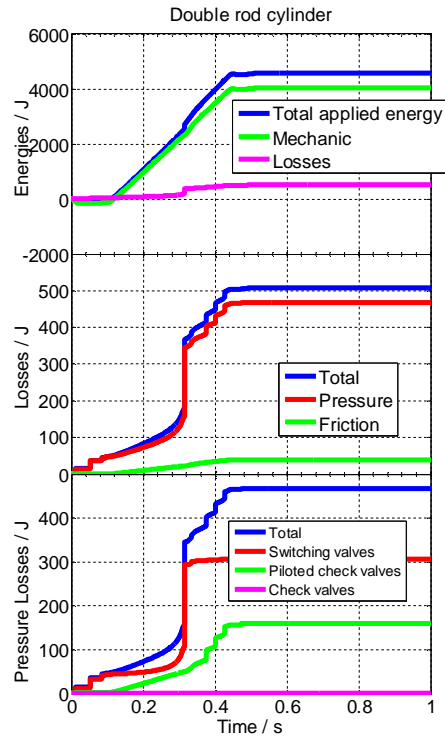
- The resulting error does not show a simple trend concerning the influence of the process force  $F_p$ . Zones with a quite stable behaviour are separated by zones with a tendency towards instability. These zones are around process force values which correspond to binary jumps of the digital hydraulic system, i.e. where the system switches between 3 and 4, 7 and 8. Here, the corresponding force levels are 12 and 24 kN, respectively. The presumable cause for this destabilization is that the state change effort of the corresponding valves causes a stronger delay time which makes the system to overshoot the position tolerance band.
- A higher valve overlap  $x_{V,ov}$  tends to make the system more stable but to increase the steady state error  $e$ .
- The area of the holding cylinder has a positive influence on stability but at the cost of a reduced hydraulic force. The latter statement is only true in the simple case without the piloted check valves and the extra control  $V_{PIL}$ .
- The additional control valve  $V_{PIL}$  improves the stability and avoids the problem of hydraulic net force reduction by the holding sub-system. However, it increases cost and system complexity.



(a)

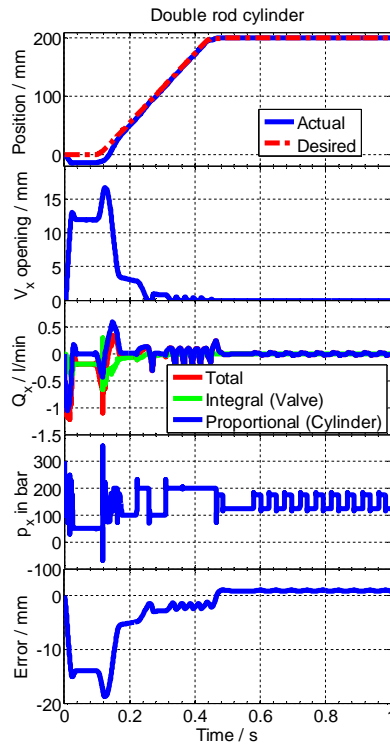


(b)

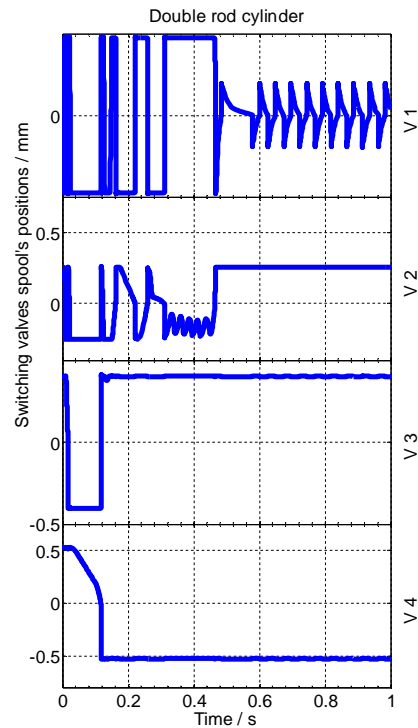


(c)

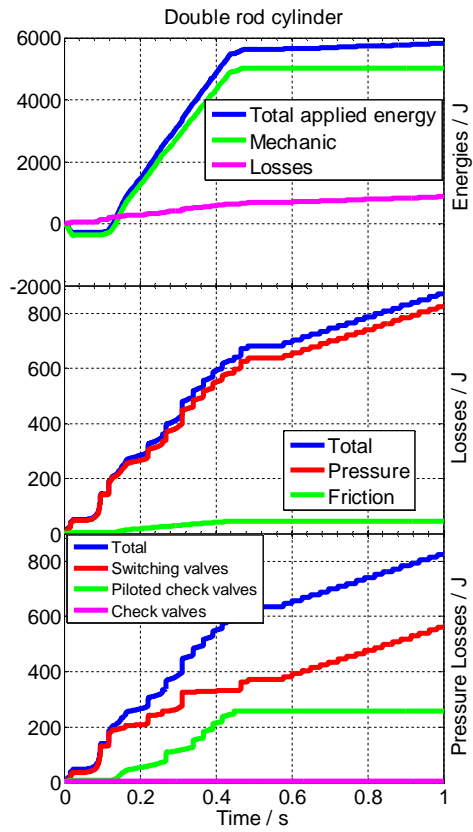
Figure 9. a,b,c: Double rod cylinder simulation results ( $A_g = 4 \text{ cm}^2$ ,  $Q_{NOM,CHK} = 14.4 \text{ l/min}$ , valve overlap = 1 mm,  $F_P = 20 \text{ kN}$ )



(a)

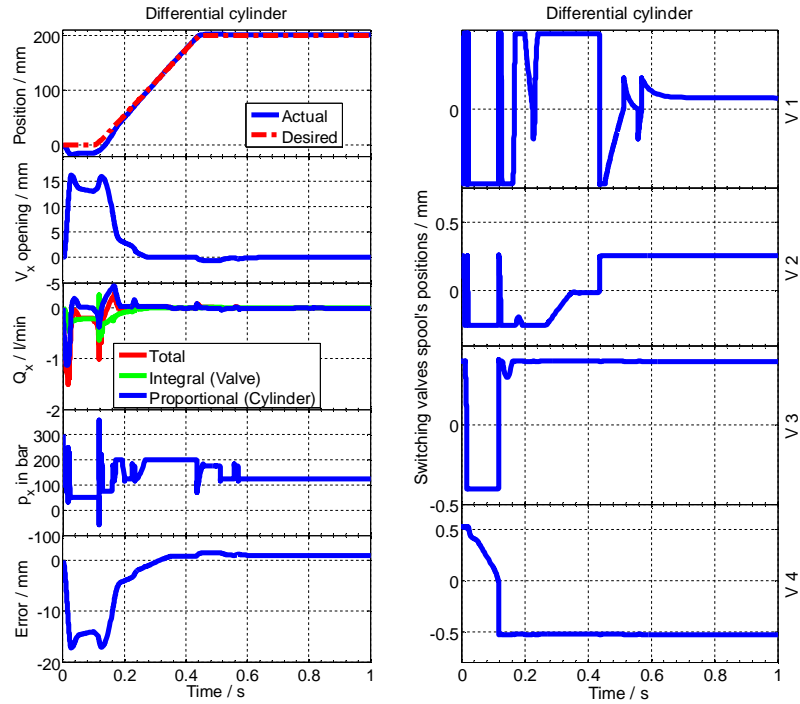


(b)



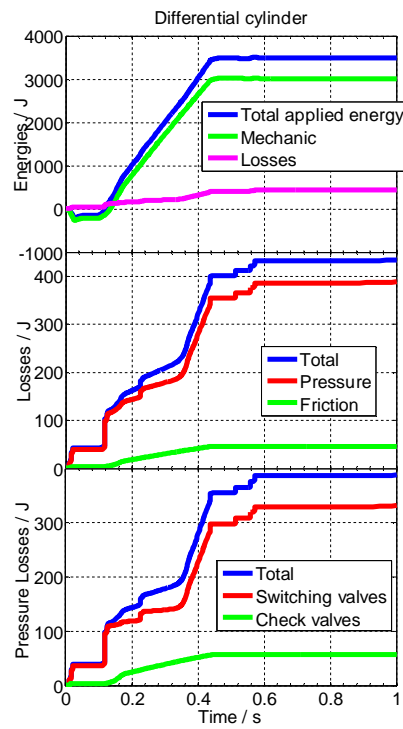
(c)

Figure 10. a, b, c: Double rod cylinder simulation results ( $A_g = 4 \text{ cm}^2$ ,  $Q_{NOM,CHK} = 14.4 \text{ l/min}$ , valve overlap = 2 mm,  $F_P = 25 \text{ kN}$ )



(a)

(b)



(c)

Figure 11. a, b, c: Differential cylinder simulation results ( $A_r = 4 \text{ cm}^2$ ,  $Q_{NOM,CHK} = 14.4 \text{ l/min}$ , valve overlap = 1 mm,  $F_P = 15 \text{ kN}$ )



Fig. 9 to Fig. 11 show plots of several system states obtained from the simulation runs for both types of holding systems. Two cases (Fig. 9 and Fig. 11) are stable and one is unstable (Fig. 10). In the unstable case one valve (V1) does a permanent periodic switching. This costs energy as can be seen in Fig. 10, c. If such a drive would have to hold a rest position for a long time the energy saving effect of the digital cylinder drive could be overcompensated by these “holding losses”. In addition, a small vibration occurs (in the simulated case of Fig. 10 with a frequency of approx. 25 Hz) which, though the velocity amplitudes are quite small, could be harmful or annoying and, therefore, is unacceptable.

#### 4. SUMMARY AND CONCLUSION

Two concepts to stabilize a linear digital hydraulic amplifier’s rest position by means of check valves have been presented. The first one just takes ordinary check valves and places these valves on one side of an additional differential cylinder or on the rod sides of one or more of the digital cylinders. The second employs an additional open centre and overlapped control valve which pilots two piloted check valves placed on the tank lines of a double rod cylinder. With both concepts a rest position can be stabilized statically. Dynamically, however, a complex stability problem arises resulting from the interplay of the digital hydraulic system with the check valves based holding device.

This stability problem was investigated by a numerical model in Matlab/Simulink for the case of a binary cylinder stepping drive. The test case was a ramp like motion. The results taught that the binary stepping is a severe problem in the sense that at those force levels where a binary jump arises and many valves have to change states, the resulting time delay endangers stability. By trend, measures that help to stabilize increase the energetic losses.

It has to be pointed out that this difficulty in avoiding instability at rest positions is mainly coming from the pure hydro-mechanical control principles of the linear digital hydraulic amplifier. With electronic control more freedom is given to obtain stability. However, the concept to employ ordinary or piloted check valves as simple means to generate an additional force for closing the gap between the finite force steps of a digital cylinder drive in rest position, may be also useful for electronically controlled digital cylinder drives.

#### REFERENCES

- [1] Biedermann I., Scheidl R., Plöckinger A. 2011. A Linear Digital Hydraulic Amplifier. Proceedings of the Fourth Workshop on Digital Fluid Power, 21-22 September, 2011, Linz, Austria, pp. 75-89.
- [2] Biedermann I. 2012. Konzeption und rechnerische Analyse einer Klasse digitaler hydraulischer Linearverstärker. Master thesis, Johannes Kepler University Linz, July 2012.

## COMPARISON AND EVALUATION OF DIGITAL CONTROL METHODS FOR ON/OFF VALVES

Dipl.-Ing. Ingo Schepers  
Dr.-Ing. Daniel Weiler  
Bosch Rexroth AG  
Industrial Hydraulics, Innovations  
97816 Lohr am Main, Germany  
Email: ingo.schepers@boschrexroth.de

Prof. Dr.-Ing. Juergen Weber  
Dresden University of Technology  
Institute of Fluid Power  
01062 Dresden, Germany

### ABSTRACT

Digital hydraulics opens a lot of possibilities to use and combine on/off valves. For example a number of parallel connected on/off valves per metering edge can be used. In this article only one on/off valve per metering edge is used. To imitate a 3-way directional valve four 2-way on/off valves can be used. To control this on/off valve configuration digital control methods are needed. In this article the most reasonable digital control methods will be introduced and compared. The most promising digital control methods will be compared more detailed.

**KEYWORDS:** Digital hydraulics, digital control methods, OPM, PWM, on/off valve

### 1. INTRODUCTION

Using on/off valves for control functions is already realized in different applications. For the former anti-lock braking system on/off valves were used for example. So the possibilities to use on/off valves for the anti-lock braking system or for other applications of the car industries were investigated by [1] until 1995 or [2] until 1984 as an example. At the moment the Technical University of Tampere and the Johannes Kepler University of Linz are investigating e.g. on/off valves or control methods for the digital hydraulics. 2011 a state of the art paper of the digital hydraulics was written by [3]. In this paper the digital fluid power is defined as:

*“Digital Fluid Power means hydraulic and pneumatic systems having discrete valued component(s) actively controlling system output.”*

This definition shows that Digital Fluid Power and also digital hydraulics covers a number of possibilities of different solutions. First at all the number of on/off valves per metering edge can be chosen. Secondly the metering edges can be independent or not. Depending on this different control strategies are needed.

Using one on/off valve per metering edge the pulse width modulation (PWM) is usually used in the digital hydraulics. In the pneumatics the pulse frequency modulation (PFM) is commonly used. Another digital control method, proposed by [4] is the optimized pulse modulation (OPM), which has a model based approach. Among other things these three different digital control methods will be compared in this paper.

## 2. DIGITAL CONTROL METHODS

An on/off valve has only two static states called activated and deactivated. Depending on the construction of the on/off valve the deactivated state can represent a closed valve, then it is called normally closed or an opened valve. In this case it is called normally open. In this paper only normally closed on/off valves are used, so the deactivated state represents the closed on/off valve and activated state represents opened on/off valve.

The command signal for the on/off valves can be a digital signal as also shown in Figure 1. The digital command signal is an alternating signal between logical zero and logical one. The length of the duration, when the signal is one is called pulse time  $t_i$ . Corresponding to the pulse time the duration, when the command signal is zero, is called pause time  $t_p$ . The command signal differs a lot to command signal of directional valves. That signal is continuously and not alternating.

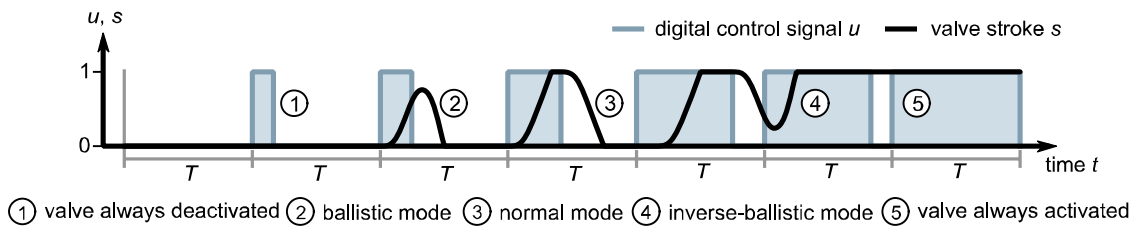


Figure 1. Behavior of a on/off valve controlled by a digital command signal

Varying the pulse time and the pause time, the on/off valve behaves in a specific way, that was also observed by [1, 2, 5] and is also shown in Figure 1. Short durations of the pulse time  $t_i$  are neglected by the on/off valve, so the valve is always closed ①. If the duration of  $t_i$  will be increased, the on/off valve opens. But the duration is as short as the valve cannot open fully. This mode is called ballistic mode ②. Go on increasing the duration of  $t_i$  leads to the result that the on/off valve can open fully. This mode is called normal mode ③. Corresponding to the ballistic mode an inverse ballistic mode ④ exists. In this mode the duration of the pause time  $t_p$  is as short as the on/off valve cannot close fully. If the duration of  $t_p$  is very short no reaction of the valve can be observed.

The digital control signal is a combination of following periods. One period is defined as the sum of the duration of the pulse  $t_i$  and the pause  $t_p$ :

$$T = t_i + t_p. \quad (1)$$

In principal the duration of the pulse  $t_i$  and the pause  $t_p$  can be varied, so that  $t_i$  and  $t_p$  are the control variables. A lot of digital control methods have only one control variable so a second equation with exceptional these three equation variables is needed. The digital control methods with one control variable will be compared in this paper. In the

following the most reasonable equations will be derived and the corresponding digital control method introduced.

One possibility for a second equation is  $T = \text{const}$ . The corresponding digital control method is the PWM. When the period  $T$  is constant, the duration of the pulse  $t_i$  is the control variable as an example and the duration of the pause  $t_p$  will be calculated. The second possibility for the second equation is  $t_i = \text{const}$ . This digital control method is called the pulse frequency method (PFM). The duration of the pause  $t_p$  is the control variable and the period  $T$  can be calculated. As the third possibility of the second equation the duration of the pause  $t_p = \text{const}$ . This control method is called in this paper the inverted pulse frequency modulation (invPFM). The control variable is the duration of the pulse  $t_i$ . The fourth possibility of the second equation is  $g = t_i/T = \text{const}$ .  $g$  is also known as the duty cycle. In this paper this digital control method is called the duty cycle frequency method (DFM). At the DFM the duration of the pulse  $t_i$  is the control variable. The period  $T$  and the duration of the pause  $t_p$  can be derived with the two equations. The second possibility of the setting a fraction constant is inverted to the DFM and will be neglected in the comparison  $t_p/T = 1 - t_i/T = 1 - g = \text{const}$ . At the DFM the ratio between the pulse duration and the period is constant, so the ratio between the pulse duration and the pause duration is also constant. So the behavior of a digital control method with a second equation of  $t_i/t_p = \text{const}$ . will be the same to the DFM. The fifth control method is the optimized pulse modulation (OPM) introduced by [4, 6]. In this control method the duration of the pause is dependent of the pulse duration. The target of that digital control method is, to ensure, that

1. the on/off valve is always closed at the end of one period,
2. the pause is as short as possible, without neglecting claim one,
3. the duration of the pulse is as long as leads to a hydraulic reaction.

Claim one is the most important one, because the on/off valve has a no sensor, so that the position of the piston cannot be detected. Without any possibility of measuring the position of the piston, the piston must start from a defined position. To ensure that the on/off valve is closed a robust – parameter can be included. This parameter enlarge the duration of the pause as shown in Figure 2

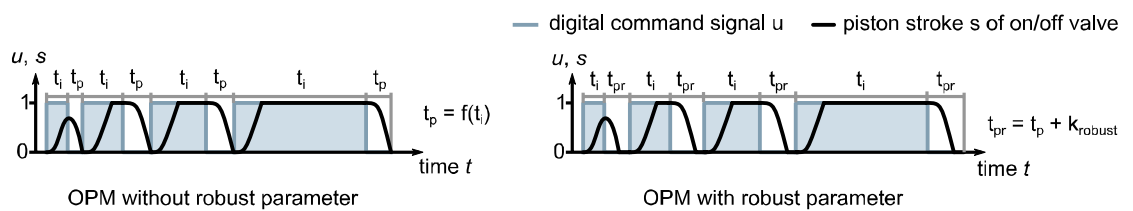


Figure 2. OPM modulated signal and piston stroke of a switching valve [4]

Of course other equations can lead to more digital control methods. But a lot of them will lead to similar digital control methods like the presented ones. The digital control methods, which are compared in this paper, fix one of the variables  $T$ ,  $t_i$ ,  $t_p$ , the fraction of  $t_i/T$  or  $t_p$  is a function of  $t_i$ . The model that is used for the comparison was introduced in [5].

### 3. MODEL OF THE ON/OFF VALVE

There are some requirements to the simulation model for analyzing and comparing the five digital control methods, mentioned in section 2. In the literature different simulation models can be found, which are used in the past. The models had different accuracies. The simplest simulation model just follows the control signal as also shown in Figure 3 (A). This can be used when switching times have no relevant influence compared to the pulse time. A simulation model with a time delay and different switching times as shown in Figure 3 (C) was used by [7]. More detailed is the simulation model that have different switching times and different dead times (D).

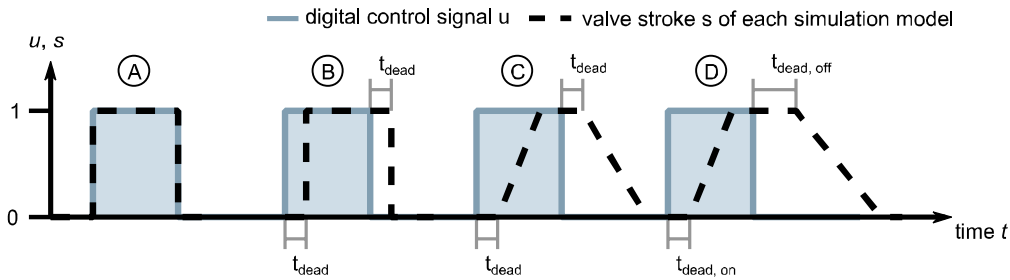


Figure 3. Simulation models for on/off valves with different levels of detail

Due to analyzing the digital control methods for digital hydraulics the model must satisfy some special requirements. But all these models shown in Figure 3 do not represent all requirements to compare the digital control methods. These requirements are:

1. Represent different switching on and off times
2. Represent different “dead times” for switching on and switching off
3. Represent that short durations of pulse time are neglected by the on/off valve
4. Represent that short duration of pause time are neglected by the on/off valve
5. Represent the five modes shown in Figure 1
  - a. valve is always closed (1)
  - b. ballistic mode (2)
  - c. normal mode (3)
  - d. inverse ballistic mode (4)
  - e. valve is always opened (5)
6. Represent a smooth transition between the ballistic mode and the normal mode
7. Represent a smooth transition between the inverse ballistic mode and the normal mode

All these requirements are covered by the novel model, which was introduced by [5]. This model is divided in two parts: the dynamic part and the hydraulic part. The hydraulic part contains e.g. the shape of the piston and other geometric parameter like the diameter. The hydraulic part also contains the type of the on/off valve e.g. directional seat valves or directional spool valves.

The dynamic part contains the switching behavior and all the mentioned requirements. The functionality of the valve is shown in Figure 4. The control signal is a digital command signal. When the valve is fully closed and the command signal switches from logical zero to logical one for the duration less than  $t_{i,min}$  the valve does not move. Is the duration longer, the valve opens and operates first at all in the ballistic mode. If the

duration of the pulse time  $t_i$  is longer than the switching on time  $t_{on}$  than the valve is fully open. Analog to the opening behavior of the valve is the closing behavior of the valve. The duration, when the valve does not close, is called  $t_{p,min}$ . When the pause is shorter than the switching off time  $t_{off}$  then the simulation model operates in the inverse ballistic mode.

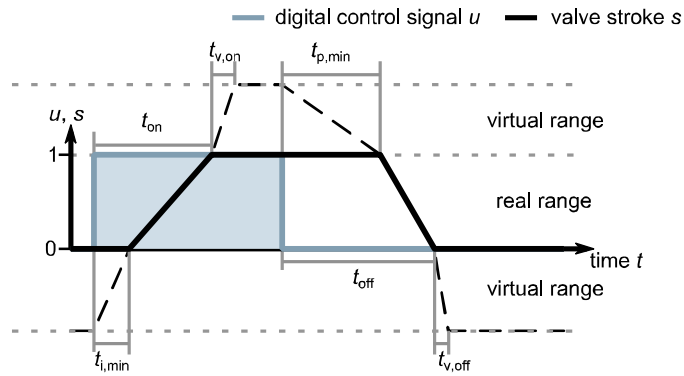


Figure 4. Novel model for the valve dynamics [5]

The virtual ranges realize that small pulses are neglected by the on/off valve as required in claim 3 and 4. Using a dead time would only lead to time lag of small pulses. If the simulation model operates in the virtual ranges there will be no movement of the piston. The real piston is either at the lower end stop or the upper end stop when a movement in one of virtual ranges exists. The parameter  $t_{v,on}$  is responsible to adjust the transition between the ballistic mode to the normal mode. Analog to the parameter  $t_{v,on}$ ,  $t_{v,off}$  adjust the transition between the inverse ballistic mode and the normal mode.

#### 4. BEHAVIOR OF AN ON/OFF VALVE IN OPEN LOOP

As mentioned the period  $T$  is the sum of the pulse time  $t_i$  and the pause time  $t_p$ . By varying the pulse time  $t_i$  and the pause time  $t_p$  the total operation range of a switching valve can be represented. Another possibility to display the total operation range is to use the duty cycle –frequency diagram as shown in Figure 5.

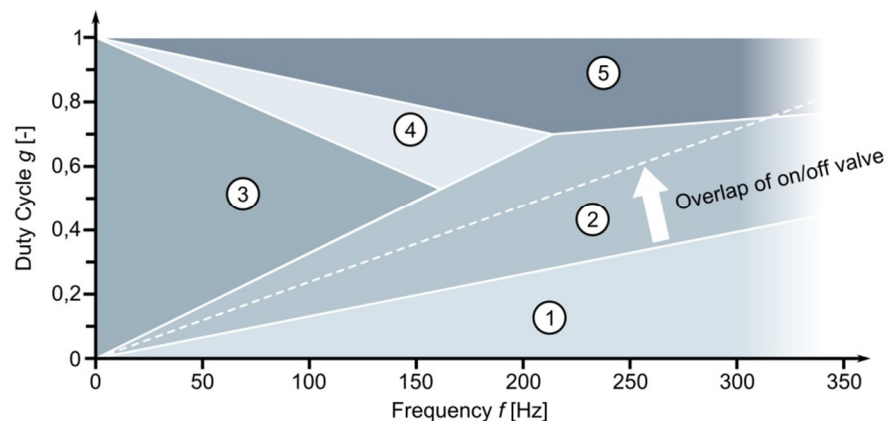


Figure 5. Duty cycle-frequency diagram of the analyzed valve

The frequency is calculated by

$$f = \frac{1}{T}. \quad (2)$$

The advantage of the diagram introduced by [5] is that the maximum of the duty cycle of is always one, independent from the frequency and the linear borders between the operation modes. The five operations modes called “the valve is always closed”<sup>①</sup>, “ballistic mode”<sup>②</sup>, “normal mode”<sup>③</sup>, “inverse ballistic mode”<sup>④</sup> and “the valve is always opened”<sup>⑤</sup> that were introduced in section 2 are also shown in Figure 5. The borders between the five operation modes are straight lines that are characterized by the parameters  $t_{i,min}$ ,  $t_{on}$ ,  $t_{p,min}$  and  $t_{off}$ . The following five formulas were derived by [5]. The border between mode <sup>①</sup> and mode <sup>②</sup> can be calculated by

$$g(f) = t_{i,min} \cdot f, \quad (3)$$

between mode <sup>②</sup> and mode <sup>③</sup> by

$$g(f) = t_{on} \cdot f, \quad (4)$$

between mode <sup>③</sup> and mode <sup>④</sup> by

$$g(f) = 1 - t_{off} \cdot f, \quad (5)$$

between mode <sup>④</sup> and mode <sup>⑤</sup> by

$$g(f) = 1 - t_{p,min} \cdot f. \quad (6)$$

The transition between mode <sup>②</sup> and mode <sup>④</sup> or mode <sup>⑤</sup> is characterized by two different straight lines. The one for lower frequencies correspond to the Eq. 5. The second part for higher frequencies can be calculated by

$$g(f) = f \cdot \frac{t_{i,min}(t_{off}-t_{p,min})}{t_{off}-t_{p,min}+t_{on}-t_{i,min}} + \frac{t_{on}-t_{i,min}}{t_{off}-t_{p,min}+t_{on}-t_{i,min}} \quad (7)$$

The analyzed valve has an overlap. So if you just have a look at the dynamic part the valve can operate in the ballistic mode without any hydraulic reaction. In this case the valve just moves in the overlap. The overlap of the analyzed valve is 50% of the piston stroke. The ballistic mode is divided in two parts of this overlap. In the part with the lower duty cycles the piston just moves in the overlap. In the second part the valve opens, too and is not moving only in the overlap. This border is characterized by a straight line with the intersection in the origin as shown in Figure 5.

#### 4.1. Static behavior of on/off valves controlled by digital control methods

In the duty cycle – frequency diagram the five digital control methods can be displayed as shown in Figure 6 to Figure 12. The four digital control methods PWM, PFM, invPFM and DFM are all straight lines in the duty cycle – frequency diagram. The OPM does not have a straight line in the duty cycle – frequency diagram because the digital control method is model based.

To create the data for the lines of the five digital control methods in the duty cycle – frequency diagram and the diagram of the normalized and averaged volume flow several simulations were done. In one simulation the control signal is for the whole time constant. That means e.g. for the PMW the duty cycle  $g = 0,5$  is constant for the whole

simulation. When the on/off valve reaches a static condition, the simulation will be stopped and the results were stored and marks one point in the diagrams. Static condition means in this case that the on/off valve behaves every period in the same way. The smallest duration of one pulse for the digital control methods is  $t_{i,dcm,min} = 2,4 \text{ ms}$ . This leads to a minimum duty cycle of

$$g_{dcm,min}(f) = t_{i,dcm,min} \cdot f. \quad (8)$$

Is the pulse shorter than the minimal pulse duration  $t_{i,dcm,min}$  no hydraulic reaction is observable at every digital control method, except the duration of the pause is very short. The minimum duration of the pulse was also chosen because the OPM does not allow shorter pulses, as defined in claim three of the OPM. So the comparability between the digital control methods is ensured. The duration of the pulse is increased by steps of  $0,1 \text{ ms}$  to the maximum duration of the pulse  $t_{i,dcm,max} = 31 \text{ ms}$ .

#### 4.1.1. Comparison of OPM and PWM

The second claim of the OPM is to optimize the pause, so that the duration is as short as possible without neglecting claim one, which ensures, that the on/off valve is always closed at the end of a period. The requirements of the two claims lead to the characteristic line that is shown in Figure 6. The OPM operates at the border between

- the normal mode ③ and the inverse ballistic mode ④,
- the ballistic mode ② and inverse ballistic mode ④ and
- the ballistic mode ② and the on off valve is always open ⑤.

The distance to the three mentioned borders depends on the chosen robust parameter, which enlarges the duration of the pause. The maximum duration of the pulse time  $t_{i,dcm,max} = 31 \text{ ms}$  leads to the maximum OPM period of  $T_{OPM,max} \approx 34 \text{ ms}$  or a minimum OPM frequency of  $f_{OPM,min} \approx 29,41 \text{ Hz}$ . The minimum duration of the pulse  $t_{i,dcm,min} = 2,4 \text{ ms}$  leads to a minimum OPM period of  $T_{OPM,min} \approx 3,3 \text{ ms}$  or a maximum OPM frequency of  $f_{OPM,max} \approx 303 \text{ Hz}$ . On the line of the OPM every marker represents a simulation. For small frequencies the simulations are close to each other. This is just the result of the chosen procedure: increasing the duration of the pulse by steps of  $0,1 \text{ ms}$  each simulation as mentioned above. So the percentage increasing per period is not linear.

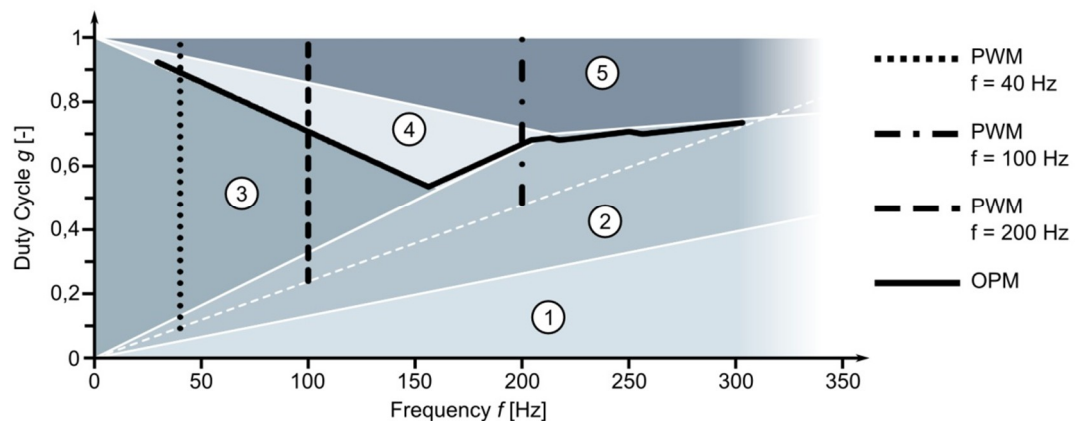


Figure 6. Comparison of OPM and PWM in the duty cycle frequency diagram



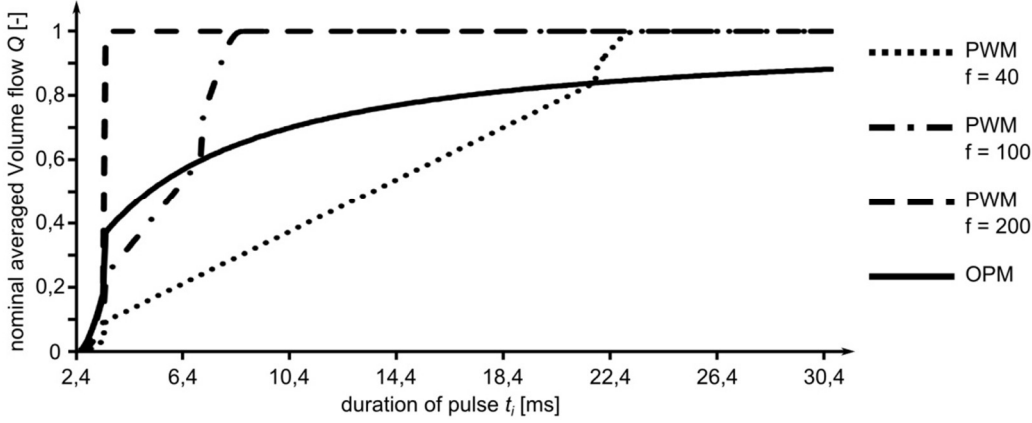


Figure 7. Comparison of OPM and PWM in the diagram of the normalized and averaged volume flow per period

The characteristic of the OPM for low frequencies is a straight line, which has an intersection with the ordinate at the value one, when the frequency would be  $f = 0 \text{ Hz}$  or the period has an infinity long duration. As long as the valve can open fully, the OPM operates at the border between the normal mode ③ and the inverse ballistic mode ④. Here the duration of the pause is constant, so the OPM is in this part characterized by

$$\begin{aligned}
 t_i &= T - t_{pr} \\
 g(f) &= \frac{t_i}{T} = t_i \cdot f = (T - t_{pr}) \cdot f \\
 g(f) &= 1 - t_{pr} \cdot f, \quad (9)
 \end{aligned}$$

where  $t_{pr}$  is the duration of the pause including the robust parameter. That no simulation between the frequency of  $156,25 \text{ Hz}$  and  $204,08 \text{ Hz}$  exist is the result of the behavior of the novel model, introduced in section 3 that is used for the on/off valve. In this case the used parameter  $t_{v,on} = 0,001 \text{ ms}$  is very short and leads to this step.

The PWM normally operates over the whole range of the duty cycle from zero to one. In this analysis the minimum pulse duration is set to  $t_{i,min} = 2,4 \text{ ms}$  as mentioned. So the on/off valve is always switching and a hydraulic reaction is observable at every period. To show a variation three different PWM frequencies are chosen:  $40 \text{ Hz}$ ,  $100 \text{ Hz}$  and  $200 \text{ Hz}$ . The duty cycles for the minimum pulse durations are  $g(40 \text{ Hz}) = 0,096$ ,  $g(100 \text{ Hz}) = 0,24$  and  $g(200 \text{ Hz}) = 0,48$ , which can be determined by Eq.8. Due to this constrain only the following duty cycles for the PWM are possible

$$\begin{aligned}
 g(f_{PWM}) &:= \in [t_{i,dcm,min} \cdot f_{PWM}, 1] \quad (10) \\
 \text{if } t_{i,dcm,min} \cdot f_{PWM} &< 1 \text{ with } t_{i,dcm,min} \in \mathbb{R}^+ \text{ and } f_{PWM} \in \mathbb{R}^+ \setminus 0.
 \end{aligned}$$

For small PWM frequencies a wide range of the normal ③ modes exists. The greater the PWM frequency the smaller is the normal mode ③ and the greater are the other four modes. The higher the PWM frequencies the smaller is also the usable range of the duty cycle, when using the on/off valve for control tasks. As an example the usable range for control tasks for a PWM frequency of  $f_{PWM} = 200 \text{ Hz}$  is just in the range between  $= 0,4 \dots 0,6$ . The usable range matches to the ballistic mode ②. This is very small compared to other PWM frequencies.

Another possibility to compare the OPM and the PWM is to plot the averaged and normalized volume flow  $\bar{Q}_{norm}$  over the pulse duration  $t_i$  as also shown in Figure 6. In this diagram the different ranges of the on/off valve can be identified too. When the duration of the pulse is longer than the period, the pulse duration is reduced to the maximum.

In the shown part of this diagram the OPM does not reach the maximum volume flow. The maximum volume flow just can be reached, when the pulse duration is infinity long. In claim one of the OPM is defined that the on/off valve has to be closed at the end of every period. So it is impossible to reach maximum averaged and normalized volume flow. The step at the duration of the pulse  $t_{i,OPM} = 3,3 \text{ ms}$  is the result of the chosen parameter  $t_{v,on} = 0,001 \text{ ms}$  which also leads to the step of the frequencies from  $156,25 \text{ Hz}$  to  $204,08 \text{ Hz}$ .

The curve of the PWM with  $f_{PWM} = 40 \text{ Hz}$  starts with the ballistic mode<sup>②</sup>. In the long linear range the on/off valve operates in the normal mode<sup>③</sup>, followed by the inverse ballistic mode<sup>④</sup>. When the normalized and averaged volume flow reaches the value one, the on/off valve is open for the whole period and operates in mode<sup>⑤</sup>. In this diagram the different sizes of the usable ranges also can be recognized. For the PWM frequency of  $f_{PWM} = 200 \text{ Hz}$  the usable range is very small as also identified in the duty cycle – frequency diagram. If any PWM will be used as the control method for the on/off valves, it is always possible to open the on/off valve for the whole period in contrast to the OPM.

#### 4.1.2. Comparison of OPM and invPFM

As shown in Figure 8 the invPFM is like the OPM frequency dependent. In this paper the invPFM is defined as  $t_{p,invPFM} = const.$  So the  $t_{p,invPFM}$  is the parameter, which can be chosen but that is constant during the control process. For the comparison with the OPM the pause duration of the invPFM  $t_{p,invPFM}$  is set to  $2 \text{ ms}$ ,  $3 \text{ ms}$  and  $5 \text{ ms}$ . The same formula as for the first part of the OPM, derived in Eq. 10, can be used to describe the characteristic of the line:

$$g(f) = 1 - t_{p,invPFM} \cdot f. \quad (11)$$

Comparing the invPFM with the OPM the digital control methods can be very similar. Using  $t_{pr} = t_{p,invPFM}$  the control methods behave in the same way on a wide range. Both have the same behavior when the on/off valve opens fully and operates in the normal mode<sup>③</sup>. In the ballistic mode<sup>②</sup> the control methods behave different. In this mode the duration of pauses are in the OPM as short as possible, but in the invPFM the duration of the pause is still constant. This is the reason why the OPM can operate in higher frequencies than the invPFM.

Using the invPFM it is necessary to know how the on/off valve behaves. If the pause  $t_{p,invPFM}$  is shorter than the switching off time of the on/off valve, the on/off valve operates on a wide range in the inverse ballistic mode<sup>④</sup> as shown in Figure 8 This is the case for  $t_{p,invPFM} = 2 \text{ ms}$ . Like in most configurations of the inv PFM, the invPFM with  $t_{p,invPFM} = 2 \text{ ms}$  operates also in the ballistic mode<sup>②</sup> when the pulses are small enough.

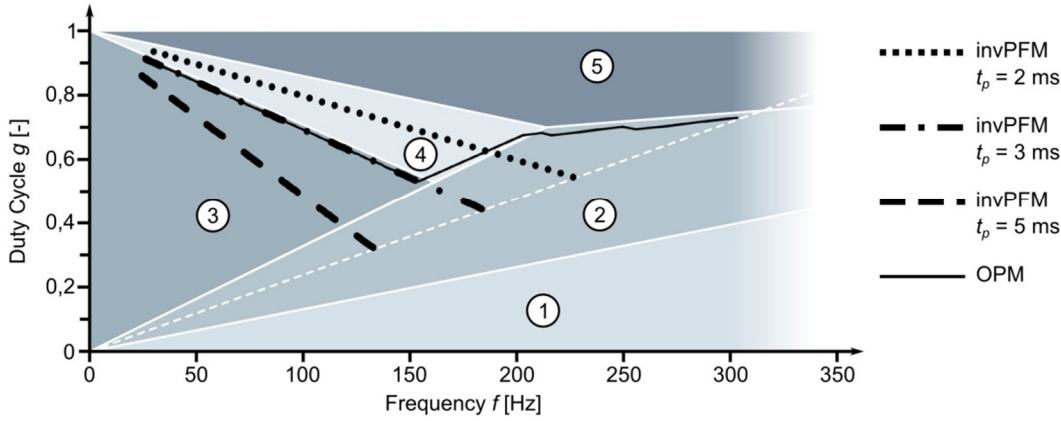


Figure 8. Comparison of OPM and invPFM in the duty cycle frequency diagram

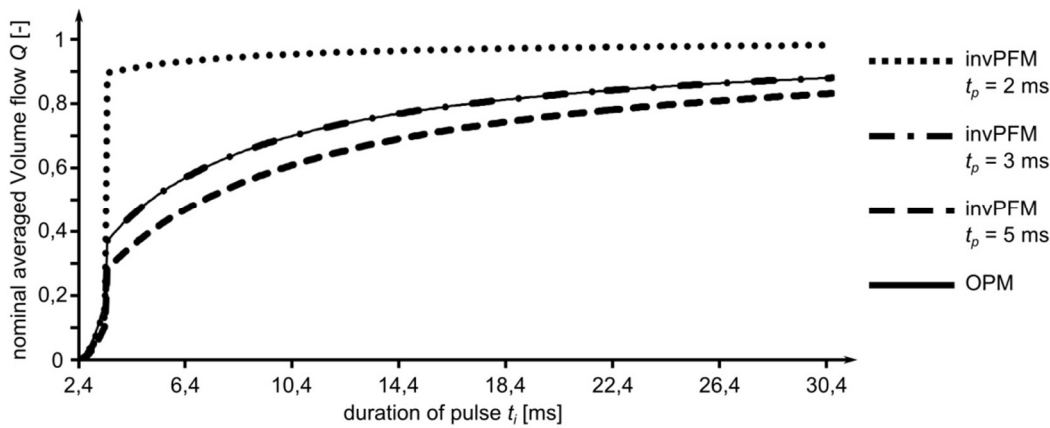


Figure 9. Comparison of OPM and invPFM in the diagram and of the normalized and averaged volume flow per period

If the pause  $t_{p,invPFM}$  is longer than the switching off time of the on/off valve, the on/off valve operates for a wide range in the normal mode<sup>③</sup>. The longer the pause is, the bigger is the distance to the border between the normal mode<sup>③</sup> and the inverse ballistic mode<sup>④</sup>. And the longer pause  $t_{p,invPFM}$  the smaller is the maximum frequency. The maximum frequency can be derived by the minimal duration of the pulse  $t_{i,dcm,min}$  and the chosen pause  $t_{p,invPFM}$

$$f_{invPFM,max} = \frac{1}{t_{i,dcm,min} + t_{p,invPFM}} \quad (12)$$

The maximum frequencies  $f_{invPFM,max}$  for the three chosen pauses of the invPFM  $t_{p,invPFM}$  of 2 ms, 3 ms and 5 ms leads to the maximum frequencies of approximately 227 Hz, 185 Hz and 135 Hz. The minimum frequency can be derived in the same way. Only the variable  $t_{i,dcm,min}$  must be replaced by  $t_{i,dcm,max}$ . This leads to the minimum frequencies of approximately 30 Hz, 29 Hz and 28 Hz.

Comparing the OPM with the invPFM in the normalized and averaged volume flow diagram almost no difference between the OPM and the invPFM can be observed. The invPFM with the pause duration  $t_{p,invPFM} = 2 \text{ ms}$  has a big step. This step is at the border from the ballistic mode<sup>②</sup> to the inverse ballistic mode<sup>④</sup>. A big step exists always at this border. The invPFM with a pause  $t_{p,invPFM} = 5 \text{ ms}$  has a smaller

normalized averaged volume flow than the one with a pause  $t_{p,invPFM} = 3 \text{ ms}$  because the pause is longer. The two graphs have the same characteristic except the step at the border from the ballistic mode<sup>Ⓜ</sup> to the normal mode<sup>Ⓝ</sup>. The longer the pause the smaller is the step at this border.

#### 4.1.3. Comparison of OPM and PFM

Any other digital control method of this paper controls the duration of the pulse except the PFM. Here the duration of the pulse is constant. The three chosen pulse durations  $t_{i,PFM}$  are  $2 \text{ ms}$ ,  $3 \text{ ms}$  and  $5 \text{ ms}$ . In case of the PFM the pause  $t_{p,PFM}$  will be controlled. The duration of the pause for the PFM corresponds to the duration of the pulse for the digital control methods  $t_{i,dcm}$ . If the PFM has a pulse of  $t_{i,PFM} = 2 \text{ ms}$ , the on/off valve only operates in the overlap as shown in Figure 10, so no hydraulic reaction can be observed. If the duration of the pulse is set to  $t_{i,PFM} = 3 \text{ ms}$ , the on/off valve is only operating in the ballistic mode<sup>Ⓜ</sup>. The PFM with  $t_{i,PFM} = 5 \text{ ms}$  operates over a wide range in the normal mode<sup>Ⓝ</sup>.

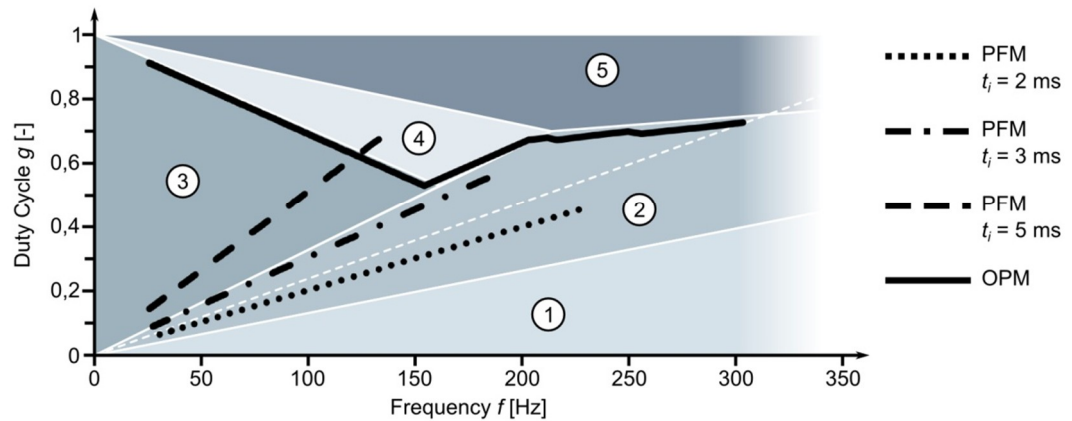


Figure 10. Comparison of OPM and PFM in the duty cycle frequency diagram

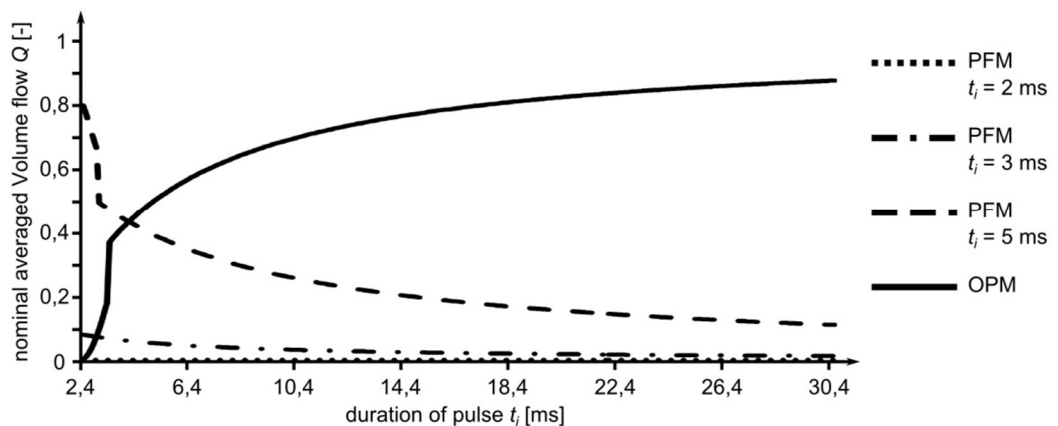


Figure 11. Comparison of OPM and PFM in the diagram and of the normalized and averaged volume flow per period

Analyzing the diagram of the normalized and averaged volume flow, the two PFM lines with durations of the pulse of  $t_{i,PFM} = 2 \text{ ms}$  and  $t_{i,PFM} = 3 \text{ ms}$  have no volume flow or the maximum volume flow is less than 10% to the volume flow, when the on/off valve

is always open. Only the PFM with a duration of the pulse of  $t_{i,PFM} = 5 \text{ ms}$  has normalized and averaged volume of  $\bar{Q}_{norm,PFM} = 0,5$ , that may be used for control tasks. But the high volume flow is at high frequencies, so the valve has to switch very often to realize high volume flows. And small volume flows just can be reached by generating a very long pause. The characteristic of the OPM and the PFM with  $t_{i,PFM} = 5 \text{ ms}$  seems to be inverted in the diagram of the normalized and averaged volume flow.

Trying to control a system with having always the same duration of the pulse leads to low control quality. In case of using small pulse duration the controlled actuator can be positioned very accurate, but the maximum volume flow is very low. Is the pulse duration longer so that the maximum volume flow is high enough the controlled actuator can not be positioned as accurate as with small pulse durations.

#### 4.1.4. Comparison of OPM and DFM

The DFM has a constant duty cycle. The chosen duty cycles are  $g_{DFM,1} = 1/3$ ,  $g_{DFM,2} = 1/2$  and  $g_{DFM,3} = 2/3$ . The DFM is a horizontal straight in the duty cycle frequency diagram. Depending on the chosen constant duty cycle the digital control method can operate in different modes. The maximum frequency is characterized by the minimum pulse duration for the digital control methods  $t_{i,dcm,min}$  and the chosen constant duty cycle

$$f_{DFM,max} = \frac{g_{DFM}}{t_{i,dcm,min}} \quad (13)$$

Analyzing the diagram of the normalized and averaged volume flow the DFMs with  $g_{DFM,1} = 1/3$  and  $g_{DFM,2} = 1/2$  are characterized by similar behavior to OPM in the ballistic mode<sup>②</sup>. Comparing the step of the DFM with  $g_{DFM,2} = 1/2$  and the OPM it has a similar characteristic, because the intersection between the ballistic mode<sup>②</sup> and the normal mode<sup>③</sup> is close to each other. If the DFM is operating in the normal mode<sup>③</sup> the range of controlling the volume flow is too small for control tasks. When the DFM has intersections with the border from the ballistic mode<sup>②</sup> to the inverse ballistic mode<sup>④</sup> or from the normal mode<sup>③</sup> to the inverse ballistic<sup>④</sup>, like the DFM with  $g_{DFM,3} = 2/3$ , the characteristics of the normalized and averaged volume has too many discontinuities. It is impossible to use an on/off valve for control tasks with one of these control methods.

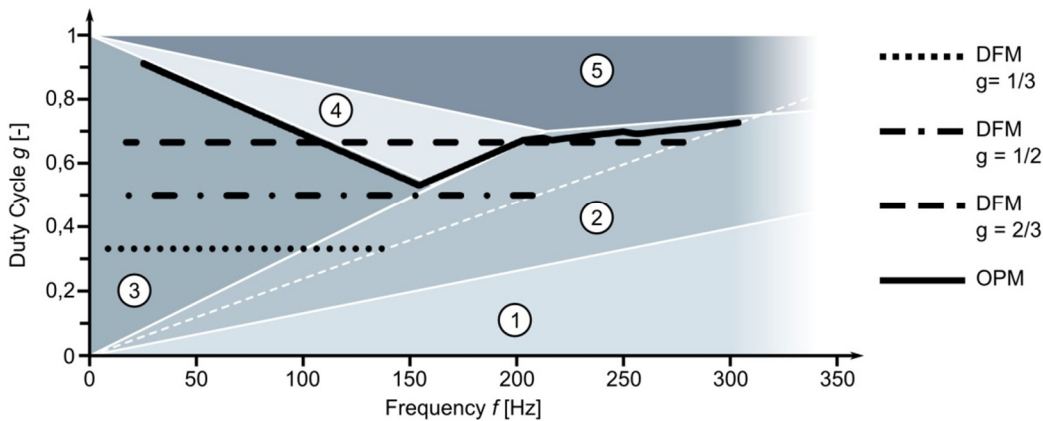


Figure 12. Comparison of OPM and DFM in the duty cycle frequency diagram

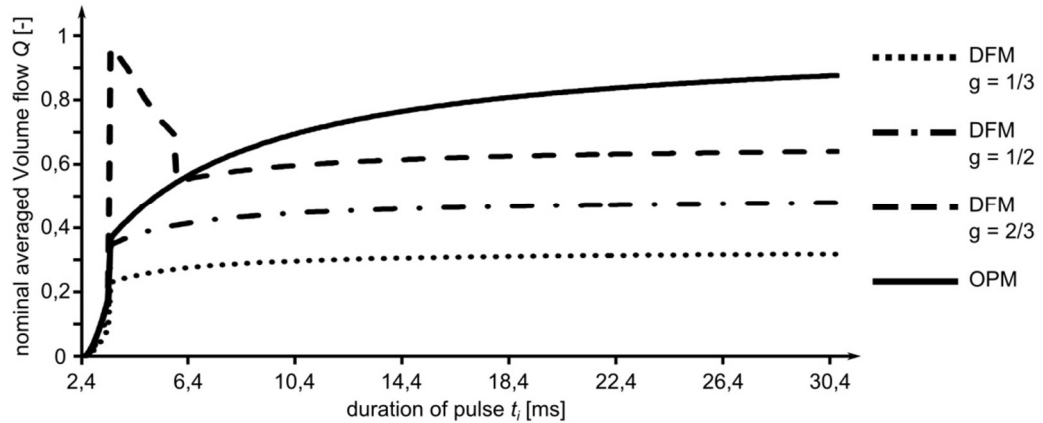


Figure 13. Comparison of OPM and DFM in the diagram and of the normalized and averaged volume flow per period

#### 4.1.5. Summary of the comparison of the digital control methods

The analysis of the digital control methods in the duty cycle – frequency diagram and the diagram of the normalized and averaged volume flow show that the DFM and the PFM is not usable for controlling a on/off valve in a configuration using only one on/off valve per metering edge. The PFM has the property that the pulse duration is constant. That leads to the conflict of accurate positioning and high volume flows, as described in section 4.1.3. The DFM has over a wide range the same averaged volume flow, so this digital control method also cannot be used for control tasks.

The invPFM can be used, when the parameter  $t_{p,invPFM}$  is chosen in the right way. Considering an ideal on/off valve that has no variation of the switching time and the switching behavior the invPFM with a pause of  $t_{p,invPFM} = 3 \text{ ms}$  can be used for the analyzed on/off valve, if it is used for control tasks. In general it means that  $t_{p,invPFM}$  correspond to the switching off time of the valve. The behavior is very similar to the OPM. The PWM can also not used with every PWM – frequency. High PWM – frequencies leads to high discontinuities. The discontinuities can lead to a low control quality. Low PWM – frequencies leads to a wide range of a linear correlation between the normalized and averaged volume flow. But the duration of one period might be very long. This lowers also the control quality, but this is detailed analyzed in section 4.2.

#### 4.2. Dynamic behavior of on/off valves controlled by digital control methods

For the dynamic analysis the PWM, the OPM and the PFM with  $t_{p,invPFM} = 3 \text{ ms}$  are chosen. In the diagrams of the normalized and averaged volume flow discontinuities are observable as shown in section 4.1.1 to 4.1.4. These discontinuities should be avoided by using the inverted lines of the normalized and averaged volume flow as shown in Figure 14. The input for the inverted characteristic line is the nominal signal. A normalized sine is chosen as the nominal signal for the dynamic analysis. This sine has the normalized amplitude of  $\hat{y}_{nom} = 0,4375$ , a mean level of  $y_0 = 0,4375$  and a frequency of  $f_{nom} = 1 \text{ Hz}$ . The amplitude was chosen so that the OPM and the invPFM can reach the maximum nominal volume flow  $y_{nom,max} = 0,875$ .

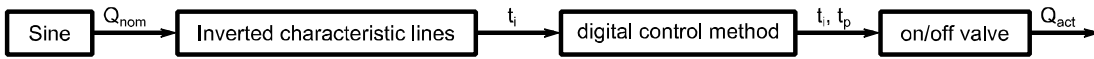


Figure 14. Structure of simulation for dynamic behavior

The PWM with a frequency of  $f_{PWM,3} = 200 \text{ Hz}$  cannot be used for control tasks as shown in Figure 15. This PWM has only a short range where the PWM follows the nominal signal. This range is just for small volume flows. After that the on/off valve opens almost fully for one period. In the range in that the PWM follows the nominal sine the on/off valve operates in the ballistic mode. Then there is a transition to the inverse ballistic mode as also shown in Figure 6. That is the reason of the discontinuity in Figure 15 of the PWM; the on/off valve opens almost fully for the whole period in the inverse ballistic mode. Only when the nominal value is zero the valve closes again and can follow the nominal sine.

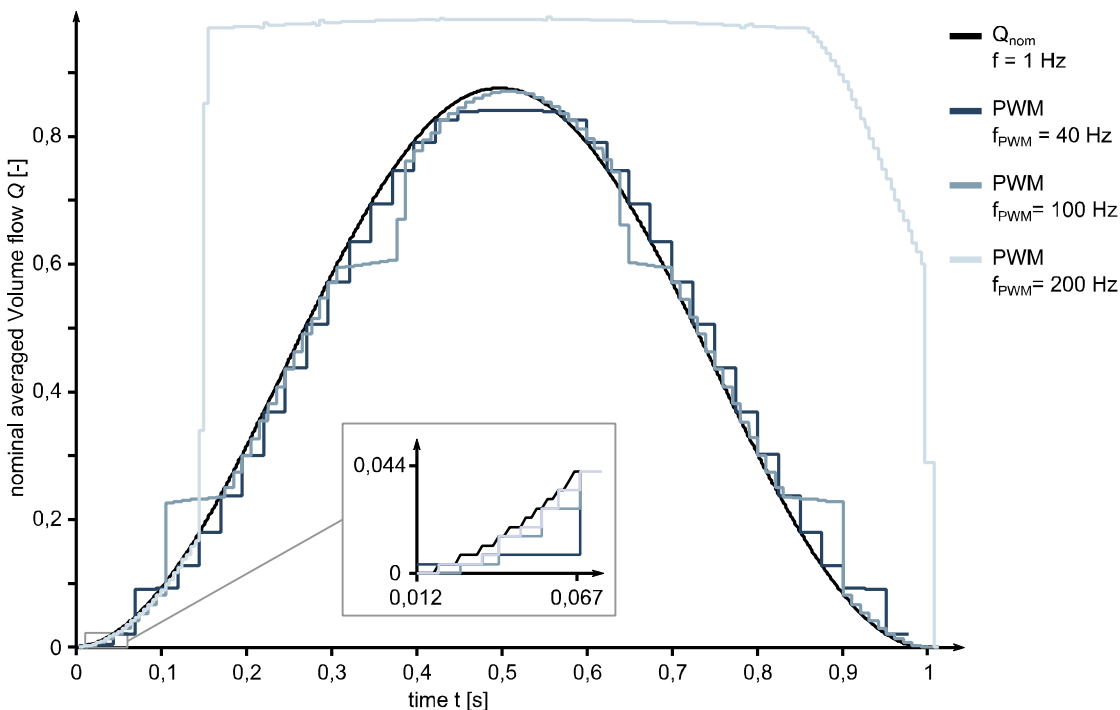


Figure 15. PWM  $f = 40\text{Hz}, 100\text{Hz}, 200\text{Hz}$

The PWM with  $f_{PWM,2} = 100 \text{ Hz}$  can follow the sine on a wider range than the PWM with a frequency of  $f_{PWM,3} = 200 \text{ Hz}$ . But the resolution of the PWM with  $f_{PWM,2} = 100 \text{ Hz}$  is not as high as with a frequency of  $f_{PWM,3} = 200 \text{ Hz}$ . The resolution is dependent from the PWM frequencies. High PWM frequencies lead to high resolutions. Here two steps are observable. For small volume flows the on/off valve operates in the ballistic mode. This PWM with the frequency of  $f_{PWM,2} = 100 \text{ Hz}$  behaves than in a different way to the one with  $f_{PWM,3} = 200 \text{ Hz}$ , because the first transition between the ballistic mode and the normal mode and not from the ballistic mode to the inverse ballistic mode. The second step indicates the transition between the normal mode and the inverse ballistic mode as shown in Figure 15.

The PWM with a frequency of  $f_{PWM,1} = 40 \text{ Hz}$  can follow the sine even on a wider range than the PWM with a frequency with  $f_{PWM,2} = 100 \text{ Hz}$ . The resolution is getting worse because of the low frequency, which leads to a long duration of the period The

duration of the period correspond to the resolution. But the steps that indicate the transitions between the ballistic mode and the normal mode as well as the normal mode and the inverse ballistic mode are still visible. The chosen nominal sine prevent that the valve operates in the inverse ballistic mode. If the amplitude of the nominal sine would be higher, the on/off valve would operate in the inverse ballistic mode and the on/off valve would follow the high values of the nominal sine. But in this case the second step is just rudimentary visible in the way that the maximum values are not reached.

The behavior of the PWM with a sine as a command signal can be summarized in three claims:

1. the higher the PWM frequency the higher the resolution of the averaged volume flow over one period,
2. the higher the PWM frequency the lower the range, where the on/ off valve can follow the sine,
3. the higher the PWM frequency the wider the range of the ballistic mode and the inverse ballistic mode.

Claim three implicates that the normal mode is getting smaller the higher the PWM frequency. Depending on the control tasks different PWM frequencies must be chosen. A general declaration which is the best PWM frequency cannot be given, because of the conflict of claim one and two.

As shown in Figure 8 the invPFM with  $t_p = 3 \text{ ms}$  has the same behavior as the OPM. The behavior of the OPM and the invPFM is the same when the two digital control methods operate in the normal mode. Both control methods does not have a constant period like the PWM. This can be observed in Figure 16. For small averaged volume flows the control methods have high resolutions, which means that the frequency for this averaged volume flows is high. For higher volume flows the OPM and the invPFM has lower resolutions, so there the frequency is lower than for smaller volume flows.

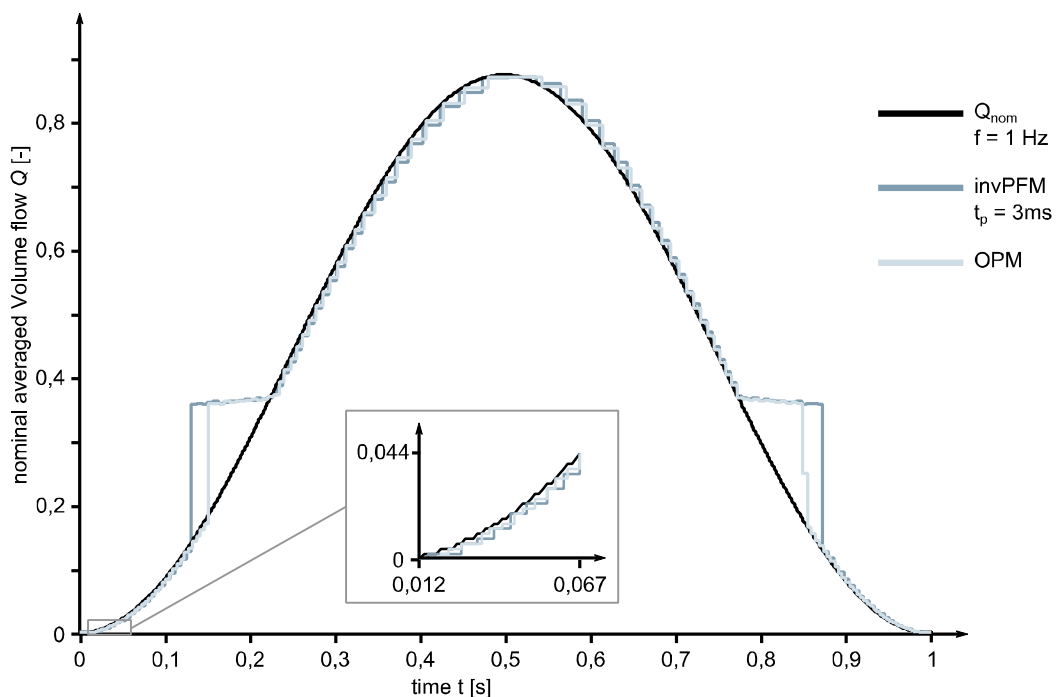


Figure 16. OPM and invPFM  $t_p = 3 \text{ ms}$



The difference between the invPFM and the OPM is that for low volume flows the OPM has a higher resolution than the invPFM. So for low volume flows the OPM uses a higher frequency than the invPFM. The invPFM have always the same duration of the pause  $t_p = 3 \text{ ms}$ . This is optimized for the range of the normal mode, but not for the ballistic mode. The OPM always has an optimum pause in the normal mode and in the ballistic mode. The second observable difference is that the ballistic mode of the OPM has a wider range than the ballistic mode of the invPFM. So the range, where the OPM can follow the nominal sine is wider than in case of use of the invPFM.

The shown behavior of the digital control methods and the used on/off valve is a mixture of the behavior of the on/off valve but also how intelligent the digital control methods can handle the discontinuities of the on/off valve. The PWM for example has often two transitions between the inverse ballistic mode and the normal mode as well as the normal mode and the inverse ballistic mode. The invPFM and the OPM have maximum one transition.

## 5. BEHAVIOR OF AN ON/OFF VALVE IN CLOSED LOOP

In most applications the on/off valves are use in a closed loop control. In this section the analyzed behavior of the on/off valve in an open loop control, as described in section 4, will be transformed to the close loop control. The OPM will be compared with the PWM with a frequency of  $f_{PWM,1} = 40 \text{ Hz}$  and  $f_{PWM,2} = 100 \text{ Hz}$ . The controller of the closed loop control is a simple proportional controller as also introduced by [6].

Several steps are the commands for the closed loop control. The controlled system is a piloted 2-way directional valve size 63 with an on/off valve pilot. The on/off valve pilot displaces a conventional 4-way directional valve. The on/off valve is a configuration of four 2-way on/off valves. The position of the main stage is measured and the feedback parameter for the closed loop system. Other parameters are not measured. The system behaves in the same way like the analyzed system of [6]. The steps are set to  $0.1 \text{ s}$ ,  $0.2 \text{ s}$ ,  $0.3 \text{ s}$ , ...,  $0.8 \text{ s}$  as shown in Figure 17 and Figure 18. So for the start of the main stage's piston movement after the step the chosen digital control method is irrelevant. The main stage's piston movement must start at the same moment, because a new period starts with the step, independent of the PWM or the OPM was used.

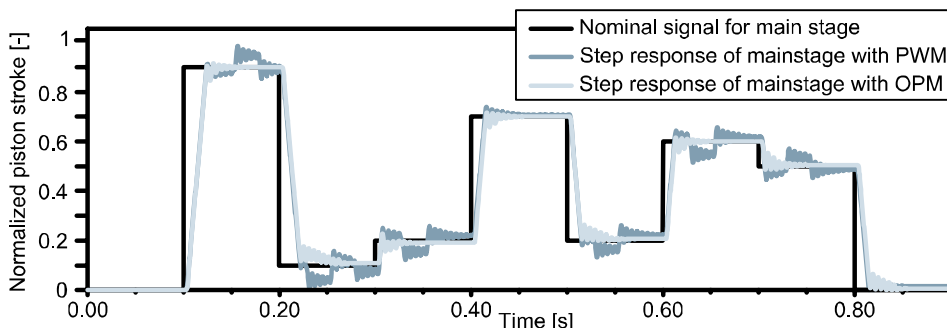


Figure 17. Comparison of the OPM and the PWM  $f_{PWM,1} = 40 \text{ Hz}$  with step responses of the main stage with switching valve pilot by [6]

Comparing the PWM with a frequency of  $f_{PWM,1} = 40 \text{ Hz}$  to ones with higher frequencies this PWM has a bad resolution as shown in Figure 15. In the closed loop

control the low frequency leads to a slow reaction as shown in Figure 17. The duration of the periods of 25 ms can be easily recognized. The opening time of the maximum step of main stage correspond to the duration of the PWM period of 25 ms, so that the opening behavior of the OPM and the PWM with a frequency of  $f_{PWM,1} = 40 \text{ Hz}$  is the same. So only the positioning behavior of these control methods is not the same.

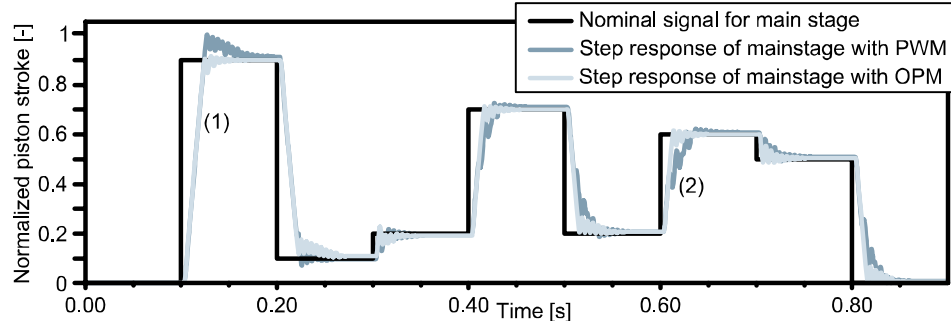


Figure 18. Comparison of the OPM and the PWM ( $f_{PWM,2} = 100 \text{ Hz}$ ) with step responses of the main stage with switching valve pilot by [6]

The step response of the PWM with a frequency of  $f_{PWM,2} = 100 \text{ Hz}$  is not optimal. At the first step from 0% to 90% (1) of the maximum piston stroke the main stage opens rapidly, but there is a big overshoot. In contrast to the first step the one from 20% to 60% (2) is much slower as the first one but the overshoot is like the one of the OPM. In this case the durations of the pulses are for the step (2) not optimal. Of course some steps also have the optimal durations to compensate the control deviation. In contrast to that the OPM can optimize the durations of the pulses as shown in Figure 18.

The PWM with a frequency of  $f_{PWM,2} = 100 \text{ Hz}$  has a higher reaction than the PWM with a frequency of  $f_{PWM,1} = 40 \text{ Hz}$ . This can be explained by the higher frequency. So in the closed loop control it can be also analyzed that higher frequency leads to a faster reaction of the pilot.

## 6. CONCLUSION AND OUTLOOK

Five different digital control methods were introduced and analyzed. The analyses' target is, to find the best digital control method for an on/off valve configuration with one on/off valve per metering edge. The used simulation model introduced by [5] is described in section 3. The simulations for the analysis are done with that model. The first analysis is the comparison of the digital control methods in the duty cycle frequency diagram and in the diagram of the normalized and averaged volume flow. These comparisons are static comparisons that mean the on/off valve moves every period in the same way. The second comparison is the dynamic comparison. A sine was chosen as the nominal signal. These comparisons were done in an open loop control. In these comparisons it could be shown that the choice of the PWM frequency is essential for control quality. A connection between the chosen PWM frequency and the resolution as well as the range, where the on/ off valve can follow the sine was found. The invPFM can be very similar to the OPM when the duration of the pause is chosen in the right way. The only difference is the behavior, when the command signal requires small volume flows. In this case the resolution of the OPM is higher than the one of the invPFM. The invPFM and the OPM just have one transition between the ballistic mode

and the normal mode. The PWM have only one transition from the ballistic mode to the inverse ballistic mode or two transitions. If the PWM just has one transition the discontinuity is very high, so that only the range of the ballistic mode can be used for control tasks. The other digital control methods, the PFM and DFM cannot be used for control tasks in combination with on/off valve configurations, which have only one on/off valve per metering edge. The PWM and the OPM were briefly compared in a closed loop control, to show that the analyses' results can explain the behavior in the closed loop control.

For the PWM some more detailed analyses can be done to find the exact connection between the frequency and the resolution or the range, where the on/off valve can follow the nominal sine. This could help to find a holistic answer to the question, which is the best PWM frequency, when using the PWM as a digital control method for on/off valves. Another question is to find the exact relation between the open loop analysis and the closed loop analysis.

The analyses were done with the same valve. But it is also known that some characteristics like the discontinuities at the transition between the ballistic mode and the normal mode as an example is the result of the characteristics of the on/off valve. An analysis of the characteristic of the on/off valve in combination with the digital control method is also reasonable.

The investigations will go on to find the answers of the asked questions in this outlook. These results of the analysis will be verified on a test bench after the mentioned investigations.

- [1] Wennmacher, G., 1995. Untersuchung und Anwendung schnellschaltender elektrohydraulischer Ventile für den Einsatz in Kraftfahrzeugen. Dissertation RWTH Aachen. Aachener Beiträge zum Kraftfahr- und Maschinenwesen, Band 9. Verlag der Augustinus Buchhandlung, ISBN 3-86073-415-6.
- [2] Lühnemann, B., 1984. Digital gesteuerte Hydraulikventile und ihre Anwendung. Dissertation TU Braunschweig.
- [3] Linjama, M., 2012. Digital Fluid Power – State of the art. The Twelfth Scandinavian International Conference on Fluid Power, May 18–20, Tampere, Finland.
- [4] Schepers, Weiler & Weber 2011. Optimize pulse modulation – A novel idea of a digital control method for on/off valves. ASME 2011 Dynamic Systems and Control Conference DSCC2011, October 31 – November 02, 2011, Arlington VA, USA, Paper DSCC2011-6007.
- [5] Schepers, Schmitz, Weiler, Cochoy & Neumann, 2011. A novel model for optimized development and application of switching valves in close loop control. International Journal of Fluid Power (IJFP), Vol. 12, No. 3 pp. 31-40.
- [6] Schepers, Weiler & Weber 2011. Analysis of control methods for switching valve configurations that control die casting machines as an example. IFK 2012 8<sup>th</sup> International Fluid Power Conference Dresden, March 26 – March 28, 2012, Vol. 1 pp 491-503.

- [7] Long et al., International Journal of Fluidpower 11 (2010): Comparitive study of position control with 2-way and 3-way on/off electrohydraulic valves
- [8] Branson III et al., International Journal of Fluidpower 9 (2008): Simulated and experimental Results for a hydraulic actuator controlled by two high-speed on/off solenoid valves
- [9] Huh et al., KSME International Journal Vol. 11 No. 4: A Study on the Stability Analysis of a PWM Controlled hydraulic Equipment



## HARDWARE IN THE LOOP MULTI OBJECTIVE GENETIC OPTIMIZATION FOR EFFICIENT VALVE CONTROL

P. Foschum\*, A. Plöckinger\*, R. Scheidl\*\*

\*Linz Center of Mechatronics

\*\* Johannes Kepler University; Institute of Machine Design and Hydraulic Drives  
Altenbergerstraße 69, 4040 Linz, Austria

E-mail: [paul.foschum@lcm.at](mailto:paul.foschum@lcm.at), Phone: +43 732 2468 6055, Fax: +43 732 2468 6005

### ABSTRACT

To control fast switching valves boosted current signals are used to drive the solenoid. A faster reaction without excessive power consumption, destroying the solenoid, is reached by optimizing this signal. Its shape gets more complex and the tuning effort rises. Production and material constraints and other ambient conditions make it impossible to find a realistic energy saving signal only using simulation. One possibility to consider the various objectives like robustness, power consumption and switching time in parallel to find the optimized current shape is to employ multi objective hardware in the loop (HIL) optimization.

In this paper a method is shown that optimizes the current signal by multi objective genetic optimization integrating a physical valve in the optimization loop.

**KEYWORDS:** hardware in the loop, HIL, current shape, controller, switching valve, multi-objective optimization, Pareto optima, genetic algorithm.

### 1. INTRODUCTION

Multi objective optimization has become a very powerful means of system design which is more and more applied in practice. It requires proper mathematical models which relate the system design parameters to the objectives placed on the system. The result is a whole set of “non dominated solutions”, also called Pareto front, which reflects the trade-off character of multi objective optimization. Of course, such optimization may concern also control parameters. In general, the used mathematical models typically neglect some physical phenomena and a real system will always deviate less or more from the designed system due to manufacturing tolerances.

Particularly optimized controllers are susceptible to system perturbations. Furthermore, for a real system, hence also for a real controller, a specific solution out of the infinitely many solutions of the Pareto front must be selected. Thus, the trade-off property is not reflected anymore in a real design. Furthermore there is a fundamental difference between hardware and software related system (or design) parameters, since the latter can be often easily and nearly arbitrarily adjusted, even at run time, much in contrast to the former parameters. This offers the opportunity to carry out a multi objective optimization at least of some software parameters. In this paper this is done for the current control of a solenoid actuated fast switching valve. The physical principles

based modelling of such valves, in particular of the solenoid, has some limitations concerning the achievable accuracy due to several complex phenomena and parameter uncertainties, respectively. Significant uncertainties are the real response of the power electronics for pulse-width control, the exact magnetic material properties, the oil stiction phenomenon, geometric tolerances, and eddy currents.

As a test case the existing fast switching valve, type FSVi [1], is used. This hardware is placed in a loop with the multi-objective design optimization software ‘MagOpt’ [1] via the integrated power electronics and some sensor signals. The software transfers each test configuration (control parameters and power peak shape) to the power electronics which communicates the measured data of the test ‘shot’ back to the optimization procedure again. The optimization objectives are: peak power consumption, switching time and hold power consumption which supports an energy efficient behaviour at high switching frequencies and robustness at high flow rates.

## 2. TEST RIG

The hydraulic part of the test rig (Figure 1, Figure 2) consists of the FSVi valve itself, the two hydraulic decoupling accumulators feeding the valve during the switching process and a set-up to pressurize the armature and solenoid chamber (leakage port). On the other hand the electric system comprises a microcontroller based power electronics developed by LCM, the eddy currents position sensor and the two pressure sensors directly applied at the valve to measure the differential pressure. A PC is used to carry out the optimization process using the optimization software ‘MagOpt’.

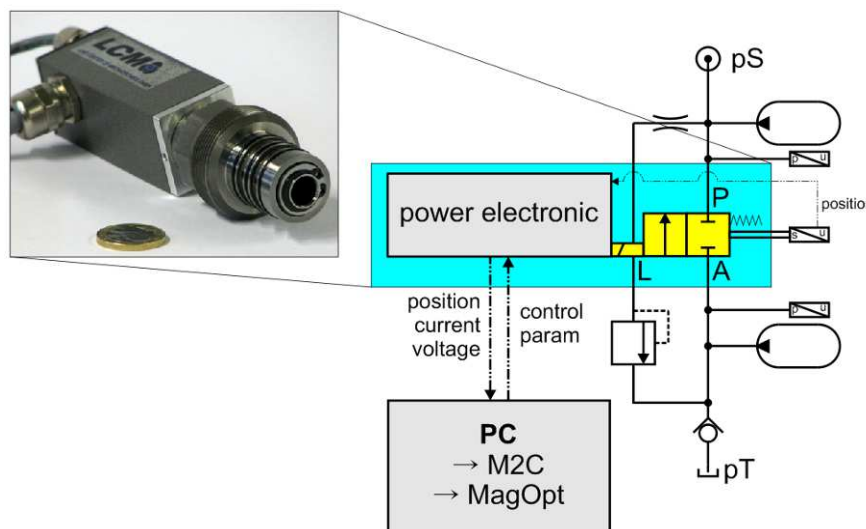


Figure 1 FSVi valve (left), schematic of HIL circuit (right)



Figure 2 Test rig with valve, power electronics, valve block and accumulators

### 2.1. System parameters

The test valve is used to demonstrate the HIL multi objective genetic optimization process. To ensure constant circumstances the oil temperature is kept at a value of 40°C and the leakage port and the armature chamber pressure at a value of 10 bar. The system pressure  $p_S$  is adjusted to 250 bar (in closed state) and stabilized by the high pressure accumulator (preloaded pressure 140 bar). The low pressure  $p_T$  rests at 1 bar which slightly increases at open state. The low pressure accumulator (preloaded pressure 5 bar) is used to reduce pulses and cavitation in the long hydraulic tank line when the valve closes.

To measure the pressure difference at the valve itself, two pressure sensors were applied directly at the NG6 adapter plate beneath the valve block.

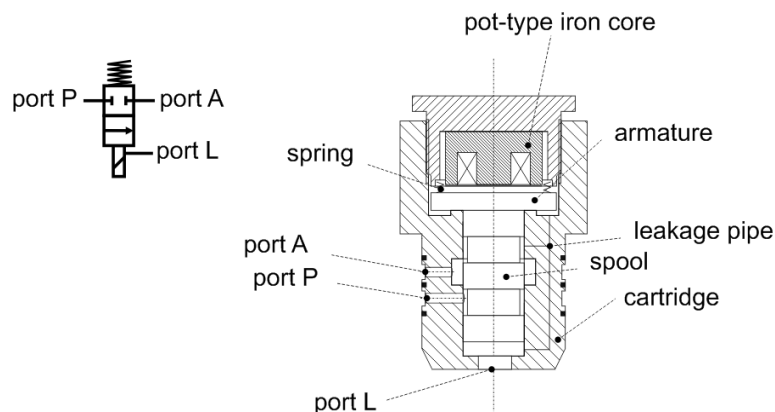


Figure 3 Schematic of the FSVi valve (with pot-core solenoid)

### 2.2. The opening process

At the beginning of each 'shot' (opening and closing again after 100 ms) the differential pressure  $dP$  is 250 bar (Figure 4). During the opening process the differential pressure



drops as the oil flow starts. During this activation the high side accumulator pressure falls and the tank side pressure slightly rises and so the differential pressure drops to about 200 bar (Figure 4). The hydraulic pump is too slow to follow this flow rate peak so all the oil flow is provided by the accumulator and the oil capacity in the system pressure pipe. Figure 4 shows the hydraulic oscillation between the hydraulic pipe and the high pressure accumulator when the valve closes. Later on the pump brings the pressure back to 250 bar for the next ‘shot’.

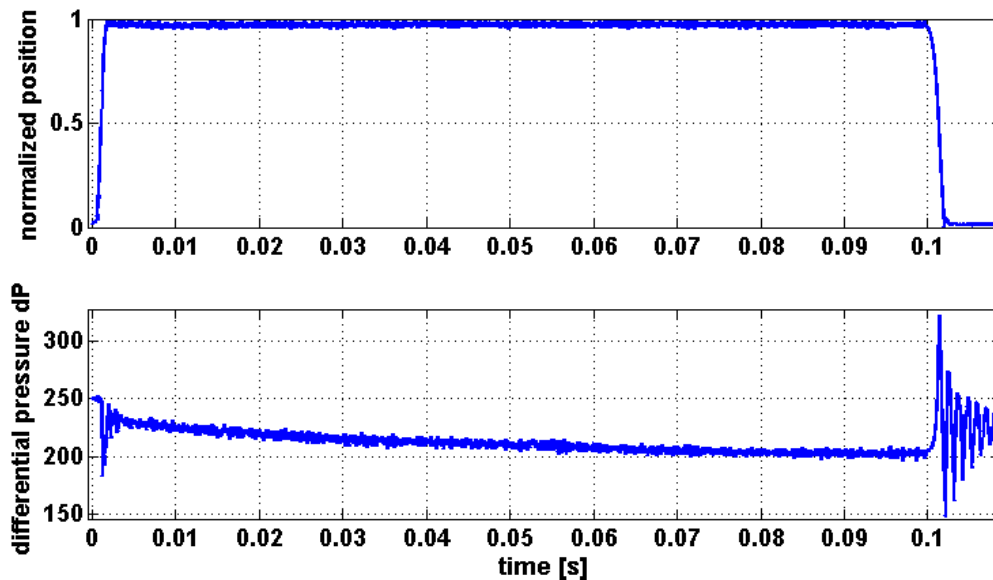


Figure 4 differential pressure drop at opening process of the spool

Table 1 FSVi characteristic

	differential pressure dP [bar]	flow rate [l / min]
nominal	5	10
	200	63
	250	70

### 2.3. The closing process

In the following considerations the closing process of the valve is disregarded because the holding voltage is just switched off and so the current reduction can't be influenced. Therefore, with the selected test procedure, the closing movement is totally independent of opening movement.

### 2.4. The measuring of single ‘shots’

The FSVi power electronics drives the current of the solenoid and in turn the spool. At first the PC carrying out the optimization transfers the parameters of the current signal shape to the microcontroller, which is placed in the power electronics case. The specified current signal shape is then applied to the solenoid which results in the reaction of the spool. To evaluate the system's response to a certain signal shape the power electronics records the position of the spool, provided by the position sensor, the current and the applied voltage. Voltage and current are directly measured inside the

power electronics. These signals are used to generate the objectives for the optimization problem, thus, they are passed on to the PC.

The pros of using the power electronics for driving and measuring without any other measuring system are the simplicity and the processing speed. The con is the small amount of possible measured values which is limited to 122 values per ‘shot’. With the maximal sampling rate of 20 kHz only 6.1ms of time can be sampled at the full rate (no down sampling). This time period is enough to reconstruct the power consumption of a hydraulic PWM frequency of 100Hz @ 50% which means 5ms on and 5ms off at a period of 10ms. To identify if the valve keeps open for the specified 100ms period, even against the applied flow forces, another ‘shot’ is carried out shortly after the first one employing down sampling (factor 20). This results in a sampling rate of 1ms and a period of 122 ms can be measured. The approach is possible because the two consecutive ‘shots’ show only negligible variation (Figure 5).

The voltage that leads to the desired current profile is applied by an electrical PWM frequency of 20 kHz. To get an accurate current sampling for the current control loop and the calculation of the power consumption, the ADC sampling of the microcontroller is carried out equidistantly at centered PWM pulses. To verify the quality all the signals were also sampled for some test ‘shots’ with an external measuring system at 500 kHz. The achieved accuracy is within 1% at a power consumption of about 35 Watt.

## 2.5. Current shape

To evaluate the generated Pareto optimal current shapes they are compared to the existing, manually set, ‘standard shot’ (SH) shown in Figure 6. The other signals and objectives are also normalized to this ‘SH’.

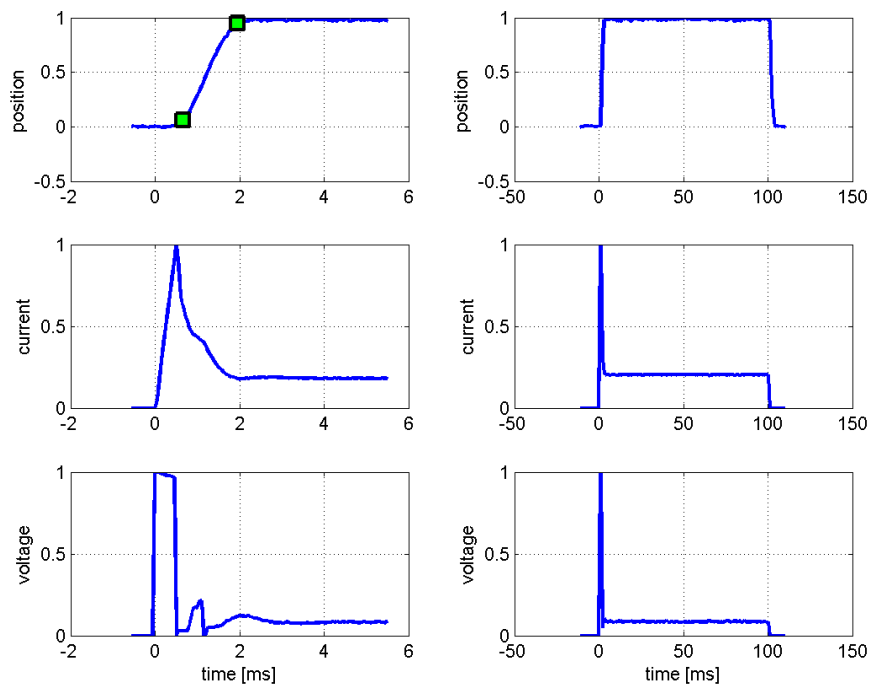


Figure 5 first part of a sample ‘shot’ fully sampled (left); full sample ‘shot’ downsampled (right); all normalized to ‘SH’

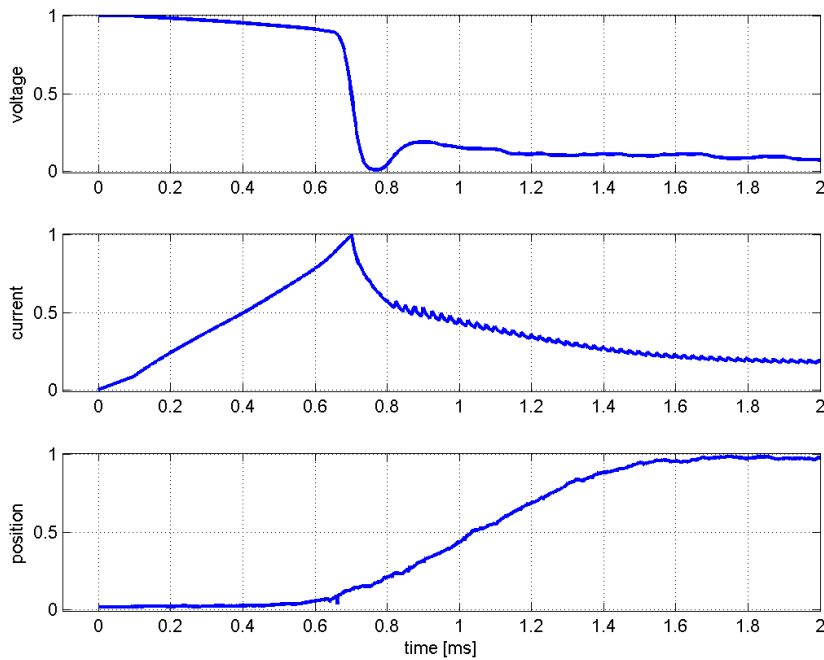


Figure 6 normalized 'SH' opening of the valve (manually set)

### 3. THE OPTIMIZATION PROCESS

#### 3.1. Generation of objectives

Multi objective optimization has the advantage of coping with several normally conflicting objectives without favouring one of them. In this case there are three objectives:

- The **switching time** which the spool needs from sending the opening impulse to the power electronics until 95% of the valve end position is reached.
- The **mean power consumption** of the **first 5ms** of the driving signal, which is used to specify the power consumption at a hydraulic PWM movement of 100Hz @ 50% duty cycle.
- The **mean power consumption** of the **rest of the 100ms** time period which can be used to evaluate the power consumption at the hold state, relevant if the valve is held open for a longer time.

The objectives are calculated by the PC between the single 'shots' and are passed through to 'MagOpt' which evaluates the single individuals standing for different driving current shapes (Figure 7 HIL optimization process).

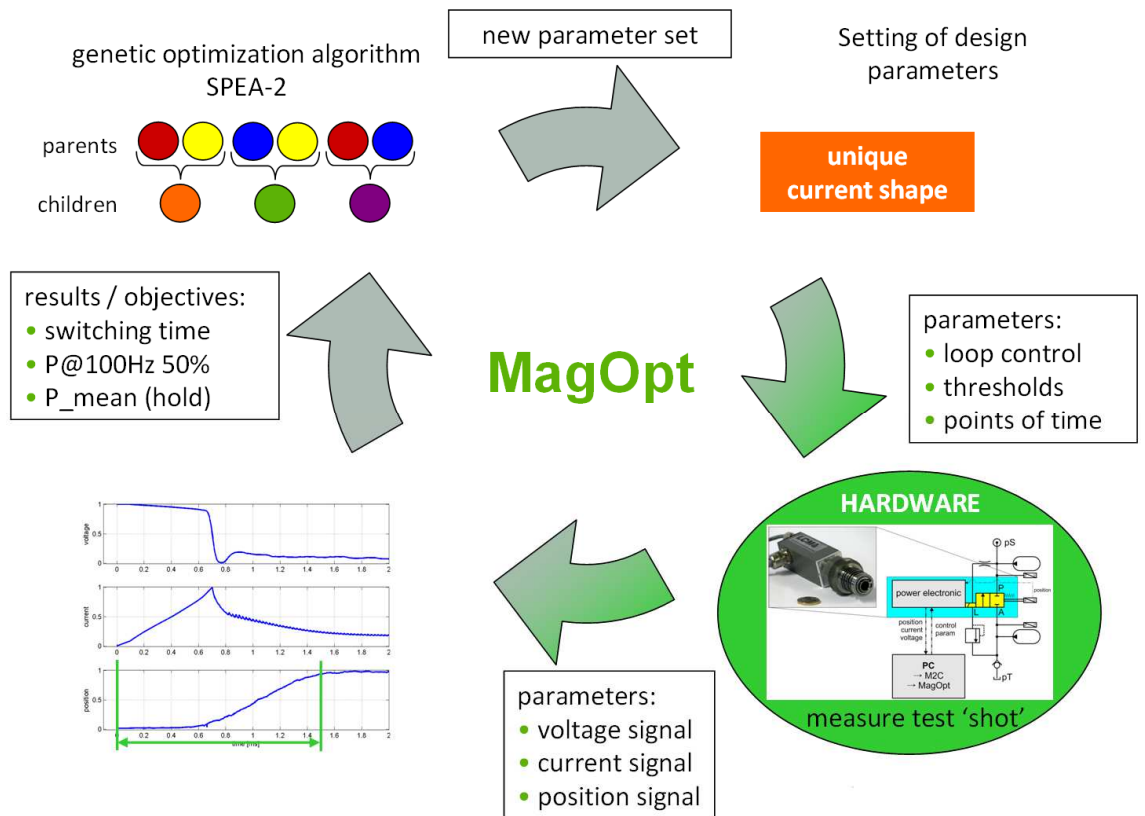


Figure 7 HIL optimization process

Beside the objectives there are also some criteria that have to be fulfilled. Otherwise an error would be triggered and the individual should be neglected. These are:

- The valve has to open fully during the time period of 100ms.
- The spool mustn't close due to flow forces until the signal is off (after 100ms).
- The hold current is controlled and has to be within 2% of the desired value.

### 3.2. Parameter variation

The 8 parameters (including controlling parameters, switching times and current levels) characterizing the actual current shape are varied by the optimization algorithm in certain limits. The range is set as wide as possible just limited by system integrity.

### 3.3. Pareto Optima

The surviving individuals which are not dominated by other ones in at least one objective are plotted with their reached objectives in Figure 8. The objectives were again normalized to the 'SH' represented by the dashed lines. Of course, there are of course individuals that reach better results in one objective compared to the 'SH'. Thus, there are some faster ones which use more energy as one with opposite results. But contrary to expectations there are also some like the one pointed out (filled bold dot) which show an increased performance by a decreased energy consumption.

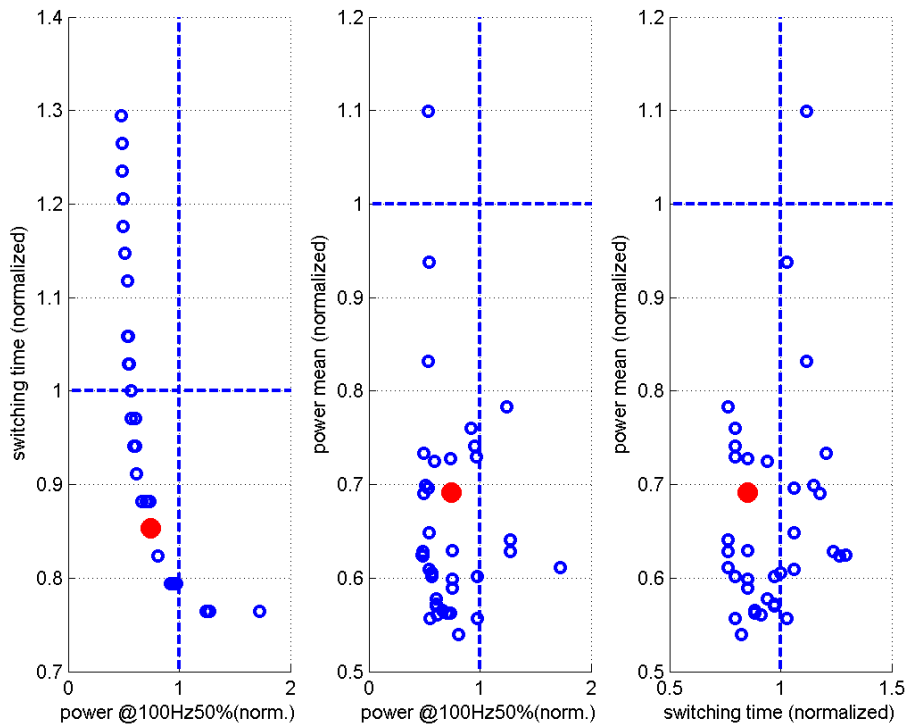


Figure 8 Pareto individuals (circles), 'SH' (dashed lines), one individual better than 'SH' in every objective (filled bold dot)

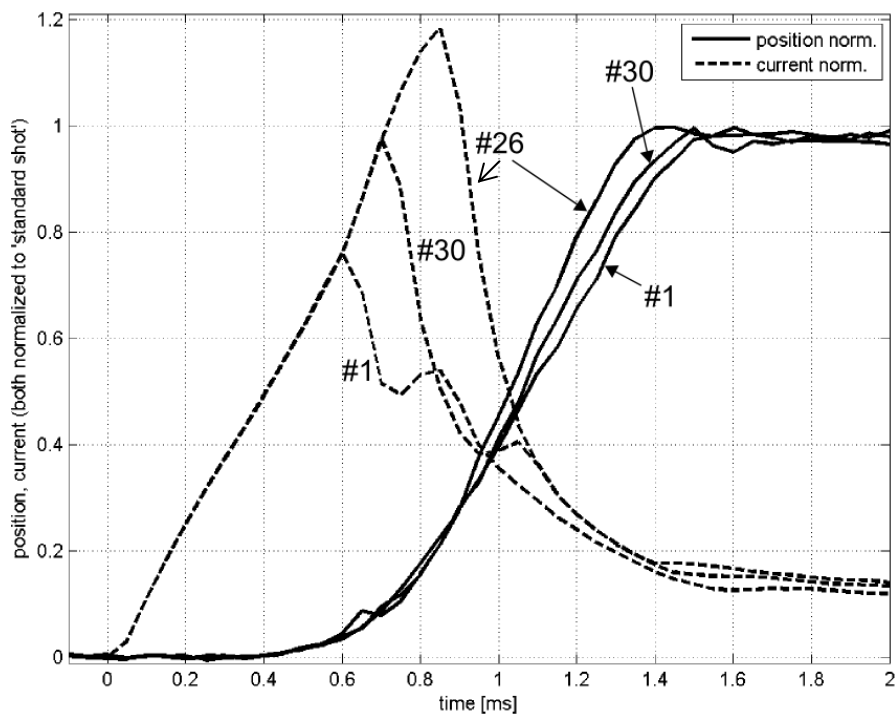


Figure 9 comparison of three Pareto optimal solutions

To compare some of the individuals three interesting ones were picked out and their normalized current and position signals are shown in Figure 9. The objectives are listed in Table 2. The first (#1) shows a moderate but quite uniform improvement over the

‘SH’. It is 3.3% faster and the power consumption @ 100Hz is reduced by 25.3%. A faster solution is #26 which has a 13.3% faster switching time. However its power consumption rises by 27.1%. The third individual (#30) lays in between and fulfils every objective slightly better than the ‘SH’.

Table 2 comparison of three Pareto optimal solutions (less is better), values normalized by those of ‘SH’

individual #	1	26	30
switching time	96.7 %	86.7 %	93.3 %
power@100Hz 50% PWM	74.7 %	127.1 %	92.0 %
mean power	70.5 %	87.4 %	98.5 %

Each individual is Pareto optimal, hence, better than any other individual in at least one objective. Individuals not fulfilling this Pareto condition or the established error criteria are not in the Pareto set. The selection of a final solution out of the Pareto set requires additional information or preferences [3].

There the aim is to maximize the switching frequency of the valve to enhance the control performance of digital hydraulic circuits. The switching time of the FSVi valve is short enough to increase the switching frequency to frequencies of some hundred Hertz and still fully open and close the valve in one cycle. The factual frequency limit is the inserted power per switching event. So the ambition is to reduce the power consumption at a switching event represented by the power @ 100Hz 50% PWM. One of the best Pareto individuals in this respect is #1. Due to its low power consumption it could be driven about 25% faster than ‘SH’ (so at 125 Hz instead of 100 Hz).

#### 4. CONCLUSION & OUTLOOK

HIL optimization systematically leads to a better performing system and takes typically less time than tuning the system parameters by hand. It requires less expertise concerning the influence of the adjustable system parameters on the system performance. Critical, however, is to set proper parameter limits for a save operation, in particular, not to destroy the system when the optimization procedure tests dangerous parameter constellations.

By applying HIL optimization to the fast switching valve FSVi to find optimal signals for switching the valve yielded a significant improvement of the valve performance. For instance, the valve can be run at 25% higher switching frequency with the same thermal loading compared to the standard current signal settings. The setting up of such an optimization and the analysis of its results provides better insight into the system. For instance, it was found out that the original parameterization of the current signal was not fully adequate to the physical characteristics of the solenoid. The correction of this deficiency not only helped to get better optimization results but gave improved insight into the physics of the solenoid. At general problem of optimized solutions is insufficient robustness. This could be experienced also in this case. Oil temperature, for instance, influences several processes in the valve. In the HIL optimisation runs oil

temperature was kept constant in experimental analyses on this influence it turned out, that some Pareto optimal individuals no more fulfil all criteria for a reliable operation.

There are two possibilities to solve this problem. The first is doing the optimization without a consideration of this robustness problem and to make a robustness check for the selected Pareto individuals. Robustness is then a major criterion to select one or a reduced set out of the original Pareto set. Another, basically better approach would be to make robustness an additional optimization objective. This however may pose severe difficulties in practical realization. Oil temperature, for instance, can not be changed rapidly and easily. Thus, incorporating the oil temperature a variation in the Pareto front search would increase the optimization run time unacceptable.

## 5. ACKNOWLEDGEMENT

The authors gratefully acknowledge the sponsoring of this work by the 'Austrian Center of Competence in Mechatronics (ACCM)' in the framework of the COMET program. This work was sponsored by the Austrian government, the federal state Upper Austria, and the Johannes Kepler University Linz.

## REFERENCES

- [1] Foschum P., Plöckinger A., Scheidl R., Multi objective genetic optimization of fast switching valves, The fourth workshop on digital fluid power, DFP11, 21. - 22. September 2011, Linz, Austria, Proceedings page 116-128.
- [2] Plöckinger A, Scheidl R., Winker B., Development and prototyping of a compact, fast 3/2 way switching valve with integrated onboard electronics, The 11th Scandinavian International Conference on Fluid Power, SICFP'09, ISBN 978-91-02-7393-588-3, 2. - 4. June 2009, Linköping, Sweden.
- [3] Foschum P., Plöckinger A., Scheidl R., Weidenholzer G., TRIZ, Design optimization and Suh's 1<sup>st</sup> axiom – a comparison on the example of fast switching valves, The 13th Mechatronics Forum International Conference, 17. - 19. September 2012, Linz, Austria.
- [4] Gruber W., Briewasser W., Amrhein W., Novel bearingless slice motor design with four concentrated coils featuring a unique operational behaviour, Proc. of the 14th European Conference on Power Electronics and Applications (EPE-ECCE Europe 2011), 30. Aug. - 1. Sept. 2011, Birmingham, UK.
- [5] Krettek J., Schauten D., Hoffmann F., Bertram T., Evolutionary hardware-in-the-loop optimization of a controller for cascaded hydraulic valves, IEEE/ASME international conference on advanced intelligent mechatronics, ISBN 978-1-4244-1263-1, 4. - 7. Sept. 2007, Zurich, Switzerland.

## SIMULATION AND EXPERIMENTAL RESULTS OF PWM CONTROL FOR DIGITALHYDRAULICS

by Andreas Plöckinger\*, Mikko Huova\*\* and Rudolf Scheidl\*\*\*

\* Linz Center of Mechatronics Gmbh.

\*\*\* Johannes Kepler University Linz; Institute of Machine Design and Hydraulic  
Drives

Altenbergerstraße 69, 4040 Linz, Austria

e-mail: Andreas.Ploeckinger@lcm.at

phone: +43 732 2468 6052

\*\* Tampere University of Technology

Department of Intelligent Hydraulics and Automation

P.O.Box 589

33101 Tampere, Finland

### ABSTRACT

The Linz Center of Competence in Mechatronics (LCM) pursues the strategy of doing digital control primarily in a Pulse Width Control (PWM) mode. Compared to the Pulse Code Modulation (PCM) [1], this approach needs a significantly lower number of switching valves and seems to be better suited for low cost realization of digital hydraulics. One disadvantage of PWM control is the noise excited by the permanent switching. An application using Pulse Width Modulation, on the test rig the so called "Seesaw" at the University of Tampere, have been tested successfully and have been experimentally demonstrated at the DFP2010 workshop in Tampere. This paper is a written report about the theoretical background, the data and the results.

**KEYWORDS:** digital hydraulics, pulse width modulation, PWM, seesaw

### 1. INTRODUCTION

The work reported in this paper has been carried out during a research stay of the first author at the Department of Intelligent Hydraulics and Automation (IHA) and in the framework of a strategic project of the Austrian Center of Competence in Mechatronics (ACCM). In the joint project between IHA and LCM a combination of PWM and PCM has been studied as well as a system with only 4 FSVi in PWM mode only. In this paper only the results of pure Pulse Width modulation are shown.



The key component of digital hydraulics is the fast switching valve. LCM developed the Fast Switching Valve with integrated electronics (FSVi) [2,3,4] with switching times  $T_s < 2\text{ms}$  and a nominal flow rate of  $Q_N = 10\text{l/min}$  at a pressure drop of 5 bar.



Figure 1. Complete prototype valve (including the integrated electronics in the (left) and 3D model and the electronic board (right)

The valve was used for research and demonstration purpose. The fast and accurate timing gives the opportunity to use it also for energy saving control by hydraulic switching convertes [5]. There are also some other special hydraulic circuits [6,7] like the so called Digi-Actuator, where the valves have been successfully tested.

## 2. SIMULATION OF THE SEESAW PWM CONTROL IN INFLOW AND OUTFLOW MODE

### 2.1. Setup

In Figure 2 a schematic of the so called “Seesaw” can be seen. There are 3 load cases which have been tested by IHA (table 1). The first simulations with the PWM only system have been done with the load case “A”.

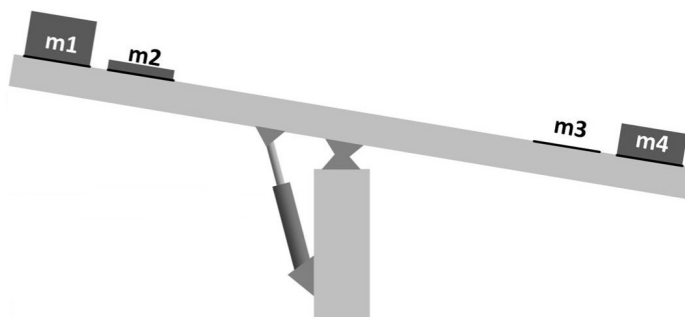


Figure 2. Test rig of the Seesaw at IHA

Table 1. Load cases for seesaw

load case	mass m1 / kg	mass m2 / kg	mass m3 / kg	mass m4 / kg
A	200	50	0	150
B	200	200	0	0
C	100	0	100	200

In this work the seesaw should be controlled by four fast switching valves FSVi (LCM) in inflow outflow mode. The hydraulic scheme is depicted in Figure 3. The idea is to open the tank side valve of the piston side chamber and the pressure side valve of the rod side chamber simultaneously. In this case the cylinder retracts. To move out the other two valves are actuated.

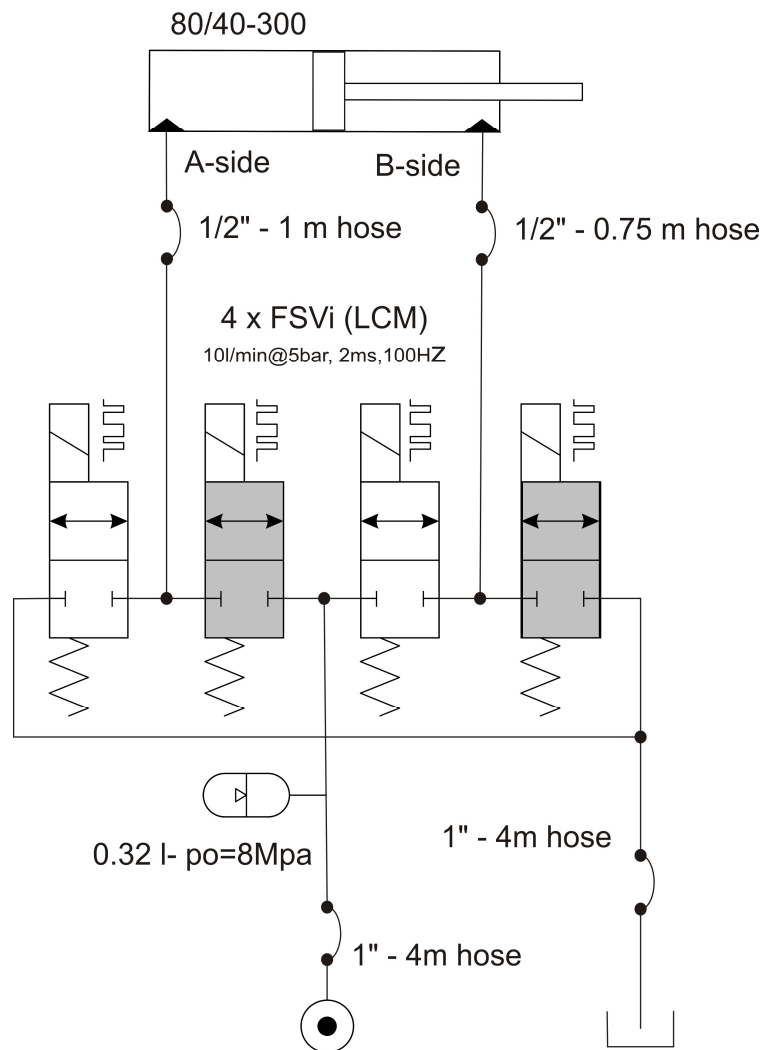


Figure 3. Hydraulic scheme of PWM controlled inflow/outflow control

## 2.2. Controller

The first approach is to use a normal PD Controller taking the error of target to actual position. Additionally, the actuation of the valves will be switched off by the controller when the target velocity is smaller than a certain value and the error is less than a certain value. The PWM frequency is kept fixed. P-type controller is presented in Figure 4.

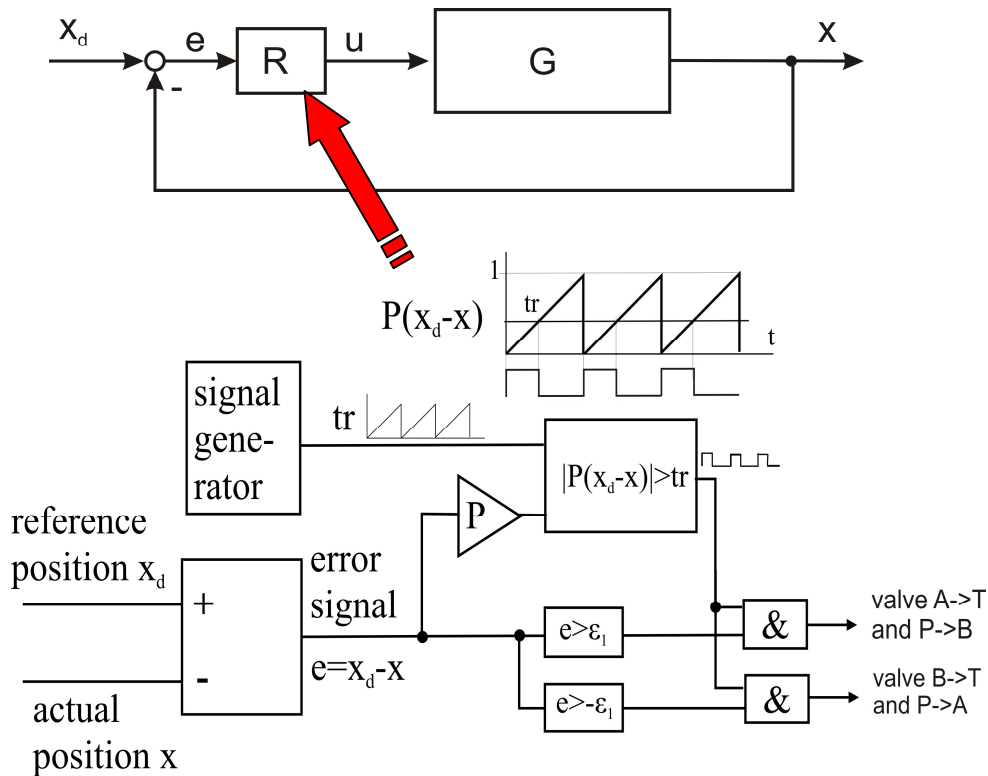


Figure 4. Simple controller circuits for Simulation

One idea for a virtual increase of the PWM frequency is to use a phase-shift PWM. In this case the two PWM outputs - one to the tank sided and one to the supply sided valve are  $180^\circ$  phase shifted. The idea is quite simple, but in the simulation results and the test on the real system this seems to have no real influence on the behaviour of the seesaw's movement. One possible explanation could be that the natural frequency of the seesaw is quite low and the inductance of the system is so high that the effect of the switching delay can be neglected.

## 2.3. Simulation model

For the simulation a controller was designed which can be implemented in the dSPACE system utilized in experimental setup. This simple simulation model includes the

controller, the four switching valves and the seesaw model provided by IHA. The seesaw model comprises the kinematics of the masses, the pressure build up relation in the cylinder chambers, a friction model and hydraulic capacitances of the pipes going to the chambers with a low bulk modulus.

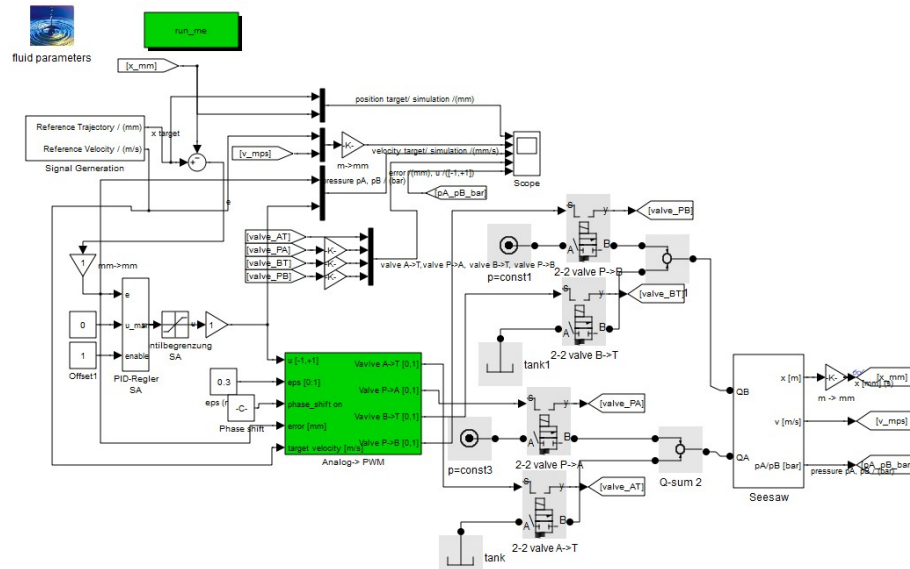


Figure 5. Simulation model for in Matlab/Simulink

#### 2.4. First Simulation results

In the next Figures 6 to 10 the first simulation results can be seen. For these different cases the PWM frequency and the switching time of the valve has been varied. The first measurements on the real system taught that the damping of the real system was lower than in the model provided by IHA. No modification of the models was done; this is left to future work.

Table 2. Different simulation cases

Case	PWM frequency / (Hz)	Switching time of the valve / (ms)	Phase shift	Comment (based on the controller used)
C1	25	10	off	in simulation not possible to stop too small stopping threshold
C2	40	10	off	in simulation not possible to stop
C3	40	5	off	in simulation not possible to stop
C4	40	2	off	quite good results - error < 0.8mm
C5	100	2	off	quite good results - error < 0.7mm

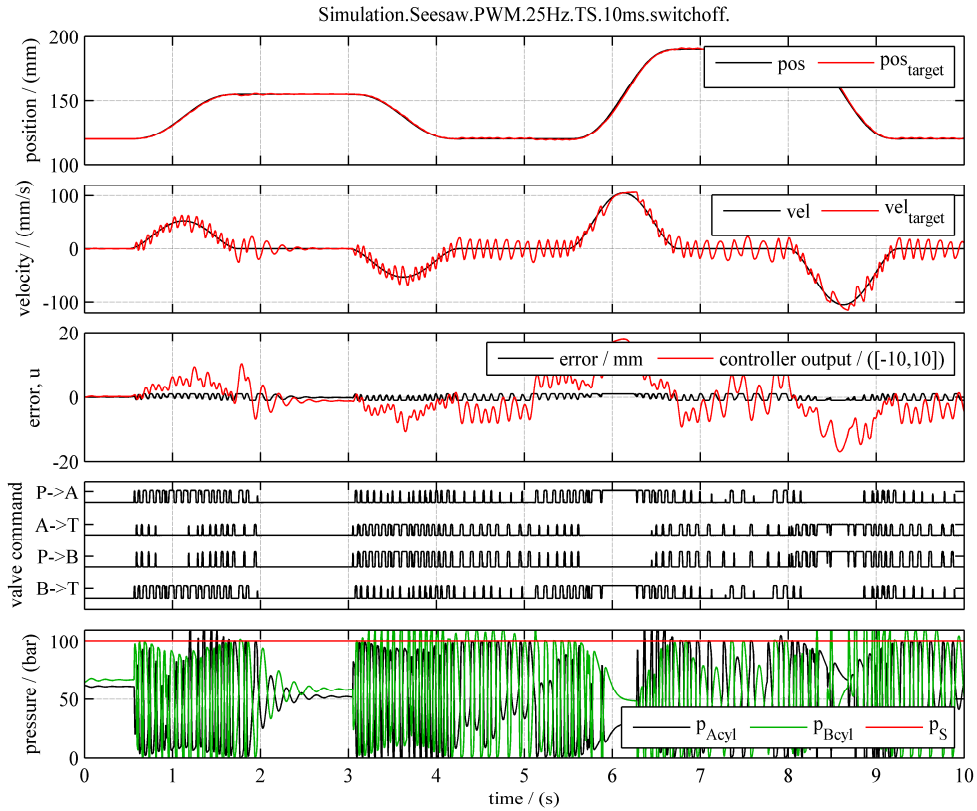


Figure 6. Simulation results case C1

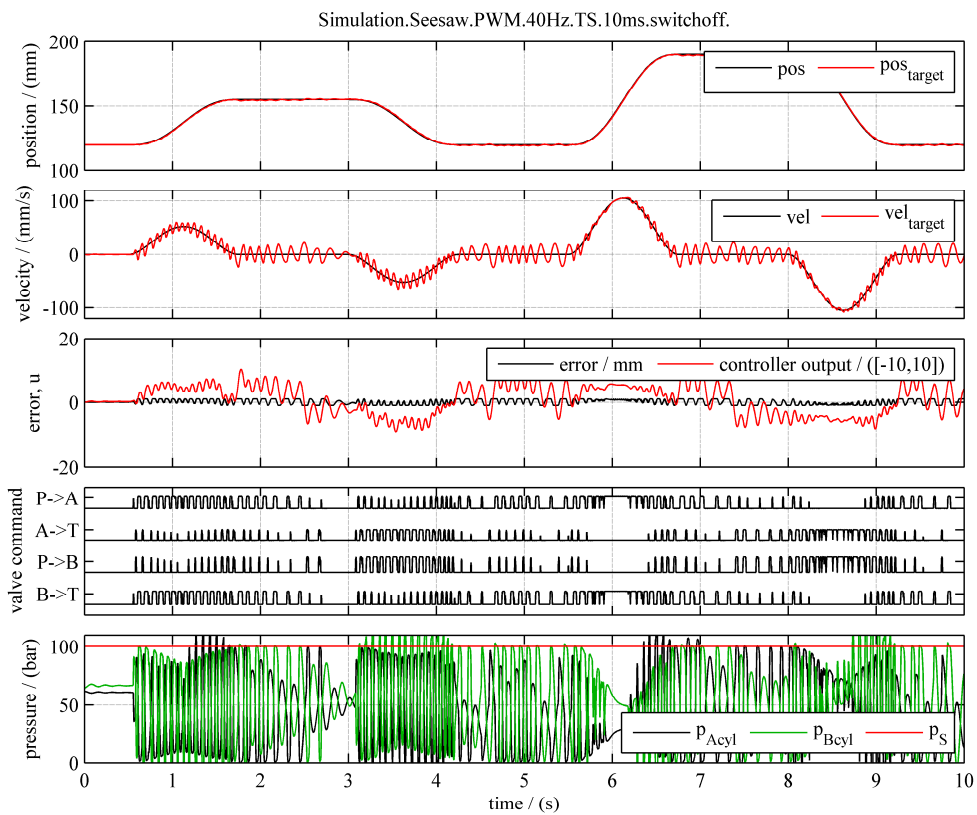


Figure 7. Simulation results case C2

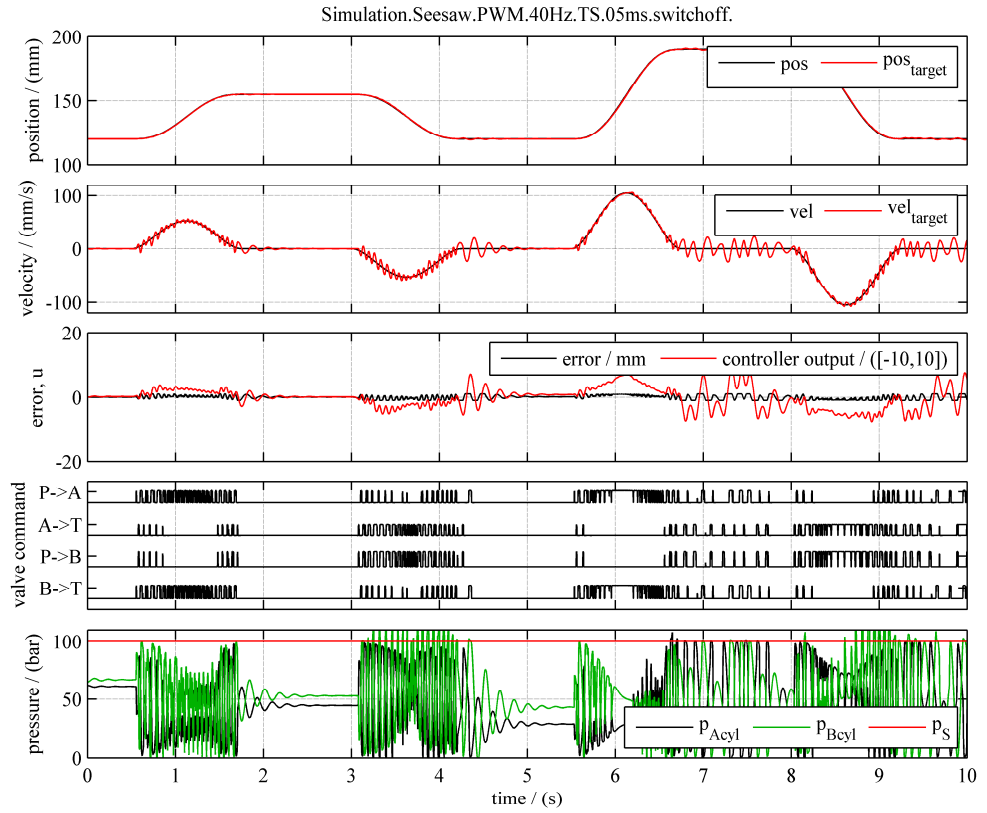


Figure 8. Simulation results case C3

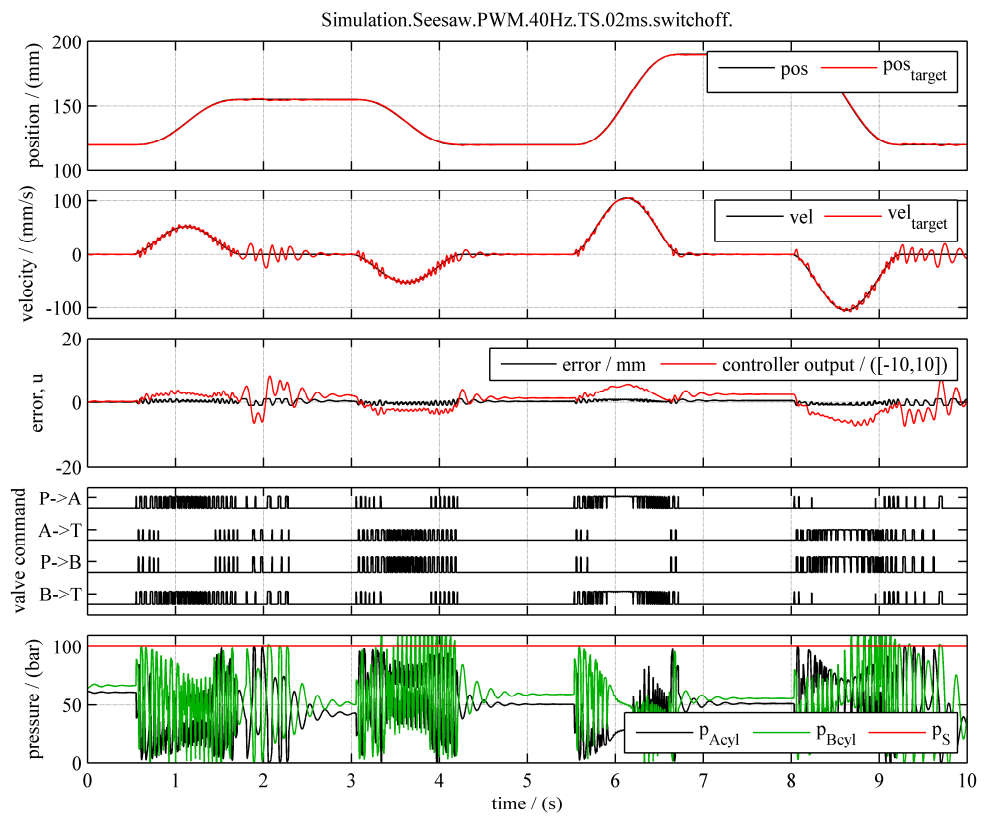


Figure 9. Simulation results case C4

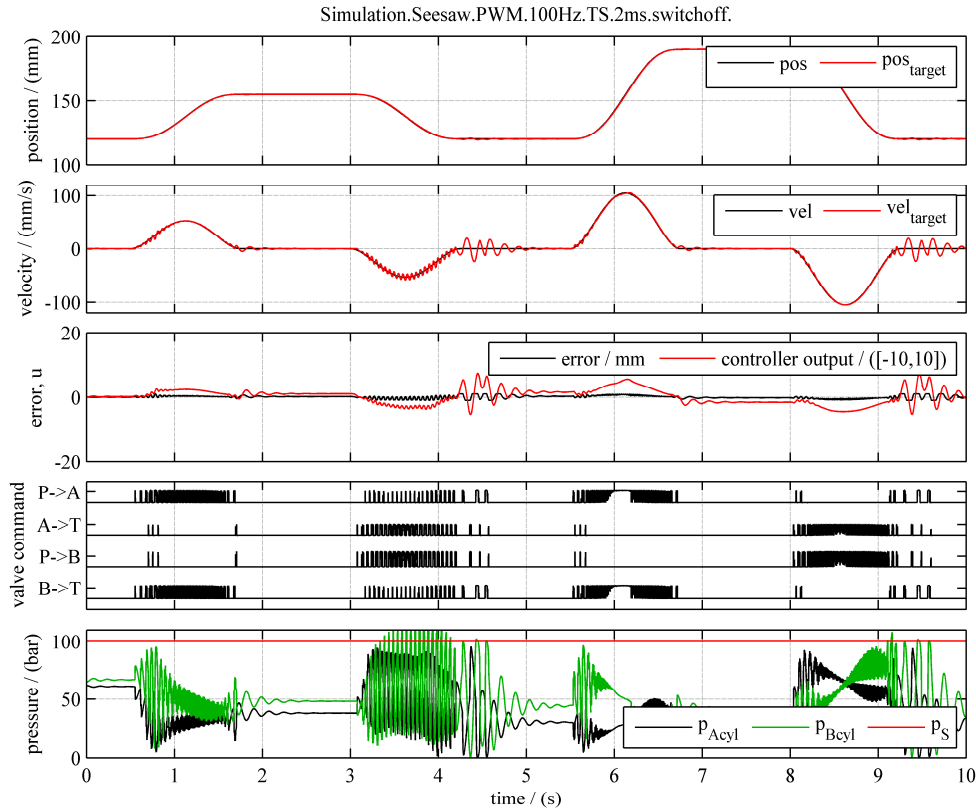


Figure 10. Simulation results case C5

The simulation results are very promising. In table 2 the different simulation cases are listed. One outcome is that for unthrottled valves and switching times  $t_s > 5$  ms without using ballistic mode the oil flow in the cylinder chamber during one opening is so much that the controller will not reach the desired dead band and so the valve actuation will not stop at zero velocity. Possibly, a combination of another controller and two valves in parallel, one unthrottled and one throttled, would do better than the PD controller is just one valve per metering edge. The fast switching valve with switching time around 2 ms can fulfil the performance and will stop at demand zero position.

## 2.5. Measurement results

The test rig has been installed in the laboratory of IHA. With this system 4 different valve configurations could be tested:

- 1 valve PWM only (with the FSVi)
- 3 valve PCM/PWM with one fast switching valve FSVi
- 3 valve PCM/PWM with only KSDE of Bosch Rexroth
- 3 valve PCM only KSDE of Bosch Rexroth

In this paper only the measurements for the PWM only system will be discussed.

### 2.5.1. Problems during first measurements

In a first attempt for the PWM only system the same controller as used in the simulation model was applied. The PWM frequency was 100 Hz. Due to some nonlinearity of the system behaviour and noise of the position sensor the system was not stable. Two modifications for gaining stability were made:

1. A combination of P-type position controller and velocity feedforward
2. Modified valve switch on and switch off thresholds for the output.

The scheme of the controller can be seen in Figure 11. The timing of the valves is triggered by a periodic triangular signal which's carrier frequency is the PWM frequency. The pulse width is obtained by comparing the value of this triangular signal with the sum of error value multiplied by the proportional gain P and the velocity reference time a gain  $P_v$ . The controller tuning was done with the nearly balanced load case A. In this case the velocity feed forward would nearly reach the desired position and the P Gain could be reduced to a very small value. To get also good results for the other unbalanced load cases the velocity feed forward factor was chosen only 75% of the reference value for the open loop control and the P Gain was increased.

A special hysteresis block was used where the minimum duty cycle  $d_{min}$  was defined by the response time  $T_s$  of the valve and the PWM frequency  $f$ . The corresponding formula is given by (1). Due to this minimal duty cycle no ballistic mode is used to avoid problems with uncertain openings.

$$d_{min} = T_s f \quad (1)$$

The minimum duty cycle for the given valve with  $T_s=1.8ms$  and eg.  $f=100Hz$  is  $d_{min}=0.18$  or 18%. The first measurements were done with  $f=100Hz$ . To achieve very low velocities of the seesaw the PWM frequency can be far below the original frequency of 100Hz. Due to the natural frequency of the seesaw of about 4 Hz PWM operation frequencies of about 12.5Hz should be feasible.

For zero velocity and low upper level control signal  $u$  the valves should be switched off. To prevent repetitive starting and stopping of the system a hysteresis was used. The duty cycle was started at  $u_{start}$  with the minimum duty cycle  $d_{min}$  kept constant till reaching  $d_{min}$  and afterwards rising in a linear way. For a falling upper level control signal  $u$  the behaviour is inverse with one small difference that the valve actuation will be shut off if  $u < u_{stop}$  (see Figure 11). This hysteresis with later stop will reduce the maximum error when reaching the stop position and is required to avoid limit cycle problems during stopping of the motion. Table 3 presents the controller parameters.



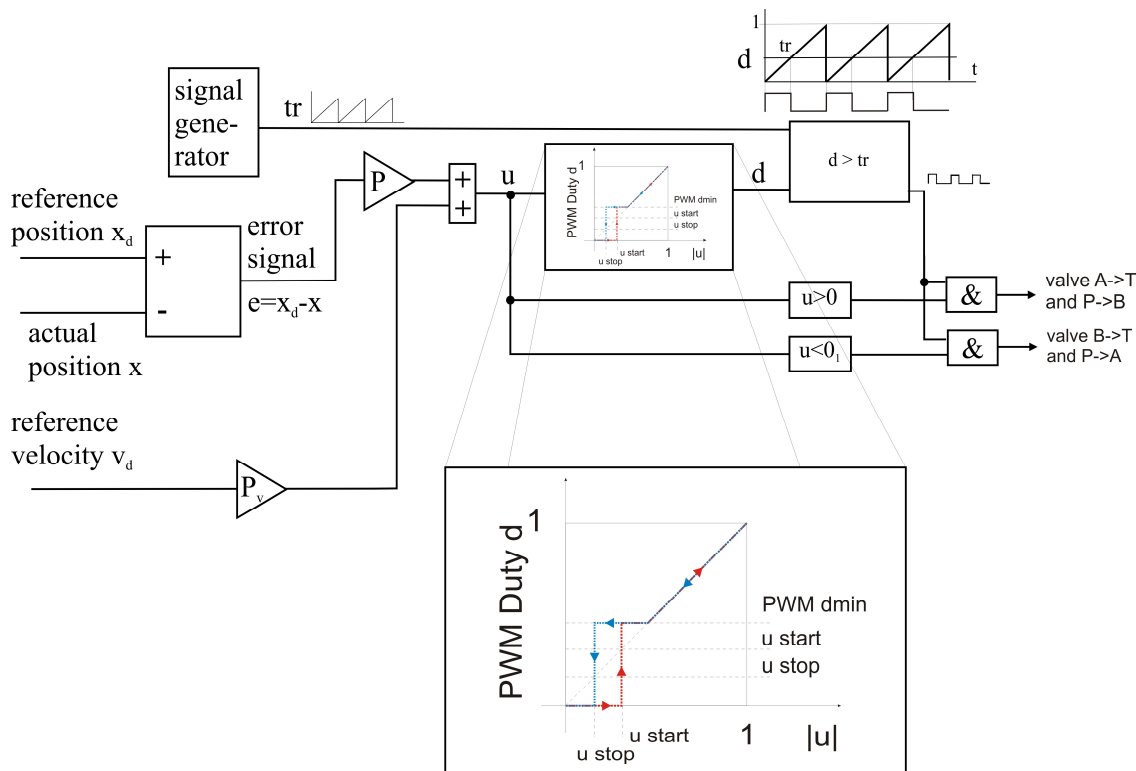


Figure 11. Schematic of the controller

The main benefit of the fast switching valves compared to valves with a longer response time is the smaller possible minimal duty cycle. Compared to a Bosch Rexroth KSDEU valve, for instance, this minimum duty cycle of the FSVi valve is about one fifth, if they are used at the same PWM frequency. Lower velocities can be realized and, in turn, a better controllability at really low velocities. The measurements were done in close loop control for all load cases and also with load case A in open loop and different PWM frequencies.

Table 3. Control parameters

Simulation			Measurement		
$P$	100	1/m	$P$	40	1/m
$\epsilon_I$	120	m	$P_v$	6	1/(m/s)
			$u_{start}$	0.4	1
			$u_{stop}$	0.1	1

### 2.5.2. Measurement results at 25 Hz load case A – closed loop

Even with this simple controller quite good results could be achieved. As there were no special decoupling methods used for the tank side the noise of the PWM only was relatively high. There was a huge difference in noise compared to the PWM/PCM combination where the smallest valve was used in PWM mode with a nominal flow of

one half of the PWM only mode. The lower noise level of the PWM/PCM combination is traded-off by a significantly higher number of valves (12 valves instead of 4).

Figures 12 – 15 present the system responses for different trajectories. On the right hand side of Figure 16 the linearity of the PWM actuation cycle can be seen. The velocity of the movement can be controlled easily with the duty cycle. For really small values of the duty cycle the oscillations are also lower than for higher duty cycles.

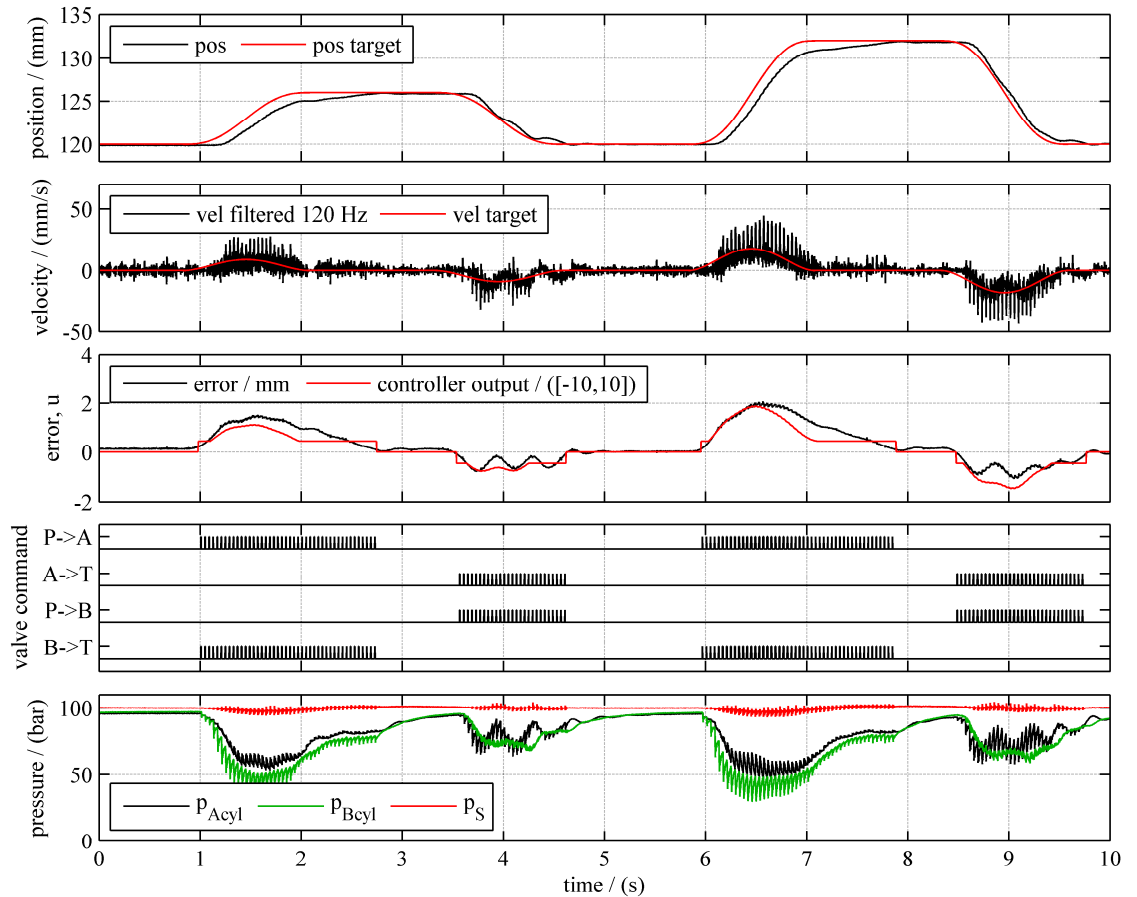


Figure 12. Measurement load case A trajectory small, PWM 25Hz – closed loop control

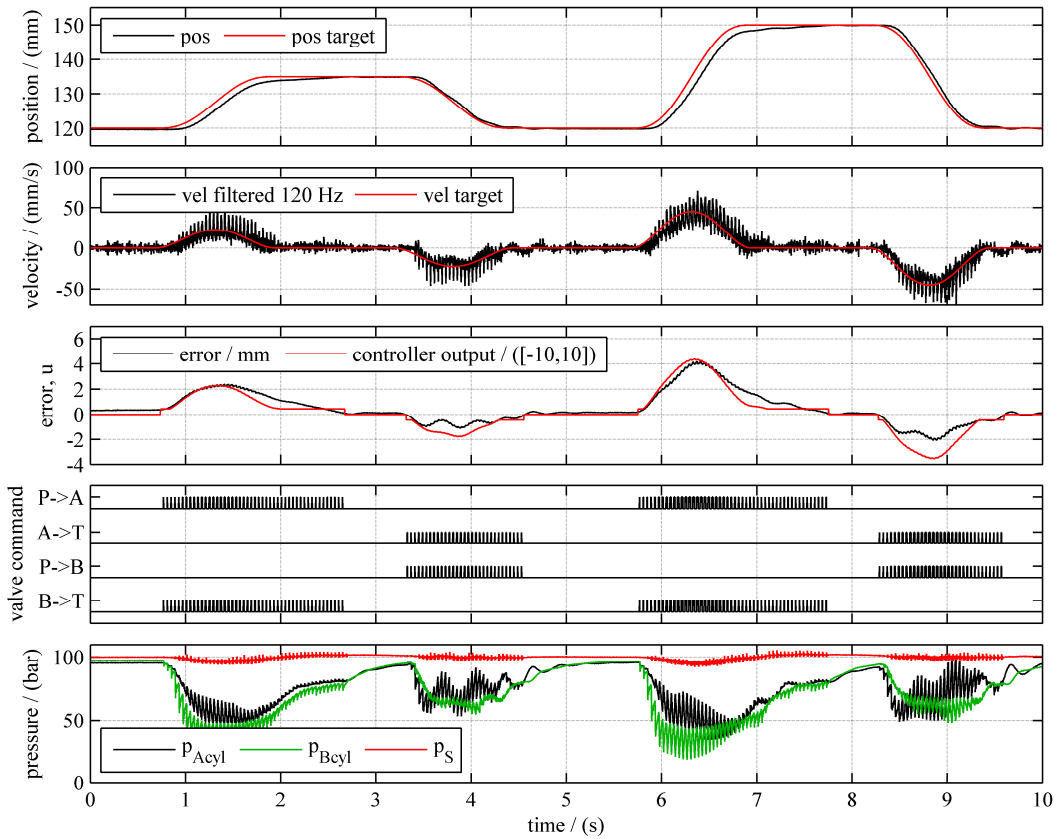


Figure 13. Measurement load case A trajectory medium, PWM 25Hz – closed loop control

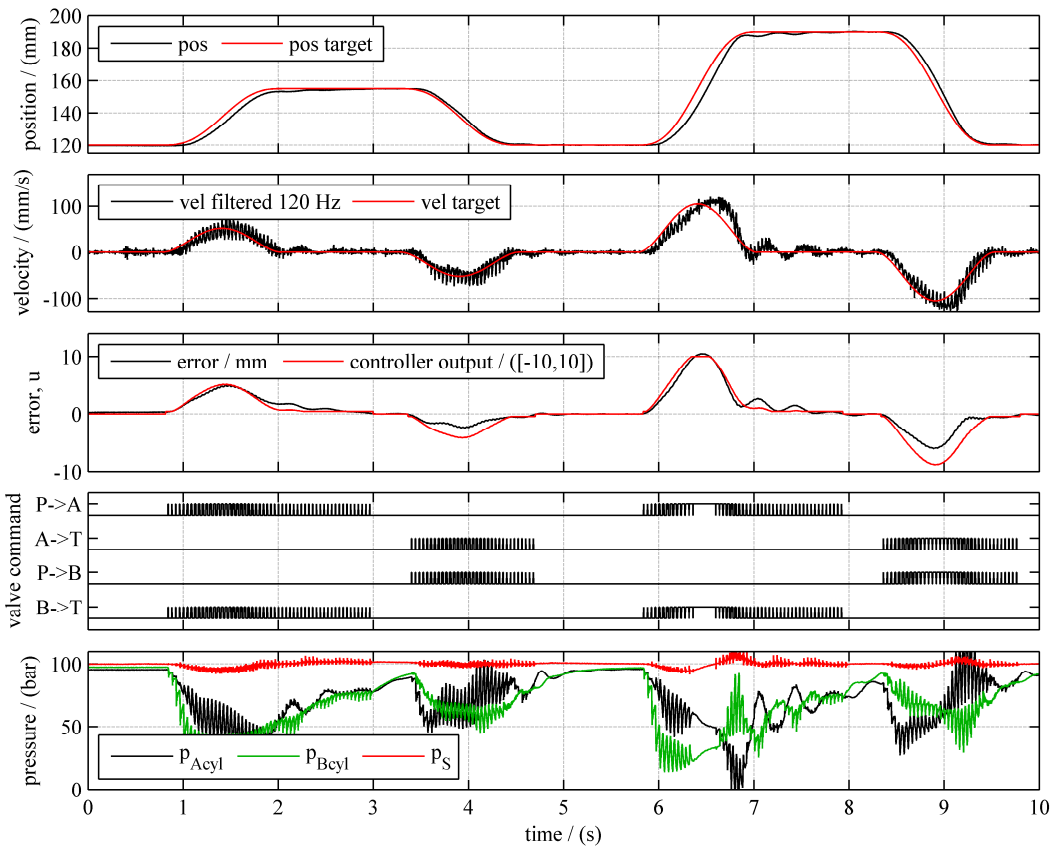


Figure 14. Measurement load case A trajectory large, PWM 25Hz – closed loop control

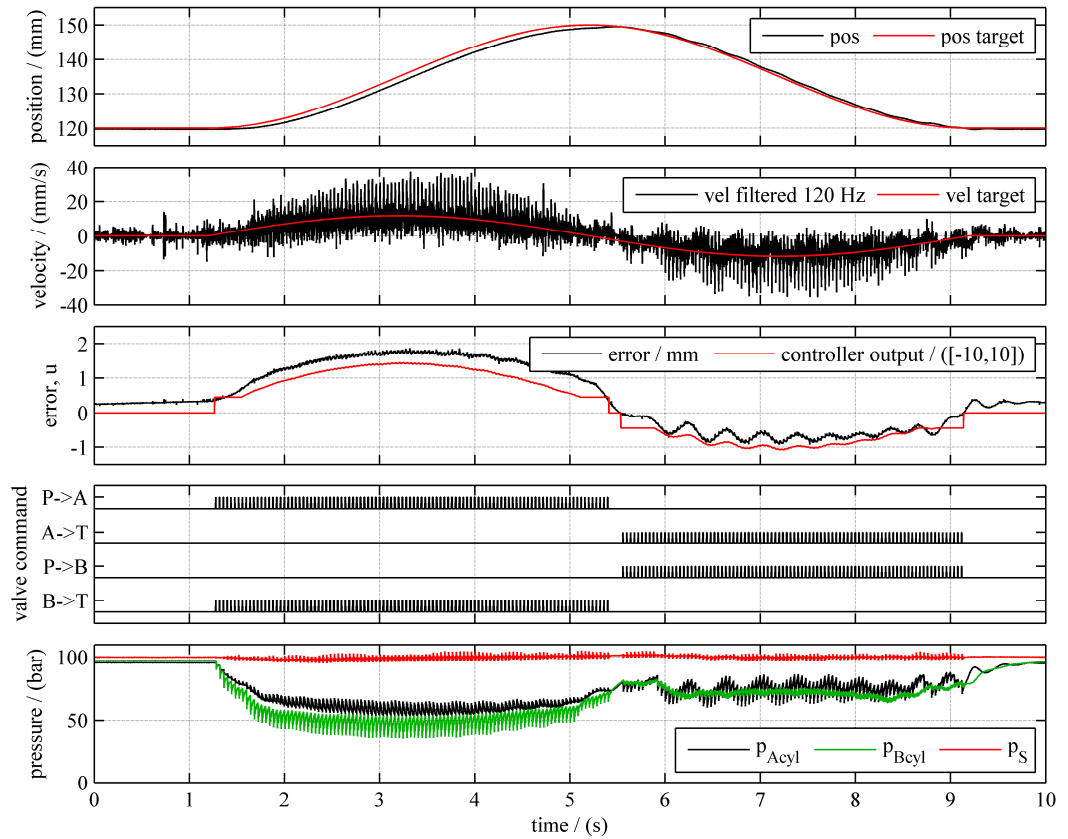


Figure 15. Measurement load case A with sinusoidal trajectory, PWM 25 Hz, amplitude: 30mm – close loop control

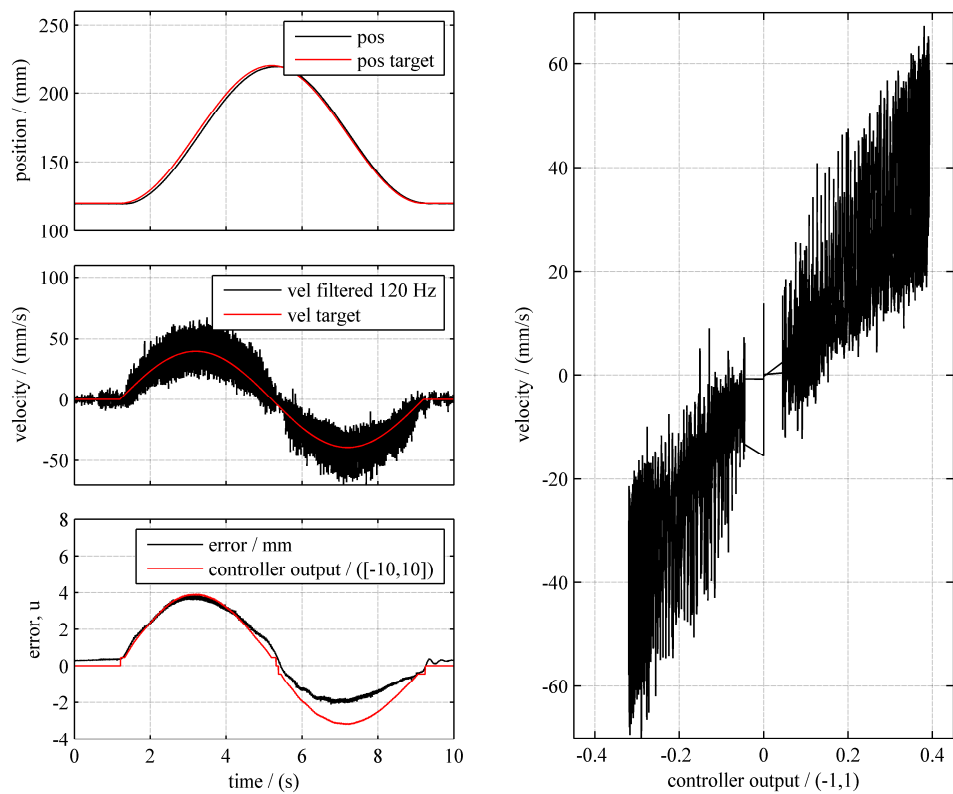


Figure 16. Measurement load case A with sinusoidal trajectory, PWM 25 Hz, amplitude: 100mm – close loop control - test linearity

2.5.3. Measurement results at 25 Hz load cases B and C with large trajectory – closed loop

Figures 17 and 18 present the results for the large trajectory for the remaining two load cases B and C. Results for load case A is presented in Figure 14. These trajectories are quite near the maximum rotational velocity of the seesaw with current valve setup. Though, there is no instability of the system. For a manual driven system such behaviour should be quite acceptable.

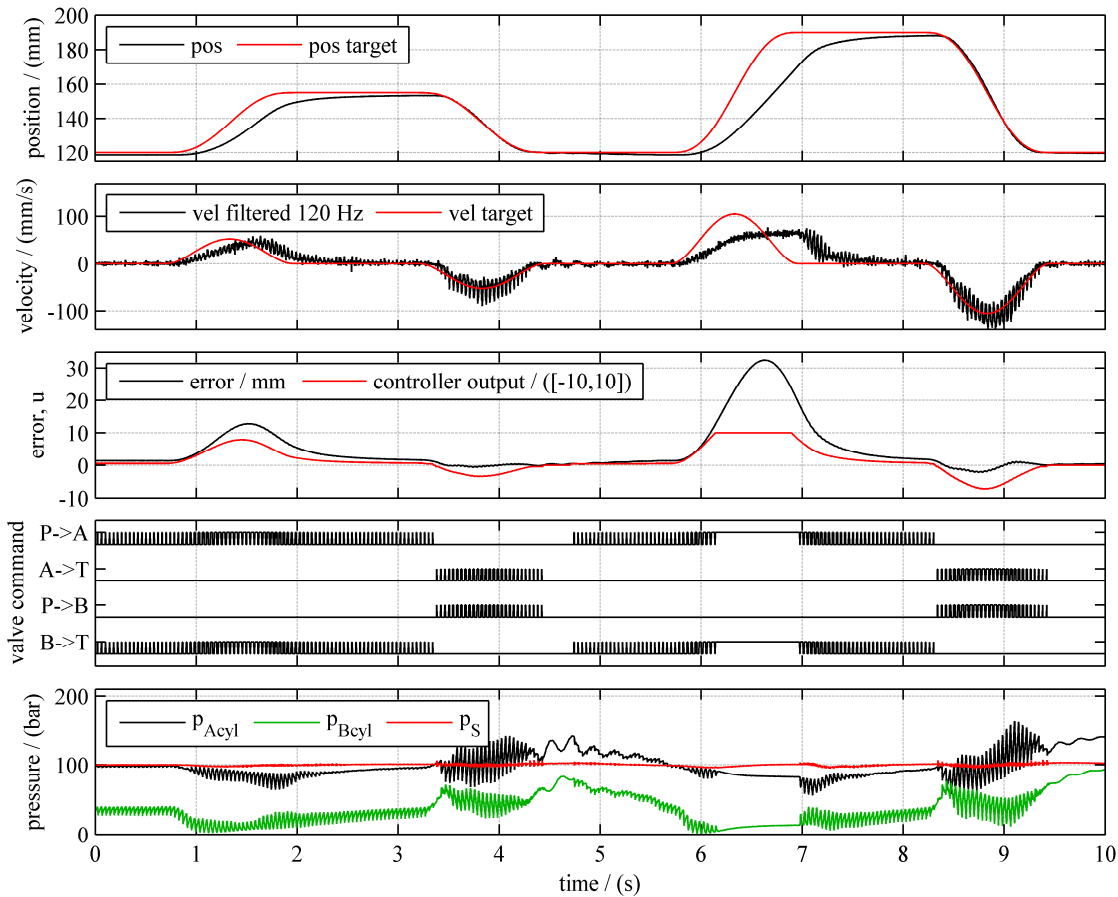


Figure 17. Measurement load case B trajectory large, PWM 25Hz – closed loop control

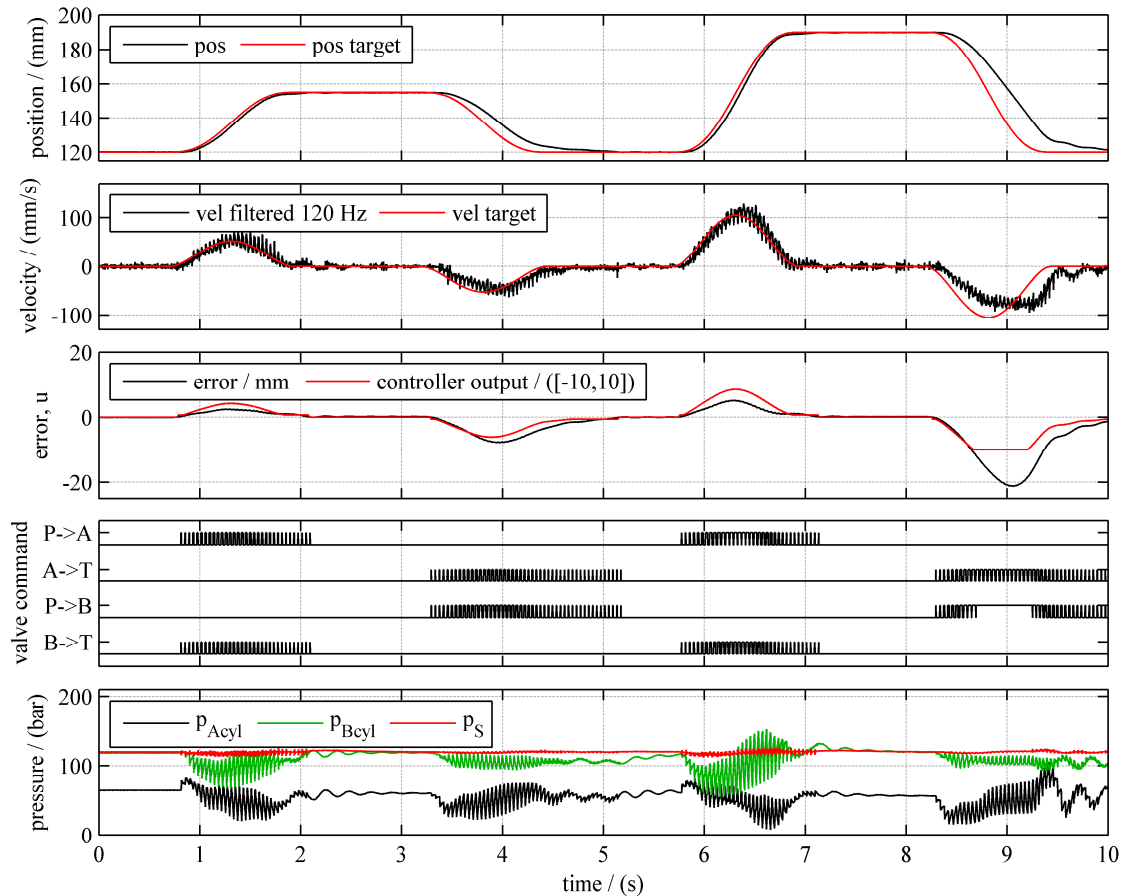


Figure 18. Measurement load case C trajectory large, PWM 25Hz – closed loop control

#### 2.5.4. Measurement results at different PWM-frequencies, load case A with sinusoidal trajectory, amplitude 100mm – closed loop control

In this part of the study different PWM frequencies were used. Figure 19 shows the results with a very low switching frequency (12.5 Hz). The pressure pulsations of 40 bar are relatively high. These pulsations can significantly be felt by putting ones hand on the seesaw boom.

For higher frequencies (Figures 20-22) the pressure peaks are decreasing, but the noise level increases and reaches really annoying levels.

The better controllability at small velocities with lower PWM frequency can also be seen from the zero crossing of the velocity. For higher frequencies the stopping is more distinctive.

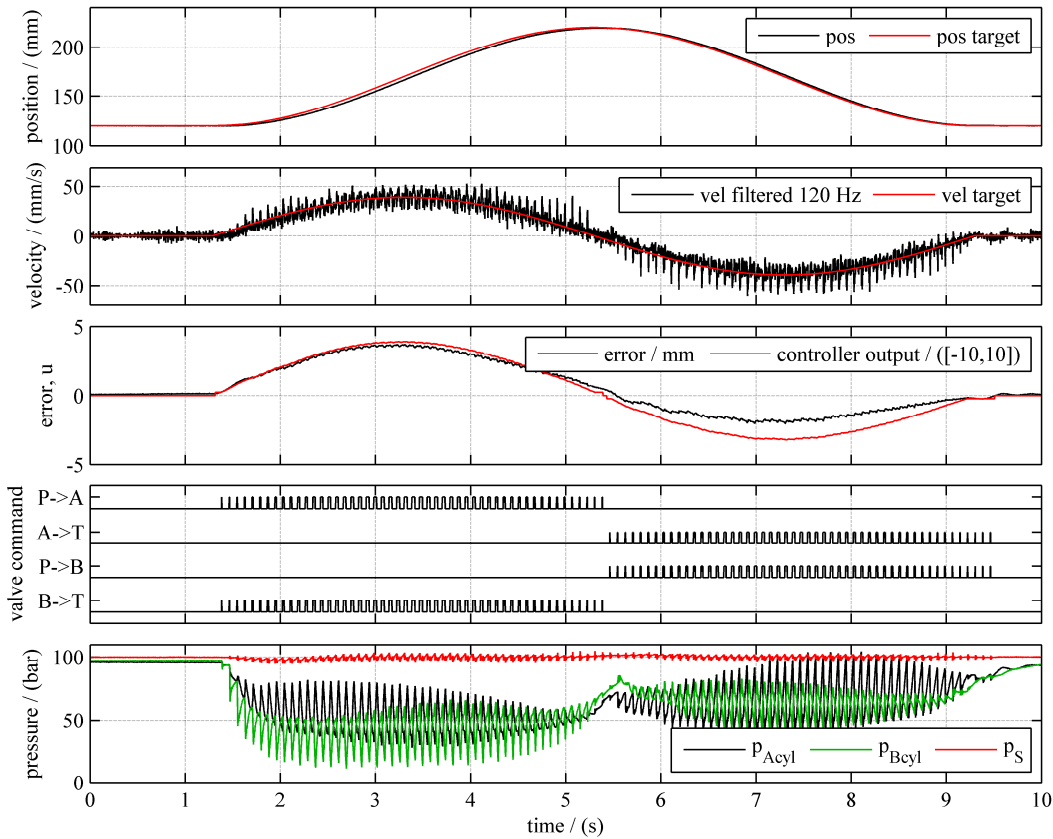


Figure 19. Measurement load case A with sinusoidal trajectory, PWM 12.5Hz, amplitude: 100mm – closed loop control

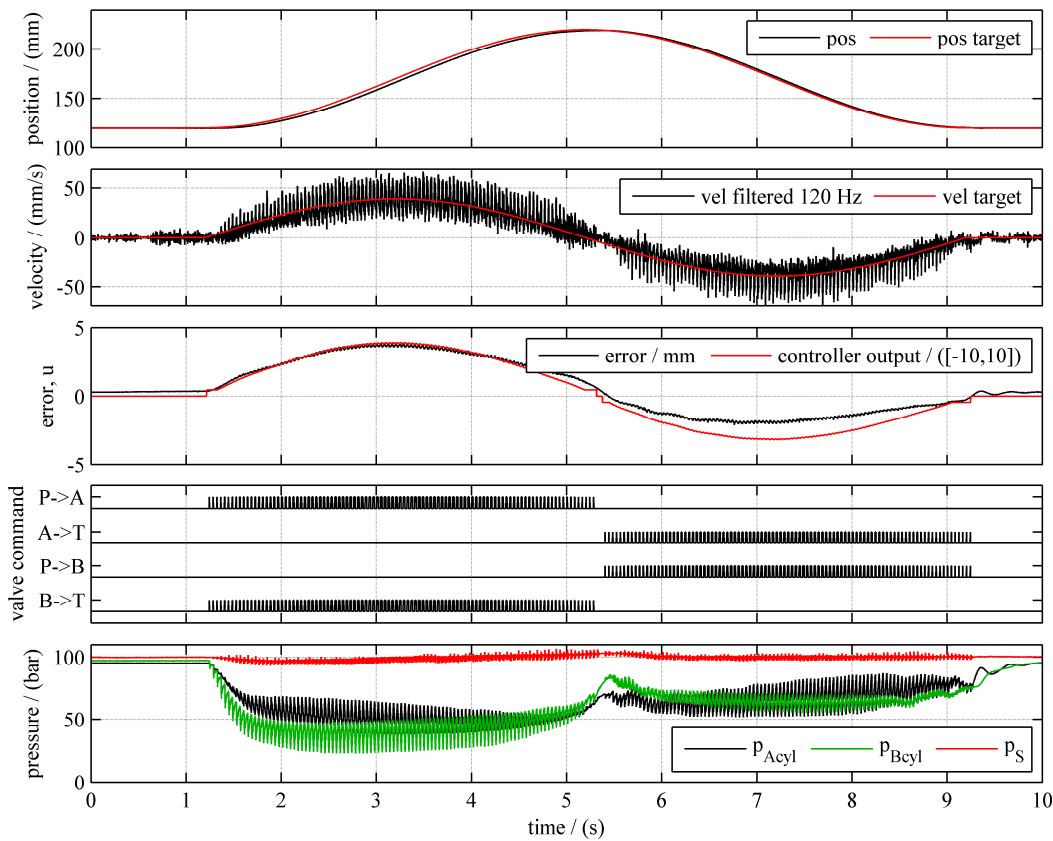


Figure 20. Measurement load case A with sinusoidal trajectory, PWM 25Hz, amplitude: 100mm – closed loop control

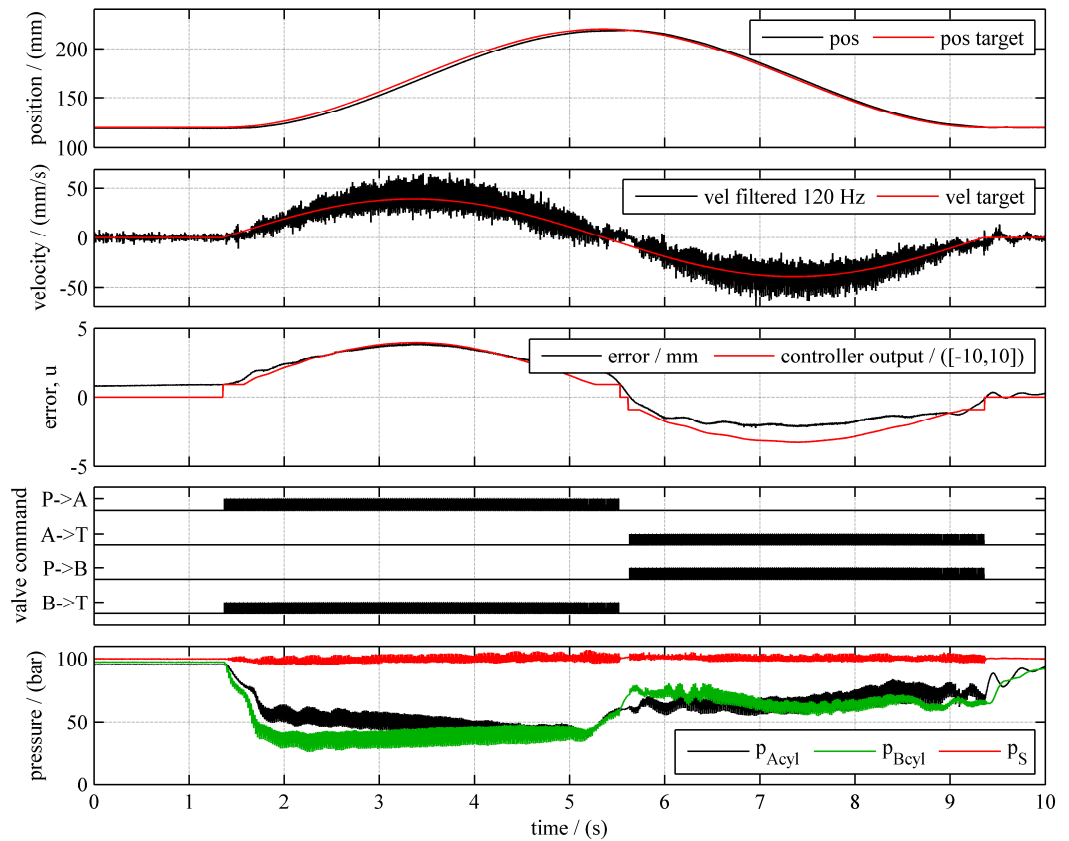


Figure 21. Measurement load case A with sinusoidal trajectory, PWM 50Hz, amplitude: 100mm – closed loop control

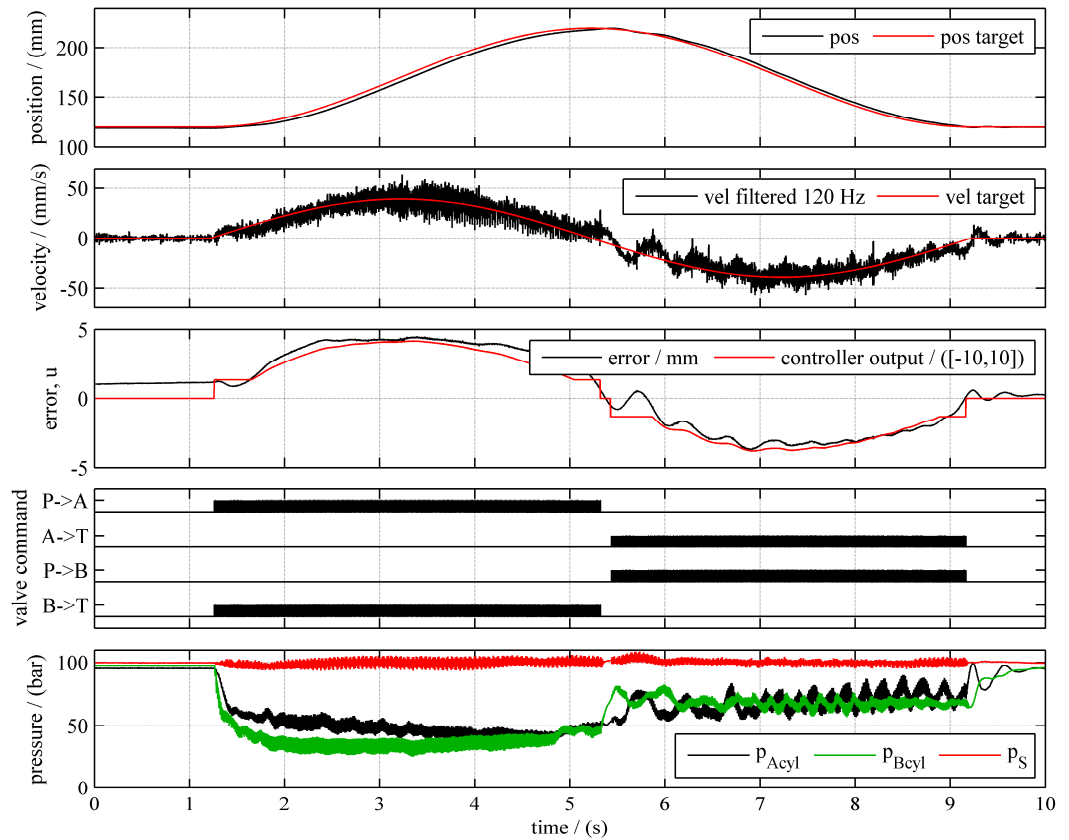


Figure 22. Measurement load case A with sinusoidal trajectory, PWM 75Hz, amplitude: 100mm – closed loop control



### 2.5.5. Measurement results at different PWM-frequencies, load case A with sinusoidal trajectory, amplitude 100mm – open loop control

To demonstrate the good and nearly linear controllability of the system also open loop measurements were done. For these the P-controller was switched off and velocity feed forward was used with amplification  $P_V = 9 / (\text{m/s})$ .

In the Figure 23 the open loop characteristic for the sinusoidal movement for a low switching frequency of 12.5 Hz and a high switching frequency of 100 Hz can be seen. In the plot on the right hand side the velocity over the control output is depicted. By comparing these results it's quite clear that due to the real switching time of the valves there is a trade-off between pulsations and accuracy. Lower switching frequencies result in higher pulsations but give the opportunity to reduce the minimum pulse-width.

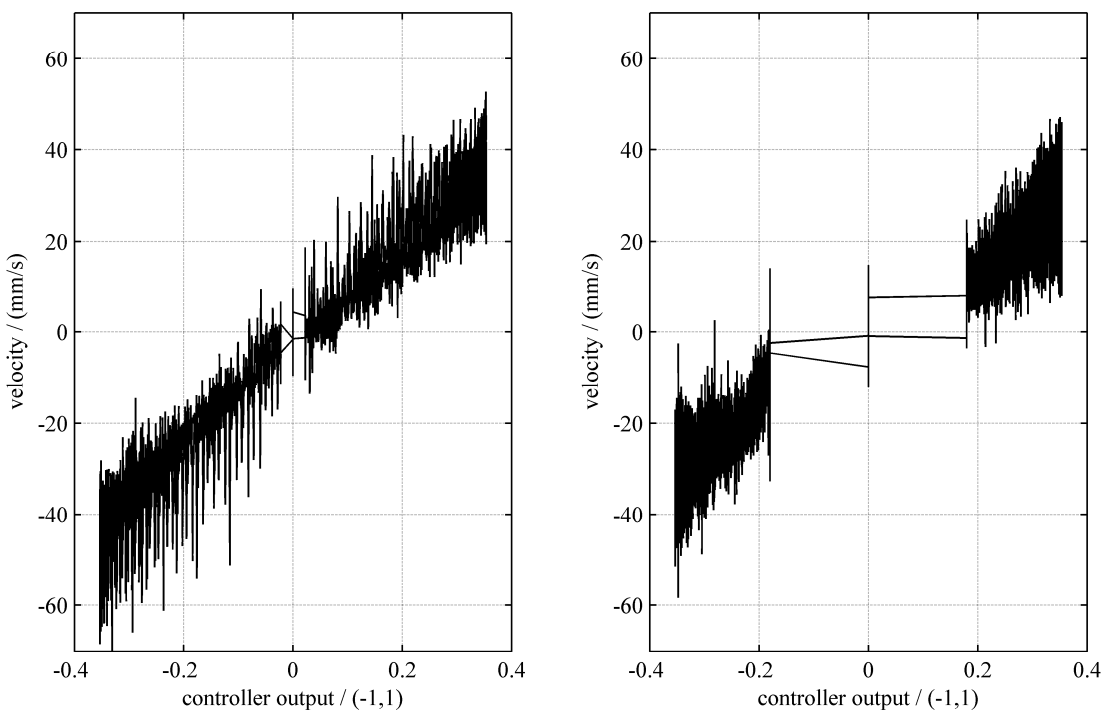


Figure 23. Measurement load case A with sinusoidal trajectory, amplitude: 100mm – open loop control. Left: PWM 12.5Hz; right PWM 100Hz.

### 3. CONCLUSION:

It can be concluded that PWM only mode is possible for the seesaw. As noise is always a problem it could be useful for PWM drives not to open the valves that fast and to employ for example some notches on the spool to smoothen the effective hydraulic response. The main benefit with the fast valves developed by LCM is to get a better controllability at small velocities compared to the system with standard switching valves. The system with only four fast switching valves provides comparable control performance like a proportional control valve [9] in terms of response dynamics and precision. By using a more advanced controller this aspect can be further improved.

## REFERENCES

- [1] Linjama, M., Laamanen, A. & Vilenius, M. 2003. Is it time for digital hydraulics? The Eighth Scandinavian International Conference on Fluid Power, May 7–9, Tampere, Finland, pp. 347–366.
- [2] Winkler B., Plöckinger A., Scheidl R., COMPONENTS FOR DIGITAL AND SWITCHING HYDRAULICS, Proc. The First Workshop on Digital Fluid Power, ISBN 978-952-15-2037-2, pp. 53-76, DFP08, October, 2008, Tampere, Finland
- [3] Plöckinger A, Scheidl R., Winker B., Development and Prototyping of a Compact, Fast 3/2 Way Switching Valve with Integrated Onboard Electronics, The 11th Scandinavian International Conference on Fluid Power, SICFP'09, ISBN 978-91-02-7393-588-3, June 2-4, 2009, Linköping, Sweden.
- [4] Plöckinger A, Scheidl R., Winker B., PERFORMANCE, DURABILITY AND APPLICATIONS OF A FAST SWITCHING VALVE, The Second Workshop on Digital Fluid Power, DFP'09, ISBN 978-3-200-01713-9, November 12-13, 2009, Linz, Austria.
- [5] Helmut Kogler\*, Rudolf Scheidl\*, Michael Ehrentraut\*, Emanuele Guglielmino, Claudio Semini, Darwin G. Caldwell\*, A Compact Hydraulic Switching Converter for Robotic Applications. In Fluid Power and Motion Control (FPMC 2010); N. Johnston and A. Plummer (Eds.); The Centre of Power Transmission and Motion Control, Bath University, UK, 2010.
- [6] Plöckinger A, Scheidl R., Winker B., Combined PWM- and Hysteresis Switching Control For A Digital Hydraulic Actuator, The Third Workshop on Digital Fluid Power, DFP'10, ISBN 978-952-15-2434-9, October 13-14, 2010, Tampere, Finland.
- [7] Huova, M. & Plöckinger, A. Improving resolution of digital hydraulic valve system by utilizing fast switching valves, The Third Workshop on Digital Fluid Power, DFP10, October, 2010, Tampere, Finland
- [8] hydroLib 3.0 / imh, Austria, <http://imh.jku.at/ftp/index.en.php> (2008.04.10)
- [9] Linjama, M., Huova, M., Boström, P., Laamanen, A., Siivonen, L., Morel, L., Walden, M. & Vilenius, M. 2007. Design and implementation of energy saving digital hydraulic control system. The Tenth Scandinavian International Conference on Fluid Power, May 21-23, Tampere, Finland, pp. 341-359.



## THE PRODUCT CALLED NORRDIGI™

Ari Sipola, Jussi Mäkitalo, Jouni Hautamäki  
Norrhydro Oy  
Niittyhaankatu 9, FI-33720 Tampere, Finland  
ari.sipola@norrhydro.com

### ABSTRACT

The NorrDigi™ product is one of the first system products in the field of digital hydraulics. This paper presents the current version of this product.

**KEYWORDS:** NorrDigi™, Product, Digital hydraulics

### 1. INTRODUCTION

Digital hydraulics has been actively researched during the last decade. Industrial research projects have also been running for several years. This paper provides a technical and economical perspective to one of the first system products in the field. This product is called NorrDigi™ – The intelligent motion control solution.

### 2. DIGITAL HYDRAULICS IN A PRODUCT: REALISTIC OR NOT

In this section, the technical and economical sides in exploiting NorrDigi™ digital hydraulic control in commercial boom applications are discussed.

#### 2.1. Linear actuators

The system solution is based on a multichamber cylinder (figure 1.), which enables the selection of effective piston area. Norrhydro has years of experience a manufacturing of commercial multi chamber cylinders. Valves and controllers are normally integrated to the cylinder, and this combination is called linear actuator.

#### 2.2. Control valves

Digital hydraulic systems typically use many on/off –valves to control pressure and flow. From the beginning of the active research era of digital hydraulics, emphasis has been given to find or design suitable valves. This discussion continues today [1]. Another problem has been the complexity of the control methods.

The Norrhydro's NorrDigi™ technology however, is functioning well with existing standard commercial valves, and has thus no urgent need for improved valve technology. Proof of this has been given in three different boom applications, including two multi degree of freedom applications. Proof of a functioning control algorithm for the secondary controlled multi chamber cylinder with three pressure levels has been received simultaneously.

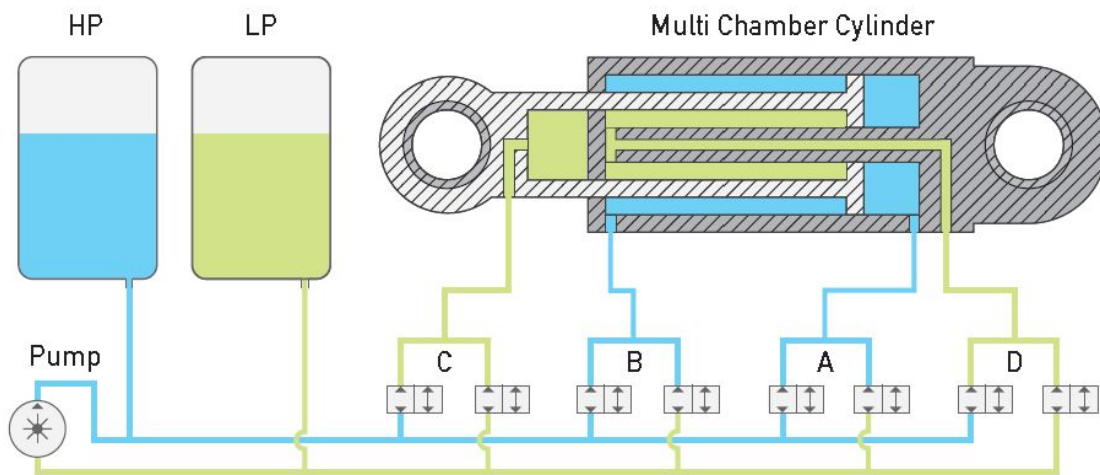


Figure 1. A four-chamber cylinder (Multi Chamber Cylinder) with valves connected to A, B, C, and D chamber, high pressure (HP) and low pressure (LP) accumulators, and a pump.

### 2.3. Power supply and energy level management

Another highly investigated topic in the field is converting power from the shaft of the internal combustion engine (I.C.E) to the needs of the (digital) hydraulic system at hand.

The (three pressure) common pressure rail (CPR) of the system with its (three) pressure accumulators need only a very simple charging method. For example, a simple fixed displacement pump (e.g. inner gear pump) can be used to pump (when needed and not pump when not needed) oil from tank to high pressure, with a very good efficiency at all times. This system enables intelligent power management of the I.C.E.

A tested invention from Norrhydro, the Energy level management unit (ELMU), is then used to transfer energy inside the NorrDigi™ system – also with a very high efficiency. The ELMU is a simple standard component of this control system [2].

### 2.4. Energy storage

A simple way to implement digital hydraulic hybrid machines, that can restore and reuse energy returning from the mechanical system, is to add hydraulic accumulator(s) to the system. The efficiency of different kind of accumulators has been widely studied.

Accumulators have mainly three reasons for not being 100% efficient: frictions or shape transformations, pressure losses due to high flow rates in or out of the accumulator, and

emitted heat due to raised temperature after an adiabatic pressure rise. The studies normally aim to neglect the last issue.

The NorrDigi™ solution aims to serve machines that have high duty ratios. This kind of machines typically operate several working cycles in a row, enabling hydraulic system to charge, discharge, and recharge its accumulator in fast cycles. In this kind of system the energy saving potential is the highest and the problem of the energy loss due to heat dissipated from the accumulators is the lowest. Therefore, commercial standard accumulators can be successfully exploited in this control system.

## 2.5. Controllers

A commercial controller that can operate the commercial digital valves with fast on and off switching times is included in the NorrDigi™ product. This was one of the critical development areas during the R&D-phase of the commercial system.

## 2.6. Price

According to present prospects, a payback time of 6 months to 1 year can be expected in solutions studied by Norrhydro. The system cost is higher than in a traditional system, but payback is gained with lowered energy consumption. This however, is very case specific, since consumption and solution methods vary from user to user and machine to machine.

## 2.7. Overview

The control technology that we use is economical and technically feasible. Case specific studies need to be made to find out the full commercial potential of adding this system to a working machine.

# 3. THE NORRDIGI™ PRODUCT

This section describes the product.

The NorrDigi™ system solution is common pressure rail (CPR) based. From the layout (figure 2.) it can be seen that the CPR is the linkage between the actuators and the energy sources, including the accumulators and the Energy level management unit (ELMU). The ELMU is connected to the pump and the pump to the internal combustion engine (I.C.E).

The NorrDigi™ product is divided into three groups:

1. Intelligent motion control system
2. Intelligent energy level control system
3. Common features

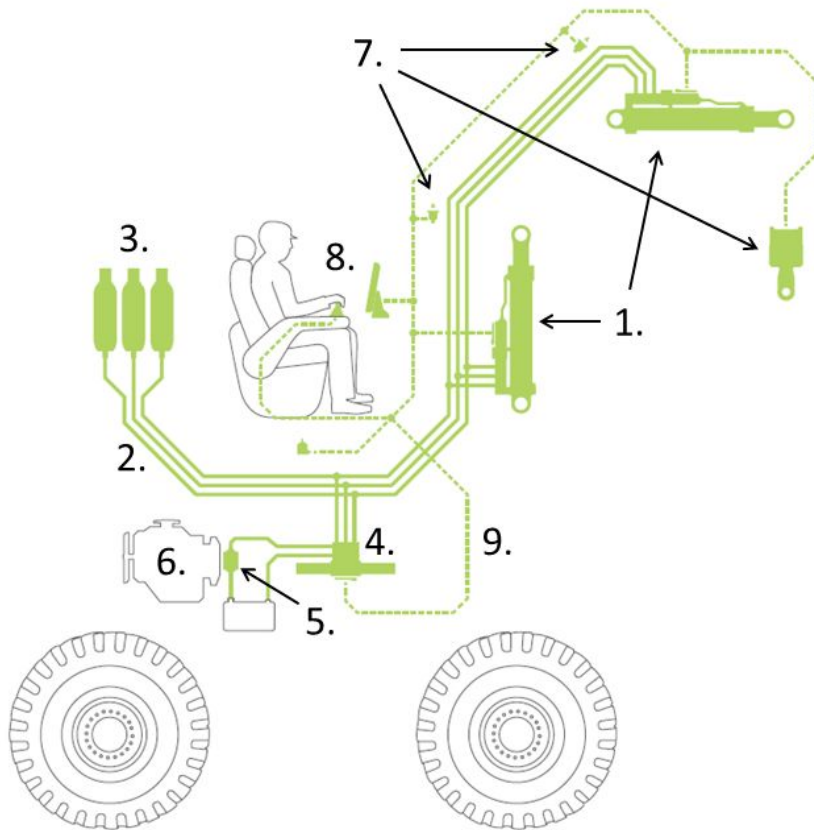


Figure 2. The NorrDigi™ system solution. 1. Actuator that consists of multichamber cylinder with integrated valves and controller, 2. Common pressure rail (CPR), 3. Accumulators, 4. Energy level management unit (ELMU), 5. (Fixed displacement) pump, 6. Customers integrated combustion engine (ICE), 7. Sensors (depend on application), 8. User with interface, 9. CAN BUS

### 3.1. Intelligent motion control system

The intelligent motion control system includes actuators with integrated controllers and digital valves as well as the needed sensors that depend on the machine.

### 3.2. Intelligent energy level control system

The intelligent energy level control enables efficient power input, recovery and reuse to/from the mechanical system or linkage. It consists of three hydraulic accumulators, the Energy level management unit (ELMU) and pump.

1. Accumulators  
Commercial piston or bladder accumulators can be used.
2. Energy level management unit (ELMU)  
The ELMU is a linear actuator that provides and optimizes efficient energy transfer.

### 3. Pump

Existing hydraulic system pump drive can be used as a charging pump unit. Preferable an energy efficient, reliable and cheap fixed displacement pump (e.g. inner gear pump) is used to supply the intelligent energy level control system.

#### 3.3. Common features

The common features include the following components:

1. **Control unit** controls the digital valves in the actuators and ELMU.
2. **Software** is the core component of the NorrDigi™ product.
3. **Intelligent fluid condition management** is a so far untested feature of this intelligent control system. This feature can in theory be used to filter all impurities from the oil using complete flushing of the system. All systems with NorrDigi™ can be equipped with this tool programmatically. That is, absolutely no additional hardware is needed, as long a traditional filtering method is included in the system.

#### 3.4. General safety standards (regulations, instructions, plans, specifications, documentation and reports) for control systems in general machinery.

The following general safety standards (regulations, instructions, plans, specifications, documentation and reports) for control systems in general machinery will be taken into account in the NorrDigi™ system solution when implemented to customer's machine:

- Machine directive 2006/42/EC
  - Machinery Decree VNa 400/2008 (in Finland)
- ISO 13849: Safety related parts of control systems
  - General principles for design
  - Validation tools for hydraulic, electrical and mechanical systems
- ISO 14121: Risk assessment: Practical guidance and examples of method
- ISO 12100: General principles for design: Risk assessment and risk reduction
- ISO 4413: Hydraulic Fluid Power: General rules and safety requirements for systems and their components (IEC 61784-3, IEC 60204-1, IEC 62061, IEC 61326-3)

Safety process flow for system solutions is the following: hazard case and operation case analysis → functionality analysis → performance level analysis (PL) → validation process → documentation.

In a safety process for different applications one important phase is validation in HIL test rig system. List of standards that are met in NorrDigi™ HIL test rig system (shown in figure 3.):

- The evaluation of the risks was carried out according to ISO 14121, ISO 12100
- The following standards are followed: ISO 13849, ISO 14119, ISO 4413, (ISO 6149, ISO 6162, ISO 6164, IEC 60204)



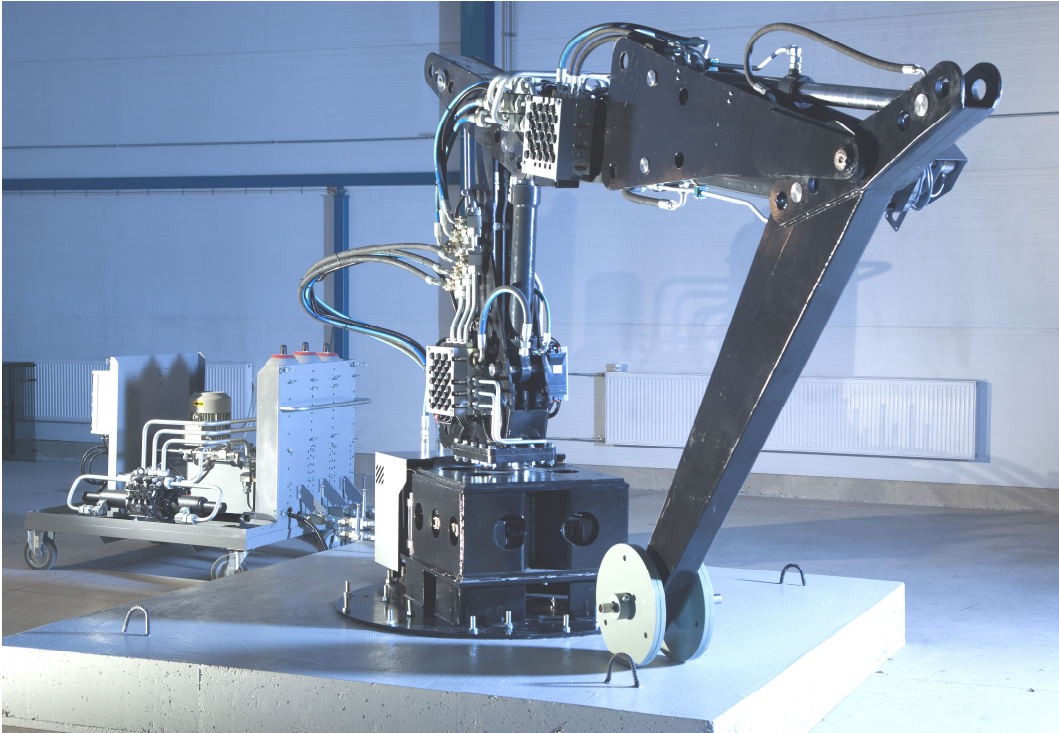


Figure 3. NorrDigi™ test rig in the test hall of Norrhydro R&D Tampere.

#### 4. COMBINING NORRDIGI™ WITH CUSTOMERS MACHINE AND/OR OTHER COMMERCIALY AVAILABLE SYSTEM SOLUTIONS

The NorrDigi™ system solution can be the only system solution in a machine, but it can also be used with other solutions: a) Inside the traditional solution (throttle controlled, pump controlled, secondary controlled), b) In parallel of a traditional system, c) In series with other hybrid solution(s). We believe that one of the most energy efficient ways to implement the NorrDigi™ system solution is to combine it with a drive transmission hybrid, e.g. secondary controlled drive transmission or electric hybrid. Some rough examples are shown in figure 4.

#### 5. CONCLUSIONS

NorrDigi™ system solution is ready to be implemented in different machines. Norrhydro normally provides early virtual validation and real test validation.

Virtual validation:

1. Static pre study and analysis
2. Dynamic simulation study and analysis

Real test validation:

1. HIL and test rig
2. Real test machine
3. Pre series  
→ Serial release

In first task, the feasibility of the customer's machine is studied. A rough level system component dimensioning is realized in this phase as well system cost estimation. If there is enough energy saving potential in the customer's machine, the payback time of implementing this system is short enough and step two can be taken.

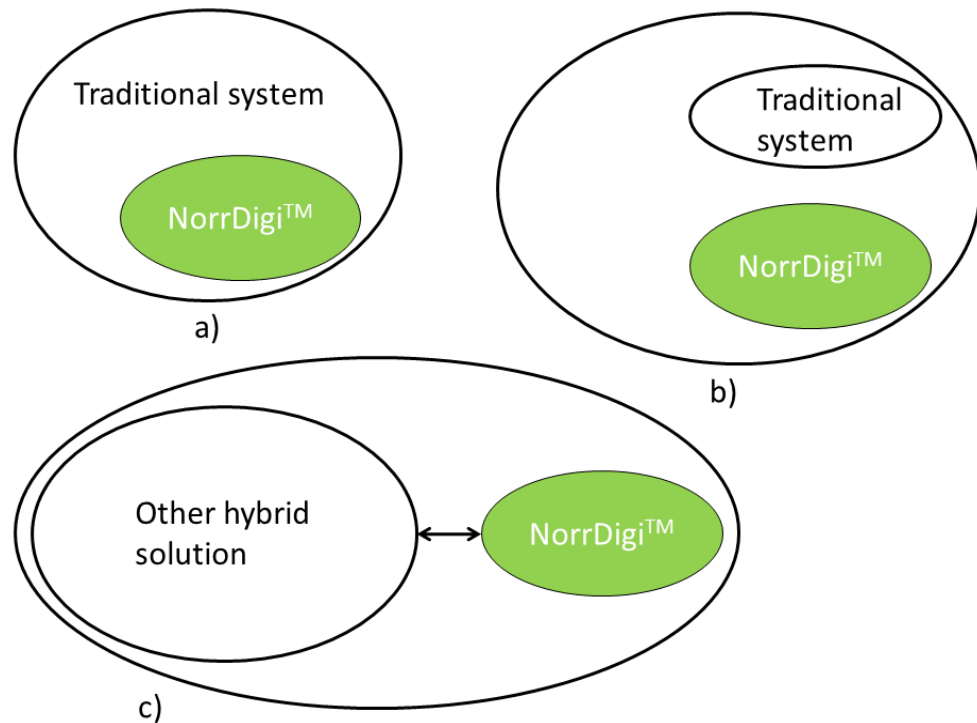


Figure 4. Possibilities in adding NorrDigi™ to a machine: a) Inside the traditional solution (throttle controlled, pump controlled, secondary controlled), b) In parallel a traditional system, c) In series with other hybrid solution

In second task, a dynamic simulation study of the machine at hand is created with NorrDigi™ implementation. Final component dimensioning and system optimization happens in this phase. Simulation results will determine if good enough controllability and productivity can be achieved. If the energy saving potential is also still high, step three can be taken.

In the real test validation, HIL in test rig is the first phase. Last step before serial testing, is to design and realize working test machine. This step should determine the market potential of NorrDigi™ system solution in real market. In this phase, the most critical is to get acceptance of operators as well as acceptance of machine builders.

Norrhydro has not faced any problem that differs from typical R&D-process of new system. All of the challenges so far have been solved over time and the system platform has been functioning very well since 2009 [3].

Biggest challenges at this moment: harmonize new concept with existing safety standards, restriction of conservative market and needed change of mind set.

## REFERENCES

- [1] Linjama, M. 2012. Fundamentals of Digital Microhydraulics. 8<sup>th</sup> International Fluid Power Conference, March 26 – 28, Dresden, Germany, Volume 1, pp.385 – 396.
- [2] NorrDigi<sup>TM</sup> datasheet, NorrDigi<sup>TM</sup> – The intelligent motion control solution, Norrhydro hand out, 2012.
- [3] Linjama, M., Vihtanen, H-P., Sipola, A. & Vilenius, M. Secondary Controlled Multi-Chamber Cylinder. Proceedings of the 11th Scandinavian International Conference on Fluid Power SICFP'09, Linköping, Sweden, June 2-4, 2009, 15 p.

## IMPLEMENTATION OF A DIGITAL HYDRAULIC VALVE SYSTEM WITH BOSCH REXROTH SEC VALVES

M.Sc. Miikka Ketonen  
Tampere University of Technology  
Department of Intelligent Hydraulics and Automation  
P.O.Box 589  
33101 Tampere, Finland  
E-mail: miikka.ketonen@tut.fi

### ABSTRACT

Bosch Rexroth SEC valve was marketed as the first digital hydraulic valve on the market when it was released at the Hannover Fair 2011. SEC is a fast Cetop 3 fittable leak-free directional valve that embodies one to four on/off seat valves in its body enabling the control of two independent flow paths with two solenoids. The company has been presenting a PWM (Pulse Wide Modulation) based control method known as ballistic control which takes an advantage of very short control pulses for which the seat is not fully opened. Ballistic control enables very accurate pressure control or cylinder velocity control with very low velocities and it gives smaller pressure ripple and noise compared to PWM-control where the valve is fully opened. Combination of ballistic control and parallel connected on/off-valves can improve the controllable velocity area and increase the maximum flow. In this paper a 4-way valve system is realized by connecting Bosch Rexroth SEC -valves in parallel and by utilizing the two separate control edges inside the valve to achieve a fully separate control of each control edge.

**KEYWORDS:** Digital hydraulics, Digital Valve System, Bosch Rexroth SEC, Ballistic control

### 1. INTRODUCTION

A system designer of a hydraulic valve system has to make a compromise between performance, reliability and cost. To improve the weaknesses, such as sensitivity for contamination, excessive pressure drop, leakage and high cost, of traditional servo and proportional valves, digital hydraulic valves have been proposed. Two different digital technologies, parallel connection of valves [1] and high frequency valve switching [2], seem both promising. Both technologies have their up and down sides and therefore combining these technologies has also been discussed [3, 4].

## 1.1. Control methods of digital valve systems

Parallel connected and pulse modulated valve systems have both several different control methods which all have their benefits and limitations. These methods have been discussed in numerous papers and will only be discussed here briefly. Summary of different control methods is presented in figure 1.

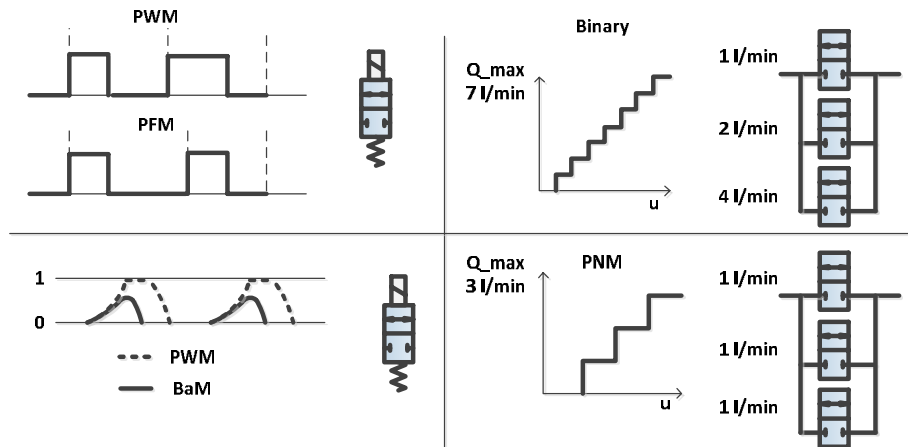


Figure 1. Summary of control methods.

### 1.1.1. Parallel connected switching valves

Binary coded (PCM, Pulse Code Modulated) series of parallel connected valves can achieve controllability comparable to a proportional valve with 5 switching valves and comparable to a servo valve with 6 or 7 switching valves per control edge [1]. 4-way cylinder control requires this number for each of the four metering edges totalling 20 – 28 switching valves. Using the sum of individual flows over the separate edges, controllability of a standard mobile proportional valve was achieved with 4 valves in [3]. Controllability is improved in cylinder applications where supply pressure can be controlled e.g. with electronic LS-control. With LS-control it is also possible to decrease the pressure difference with small openings to improve the control resolution.

PNM-control (Pulse Number Modulation) requires a large number of switching valves to achieve good controllability. With current commercial switching valves this would lead to a very large and expensive valve packages and therefore a special switching valve optimized for PNM-coded digital valve systems is needed. A PNM-coded valve systems and valve miniaturization has some benefits which makes it an interesting possibility. Fault tolerance becomes very good and a fault in one valve is hardly noticeable in the output flow. Also the certainty of flow rates during state transitions will improve the pressure behaviour compared to state transitions of PCM-coded DFCUs. PNM-coded valves can also have different flow rates and even different response times can be tolerated.

Binary and PNM coding methods can be mixed with different control schemes. One of them is the Fibonacci-coding (1:1:2:3:5...) which reduces transitional pressure peaks between states.

### *1.1.2. Pulse modulated control methods*

An alternative way to realize digital valve system is to use PWM (Pulse Width Modulation) or PFM (Pulse Frequency Modulation) that requires only a single valve for each metering edge. This minimizes the purchase costs and leads to simple configuration of the system. The main challenges of PWM control are the discontinuous flow which creates pressure pulsation, noise and jerky motion of an actuator, and the uncertainty of effective valve opening especially with small and large duty ratios. Pressure variations can be minimized by using very fast switching valves which enable high switching frequencies. High activity of the valve demands durable valves and as only a single valve is utilized the fault tolerance is poor.

Pressure variance and noise can be decreased if PWM control signal is switched on for only a short duration during which the valve stroke is not complete. This control method was recently proposed by Bosch Rexroth in [5]. Ballistic Mode (BaM) is well suited for cylinder position control or pressure control while piston is not moving, and it is capable of very high resolution. Uncertainty of the effective opening of the valve requires always some filtered feedback signal from the system. Big challenge for the ballistic control is to maintain wide enough controllable range in terms of the maximum allowed frequency since the time window during which the valve member is moving is very short for fast switching valves. Uncertainty of the valve delay and response time and the possible electromagnetic phenomena due to residue magnetism can also reduce the ballistic range. Optimized pulse modulation (OPM) that utilizes a valve model was introduced in [6] to improve the controllability.

### *1.1.3. Combining parallel connected valves with pulse modulation*

Combining ballistic control with parallel connected valves can reduce the number of valves needed. A DFCU combining binary coding and PWM-control was presented by Huova & Plöckinger in [3]. It was noticed that the usage of small PWM-controlled valve in parallel with on/off valves can improve the control resolution significantly with relatively small pressure variations. Simplest way to combine these control methods is to use similar valves from which one can be controlled with PWM. By utilizing ballistic control it is possible to achieve very small velocities and yet to achieve reasonable controllability with higher velocities. In many applications moderate velocity accuracy can be tolerated with medium or high velocities. In such cases it could be advantageous to use for example a PNM-coded series of progressively increasing flow rates and to control one of the valves with ballistic control. If the ballistically controllable range is limited to small duty ratios, the valve should have an adequate flow rate. Optimal control methods for combining binary or PNM coding with ballistic control is to be studied in the future.

## **1.2. Bosch Rexroth SEC directional valve**

The Bosch Rexroth SEC embodies in standard Cetop3 fittable structure up to four inner spring-loaded poppet valves and one or two actuating solenoids. Each of the inner poppets can be replaced by a plug which results in 15 different available configurations. Flow rate according to the manufacturer is 10 l/min @ 1 MPa. Standard version with

four poppets is presented in figure 2 on the left and the configuration studied more closely in this paper on the right.

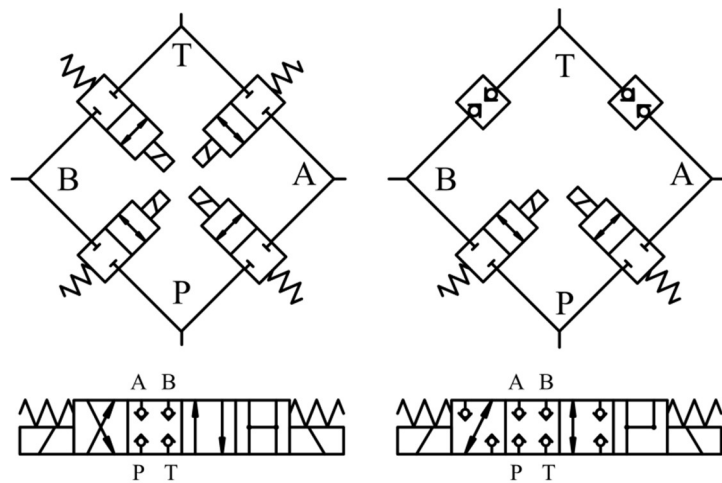


Figure 2. Operating principles of two configurations of the SEC-valve (4SEC 6 E & 3SEC 6 E13).

In the studied configuration, one solenoid is actuating only one poppet valve instead of two and thus faster performance can be assumed although it is not measured in this paper. The valve coil and control schematics of the power electronics have also significant role when the valve response time is optimized. To achieve high response times the solenoid current has to be raised fast with a high pull-in voltage.

### 1.3. Digital valve system realizations

So far most of the digital valve systems have included poppet type cartridge valves physically arranged according to the example in figure 3. The valve block is a 6-bit 4-way digital valve block with 24 pcs of Bosch Rexroth KSDEU-valves. Dimensions of the system in figure 3 are roughly 290mm x 310mm x 100mm (9 dm<sup>3</sup>) without the connectors. Cartridge valves have many well-known good features e.g. good flow/volume ratio and compact structure. The flow rate of a single valve is around 14 l/min @ 1MPa according to the manufacturer. For comparison, the ratio between the flow rate of an ideally binary coded DFCU @ 1MPa and the block volume is 3.06 (l/min)/dm<sup>3</sup>. On/off cartridge valves have potential to be smaller and faster than the current state of the art valves, which enables smaller and more effective valve packages. Currently most on/off poppet valves have a diameter of around 36 mm which defines the valve block size.

Valves designed for Cetop 3 subplate are usually spool valves that have noticeable leakage. Also the physical structure of the valve makes it less convenient for digital hydraulic valve packages. SEC-valve offers two separately controllable control edges, which lowers the number of valves needed in a digital valve system.

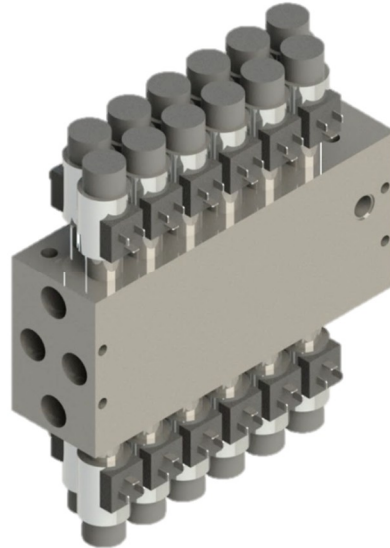


Figure 3. Typical 4-way 6-bit digital valve system.

If each meter-in and meter-out edge of a 4-way digital valve is separately controlled, four DFCUs are needed which requires two rows of 3SEC 6-valves (figure 4). The 6-bit valve design in figure 4 fits the cuboid of 240 x 315 x 185 (14dm<sup>3</sup>). The flow rate – block volume ratio is 1.4 (l/min)/dm<sup>3</sup>. Each bit to DFCUs adds extra 50 mm to the length of the valve package. Design allows only small tank line pressures specified in data sheet of the valve.

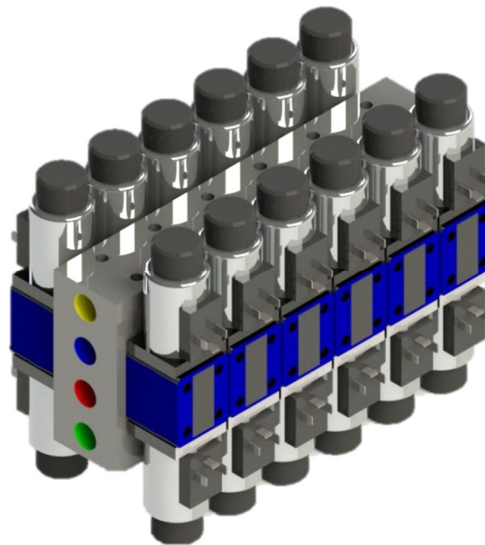


Figure 4. 4-way 6-bit digital valve with separated control of meter-in and meter-out edges.

If the SEC-valves are equipped with 4 poppets, edges P→A and B→T and vice versa edges P→B and A→T are controlled with the same solenoids. In the valve system of figure 5 the number of the valves is reduced but the benefits of separately controlled meter-in and meter-out edges are lost. This design fits the cuboid of 240mm x 315mm x 110mm (8,3 dm<sup>3</sup>). It could also be utilized as a 3-way digital valve system if SECs with two poppets are used.



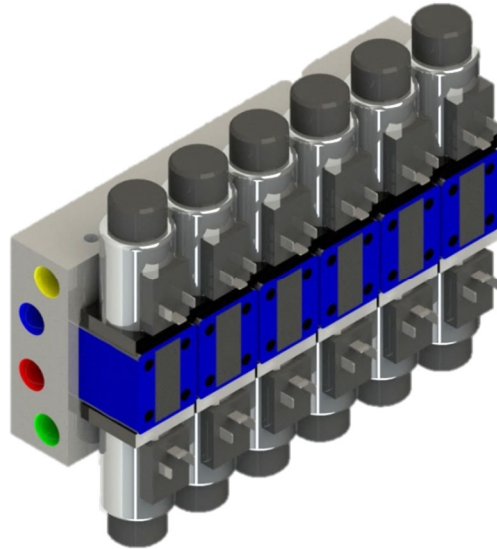


Figure 5. 4-way 6-bit digital valve with coupled control of meter-in and meter-out edges.

## 2. 4-WAY DIGITAL VALVE SYSTEM WITH 3/3 SEC-VALVES

The 4-way digital valve system built in this paper consists of 12 pieces of similar 3/3 two poppet 3SEC 6-valves with 12 VDC coils. Since each valve is similar, half of the valves have to be connected so that P-ports of the SEC-valves are connected to the T-port of the valve block. The valve system is built with a drain port for the disabled tank ports of the valves to allow the possibility to use higher tank line pressures than specified in the data sheet (2 MPa). The valve block is presented in figure 6.

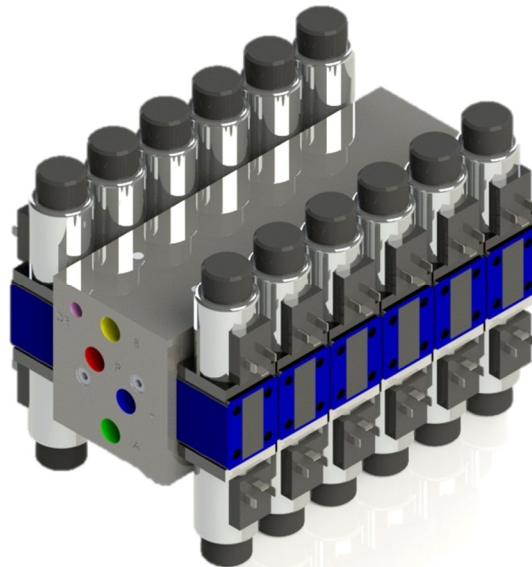


Figure 6. 4-way 6bit digital valve system with 12 x 3SEC 6 E13 valves.

The thinner design of figure 4 could have been realized if the operation had been guaranteed with higher tank line pressures. Flows of four of the A and B ports are throttled with 2.0, 1.5, 1.0 and 0.8 mm orifices. Two A-ports and two B-ports are left

without throttling to increase the maximum flow of the valve and thus results in 47 different available flow rates instead of 63 of the standard 6-bit DFCU.

### 3. EXPERIMENTAL SYSTEM

The measurement system presented in figure 7 is built to analyse first a single valve and after that each of the DFCUs. The measurement of the 3SEC 6 valve is done by applying DC voltage to both a 12 VDC and 2.5A coil, and a special 2Ω and 2.5A coil.

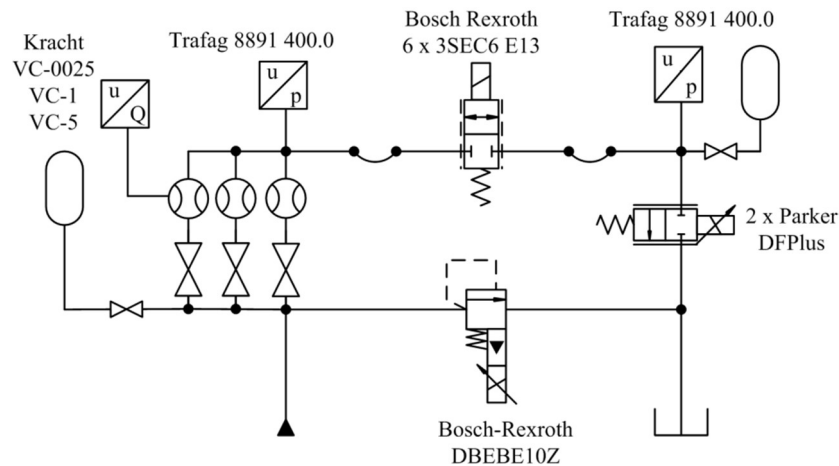


Figure 7. Experimental test system.

Measurement system is realized with dSPACE-1103 controller board. Pressure transmitters are Trafag 8891 with maximum pressure of 40 MPa and the flow is measured with Kracht VC1 and VC5 flow meters. Valve response times are analysed utilizing a clamp type current sensor from Fluke and a voltage meter. Supply pressure is controlled with a proportional pressure relief valve Bosch Rexroth DBEBE10Z. Flow is supplied by a pump unit with a maximum flow of 250 l/min and maximum pressure of 32 MPa. Back pressure is controlled with two parallel connected Parker DFPlus proportional 2/2 valves for sufficient flow rate. Oil temperature in the measurements is  $35 \pm 2$  °C.

For a single valve measurements two booster electronics are tested. Bosch Rexroth VT-MSFA1 booster for the 2Ω-coils is tested with the 2Ω-coils and a booster amplifier built at the Tampere University of Technology, IHA-booster, is tested with both 2Ω- and 12 VDC-coils. The VT-MSFA1 is designed for a single coil and its boosting parameters (pull-in voltage, pull-in time and hold-voltage) are defined by the manufacturer while our amplifier is designed for 24 valve outputs and it allows flexible tuning of each parameter. VT-MSFA1 realizes a pull-in voltage of 48 VDC for 5.5 ms which is followed by a 10 ms period of lower pull-in voltage of 22 V with current limited to 5.5A. After 15.5 ms the voltage is dropped to around 6 VDC. For the 12 VDC-coils the pull-in voltage is set to 48 V for a pull-in time of 12 ms. Hold-voltage is set to around 8V which was determined to be sufficient for keeping the valve open with high pressure differences.

#### 4. EXPERIMENTAL RESULTS

Static characteristics of the built valve system are presented in figure 8. Static measurements involve measuring pQ-characteristics of each poppet valve.

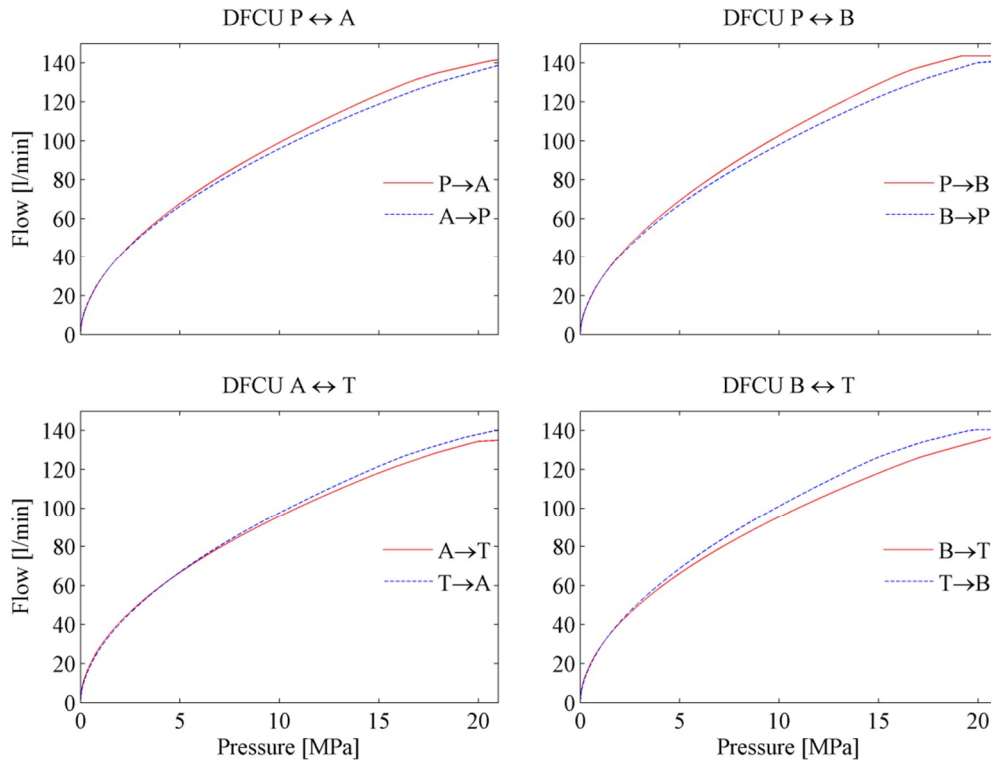


Figure 8. Characteristic curves of each DFCU to both directions and all valves open.

DFCUs have some variance partially due to the valve block design and partially due to the variance in valve flows. Flows of each DFCU are around 55 l/min @ 3.5 MPa that equals to 3.7 times the flow rate of a single valve which was around 15 l/min @ 3.5 MPa. Individual static measurements are presented in figure 9.

Especially the flows of two un-throttled valves (valves 5 & 6) have significant variation in some of the flow directions. Flows of 3SEC 6 seem to be slightly bigger in direction  $P \rightarrow A$  and  $P \rightarrow B$  than to directions  $A \rightarrow P$  and  $B \rightarrow P$ . Also the block might have a small effect on the flows.

Operation limit with the 12 VDC-coils is determined to be 120 l/min and the only jamming occurs with flow direction  $T \rightarrow A$  when a DFCU partially jams open for a short time at pressure differences over 20 MPa when closing from the full state. Operation limit with the 2Ω-coils is determined to be slightly lower and a maximum flow of 35 l/min @ 16 MPa is measured with a single valve with flow direction  $P \rightarrow A$ . Increasing the hold voltage does not improve the operation limit since the problem was noticed with the closing of the valve that is actuated by the spring. A single valve is measured to function with a flow of 35 l/min @ 30 MPa when 2.0 mm throttle is used to limit the flow. It can be concluded that the actual operation limit of a single valve is around 35 l/min and that for large pressure differences throttling should be used.

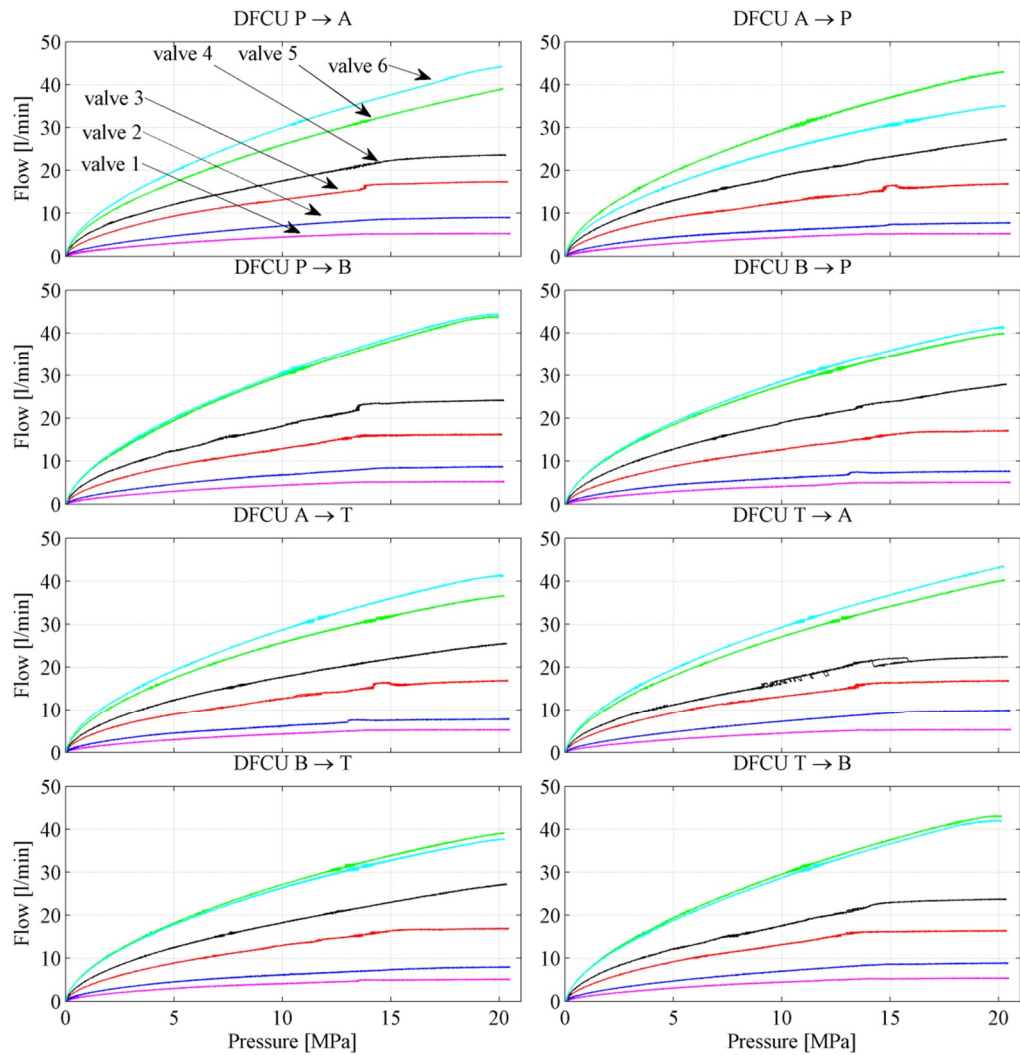


Figure 9. Characteristic curves for each valve in both directions.

Available flow levels with three different pressure differences are presented in figure 10. The selected set of orifices realized a rather large flow rates compared to a single valve. The control resolution is quite similar in the whole range. Resolution, i.e. the relation of the largest flow step and the maximum flow rate, is varying from 22.2 to 23.4. By selection of the orifice series it is possible to affect whether the series has good controllability in the whole velocity range or whether the high resolution is targeted to small velocities.

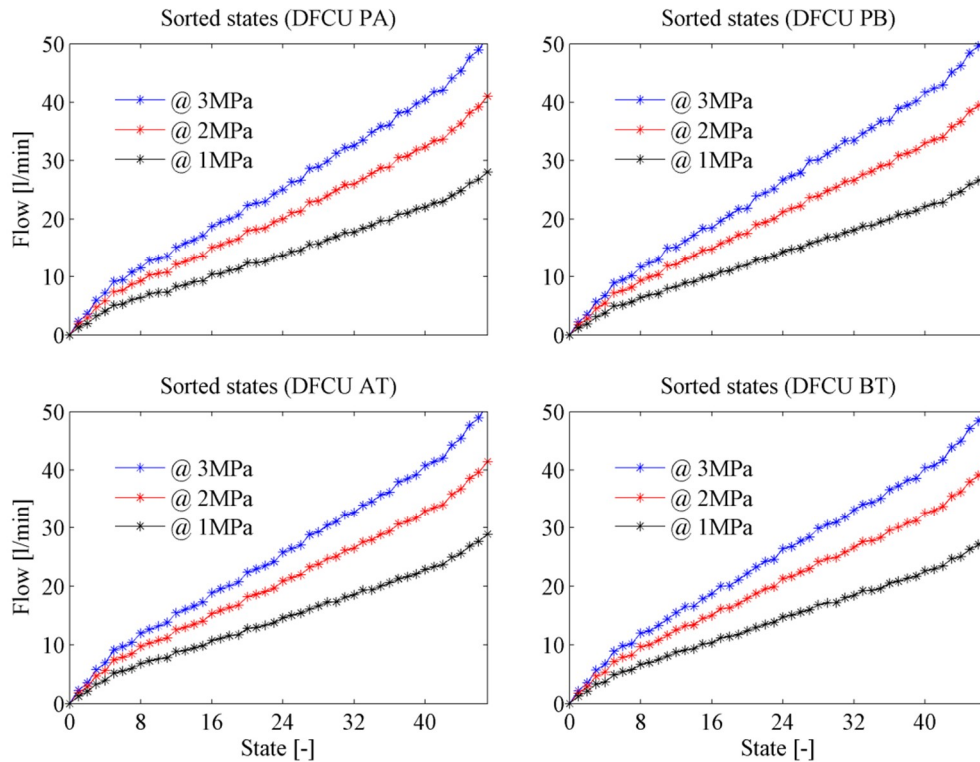


Figure 10. Achievable flow rates of each DFCU with a pressure difference of 1, 2 and 3 MPa.

Dynamic properties of a single 3SEC 6 -valve with  $2\Omega$ -coils and with the IHA- booster is presented in figure 11. Summary of the delays and response times is presented at the final chapter. From the figure 11 main dynamic characteristics can be estimated without the need to measure the position of the poppet. Points 1 and two 2 proposes that the valve delay is around 4 ms in opening and 4 ms in closing. Due to the low resolution of the flow meter, total response time can be estimated more precisely from the current to the solenoid coil and from the voltage over the coil due to changes in the inductance of the coil when the valve collides to the housing of the valve. The pull-in time for the 48V pull-in voltage is set temporally too long to be able to observe the effect of the changes in the current when the valve hits the end in 6 ms at point 5. Proper pull-in time would be close to that time. Closing of the valve can be estimated to be around point 6 which gives a closing time of also around 6 ms. With pressure differences close to the operation limit valve closing time slightly increases to directions  $P \rightarrow A$  and  $P \rightarrow B$  and vice versa decreases to directions  $A \rightarrow P$  and  $B \rightarrow P$ .

Dynamic characteristics of the built valve system with 12 VDC coils are presented in figure 12 and 13. 3SEC 6 -valve with 12 VDC valves has an opening delay of around  $8 \pm 1$  ms and total opening time of  $9.5 \pm 0.5$  ms. Closing delay is  $7 \pm 1$  ms and total closing time around  $8 \pm 1$  ms.

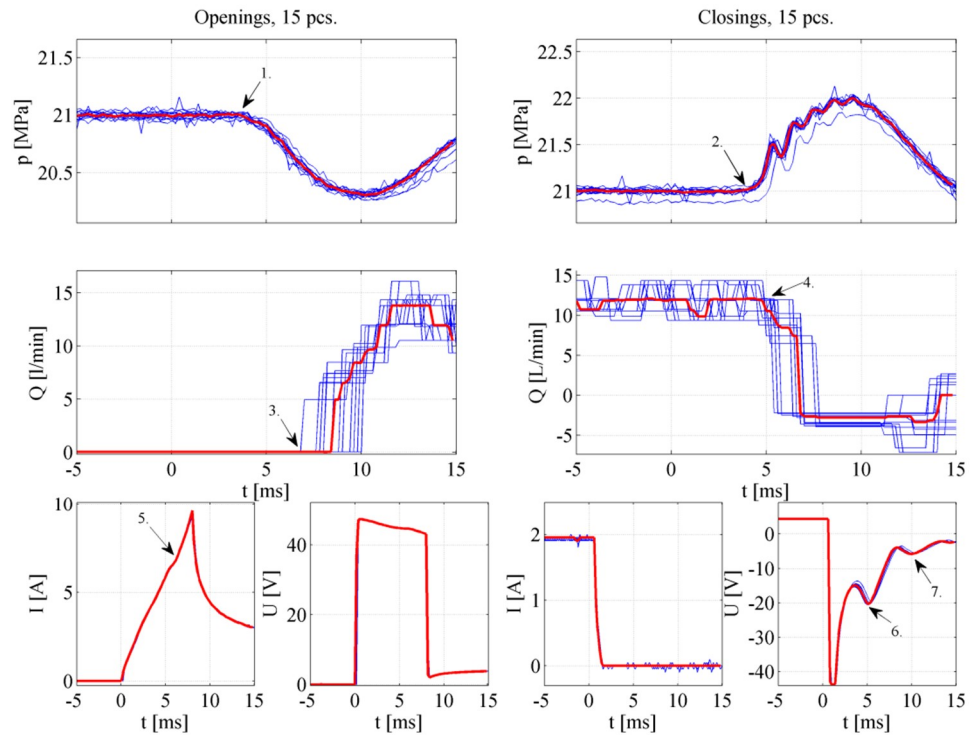


Figure 11. Opening and closing of a single 3/3 SEC-valve to flow direction P → A with the 2Ω-coil @ 2 MPa.

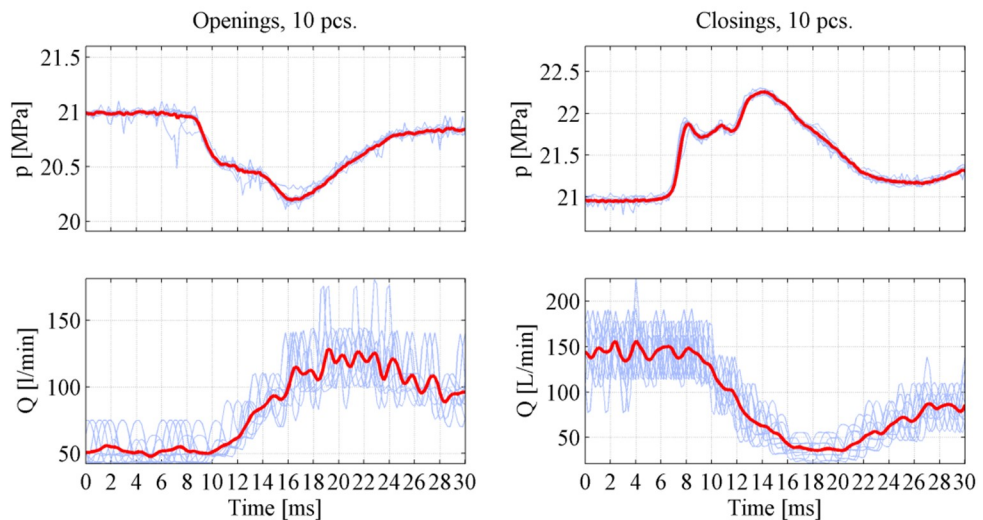


Figure 12. State transition 7 ↔ 47 of the DFCU controlling the flow direction P → A and the 12 VDC-coils @ 10 MPa.

In figure 12 the state transition is a so called good state transition where no valves are switched on and off simultaneously. State 7 equals the valve control output [1 1 1 0 0 0] whereas the state 47 equals output [1 1 1 1 1 1].

State transition 7 ↔ 40, where three of the valves are opened and three valves are closed simultaneously equaling the valve outputs [1 1 1 0 0 0] and [0 0 0 1 1 1], is presented in figure 13. The faster closing of the valve is noticed as a pressure peak in the supply pressure. For a PCM-coded digital valve system the variance in valve response time is important to be very small. Although the valve system was noticed to have a faster

closing than opening, the difference remains relatively fixed for flow rates under 120 l/min. This allows an easy compensation by delaying the valve closing commands.

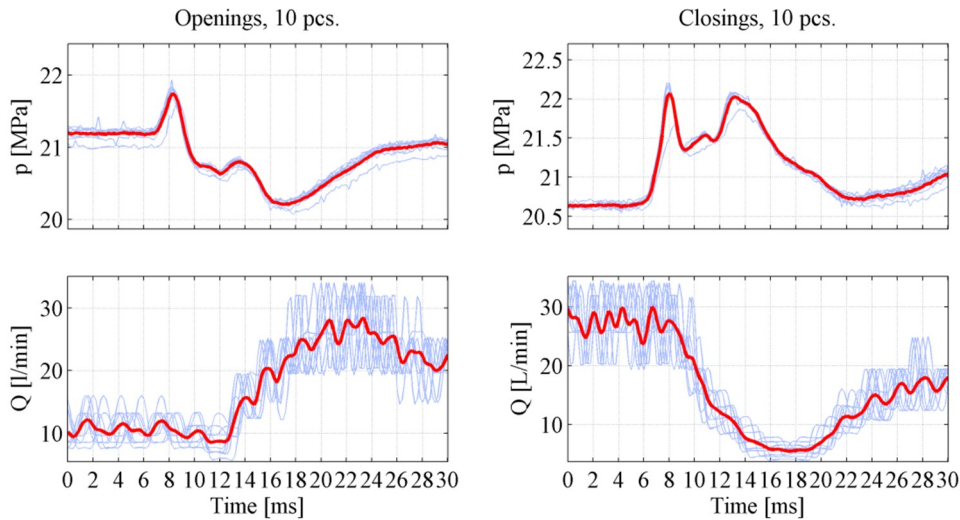


Figure 13. State transition 7↔40 with flow direction P→A and the 12 VDC-coils. and with pressure difference of 10 MPa.

## 5. SUMMARY

The purpose of this study was to gain knowledge on the characteristics and possibilities of the Bosch Rexroth 3SEC 6 valve as a part of a digital hydraulic valve system. Studied valve system is able to achieve fully independent control of metering edges with a nominal flow of 55 l/min @ 3.5 MPa and control resolution of around 23. Maximum flow was determined to be over 120 l/min and the valve system has zero leakage. Response times with both 2Ω- and 12 VDC coils are presented in table 1.

Table 1. Dynamic characteristics of 3 SEC 6 with 2Ω- and 12 VDC coils.

	2Ω-coil		12 VDC coil	
	2 MPa	8 MPa	2 MPa	10 MPa
Opening delay	3.6 – 5.2	3.8 - 5	6.4 – 7.8	5.4 - 6.8
Opening time	6 – 6.8	6.4 – 6.6	8.8 – 10.0	9.2 - 9.4
Closing delay	3.6 – 4.8	3.0 – 4.0	5 – 6.2	3.6 – 6.2
Closing time	5 – 5.8	4.0 – 6.0	6.0 – 6.8	6.2 – 6.9

It can be seen that closing is a bit faster with both coils. With 12 VDC coils a closing delay compensation of around 2 ms should be utilized to improve the behavior in state transitions.

Achieving very accurate low and high velocities simultaneously has been hard to realize with digital valve systems without adding several new valves to the DFCU. Ballistic control has been introduced and shown to have good potential for very accurate position and pressure control and the characteristics of 3SEC 6 is proved to be . Combining the ballistic control with the built 6-bit DFCU has potential for very high resolution

pressure and position control combined with accurate velocity control and 3.5 times higher flow rate than with the single valve. Challenge lies ahead in finding the optimal control strategy for the resulting valve system.

#### ACKNOWLEDGEMENT

This research was supported by Academy of Finland (Grant no.139540).

#### REFERENCES

- [1] Linjama, M. & Vilenius, M. 2007. Digital hydraulics – Towards perfect valve technology, The Tenth Scandinavian International Conference on Fluid Power, May 21–23, Tampere, Finland.
- [2] Winkler, Plönckinger & Scheidl 2010. A novel piloted fast switching multi poppet valve. The Second Workshop on Digital Fluid Power, November 12 – 13, 2009, Linz, Austria. pp. 116 – 128.
- [3] Huova, M., Plöckinger, A 2010. Improving resolution of digital hydraulic valve system by utilizing fast switching valves. The Third Workshop on Digital Fluid Power, October 13 – 14, 2010, Tampere, Finland. pp. 79 – 92
- [4] Försterling, Stamm & Roth 2011. Tailored solutions limit complexity. The 4th. Workshop on Digital Fluid Power, September 21–22., 2011, Linz, Austria, pp. 51-58
- [5] Schepers, I., Schmitz, D., Weiler, D., Cochoy, O., Neumann, U. 2011. A Novel model for optimized development and application of switching valves in closed loop control. International Journal of Fluid Power 12 (2011), No. 3, TuTech, ISSN 1439-9776, pp. 31-40.
- [6] Schepers, Weiler & Weber 2011. Optimize pulse modulation – A novel idea of a digital control method for on/off valves. ASME 2011 Dynamic Systems and Control Conference DSCC2011, October 31 – November 02, 2011, Arlington VA, USA, Paper DSCC2011-6007





## A HIGH FLOW FAST SWITCHING VALVE FOR DIGITAL HYDRAULIC SYSTEMS

Sylwester Kudzma, Nigel Johnston,  
Andrew Plummer, Nathan Sell, Andy Hillis, Min Pan

### ABSTRACT

Digital hydraulic systems can provide efficient control of pressure and flow. Switching valves can be used in a form of pulse-width modulation. The performance of the switching valve influences the effectiveness of the whole system. Low leakage, low pressure drop and fast switching are needed.

A spool type linear-acting fast switching valve is described. This is a 3-way device with one common port and two switched supply ports, and the spool can take two positions. The valve construction enables low flow resistance (65L/min at 10bar), low leakage and very high flow gain. The valve spool is driven by a servo-hydraulic actuator. This actuation module enables the valve to switch flow between high and low pressure supply ports in less than a millisecond and achieve a response close to a square wave. The duty cycle, which is defined as the ratio of time between the high pressure supply port open and low pressure supply port open, can be changed from zero to 100%. The design and performance of this valve are explained in the paper.

**KEYWORDS:** fast switching valve, multi groove spool

### 1. INTRODUCTION

Fast switching valves are an integral part of digital hydraulic systems. The valve presented in this article is designed for use in a flow or pressure booster, based on the switched inertance or switched reactance principle [1]. A switched inertance device basically consists of an inertance tube and a fast switching valve, and is used for continuous control of fluid pressure or flow. The operating principle relies on rapidly switching the fluid inertance between high and low pressure supply ports for the flow booster and between output (return port) and load (delivery port) for the pressure booster. The concept of switched reactance control is essentially energy conservative apart from parasitic friction and leakage losses. Additionally, the outlet pressure or outlet flow can be stepped up or down. A step up of pressure is associated with a step down of flowrate, and a step down of pressure is associated with step up of flowrate [1, 2]. The most crucial role is played by the fast switching valve. In order to achieve good and effective performance, the valve has to meet the following criteria:

- it has to have a variable switching ratio to enable pulse width modulation (PWM) ;
- time of switching has to be very short (typically below 1ms);
- It must have low resistance;
- It must have low leakage.

Research on fast switching valves for digital hydraulics has been already done by Winkler, Scheidl and Plockinger [4–7]. They present 2/2-way and 3/2-way spool and seat type valves. However, for the purpose of continuous control of pressure or flow using the flow or pressure booster the 2-position 3-way valve described in this paper seems to be a useful alternative to using two 2/2-way valves.

## 2. VALVE DESIGN

The prototype linear-acting fast switching valve has a modular design. It consists of two main components, shown in Fig. 1: main valve and actuation block.

A few types of main valve actuation were analysed. In the first instance a piezo-actuators were considered. However, devices available on the market do not provide sufficient force with relation to the maximum stroke and time of switching. A membrane actuator was also considered but simulations reveal that 0.2mm stroke consumes much more oil volume than a conventional actuator which significantly slows down the control. On the other hand a small diameter of membrane causes too large stresses for the demanded deflection. For this prototype, actuation is provided by a fast-response electrohydraulic servovalve driving a very small linear actuator.

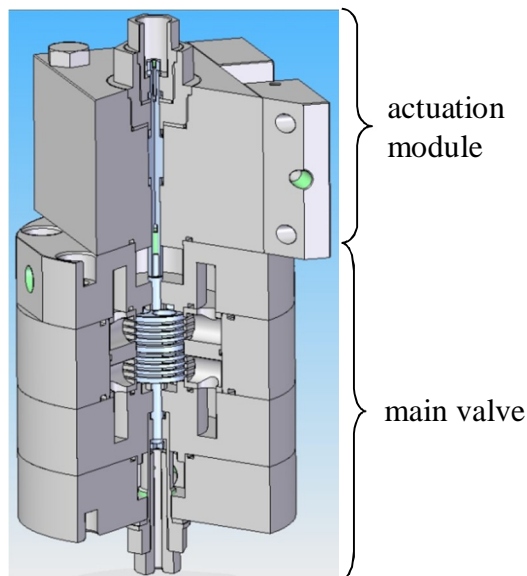


Figure 1. Linear valve

## 2.1. The main stage of the valve

The main stage of the valve (shown in Fig. 2) is composed primarily of a stationary sleeve and moving spool (Fig. 4) and additionally housing, three covers and screws for sensor mounting. Material chosen for valve components is AISI type 304 (stainless steel).

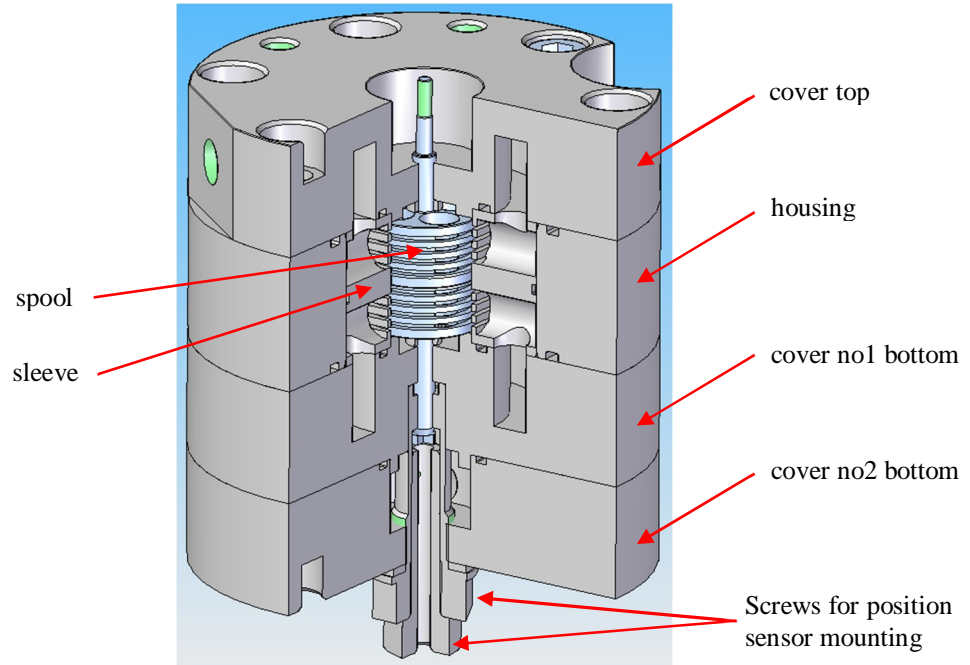


Figure 2. Main valve

Reciprocating movement of the spool switches flow between two supply ports and a common port. This is shown schematically in Fig. 3.

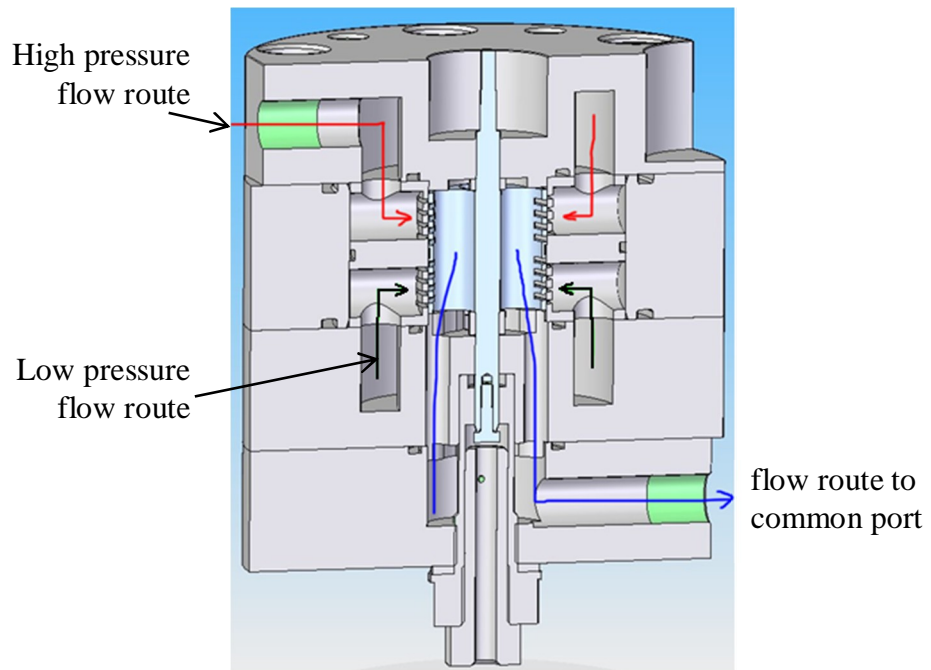


Figure 3. Schematic flow routes in the main stage of the valve

The novel feature of this valve is the use of multiple grooves to obtain an exceptionally high flow gain. A very small linear movement produces a large flow area. The spool is 30mm in diameter and 30mm in height. It has 4 holes through and 8 grooves on outer cylindrical surface (4 for each port) to enable the flow to port A as shown in Fig 4. Piston reciprocating movement is  $\pm 0.1$ mm.

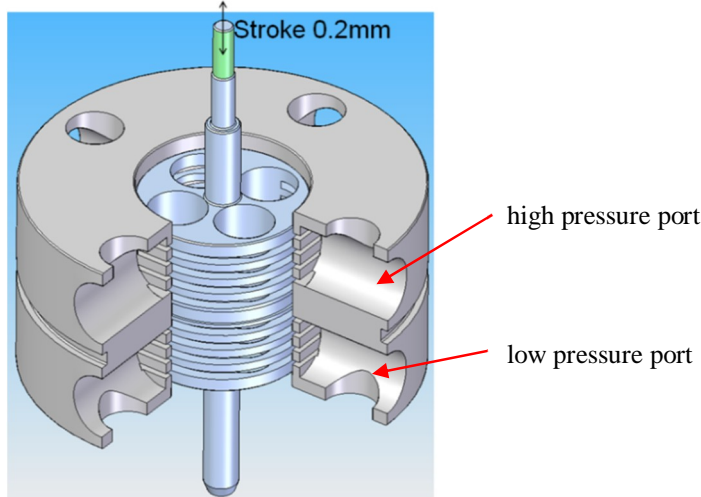


Figure 4. Sleeve and spool

The grooves in the piston and sleeve are cut in such a way that spool movement 0.2mm up makes 0.1mm gap in four grooves enabling flow from high pressure port to holes in the spool and then down to the port A. At the same time 4 other grooves are closed and overlapped 0.1mm. This is shown in Fig. 5a. When the spool is moved 0.2mm down (see Fig. 5b) then the low pressure port is open (0.1mm gap) and high pressure port closed (0.1mm overlap).

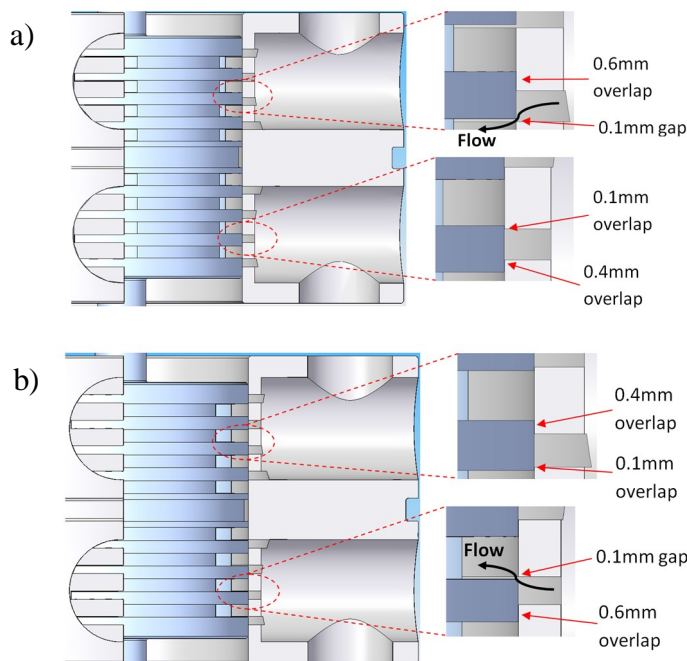


Figure 5. Cross-section view of the spool – sleeve, a) extreme upper spool location, b) extreme lower spool location

The theoretical cross-section area of the fully open gaps for one port is equal to:

$$A = \text{gap}_{\text{width}} \cdot \pi \cdot d \cdot \text{No}_{\text{grooves}} = 0.1\text{mm} \cdot \pi \cdot 30\text{mm} \cdot 4 = 37.7\text{mm}^2 \quad (1)$$

Using orifice equation Eq. 2 a theoretical flow, at  $\Delta p=10\text{bar}$  pressure drop across the valve, can be roughly calculated.

$$Q = A \cdot \alpha_d \cdot \sqrt{\frac{2}{\rho}} \cdot \sqrt{\Delta p} = 65\text{L/min} \quad (2)$$

$\alpha_d$  - discharge coefficient:  $\alpha_d=0.6$   
 $\rho$  - density of oil  $\rho = 870\text{kg/m}^3$

### Leakage estimation:

Leakage in the valve was estimated using the following equation:

$$Q_L = \frac{w \cdot \Delta p \cdot c^3}{12 \cdot \mu \cdot L} \quad (3)$$

Where:  $w$  – width of the gap,  $c$ -clearance,  $L$  – length of the gap,  $\Delta p$  – pressure difference,  $\mu$  – dynamic viscosity.

The clearance between spool and sleeve was designed for a maximum of 6 microns; however, after machining the measured clearance is about 7-10 microns. It is worth to mention that geometrical inaccuracy of the sleeve hole and the spool cylindrical surface can also play important role, however they were not measured after machining.

An estimation of the leakage, when spool is at rest, at extreme lower location is shown. In that position low pressure port is closed and there is a flow from high pressure port to A port. The total leakage into low pressure port is estimated as follows:

$$Q_{LT} = 4 \cdot \frac{w \cdot \Delta p \cdot c^3}{12 \cdot \mu \cdot L_1} + 3 \cdot \frac{w \cdot \Delta p \cdot c^3}{12 \cdot \mu \cdot L_2} + \frac{w \cdot \Delta p \cdot c^3}{12 \cdot \mu \cdot L_3} = \frac{w \cdot \Delta p \cdot c^3}{12 \cdot \mu} \left( \frac{4}{L_1} + \frac{3}{L_2} + \frac{1}{L_3} \right) \quad (4)$$

In calculations the following data were assumed:  $w = \pi d = \pi \cdot 30\text{mm}$ ,  $c_{\text{min}} = 7\text{microns}$ ,  $c_{\text{max}}=10\text{microns}$ ,  $\mu = \rho \cdot \nu$ ,  $\rho = 870\text{kg/m}^3$ ,  $\nu_{\text{min}} = 32\text{cSt}$ ,  $\nu_{\text{max}} = 60\text{cSt}$ ,  $\Delta p=10\text{bar}$ ,  $L_1$ ,  $L_2$ ,  $L_3$  – values of length of gaps are shown in Fig 6.

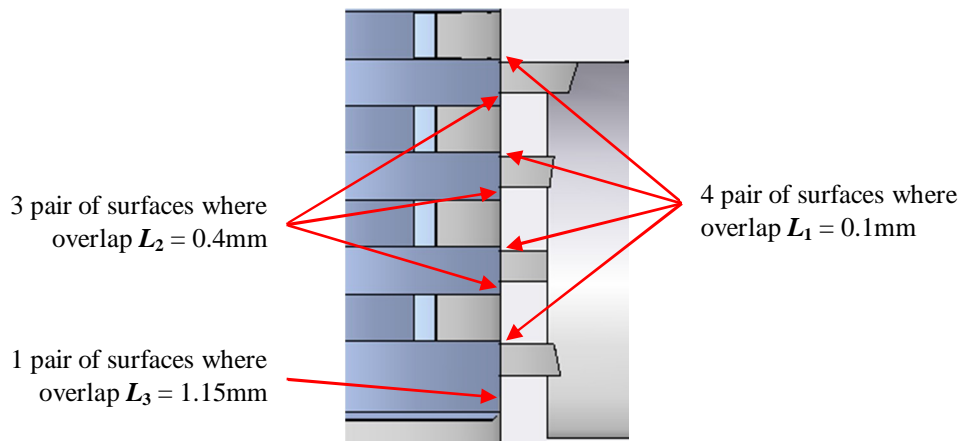


Figure 6. Length of the leakage gaps

Total leakage for above data:  $Q_{LT\_max} = 0.82\text{L/min}$ ,  $Q_{LT\_min} = 0.15\text{L/min}$ .

## 2.2. The actuation module

The actuation module consists of piston, block, and manifold plate and two screws for sensor mounting as shown in Fig 7.

Diameter of the piston is  $D=10\text{mm}$  and diameter of the piston rod is  $d=6\text{mm}$ , so pressurized area of the piston is  $A_p=50.26\text{mm}^2$ .

Assuming  $\Delta p=200\text{bar}$  in cylinder chambers, force acting on piston  $F=\Delta p A_p \approx 1\text{kN}$ .

The mass of the moving set i.e. piston connected to spool and screws for sensors plus weight of accelerometer was estimated in CAD Solid Edge system. (density of 304 stainless steel =  $8027\text{ kg/m}^3$ )

$$M = m_{\text{piston}} + m_{\text{spool}} + m_{\text{screw-A}} + m_{\text{screw-P}} + m_{\text{accelerometer}} = 81\text{g} + 26\text{g} + 1\text{g} + 2\text{g} + 2\text{g} = 112\text{g}$$

The mass of the moving set is rounded up to **115g** to take into account the weight of the cable and connector attached to accelerometer.

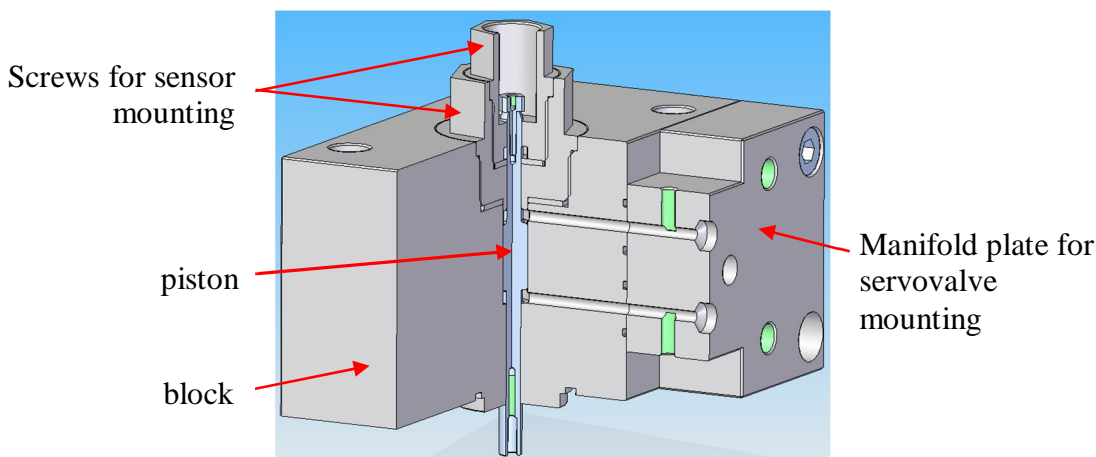


Figure 7. Actuation module

The flow into the chambers of the cylinder is metered in and metered out by a Moog servovalve. Valve model number: E050-899, valve serial number: e101 (Specification similar to E050-810) shown on Fig. 8. Installation details (mounting plate) are the same as servovalve 31 series.

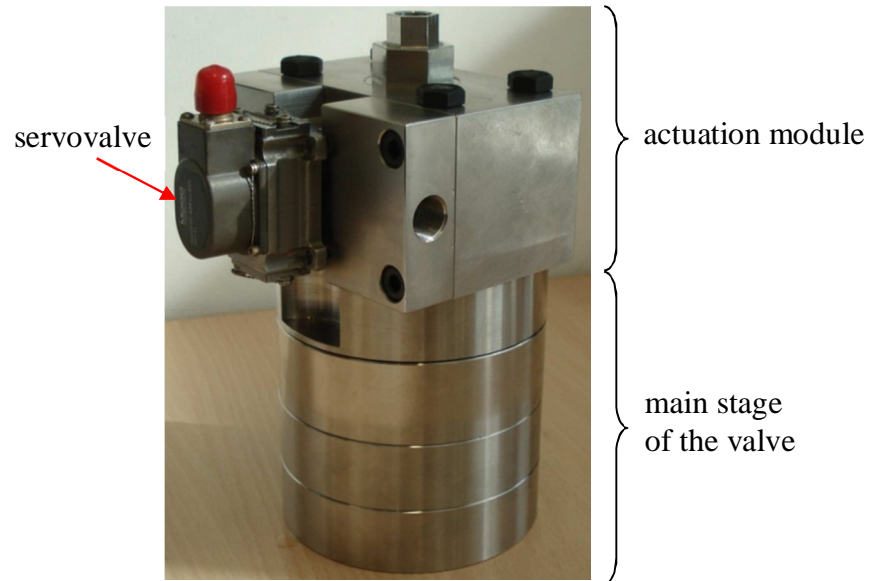


Figure 8. Prototype of the valve with mounted servovalve

### 3. OPERATION OF THE VALVE

Spool position is controlled with a closed loop system instead of just driving between mechanical limits. This was chosen in order to avoid unwanted noise, mechanical vibrations and internal impact damage which may particularly increase in the case of high frequency switching. Additionally, feedback control can allow this device also to work as a proportional valve.

In order to regulate position, time of switching, frequency and duty cycle of the spool a number of sensors is used and linked with the xPC Target system and Matlab-Simulink. This is shown schematically in Fig. 7. The control system is being developed.



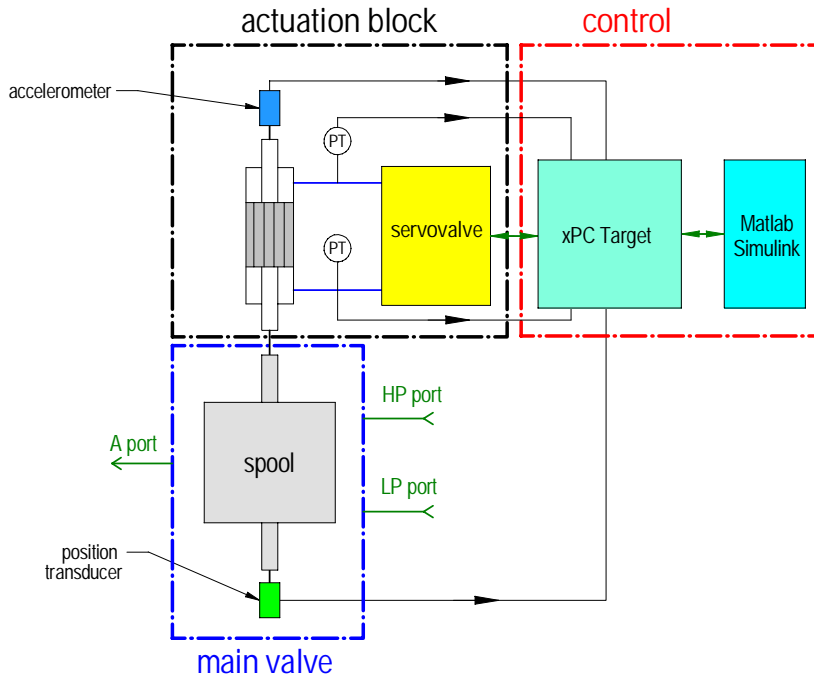


Figure 9. Schematic diagram of the valve control system

#### 4. EXPERIMENTAL RESULTS

The first step to determine the performance of the main stage valve was to conduct steady state experiments.

##### 4.1. Steady state performance

There were two different arrangements of steady state measurement circuit, shown in Figures 10a and 10b. Flow characteristics were obtained for both HP-A and LP-A switches and also for different gap opening. The results of the steady state experiment can be seen in Fig 10c – flowrate vs. spool position at 80bar and Fig 11 – flow characteristics.

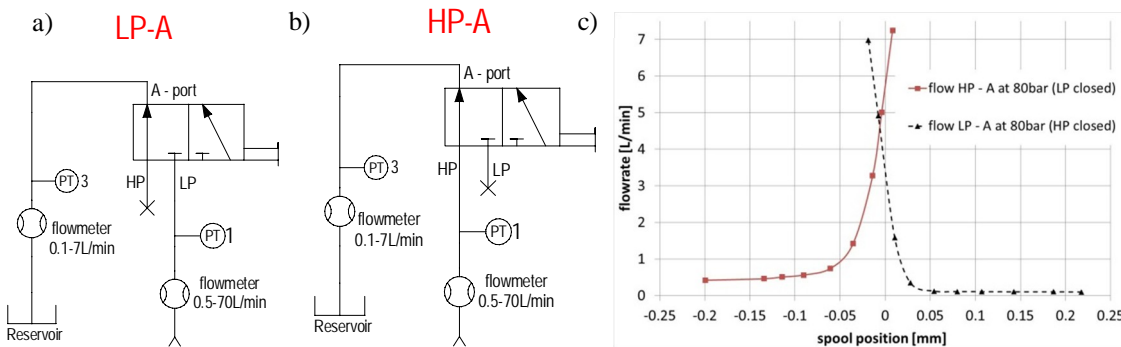


Figure 10. Schematic view of the valve and sensor arrangement for steady state tests: a) LP-A and b – HP-A and c – flow vs. spool position at 80bar

HLP 32 mineral oil was used as a working fluid and temperature was kept in the range 28-33C deg. what results in kinematic viscosity approx. 55cSt.

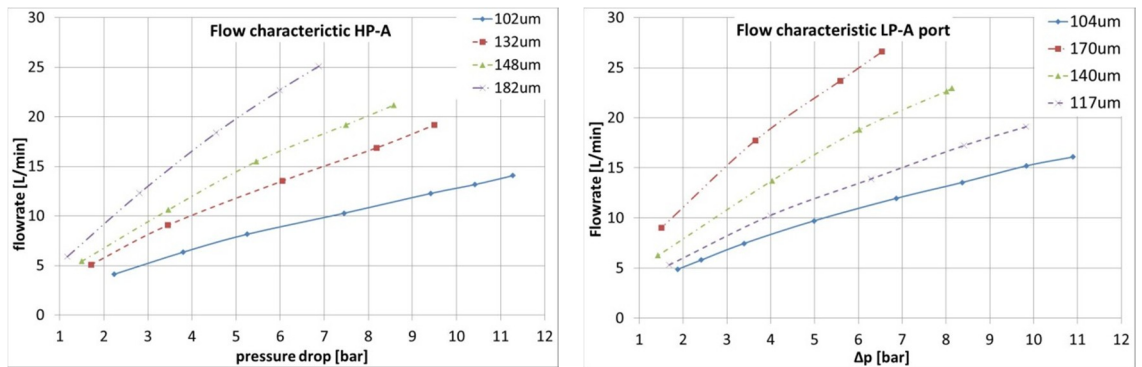


Figure 11. Steady state flow characteristics as a function of spool displacement from 'zero' position

The above test shows that valve does not meet its initial requirements. The flowrate at 10bar and gap opening circa 100micron reach only 15L/min. This is because grooves in the spool are too narrow in fact. That means that in 'zero' position there is overlap between sleeve and spool metering edges and in case of spool displacement gap is smaller than initially assumed.

The leakage in the valve was determined with the circuit arrangement shown in Fig 12a. The results of the leakage test at 13.5bar and 80bar can be seen in Fig. 12b.

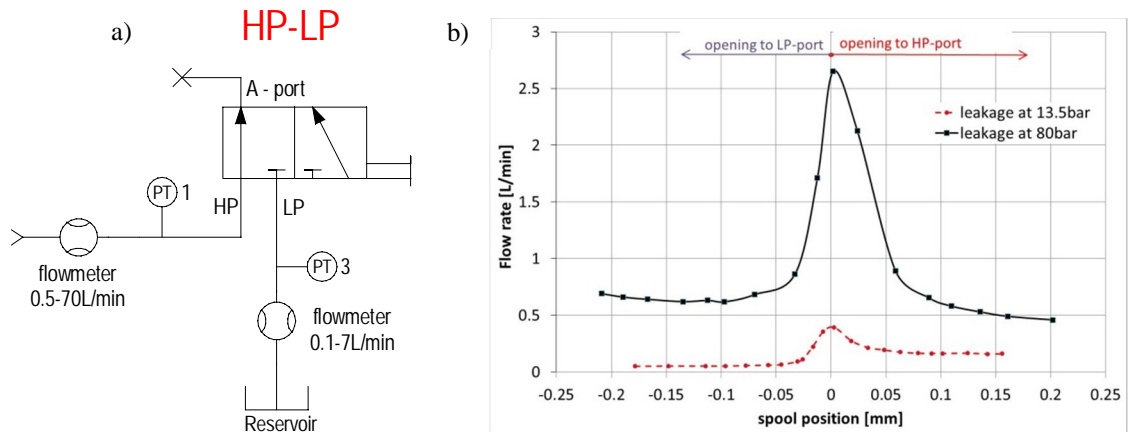


Figure 12. Leakage in the valve between HP and LP port

The spool 'zero' position i.e. centre spool position (theoretical zero overlap for both ports) was found experimentally using circuit arrangement shown in Fig. 13a. The test result can be seen in Fig. 13b.

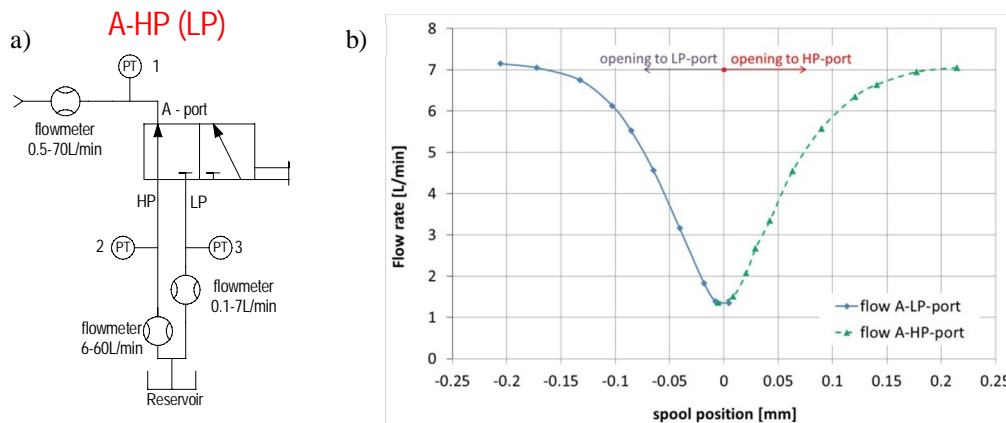


Figure 13. Flow rate A-HP (LP) as a function of spool position

## 4.2. Preliminary experimental dynamic performance and simulation

### 4.2.1. Simulated dynamic performance

Prior to experimental tests the numerical model of the valve was built in order to develop its control strategy. The intricacies of this model will not be discussed but a general overview is given in Figure 14.

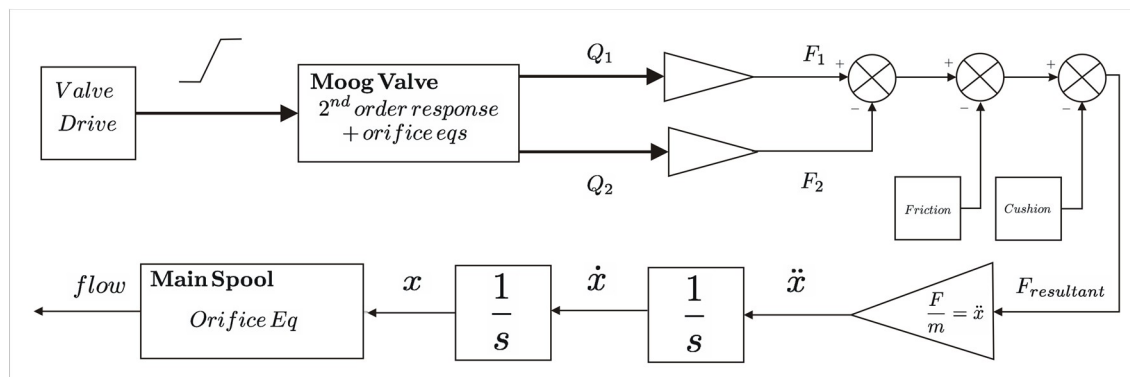


Figure 14. Simplified Diagram of Valve Model

This model is very complicated and contains various non-linear and switching blocks. Therefore model was linearized using perturbation theory what results in two transfer functions for spool position and acceleration. This is sufficient for the development of a control scheme as results using transfer functions and non-linear model are very similar. There was analysed a few strategies of control and the most successful was Iterative Learning Control (ILC), introduced first by S. Arimoto et.al. [3]. The valve model was tested for its response on square wave demand signal. The results can be seen in Figure 15.

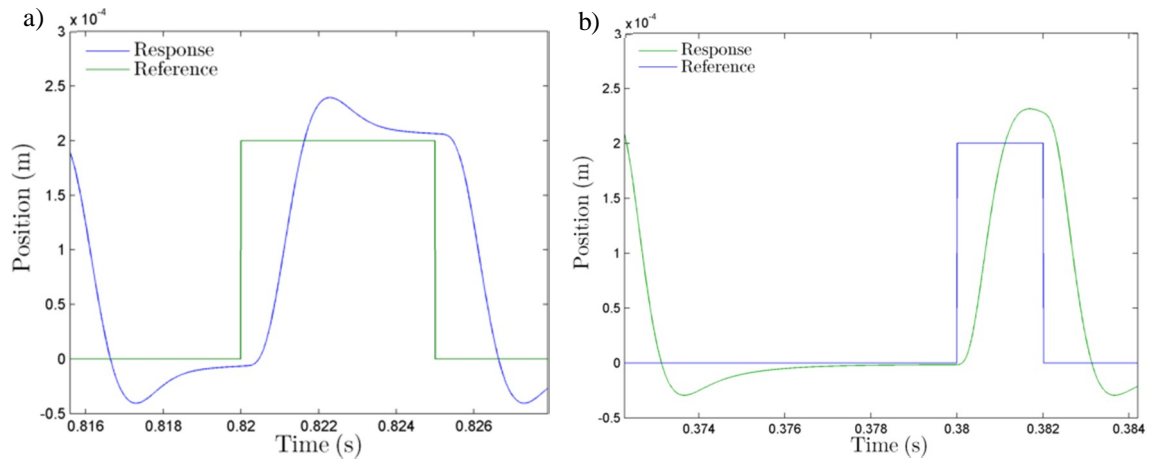


Figure 15. Response of the ILC model to a 50% (a) and 20% (b) duty cycle pulse at 100Hz

From above results following parameters can be read: Rise time=0.69ms, setting time=3.5ms and overshoot=12.8%.

#### 4.2.2. Preliminary experimental dynamic results

The strategy of control system implementation to the real valve is to start from simple PID controller and then gradually increase control complexity. At current stage PID controller with spool position feedback is applied. Position is measured by high speed and high accuracy inductive displacement sensor (resolution – 0.4 $\mu$ m, response time – 0.075ms). Dynamic performance of the valve spool using this controller can be seen in Figures 16–18.

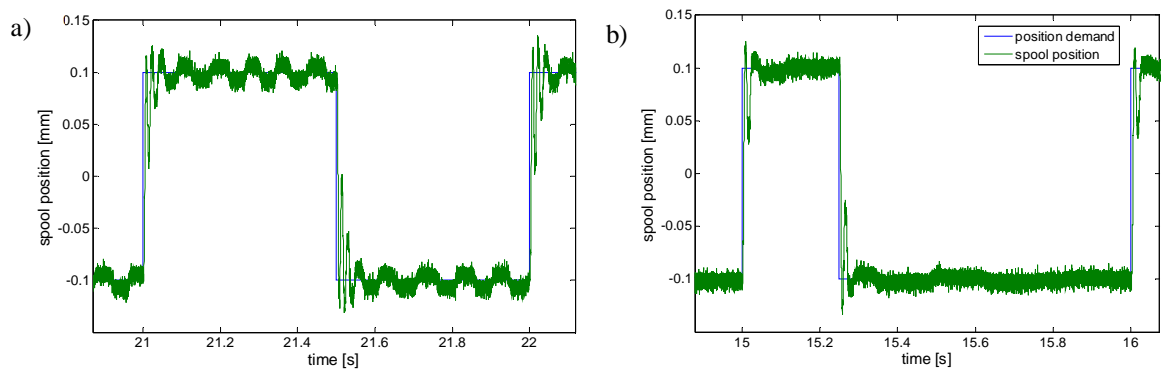


Figure 16. Response of the valve spool at frequency 1Hz; (a) 50%, (b) 25% duty cycle

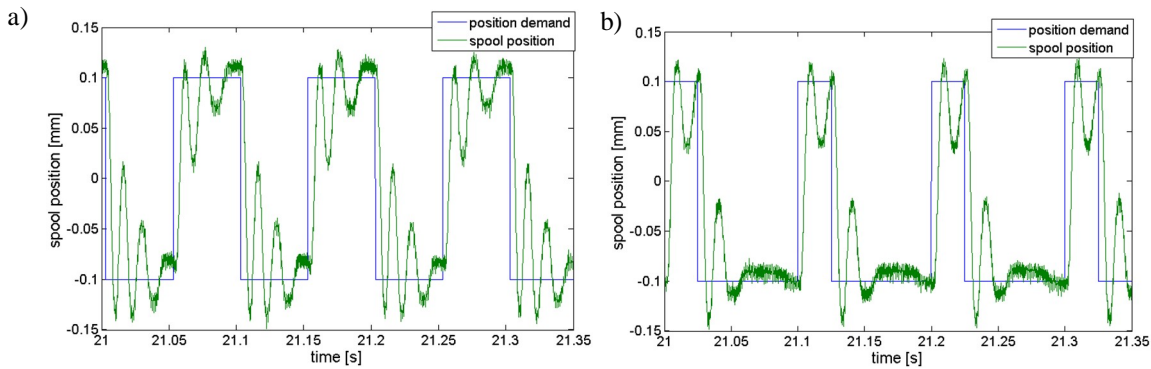


Figure 17. Response of the valve spool at frequency 10Hz; (a) 50%, (b) 25% duty cycle

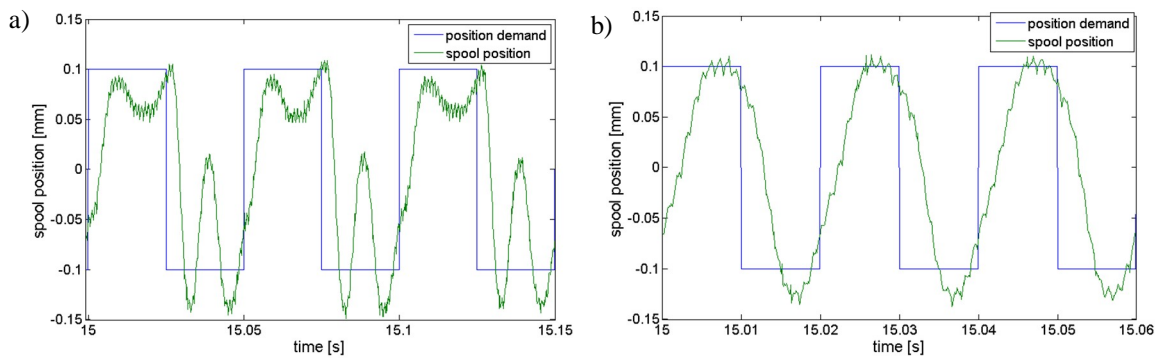


Figure 18. Response of the valve spool at frequency (a) 20Hz, (b) 50Hz; duty cycle 50%

The above figures show that oscillations play important role in the response signal. This is typical behaviour of the PID controller at early stage of system tuning. It is clear that controller need to be improved to match better demand signal and especially shorten the rise time. The next step in controller development will be implementation of the iterative learning control (ILC) system.

## 5. CONCLUSIONS

The paper has presented design and experimental results of a linear (3way/2position) valve with reciprocating motion for digital hydraulics. The idea of multi-groove concept was used for spool design. Four metering edges are used for each port what results in a large gain flow for small spool movement. But on the other hand the small spool movement leads to tiny sealing land what results in increased leakage at higher pressures. Steady state characteristics show that flow gain is much smaller than expected. The reason for this is too narrow grooves in the spool due to not enough precision during machining which means that when piston is in the extreme position the gap is much smaller than initially design. This will be fixed in the future.

Simulations of valve dynamics are promising and reveal that minimum switching time is 0.69ms, however, the experimental research are on too early stage to confirm this performance. Applied simple PID controller results in excessive spool oscillation and relatively long switching time. Next step of controller development is in progress.

## 6. FUTURE WORK

The work is ongoing. The development of the valve controller includes an Iterative Learning System application, its discretization with reference to the sampling frequency and finally testing and tuning for different values of frequencies and duty cycles. Further development of the valve comprises also metering edges improvement to increase flow gain and betterment of the cooperating surfaces of the spool and sleeve by hardening to protect them against wearing off process.

## ACKNOWLEDGEMENTS

This work is supported by UK Engineering and Physical Sciences Research Council (EPSRC EP/H024190/1), together with Instron, JCB and Parker Hannifin. Their support is greatly appreciated.

## REFERENCES

- [1] Johnston DN. A switched inertance device for efficient control of pressure and flow. In: Bath/ASME Fluid Power and Motion Control Symposium, Hollywood, USA, 2009.
- [2] Brown FT, Tentarelli S and Ramachandran S. A hydraulic rotary switched-inertance servo-transformer, *Journal of Dynamic Systems, Measurement, and Control*, vol. 110, pp.144-150, 1988.
- [3] Arimoto S., Kawamura S., and Miyazaki F. Bettering operation of robots by learning. *Journal of Robotic Systems*, 2:123-140, 1984.
- [4] Winkler B., Scheidl R. Optimization of Fast Switching Valve for Big Flow Rates, *Power Transmission and Motion Control*, University of Bath, UK, 2006.
- [5] Winkler B., Plockinger A., Scheidl R. Components for Digital and Switching Hydraulics, *The First Workshop on Digital Fluid Power*, Tampere, Finland 3<sup>rd</sup> October 2008.
- [6] Winkler B., Plockinger A., Scheidl R. A Novel Piloted Fast Switching Multi Poppet Valve, *The Second Workshop on Digital Fluid Power*, Linz, Austria, 12<sup>th</sup>-13<sup>th</sup> November 2009.
- [7] Winkler B., Plockinger A., Scheidl R. Refined Dynamic Measurements of a Piloted Fast Switching Multi Poppet Valve, *The Third Workshop on Digital Fluid Power*, Tampere, Finland, 13-14 October 2010.



## COMMERCIAL HIGH FLOW ON/OFF-VALVES FOR DIGITAL HYDRAULICS

Ilari Hyöty, development engineer in Engine Ancillary Systems group, Wärtsilä Finland Oy, P.O.Box 244, 65101 Vaasa, Finland. E-mail: [ilari.hyoty@wartsila.com](mailto:ilari.hyoty@wartsila.com)

### ABSTRACT

An approach where a commercial 4/2-directional valve is used as a 2/2-on/off valve is introduced, and this method is also tested with three existing and easily available valves in laboratory environment. The results of the measurements verify that this technique can be used to achieve a high flow capacity digital valve.

**KEYWORDS:** Digital hydraulics, Solenoid valve, on/off-valve, commercial, high flow valve

### 1. INTRODUCTION

The development of digital hydraulic valve technology has been more concentrated on relatively small flow capacity valves. In order to apply digital hydraulics to larger or very high flow rate systems, bigger valves are needed. One of the major challenges with bigger components is to achieve the peculiar fast time response of digital hydraulics. An arrangement where a 4/2-directional valve is converted into a 2/2-directional valve could offer a good alternative, instead of increasing the size of 2/2-valves, in the search for a high flow digital valve.

### 2. TEST RIG AND TEST INTRODUCTIONS

The measurements of the valves took place in Tampere, at the Tampere University of Technology, in the laboratory of the department of Intelligent Hydraulics and Automation between 23.1.2012 and 3.2.2012. The idea of 4/2-directional valve conversion to 2/2-directional valve is seen in figure 1. [1]

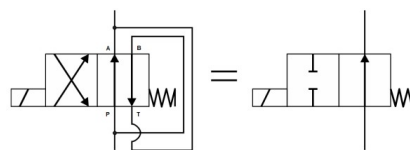
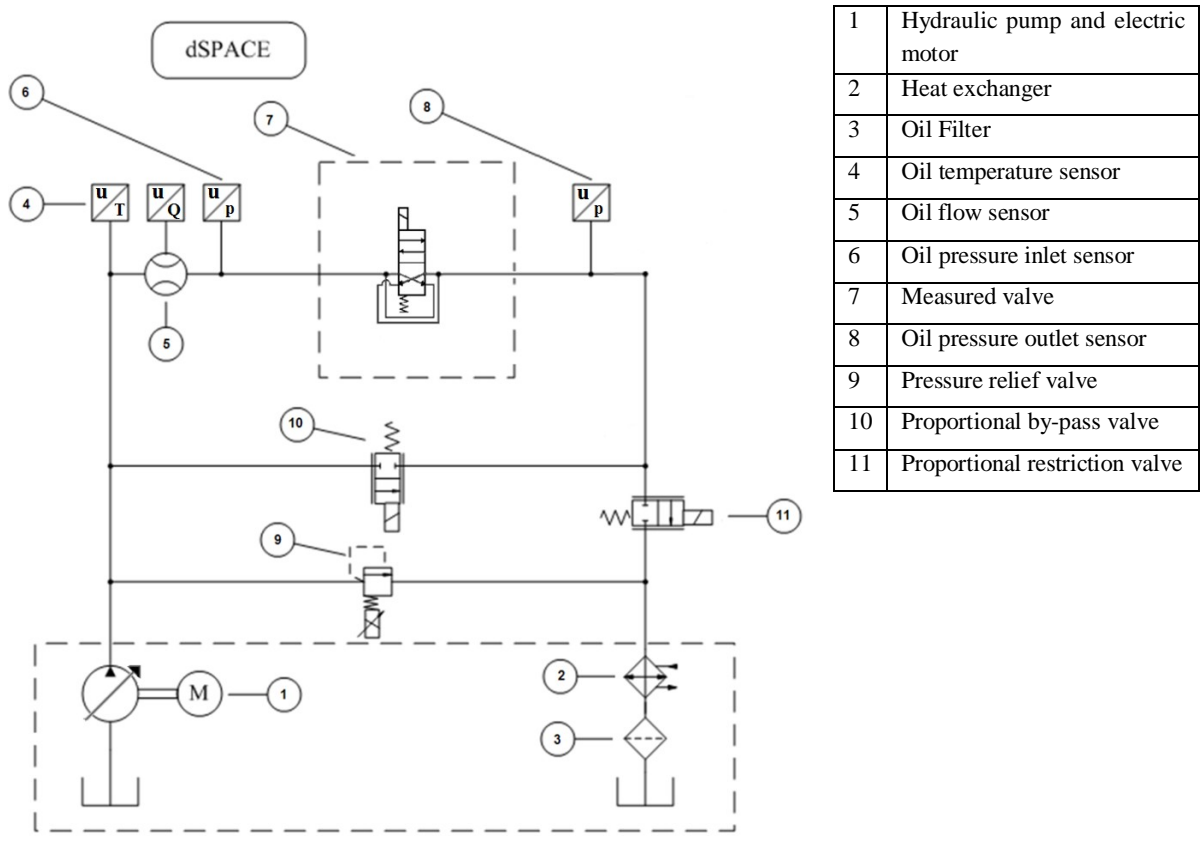


Figure 1. Valve conversion



The test system hydraulic circuit can be seen in figure 2. The pressure level after the measured valve is controlled by two Parker DFPlus proportional valves (11). The flow is restricted with these two valves and this causes pressure to rise after the valve. The pressure represents the load induced pressure in normal usage. The supply pressure is controlled with one proportional pressure relief valve (9).



1	Hydraulic pump and electric motor
2	Heat exchanger
3	Oil Filter
4	Oil temperature sensor
5	Oil flow sensor
6	Oil pressure inlet sensor
7	Measured valve
8	Oil pressure outlet sensor
9	Pressure relief valve
10	Proportional by-pass valve
11	Proportional restriction valve

Figure 2. Test rig hydraulic diagram

One DFPlus valve is also used as a bypass valve to surpass the measured valve (10). This oil flow will, however, go through the DFPlus restriction valves. This way, the pressure level after the measured valve can be increased even if the measured valve is kept at the closed position. Pressure levels are measured before and after the measured 4/2-directional valve. Temperature of the oil was measured from a volume close the measured valve. Different flow sensors were used to ensure accurate measurements through hugely varying flow rates (5). The used hydraulic oil was Shell Tellus S46. The oil temperature was kept at 40 +-1 degrees Celsius. The used booster uses two voltages for the valve coil, a voltage of 48 volts for the boost phase, and 12 volts for holding current. Module 1 is a current source for 12 volts, module 2 for 48 volts, and module 3 for 24 volts. The 24 volt source is used for different sensors in the measuring system and for the proportional pressure control valves. The module 4 is the actual booster which controls which voltage is applied. A control voltage of 3-10 volts is applied to the booster, and this voltage determines the time duration of the boost phase (maximum of 15 ms). A list of the measured valves, valve blocks and coils can be found in the table 1.

Table 1. Part list

Valve	Bosch Rexroth KKDE R 1EA/HN0V 4/2-directional spool cartridge valve
Block	MNV/S – Valve body iron Sun hydraulics 1/2"
Coil	Bosch Rexroth 12V 37-K4 -22G12 00
Valve	Parker DSH104 4/2-directional spool cartridge valve
Block	Parker block B10-4-6B, steel, 3/8"
Coil	Parker super coil 28W, 24VDC
Valve	Bosch Rexroth 4WE 10 EB3X/CG12N9K4 4/2 directional spool valve, sub-plate mounted
Plate	NG10 size mounting plate
Coils	Solenoid coil 12V GZ63-4 12V K4

### 2.1. Valve block modifications

The smaller valves (Bosch Rexroth KKDE and Parker DSH104) are block mounted cartridge valves. The block connections are slightly different between these blocks; the port 1 is in a different spot in these two blocks. The connections 2, 3 and 4 are in similar spots. The blocks and port numbering can be seen in the figure 3.

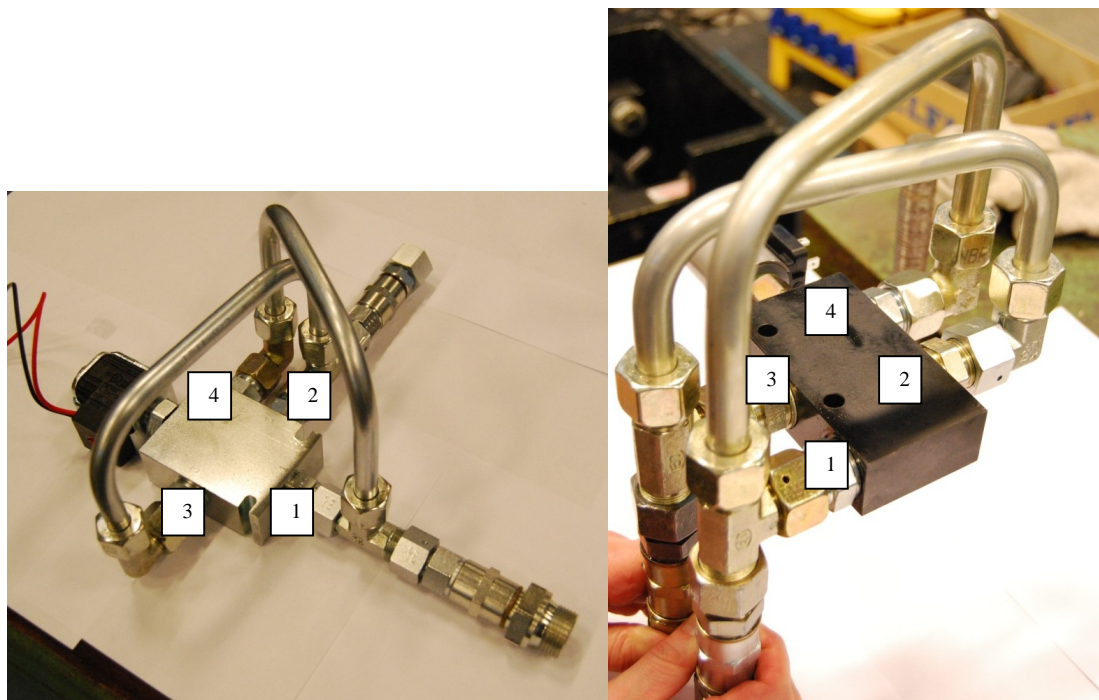


Figure 3. Parker DSH104 and Bosch Rexroth KKDE 2/2-modification

The valve blocks had to be modified to implement the connection principle seen in figure 1. These connections were made by using pipe connectors and making u-shaped pipes to connect the desired ports. In both blocks, the ports 3&2 and 4&1 were made a pair to achieve the arrangement seen in figure 4.3. These connections could also be made straight to the block by drilling more flow channels into them, but this procedure would have needed slightly bigger blocks and more time to make the modifications. By

using pipes, we could buy a standard commercial block, and make the connections outside the block in little time and with less effort. This arrangement suits the test circumstances well, and shouldn't have remarkable impact on the results. If this kind of a port connection arrangement would be used for commercial products, it would be smart to do the flow channels into the block to minimize the used space.

## 2.2. Tests

Two different pressure ramp tests were done to obtain pQ-characteristic curves for the valves. The first test was an upstream pressure ramp, and the second a downstream pressure ramp. The next test was an operating limit test, which shows the critical pressure difference over the valve at which the valve is still able to function normally. The response time tests were done also to find out how quickly the valve can switch from one position to another. Leakage tests were also done to find out how much these spool type valves leak.

All the tests were done in both flow directions of measured valves. Basically, this means that all the tests were done on a valve, and then the valve was turned around to do the same tests with the opposite flow direction. The properties of a valve can vary depending on the direction of the flow, for example, because of pressure and flow forces or because the flow path geometry affects the flow differently in opposite directions. All the tests were also made at several different pressure levels and pressure differences to find out what kind an impact different circumstances cause in the valve actuation.

The pressure sensor accuracy is NLH at +25°C  $\pm 0,07\%$ . This means that with a 400 bar pressure sensor the error is 0,28 bar. This measuring test rig has pressure sensors on both sides of the measured valve, so the cumulative pressure error may be 0,56 bar. The delay of the pressure sensor is 1 millisecond in a pressure change from 10% to 90% of the sensor range. The used sensor was a 400 bar sensor so a typical delay from 60 bar pressure to 360 bar pressure is 1 millisecond. This delay should be taken into consideration as the response time tests valve delay times are deduced from the pressure graphs. However, the changes in the pressure in the measurement are much smaller, typically under 50 bars, so the delay from the pressure sensors can be assumed as well below 1 millisecond.

## 3. PQ-CHARACTERISTIC CURVES WITH PS-RAMPS

The pressure ramps durations were 60 seconds, 30 seconds for increasing and 30 seconds for decreasing of the pressure. The ramps were lengthy so that accurate results could be obtained. The used maximum pressure difference was 15-20 bars, since usually the flow capacity of a valve is given at 5 bar pressure difference over the valve, and a bigger difference would have made the graph harder to read with small pressure differences. The maximum flow tests are done separately, where the pressure differences will reach over 100 bars. In some graphs, the downstream pressure is marked as 0 bars but due to restrictions in the tank line, this pressure couldn't be kept at exactly 0 bars as the flow rate grew. The downstream pressure in these cases rose to

about 3-8 bars, however, the pressure difference over the valve is the thing that matters the most, and all the calculations and graphs are made based on those values.

The first pQ-test was a Bosch Rexroth KKDE supply pressure ramp test. The pressure after the valve is kept at the same level as the supply pressure before the ramp. This test represents the valve being used for example at the downstream of an actuator, hydraulic motor or cylinder. The figure 4 illustrates how the flow is dependent on the flow direction.

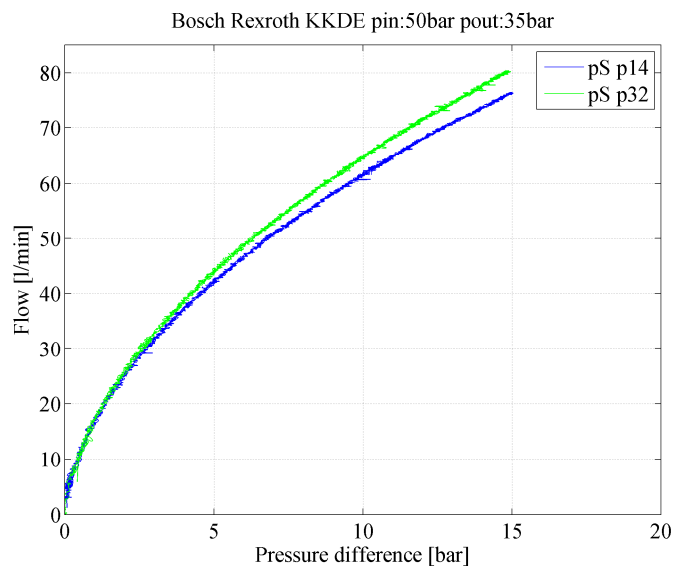


Figure 4. Supply pressure ramp pQ-curve

The flow at five bar pressure difference is 44,3 lpm when pressure is applied to ports 3 and 2. The flow to the other direction with the same pressure difference is a bit less; 42,4 lpm. This is due to the fact that the flow path geometry affects the flow differently in opposite directions. At ten bar pressure difference, the flows in both directions are over 60 lpm.

The parker pS-ramp tests were run next, and almost instantly, it was noticed that the flow rates are not even close to what was expected based on the manufacturer's brochure. There are pQ-characteristic curves for each flow path, and from there it is possible to obtain some kind of an estimate what the flow rate could be with this kind of special connections. The manufacturer's brochure gives approximately, both flow paths combined, a 45 lpm flow rate with the pressure difference of 5 bars. Now the measured flow rate at 5 bars (in pressure ports 3 and 2 direction) is only about 27 lpm. It was clear that either the valve is not at all suitable for this kind of connections, or there is something wrong with measuring rig setup. The other flow direction showed a bit better results, but the flow was still far from what had been expected; 32 lpm flow at 5 bar pressure difference.

One thing that had been under suspicion from the beginning, were the quite small drillings of the block. The valve block itself was also quite small, and the drillings therefore quite close to each other, which prevented bigger pipe connector installations. The valve block drillings diameters were increased to from 6,25mm to 8mm but there

was still suspicion if they would cause too much pressure loss. On the other hand, the holes could not be drilled any bigger, since the edges of the drillings were getting close to the seals of the valve spool liner. After some thought, it was discovered that the holes could be made bigger, not by drilling, but by enlarging the holes to only one direction, making them asymmetric. This was done with a milling cutter, and now the holes were bigger, yet the sealing surfaces stayed intact. The directions the holes were enlarged to and the hole area geometries can be seen in figure 5.

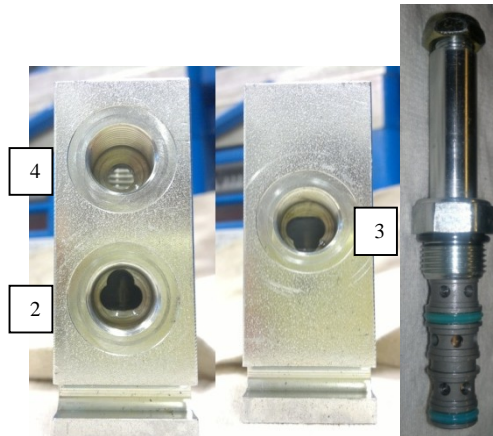


Figure 5. Parker block and spool liner modifications

It was also discover that since the block ports 3 and 2 are always connected to each other by the pipe connection, the middle seal in the valve spool liner separating volumes of ports 3 and 2, is unnecessary, and was therefore removed. This allows the oil flow a bit more freely through the valve and should affect the measurements as increased flow. To make the modification even more effective, bigger pipe connectors were installed by rounding the edges of the tightening nuts, so that the connectors could be fitted side by side to the block ports 2 and 4 side. These bigger connectors, further on, enabled bigger pipes to be installed which reduced the pressure loss. The old pipe diameter was 12mm and the new was 16mm.

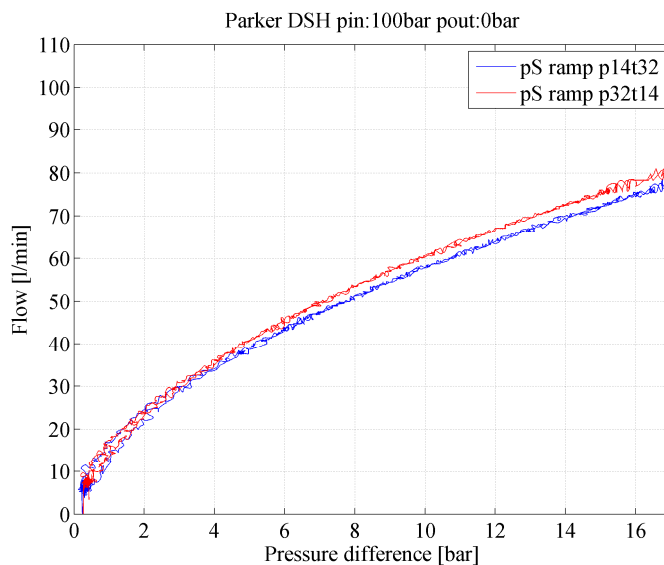


Figure 6. Supply pressure ramp pQ-curve

When ports 1 and 4 are on the supply pressure side, the flow with 5 bar pressure differential over the valve is 41,1 lpm (old value  $Q=33\text{lpm}$ ). The flow to the opposite direction with the same pressure differential is 39,2 lpm (old value  $Q=27\text{lpm}$ ). This valve shows that there is a small difference in the flow rate depending on the direction of the flow. It is notable that as the flow rate difference after the modifications was only 2 liters, it was a significant 8 liters before the modifications. The difference is about the same as pressure difference is increased; at 10 bars, the flow rates are 57,8 lpm and 60,3 lpm. The new supply pressure ramp pQ-characteristic curves show bigger flow capacity with the same pressure difference than before, so it can be said that the modifications improved the results.

The NG10 size Bosch Rexroth 4WE was the biggest of these three valves. Again, a small difference in the flow rates could be spotted, depending on the direction of the flow. The direction supply pressure to ports P and B provided a flow rate of 77,6 lpm whereas the other direction provided 76,4 lpm with a pressure difference of 5 bars. The flow rate varies only about 2 per cent, so the valve has almost the same flow capacity to both directions. At 10 bar pressure difference, the flow rates are 111,0 and 108,3 lpm, the percentage difference remains approximately the same. The variation is very little, and could even be due to pressure sensor error. Therefore it can be said that the flow is equal to both directions.

#### 4. PQ-CHARACTERISTIC CURVES WITH PT-RAMPS

In the next pQ-tests, the pressure at the downstream port of the valve is varied, and the supply pressure is kept constant. This situation represents the valve being used as directional valve for a cylinder or hydraulic motor, because the downstream pressure changes, that is, for example, a working load caused pressure at the B port of the valve. The downstream pressure ramps had to be measured in multiple parts at low pressure values because of the downstream pressure causing proportional restriction valves. These valves caused a pressure higher than was intended, even though they were fully open, when the flow rates were big enough. In order to avoid this, a mechanically controlled by-pass valve had to be opened in parallel to the restrictive proportional valves. This way the downstream pressure could be controlled, but the actual pressure control valves didn't prevent low downstream pressure rates. At higher pressure rates, this did not matter, because the downstream pressure was always kept higher than 30 bars. From the Bosch Rexroth KKDE pT-ramp pQ-characteristic curves it could be seen, that the flow rates are approximately 42,1 (supply pressure ports: 1&4) lpm and 43,5 lpm (supply pressure ports: 3&2) with 5 bar pressure difference. The flow rates are over 60 lpm with ten bar pressure differential in both flow directions. The flow geometry seems to have less flow resistance in the direction where pressure is applied to ports 3 and 2.

The first configuration of Parker DSH104 valve test setup results are not provided here because the results were at a similar level with the first pS-ramps, so the improved setup results are provided only. Figure 7 shows the downstream pressure ramp pQ-curve of Parker DSH 104 valve.

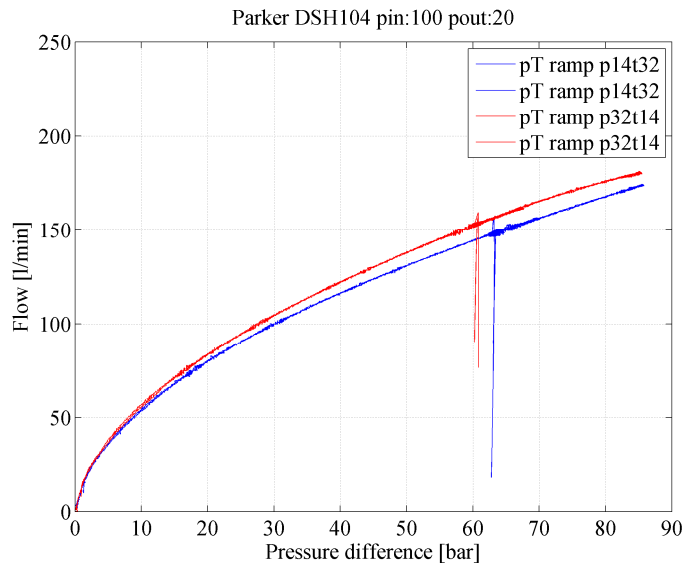


Figure 7. Downstream pressure ramp pQ-curve

The upper curve represents the situation where supply pressure is applied to ports 3 and 2, the valve downstream volume is connected to ports 1 and 4. The lower curve has the connections vice versa. This graph shows that the pressure drop is smaller if the flow is directed so, that the oil goes in to the valve via the ports 3 and 2, and out of the valve via the ports 1 and 4. This valve shows similar behaviour as the Bosch Rexroth valve, the hydraulic resistance with the same flow path geometry changes depending on the direction of the flow.

Figure 8 shows the downstream pressure ramp pQ-curve of Bosch Rexroth WE4 pT – ramps

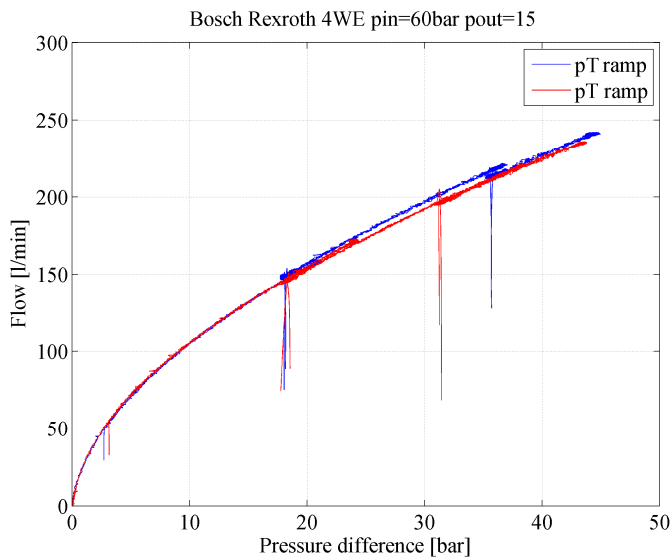


Figure 8. Downstream pressure ramp pQ-curve

This graph shows that Bosch Rexroth valve type 4WE has very little difference in the pressure loss depending on the flow direction. The middle part in the blue curve has

some error, and therefore two discontinuous spots, probably due to measuring error. The last section of the blue curve seems to be in line with the first section. The upper curve was measured when supply pressure was applied to ports A and T, and the ports P and B were connected to the tank side.

## 5. OPERATING LIMIT TEST

This test was done to find out at which pressure differential over the valve the valves can still operate. The pressure reference value at the downstream port of the valve was kept constant, and a supply pressure ramp was applied to the valve upstream port. The valve was switched on and off with a constant frequency, for example, 0,5 hertz. The initial supply pressure is the same as on the downstream side of the valve.

There is always a figure of the whole pressure ramp, and then a zoomed figure from the point that the valve shows abnormal operation. Whenever the valve switches to open or closed position, the pressure starts, after the first peaks, to slowly decrease or increase. This is because the supply pressure side pressure control valve starts to adjust the pressure towards the desired supply pressure reference value. The valve supply pressure and valve opening signal are shown in the graphs also.

The first operating limit ramp can be seen in the figure 9. The blue pressure graph is the pressure difference over the valve and the red signal is the valve control signal. The control signal does not have a unit, it is scaled to 0 and 100 to indicate the commanded position (0=close position and 100=open position).

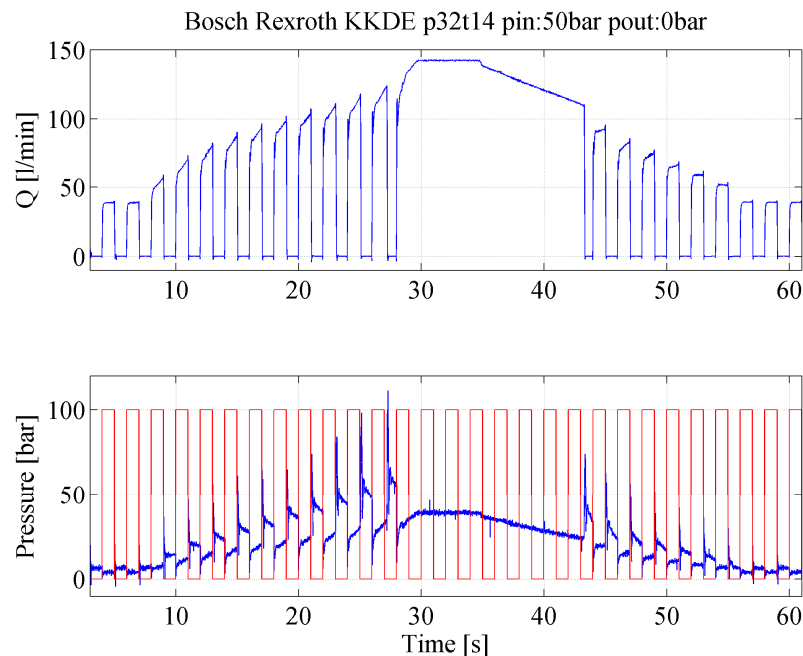


Figure 9. Operating limit test

It can be seen in the figure 9 that when the reference supply pressure reaches approximately 40 bars, the valve will not switch to closed position. The valve stays in



the open position which can also be seen in the flow graph, as the flow settles to approximately 140 lpm. The maximum flow before the operating failure is 120 lpm.

There are natural pressure spikes whenever the valve is switched. When the valve is suddenly switched to off-position, there is a pressure rise due to very fast change in the flow velocity. The kinetic energy of the fluid is converted to potential energy stored in the system pipes, hoses and in the fluid. This increase in the potential energy is seen as rapid pressure rise.

The pressure drop when opening the valve is due to the pressure difference over the valve. The potential energy stored in the fluid is released back to kinetic energy, which can be seen as a rapid flow rise in the flow graph. The pressure in the downstream of the valve is close to initial starting pressure, and therefore the oil flows from the high pressure side to the low pressure side.

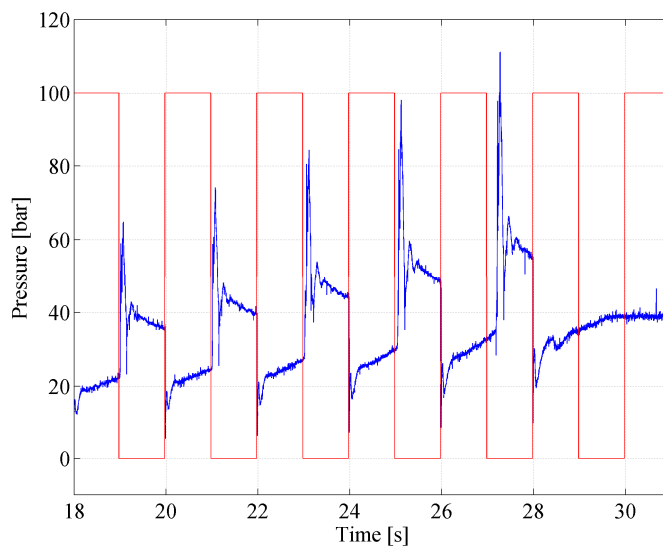


Figure 10. Operating limit test zoomed view

From this zoomed view, figure 10, it can be seen that the sudden pressure (in blue) rise occurs later and later, compared to the control signal (in red). This is a sign that the valve does not switch to closed position normally. The delay becomes longer as the supply pressure increases, and after a few misbehaving switches, the valve does not close at all.

The next working boundary condition test is run with opposite flow direction. It can be seen from the flow graph that the valve does not remain fully open when it is opened with bigger pressure differentials. The operating limit test graph can be seen in the figure 11.

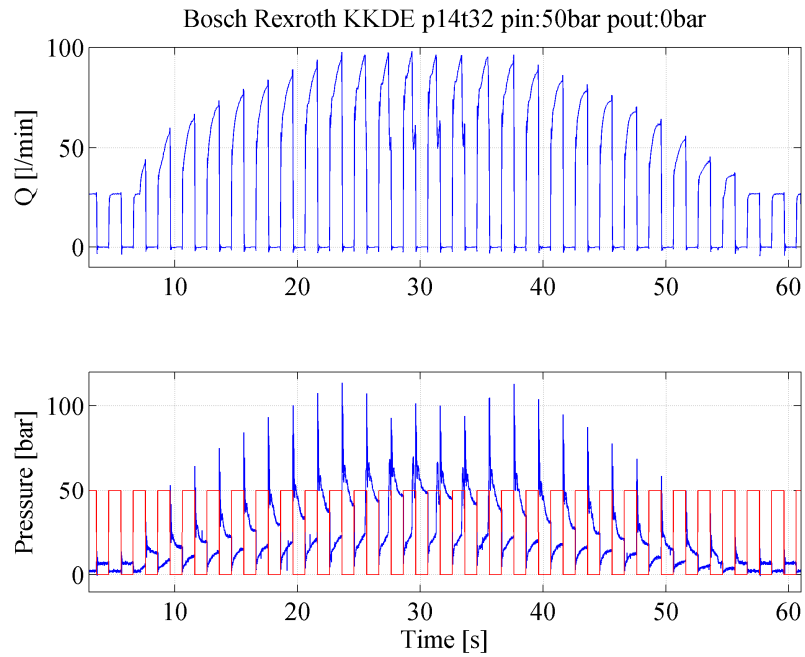


Figure 11. Operating limit test

This phenomenon does not seem to result in total valve operation failure with a pressure ramp of 0 to 50 bars in the flow direction where supply pressure is applied to ports 1 and 4. The pressure spikes do not seem to grow naturally as the ramp pressure increases and this indicates slower valve closing. Before any misbehaviour, the flow reaches almost 100 lpm, which is quite a big flow rate for this valve.

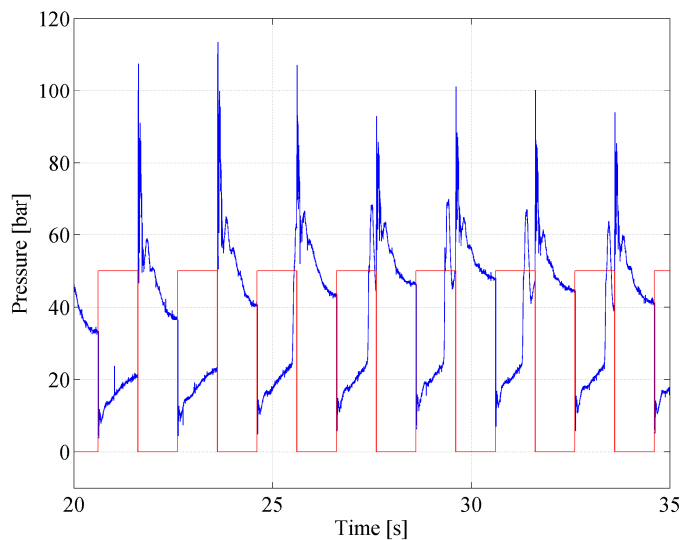


Figure 12. Operating limit test zoomed view

The pressure graph indicates early valve closing because the pressure level rises rapidly before the valve is commanded to close. The next measurement was the same situation, but with a bigger pressure ramp, a ramp from 0 to 100 bars. This bigger ramp should make the phenomenon pop out a bit more. When the valve starts to fail ( $t=15s$ ), it was seen from the flow graph that the valve opens almost fully but starts to close

immediately after the opening and switches to a position somewhere between open and closed position. The flow rate seems to stabilize to 45-50 lpm with the abnormal functioning. The zoomed view showed that the supply pressure rises before the valve is commanded to close position. This indicates that the valve starts to close, even though it is being held open with holding current. This phenomenon becomes more evident as the supply pressure ramp grows. At opening command at 22 seconds, the pressure spike is almost as big, as in a normal fast valve closing.

There is a pressure drop in the supply pressure, whenever the valve is opened due to the big pressure difference over the valve. The pressure drop remained as it should be, showing that the valve does open, but after that, especially towards the end of the zoomed view, the supply pressure rises to a value that isn't in line with the supply pressure values seen in the beginning of zoomed view. This showed that the valve restricts the flow more than it does when in fully open position, and is seen as increased supply pressure values. This means that the valve switches to some "middle position".

It is interesting, that when the supply pressure is applied to ports 3 and 2, the valve tends to stay open, and on the contrary, when supply pressure is applied to ports 1 and 4, the valve tends to close, when the supply pressure ramp is run. This refers to the fact, that the pressure forces are the ones that set the limit to the functioning of this valve, in this kind of operation. When this test was done with higher overall pressure levels, 300 bar and 240 bar, similar kind of an effect can be seen. It can be deduced that the general pressure level has little impact on this phenomena, it is more a function of pressure difference over the valve.

The parker operating limit test, with the supply pressure applied to ports 3 and 2 shows very similar looking results with KKDE valve. The supply pressure was also connected to ports 3 and 2 in KKDE, when this similar looking data was obtained. The valve seems to be working fine until 80 bar pressure difference. However, from that point on, the valve does not close at all. The flow increases as the supply pressure ramp reaches higher values. The function returns to normal when the pressure difference becomes approximately 80 bars and below that.

The next test was the same test but with opposite flow direction. This direction, again, showed very similar results to KKDE valve. However, it was notable that the maximum flow reaches over 200 lpm, against KKDE's maximum 125 lpm. The valve block and spool liner modifications had also an impact on this test, as before the modifications, the peak flow was about 20 per cent smaller at 80 bar pressure difference. The zoomed view showed the valve closing before the close command as the pressure difference reaches approximately 125 bars. The Bosch Rexroth 4WE valve could not be measured to critical fail point, since the hydraulic unit used had a pump that could provide a maximum of 250 lpm, and the valve showed perfectly normal actuation within the range 0...250 lpm.

## 6. RESPONSE TIME TEST

The delay time is the time between the control signal and when the moving element actually starts to move. Movement time is the time spent from the beginning of the movement to the end of the movement. The response time is the sum of delay time and

movement time. The response time can be deduced from the electrical current applied across the solenoid. Actually, the delay is determined from the pressure rate, and the end of the movement is determined from the electrical current. This way we get the delay, movement and response time. [2, p.42]

The plunger movement inside the solenoid affects the current. This phenomenon is known as the back EMF (electromotive force), and it strives to slow down the rise of the current. The current can even decrease from the level it has reached due to this phenomenon. The back EMF effect ends as the movement of the plunger ceases. The response time can therefore be deduced from the current graph as the ending point of this phenomenon. In practice this means that in the opening of the valve, there is a small notch in the current curve, and that means that the valve moving part has reached the end of the movement. If there is not a notch, the second beginning of current change speed increase can be interpreted as the spool reaching the end of the movement. The beginning of the movement can be seen as a small sudden drop in the supply pressure level. [2, p.40]

The closing of the valve, on the other hand, is seen from the voltage applied across the solenoid. The voltage reaches -48V when the valve is commanded to close, and after a few milliseconds it starts to rise. There is a notch or a saddle point in the voltage graph, and the valve has reached the end of the movement when the voltage starts to increase after this point. The closing cannot be deduced from the current curve.

One thing that was seen on the operating limit tests was that the flow direction where supply pressure was applied to ports 1 and 4 seemed to close the valve with big pressure differentials. It was deduced that the pressure forces caused this closing to occur. It will be interesting to see if the response time tests in this flow direction support this theory, that is, does the flow direction affect the response time. It could become visible so that the opening is slower and the closing faster, in this flow direction. If there is no, or little, difference in the response times between pressurized and un-pressurized measurements, this phenomenon, obviously, will not be visible here. The valve time response is presented for every valve, both opening and closing. Different pressure levels were used to find out if the general pressure level has an impact on the response time. Some tests were also done with a bigger pressure differential over the valve to find out whether this has an impact on the response time or not.

#### 6.1. Bosch Rexroth KKDE response time test

The response time was first measured with zero pressures. Deducing from the notch in the current graph, the response time was approximately 8 ms. The booster voltage was used for 10 ms, only 2 ms longer than the actual opening, and is therefore adjusted quite accurately. Next measurements were done to find out whether the rise of the general pressure level or pressure difference has an effect on the response time. Now, when we have higher pressure rates, when can determine the delay time also. The response can be seen in figure 13.

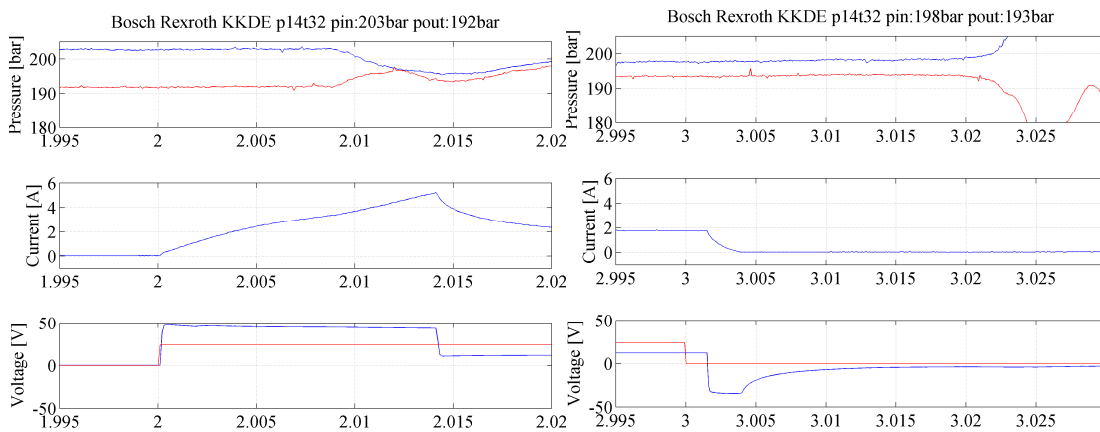


Figure 13. Response time test for valve opening and closing

The blue pressure curve is the inlet pressure and the red curve the outlet pressure. Valve control signal (in red) can be found in the voltage graph, it is unitless and is scaled to reasonable values so that the valve state can be seen. There is a discontinuous spot in the current graph when the voltage is switched from 48V to 12V. The delay is 9 ms, and the movement time 1 ms, total response time is 10 ms. The booster 48V pull phase voltage is applied almost right away, this delay is approximately 0,3 ms. The response time is 1 ms longer than without pressures. Figure 11 shows also the response for valve closing. The voltage drops to -38V when the valve is commanded to close position. Here we can see the delay that comes from the booster itself, a millisecond or two passes from the control command before the booster actually gives the -38V voltage. The voltage is supposed to rise from the -38V to a saddle point somewhere between -38V and 0V. The valve reaches the closed position when the voltage starts to rise from this value. From the valve closing, it can be seen that the booster delay is 2 ms. The first reaction in the pressures can be seen at 19 ms. This means that the valve delay time is 17 ms, in closing movement. The voltage seems to start the increasing at 25 ms, making the response time 23 ms. This is 3 ms slower than without the pressures.

Next measurements were done to find out whether the increase of the pressure difference has an effect on the response time or not ( $dp=150\text{bar}$ ). Based on the previous data information, it will be interesting to see if the direction where supply pressure is applied to ports 1 and 4 will have a faster closing and slower opening with bigger pressure differential. The delay time was now 9 ms and the response time 10ms. This value is 2 ms bigger than without the pressures, it can be said that it matters whether the system is pressurized or not, and further on, the pressure difference over the valve affects the results as well. The influence of pressure ( $dp=120\text{bar}$ ) becomes even more evident with valve closing, first changes in the pressure curves could be seen at 10ms, and the voltage curve shows that the valve closes 14 ms after the switch command. The booster delay is 2 ms, so the actual valve response in only 12 ms.

As expected, the pressurized system makes the opening a bit slower, and the closing a bit faster when the supply pressure is applied to ports 1 and 4. The next results, figure 14, were measured with the opposite flow direction and they will show whether this phenomena will make the valve open faster and close slower in the opposite direction when the system is pressurized. Figure 14 shows the response in the other flow direction with a pressurized system.

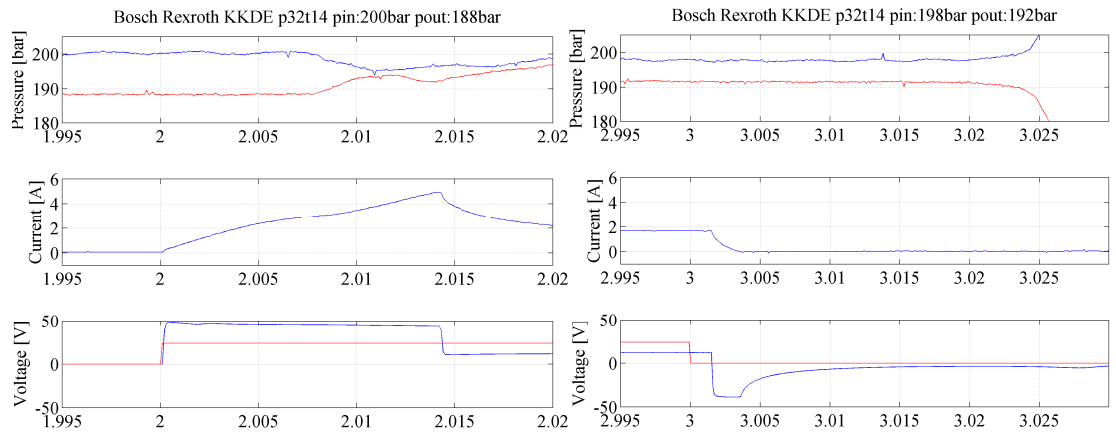


Figure 14. Response time test for valve opening and closing

When a pressure level of 200 bar is applied, figure 14, the first signs of change in the supply pressure can be seen at 8 ms from the opening signal. Deducing from the current curve, the response time is 9 ms. In valve closing, the first signs in the pressure level can be found at 3,020 seconds, and the voltage curve gives the total response time; 28 ms. The booster delay is 2 ms, so the actual closing time response is 26 ms. This response time is 14 ms longer than with the opposite flow direction, with same pressure difference and general pressure level. The opening with a bigger pressure difference over the valve results in a response time of 9 ms. First changes can be seen in pressure curves at 8 ms from the opening control command. The pressure effect is very clearly visible in the last KKDE valve closing measurement, the response time for closing is a staggering 52 ms, while the first changes in the pressure can be observed at 43 ms. The booster 2 ms delay does not make the real response time 50 ms look much better. All in all, it is clear that the response is affected by both, whether the system is pressurized or not, and the pressure difference over the valve. Also, it has a very clear impact on the response time which way the valve is connected.

## 6.2. Parker DSH104 response time test

The first measurements were done with unpressurized system. The response without pressures, is quite fast, only 7 ms. Figure 15 shows the response with pressurized system.

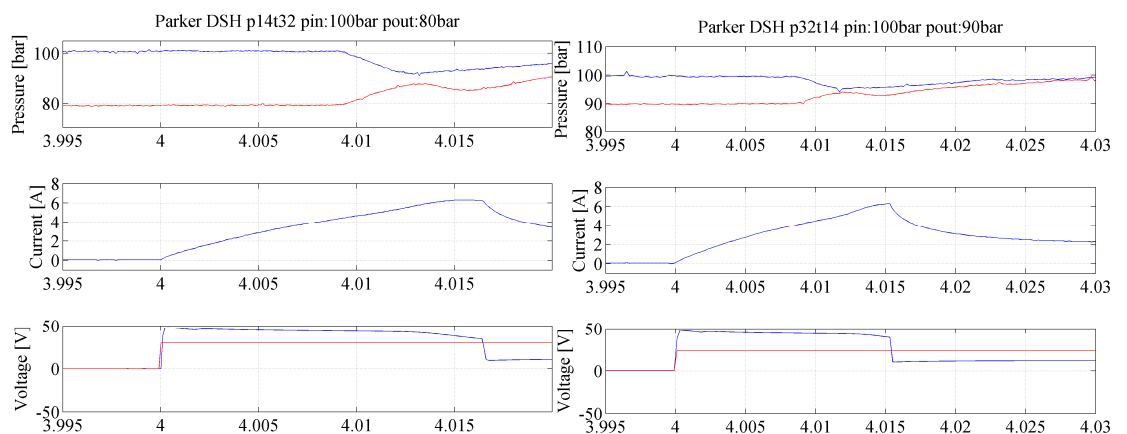


Figure 15. Response time test for valve opening in both flow directions

The first changes can be found at 9 ms from the control command. The response time is determined from the current curve; 12ms. The movement time is therefore 3ms, which 1-2 milliseconds slower than Bosch Rexroth KKDE valve. This flow direction was noticed, in the critical boundary test, to close the valve when bigger pressure differentials are applied. The general pressure level definitely has an effect on the response time, the pressurised valve response time is 5ms longer than without the pressures. Next measurements were done to find out how long the response time for valve closing actually is without negative control voltage and the result was over 50ms.

After a coil modification (a diode was removed from the coil which prevented the negative voltage), the response time is 12ms, and the first changes in the pressure were seen at 8 ms, so the delay was 8 ms and the movement time 4 ms. The modified coil was also tested in this direction without pressure, and the response time was 11 ms. This supports the conception that the sum pressure forces act in the opening direction with this flow direction.

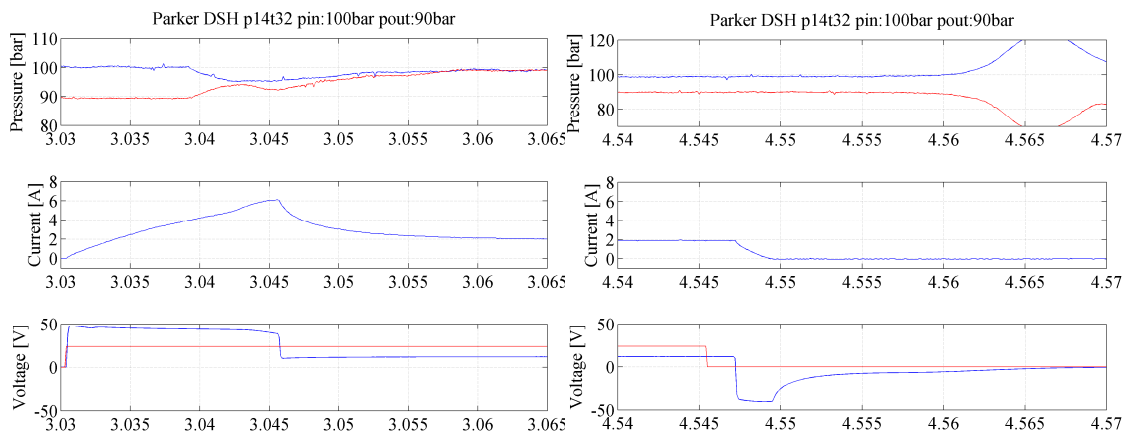


Figure 16. Response time test for valve closing and opening

The opening response, figure 16, in this flow direction is also 12ms, so there is no deviation between the flow directions regarding the response time. The figure 16 shows also the closing of the valve. The first changes in the pressure can be seen at 13ms after the control command, but the end of the movement is quite difficult to deduce from these graphs. The booster delay is 1 ms, and the end of the movement is approximately at 15 ms, so the actual response time is approximately 14ms.

In valve closing in flow direction p32t14, the first changes in the pressure were seen at 16 ms from the close command but the end of the closing was quite hard to see. The end of the movement, deducing from the voltage graph, could be approximated to occur at 18ms. The booster delay was 2ms so the actual response is 16 ms.

These were all the measurements that were done after removing the diode. From the measurements before the modification, it can be said that the general pressure level did not affect the opening response time. Increasing the pressure difference over the valve, also, did not affect the response time in either direction. When the Parker DSH valve was measured, the closing could be seen quite clearly from the voltage curve when the system was un-pressurized. A clear notch in the voltage curve could not be found when the system was pressurized, this made it a bit hard to determine the closing response time.

### 6.3. Bosch Rexroth 4WE response time test

The used booster could give the maximum 48V voltage at maximum for only approximately 15 milliseconds, and this proved to be a too short time for some measurements. The valve doesn't always switch position within this time, and yet, the boost voltage ends. There is a discontinuous spot in the current graph when the voltage is switched from 48V to 12V. After that, the current decreases and settles to holding current value. The notch seen in the previous valve measurement data current graphs is not seen because the valve does not reach the other position during the rise of the current. This makes it very hard to deduce the movement time of the valve. The beginning of the opening, on the other hand, can be seen very clearly from the pressure graphs.

The first measurements were done by using one coil. In this setup the coil is used to open the valve and a spring is used to return the valve. Measurements provided here were done with pressurized system because the voltage and current graphs from measurements with unpressurized system were quite uninformative; e.g. the notch in the current curve could not be found or the boost current ended before anything happened. The response can be seen in figure 15 and the flow direction is marked in the graph title.

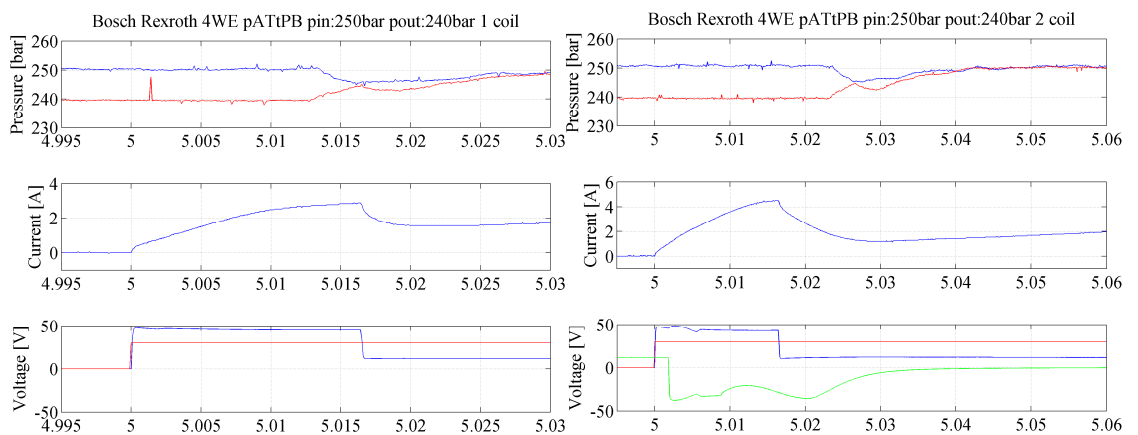


Figure 17. Response time test for valve opening

Figure 17 (lhs) shows a quite fast actuation, the first changes in the pressure can be found at 13 ms after the control command. The response time cannot be deduced from this graph. The next measurement, figure 17 (rhs) is done by using two coils, the graph voltages are taken from separate measurements because only one voltage meter was available. The two coil response for opening is slower. The first changes in the pressures can be found as late as at 23 ms. This implies that the second coil, the coil that keeps the valve closed, restricts the movement in the opening. The closing coil is switched off when the valve is opened, but as the graph shows, the voltage doesn't drop instantly from the 12 V holding voltage. The booster delay for switching the valve closing coil control voltage from 12V to -40V is 2 ms while the opening coil voltage increases immediately. The fact that the other coil voltage does not drop immediately, induces a restricting force to the valve from the closing coil in the beginning of the opening. A solution to this problem is adjusting the booster so that the voltage drops immediately when the control command to switch the valve open is given.



So the opening was slower when two coils were used, because of the bad booster adjusting, but it will be interesting to see how the closing coil will affect the closing time response, compared to spring return version of the valve. A measurement was done with only the opening coil, and it is switched off, and the returning spring does the return movement. The first changes in the pressure were seen 32 ms after the closing command. Next measurement was the same situation but with two coils in use. The first changes in the pressure can be seen at 21 milliseconds, which is 11 milliseconds faster a time than with the spring return. Figure 18 shows the response for the other flow direction.

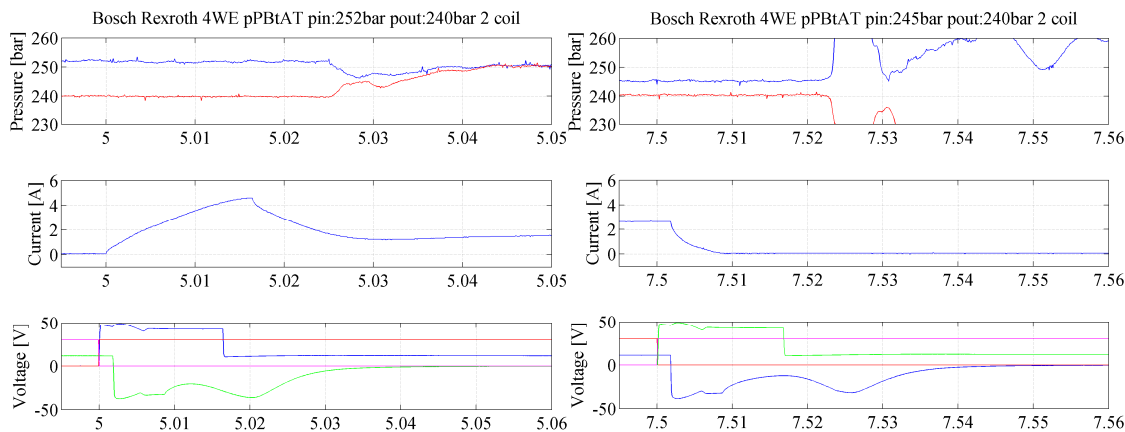


Figure 18. Response time test for valve opening and closing

The coil control signals are marked with red and purple. The corresponding voltages can be seen in blue and green. Again, there is a booster delay of a few milliseconds on the closing coil (green curve) and this slows down the opening. The first changes in the pressure can be seen at 26 ms. Figure 18 (rhs) shows the closing of the valve. First changes in the pressure can be found at 23 ms. The valve delay is 3ms shorter with closing than it is for opening. Closing with a coil is 9 ms faster than with a spring.

## 7. LEAKAGE TEST

A small capacity flow meter was used to determine the leakage flow across the closed valve with a pressure differential of 200 bars. The Bosch Rexroth KKDE leakage was in the flow direction p32 & t14 0,03 lpm, and in the p14 & t32 direction 0,05 lpm. The Parker DSH104 leakage was in the flow direction p32 & t14 0,03 lpm, and in the p14 & t32 direction 0,035 lpm. The Bosch Rexroth WE10 leakage flow is 0,04 lpm when the closing coil is on, and 0,08 lpm when the closing coil is off. These leak flow rates are within a very reasonable range if these valves are used to control a dynamic continuously state changing system. Valves in digital hydraulic systems are known to be leak free. This is because the used valves in the DFCUs are poppet type valves. However, digital hydraulic systems can also be implemented with spool type on/off valves. This solution will cause some leakage in the valves, but could provide quite fast operating high flow capacity DFCUs. A DFCU could also be combination of spool and poppet type valves, for example so that the poppet valves are for small flow rates and the spool valves for bigger flow rates.

## 8. VALVE MEASUREMENT CONCLUSIONS

Based on the quite fast returning operation of the biggest valve, it can be said that it would bring benefit and better controllability, to especially bigger flow capacity digital valves, if the valve was operated with two solenoids. This way the valve would have one solenoid for the opening, and another for the closing. Now the opening time is determined widely by the solenoid operation, whereas in the return movement, the response time is widely determined by the return spring. Stiffer springs can be used to make the return faster, but this results in bigger force requirements for the opening. This issue becomes more evident as the valve size grows.

A very precise controllability of a DFCU is hard to achieve if the switching times vary depending on if the valve is closed or opened. From a control point of view, it would be really good if the valve would open and close within the same time. For smaller valves, it may be sufficient that they are closed with springs, but as could be seen from the measurements, for bigger valves, the spring return does not work very well. The two coil usage would, of course, increase the valve size a bit, but the benefits of precise control would probably overcome the valve size change in applications where the physical size of the valve is not absolutely critical.

Some modifications (drillings in the valve block, removal of a seal and a diode) were made during the measurements and they showed clearly visible changes in the results. Further modifications would have upgraded the valve performance even more. The flow channels should be drilled straight to the block, the valve spool overlap could have been machined to be approximately 2mm smaller. Now the two middle ports were connected to each other with a u-shaped pipe; these volumes should be united as a one big volume inside the valve block.

The operating limit tests showed the critical boundaries for the valves, but also that it really matters which way the valve is assembled a valve to a system. The valves tended to stay in the open position when critical pressure difference was applied while in the other flow direction, the valve would switch to closed position or stay closed. No chocking of the flow was detected; the flow rate grew as the pressure difference became bigger. Some crucial measurement data can be seen in table 2, but to get a good overview of the valve operation, the actual valve measurement chapter should be read.

*Table 2. Summary values*

	BR KKDE	Parker DSH104	BR 4 WE
Flow (dp=5bar) pS ramp	43 lpm	41 lpm	77 lpm
Flow (dp=5bar) pT ramp	43 lpm	37 lpm	77 lpm
Operating limit (dp/flow)	40 bar/125 lpm	80 bar/175 lpm	unmeasured
Response time (open – close)	10 ms / 14 ms	12 ms / 16ms	15 ms / 15 ms
Leakage (dp=200bar)	0,05 lpm	0,035lpm	0,04 lpm

The largest valve showed unexpectedly small flow rates, compared to the valve size. However, it showed that the two coil operation brings great benefit to the valve control. The response time for this size valve and spool was quite good. With a different spool, probably a flow rate of approximately 150 lpm could be achieved with the same response time. The smaller valves showed quite close to expected results, validating the feasibility of this kind directional valve usage in digital hydraulics. It might not be reasonable to use the same size valves if the required flow scope is very wide. For a DFCU with a capacity of 600 lpm, for example, it is reasonable to have different size valves if binary coding is used to dimension the valves.

It can be also said that the valve behaviour was affected a bit by pressure conditions. The valve behaviour is of course mostly determined by the control electronics and driving voltage. When creating a digital hydraulic system controller, the used valves should be measured to obtain the parameters of valve dynamics to create a properly working controller.

## 9. ACKNOWLEDGEMENTS

This research is funded by the DIGIHYBRID-project which is part of EFFIMA-program of the Finnish Metals and Engineering Competence Cluster, FIMECC Ltd.

## REFERENCES

- [1] Mikkola, J., Ahola, V., Lauttamus, T., Luomaranta, M., Linjama, M. & Vilenius, M. 2007. Improving Characteristics of On/Off Solenoid Valves. The Tenth Scandinavian International Conference on Fluid Power (SICFP'07), May 21–23, Tampere, Finland, pp. 343–353 (Vol. 3).
- [2] Linjama, M., 2009. Digitaalihydrauliikka –course lecture material, IHA-2570 course lecture material

## MODELLING OF FLOW CHARACTERISTICS OF ON/OFF VALVES

Matti Linjama, Mikko Huova & Matti Karvonen  
Department of Intelligent Hydraulics and Automation  
Tampere University of Technology, Finland  
E-mail: matti.linjama@tut.fi

### ABSTRACT

One benefit of digital hydraulics is that control valves have predictable characteristics. By definition, on/off valve is either fully closed or fully open and the transition between these states happens quickly. If the flow characteristics of the valve are known accurately, it is possible to predict what would happen in the system if certain valves were open. This model-based control approach has been used successfully in the control of hydraulic actuators with parallel connected valve systems. The challenge is that valves have individual characteristics because the flow capacities are adjusted according to powers of two. This paper studies the accuracy of the generalized exponent flow model in the modelling of flow characteristics of different valve-orifice geometries. Results show that the standard square root model is inaccurate but general exponent model gives very good fit in most cases. The effect of orifice diameter on the exponent is also analysed.

**KEYWORDS:** Digital hydraulics, on/off valves, modelling

### 1. INTRODUCTION

Parallel connected on/off valve systems, aka. digital valve systems, have been used successfully in the implementation of demanding control tasks [1-3]. Figure 1 shows typical valve configuration used to control double acting cylinder. Each flow path is controlled by 4-7 parallel connected on/off valves, and the flow areas of the valves are adjusted by screw-in orifices to approximately follow the binary sequence 1:2:4:8: etc.

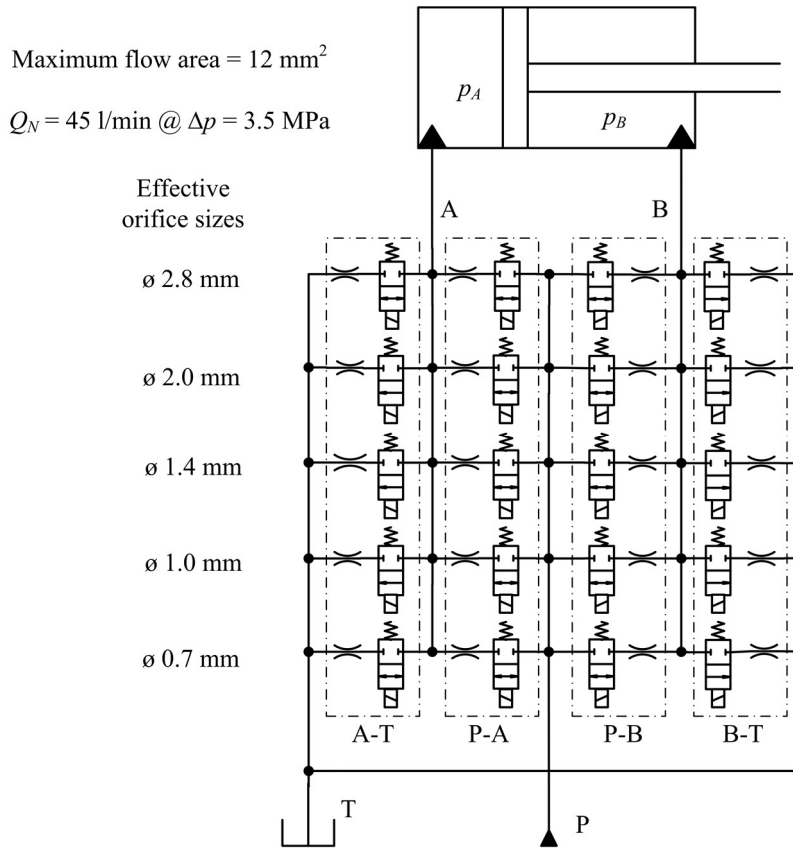


Figure 1. Example of digital valve system connected to hydraulic cylinder.

If flow characteristics of the valves are modeled accurately, it is possible to predict the system output and select the best opening combination at each sampling instant. As on/off valve is – by definition – either fully open or fully closed, it is normally enough to have model for combination of open valve together with its orifice. If the valve has leakage, the model for closed valve may also be needed, but it is not discussed in this paper.

The modeling of flow rate of the valve or valve-orifice combination is closely related to the modeling of the flow rate through turbulent orifice. The well-known formula for the orifice flow is

$$Q = K_v \sqrt{\Delta p} , K_v = C_q A \sqrt{\frac{2}{\rho}} \quad (1)$$

where  $A$  is flow area,  $\rho$  is density and  $C_q$  is tuning parameter. As the fluid density is practically constant, the equation can be parametrised by using only one combined flow coefficient  $K_v$ . The square root uniquely determines the shape of the  $p$ - $Q$  curve and flow coefficient can be calculated by measuring one  $p$ - $Q$  data point. Our experience is that this model is far from accurate and more accurate model is needed. Two main reasons for inaccuracy is that the shape of the  $p$ - $Q$  curve is fixed to follow square root formula and that cavitation choking strongly affects the flow rate at small outlet pressures [4]. The square root model is particularly inaccurate with small orifices.

## 2. MODELLING OF FLOW RATE

### 2.1. Flow Model

The flow path through a DFCU consists of connectors, drillings, bends, valve, and possibly orifice, which is used to reduce flow capacity of the valve to the target value. It is assumed that valve-orifice combination dominates the flow characteristics and that the fluid volume between them is small. It is then possible to model each valve-orifice combination as a one flow restrictor. The generalized exponent model is used to model the flow rate:

$$Q(p_{in}, p_{out}) = \begin{cases} K_{v1} (p_{in} - p_{out})^{x_1}, & b_1 p_{in} < p_{out} \leq p_{in} \\ K_{v1} [(1 - b_1) p_{in}]^{x_1}, & p_{out} \leq b_1 p_{in} \\ -K_{v2} (p_{out} - p_{in})^{x_2}, & b_2 p_{out} < p_{in} < p_{out} \\ -K_{v2} [(1 - b_2) p_{out}]^{x_2}, & p_{in} \leq b_2 p_{out} \end{cases} \quad (2)$$

$$p_{in} \geq 0, p_{out} \geq 0$$

where  $p_{in}$  and  $p_{out}$  are pressures at the “inflow” and “outflow” side of the valve,  $K_v$  is flow coefficient,  $x$  is exponent and  $b$  is critical pressure ratio. The subscript 1 denotes the flow direction from inflow to outflow side and the subscript 2 the flow direction from outflow side to inflow side. The parameter values are usually different for different flow directions. The exponent value  $x = 0.5$  gives the standard square root model while value  $x = 1$  corresponds to fully laminar flow.

Figure 2 depicts the shape of the flow rate function for certain parameter values. The cavitation choking affects the flow rate when the outflow side pressure is smaller than  $b$  times the inflow side pressure. The flow rate does not increase even if the outflow side pressure is further reduced.

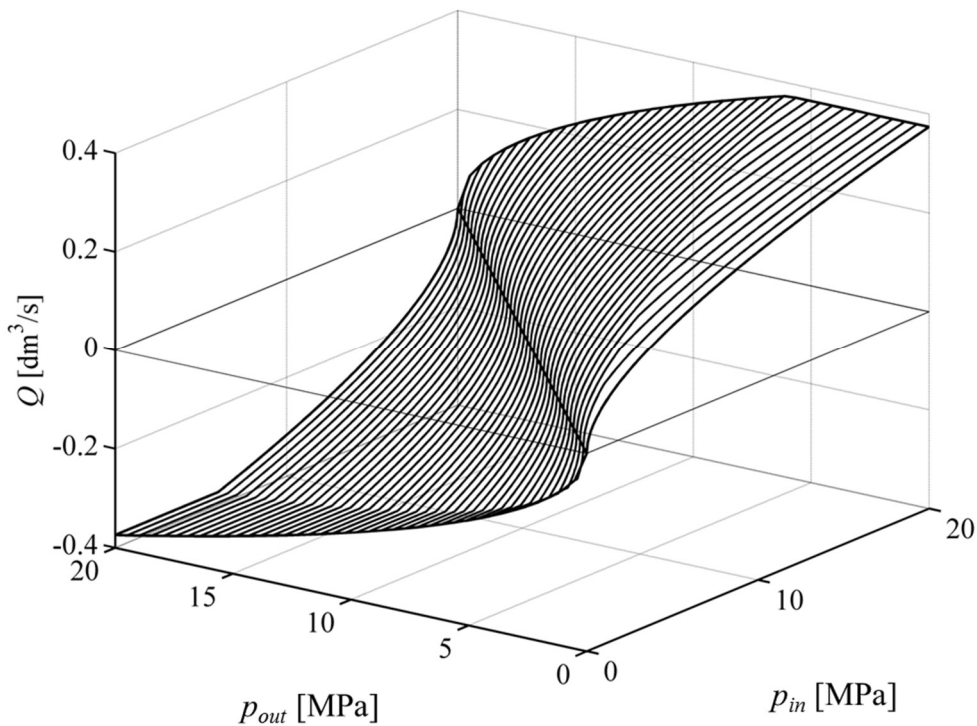


Figure 2. The value of the flow model with following parameters:  
 $K_{v1} = K_{v2} = 10^{-7} \text{ m}^3 \text{ s}^{-1} \text{ Pa}^{-x}$ ,  $x_1 = x_2 = 0.5$ ,  $b_1 = b_2 = 0.3$ .

## 2.2. Calibration Measurements

Two calibration measurements are suggested in order to determine the parameter values of the flow model:

- 1) Keep the inlet pressure constant and adjust outlet pressure from inlet pressure to zero and back.
- 2) Keep the outlet pressure at zero and raise inlet pressure from zero to maximum value and back.

The signals to be recorded are inlet and outlet pressures, oil temperature (preferably both before and after the valve), and flow rate. It is important consider following things:

- Pressures must be adjusted slowly and smoothly. Ramp type adjustment with ramp time about one minute is usually slow enough, but this depends on the flow capacity of the valve and hydraulic capacitances of the measurement system.
- Sensors must be accurate enough. Different sizes of flow sensors may be needed because digital valve systems have valves with order of magnitude different flow capacity. Recommended accuracy for pressure measurement is 0.01 MPa as we are many times interested on flow rates at 0.5 MPa pressure differential.

- Oil temperature must be controlled accurately. The ISO 10770-1 standard recommends temperature of  $40 \pm 6$  °C, but even 2 °C temperature change can be seen in the flow rate in the case of small orifices [5]. The preferred accuracy is  $\pm 2$  °C, but this is difficult to arrange in practice. The valve, valve manifold and piping must be preheated by keeping the valve open and letting the oil flow warm up the system.

Figure 3 shows the simplified hydraulic circuit diagram of the IHA's valve measurement rig. The pressure control is implemented by a proportional pressure relief valve, high response directional servo valves and closed loop controllers, which allow accurate control and fully automatic measurement sequences. Three flow sensors are used in order to maintain the flow measurement accuracy in the range from 0.008 to 250 l/min. The bypass valve can be used to improve controllability because only part of the flow goes through the valve studied. The bypass flow also helps to control temperature with small valves.

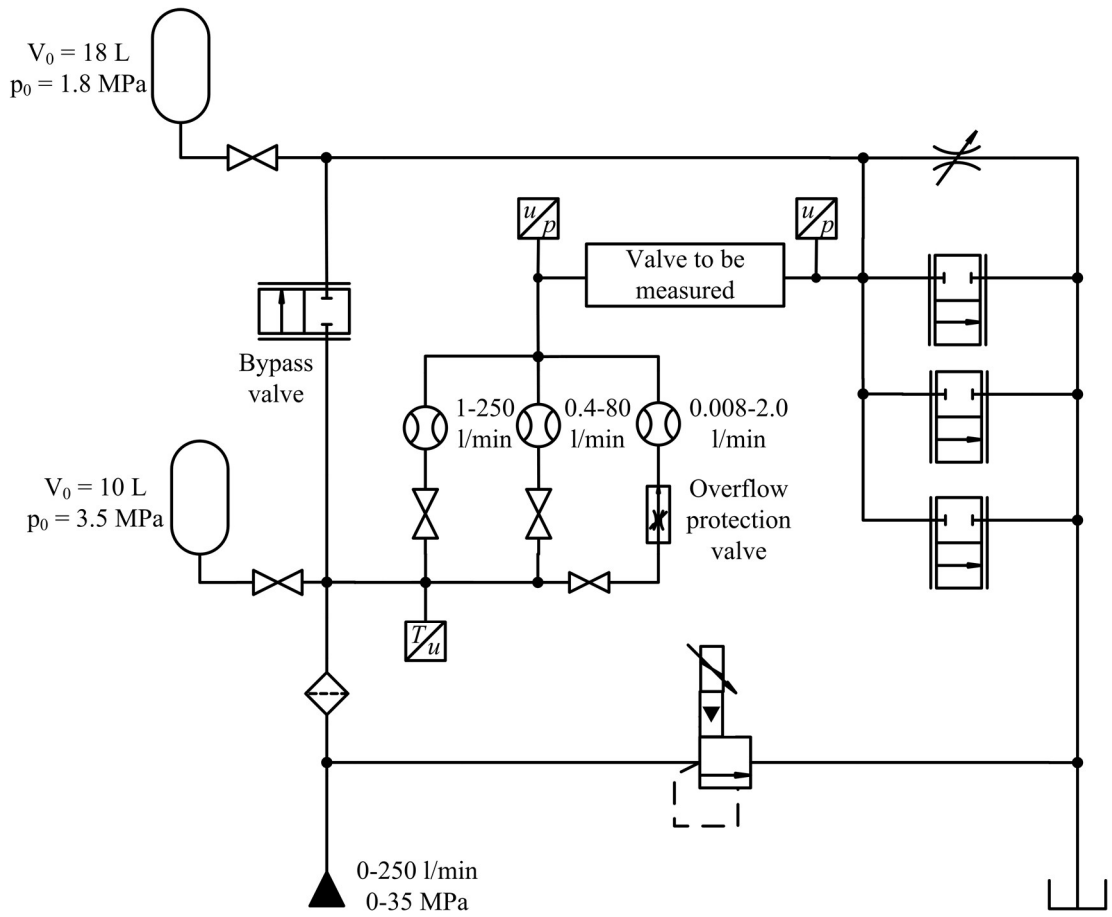


Figure 3. Hydraulic circuit diagram used in the valve calibration measurements.

### 2.3. Parameter fitting procedure

The parameter fitting is explained by using an example measurement. The 20 MPa constant inlet pressure data is shown in Figure 4. It is seen that the ramp time is 30 s and that the zero outlet pressure is not achieved because of flow losses at the outflow side.



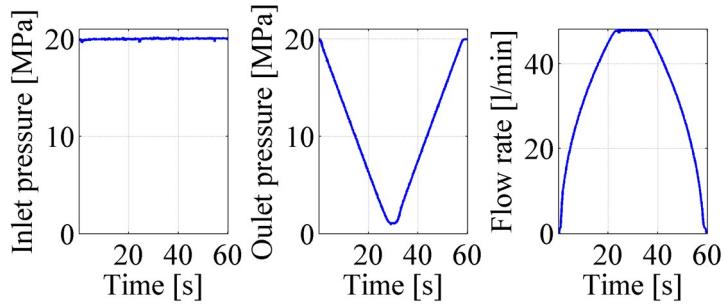


Figure 4. Example measurement with 20 MPa inlet pressure.

The flow rate versus pressure differential is plotted in Figure 5. The cavitation choking starts at 15.5 MPa pressure differential and effect is clearly seen. It is also seen that the curve has only minor hysteresis. If the hysteresis was bigger, the ramp time should be increased.

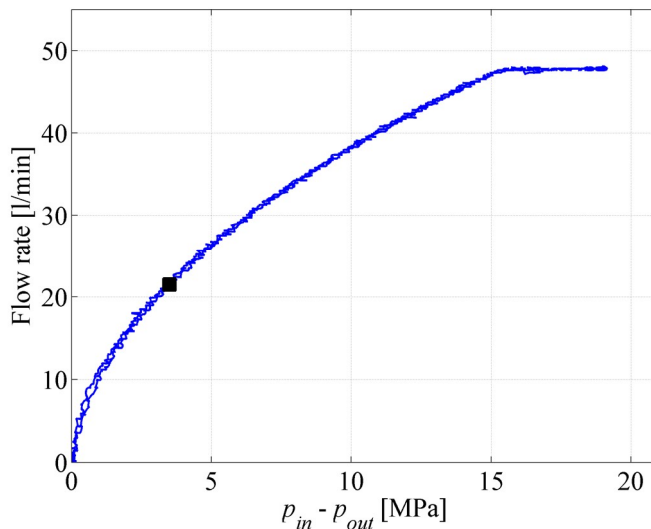


Figure 5. Flow rate versus pressure differential for the example measurement.

The first task is the determination of the nominal pressure differential, which should be selected according to the typical operation point of the valve. Here it is assumed that the valve works usually with 2-5 MPa pressure differential and the nominal pressure differential is selected to be 3.5 MPa. The corresponding flow rate is 21.5 l/min and the nominal  $p$ - $Q$  point is shown in Fig. 5. The next step is to determine exponent  $x$ . The flow coefficient  $K_v$  and exponent are related by

$$K_v = \frac{Q_N}{\Delta p_N^x} \quad (3)$$

The starting value for the exponent is 0.5 and the result is shown in Figure 6 (a). It is seen that the square root model  $x = 0.5$  is not accurate at all. Some experiments yield  $x = 0.54$  and corresponding flow coefficient is  $1.05 \times 10^{-7} \text{ m}^3 \text{ s}^{-1} \text{ Pa}^{-x}$ . The result is shown in Figure 6 (b) and the fit is perfect if cavitation choking is not considered.

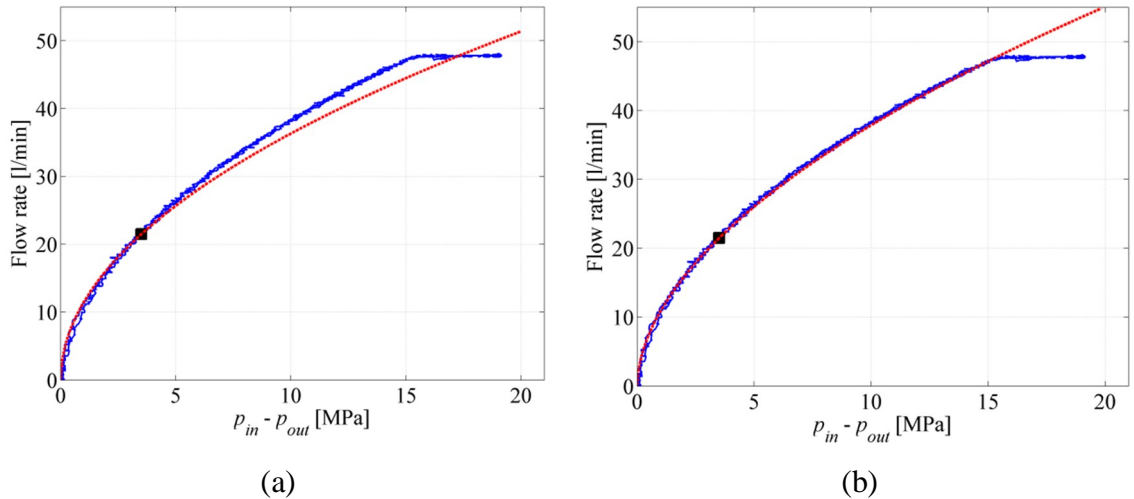


Figure 6. Model fit with  $x = 0.5$  (a) and  $x = 0.54$  (b).

The cavitation choking parameter  $b$  can be found by plotting the flow function of Eq. 2 with different values of  $b$  together with measured  $p$ - $Q$  curve until the best fit is found. In the example case the correct parameter value is  $b = 0.23$  and the result is shown in Figure 7 (a). If the model was perfect, it would give good accuracy for the zero outlet pressure measurement also. This is not the case as Figure 7 (b) shows. The result is obtained by calculating the value of Eq. 2 with the measurement data of Figure 7 (c). It is possible to fit parameters for the zero outlet pressure case but then the constant inlet pressure case would not be accurate. It is also possible to use some average parameter values which give reasonably good fit for both cases. Probably the best approach is to select the parameters according to the actual installation location of the valve. If the valve is installed in the tank side DFCUs, the parameters should be fitted to the zero outlet pressure data. If valves are in the pressure side DFCUs (from P to A or from P to B), the parameters should be fitted to the constant inlet pressure data.

### 3. THE EFFECT OF VALVE AND ORIFICE SIZE ON FLOW RATE

#### 3.1. Introduction

The calibration measurements have been performed for hundreds of valve orifice combinations and some of the results are presented in this chapter. Results are shown for constant inlet pressure measurements, because it is then possible to study cavitation choking also. The flow capacity of the valve is described by flow rate at 3.5 MPa pressure differential. The value is obtained from the valve model, not from the measurements. The oil is VG46 and inflow oil temperature 35-45 °C unless other specified.

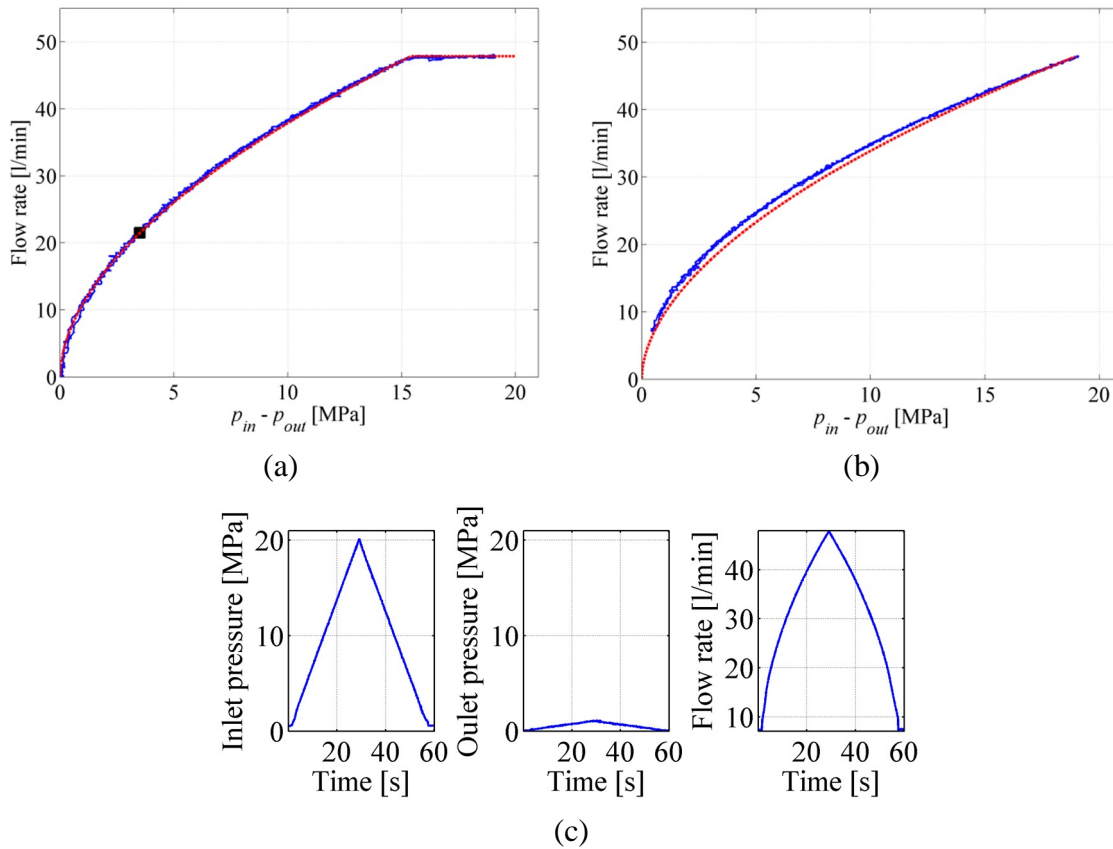


Figure 7. Model fit for constant inlet pressure measurement (a);  
 model fit for zero outlet pressure measurement (b);  
 measurement data of the zero outlet pressure case (c).

### 3.2. The effect of valve geometry

The valve geometry has an effect especially on the cavitation choking. Cavitation choking does not happen in valves where the dominating orifice is short. Spool valves are the most common example. Seat valves with “mushroom” type armature may or may not have cavitation choking while the strongest cavitation choking occurs in valves where the flow path is sharp edged orifice with significant length.

Figure 8 presents measurement results for three 4/2 spool type valves without orifices [6]. The P & B as well as T & A ports of the valves are connected externally together, which allows the utilization of both flow edges. All measurements suffer from too big flow losses in the return side and it is impossible to draw any conclusions about the existence of cavitation choking. The model fit is good in all cases and exponents are significantly bigger than 0.5.

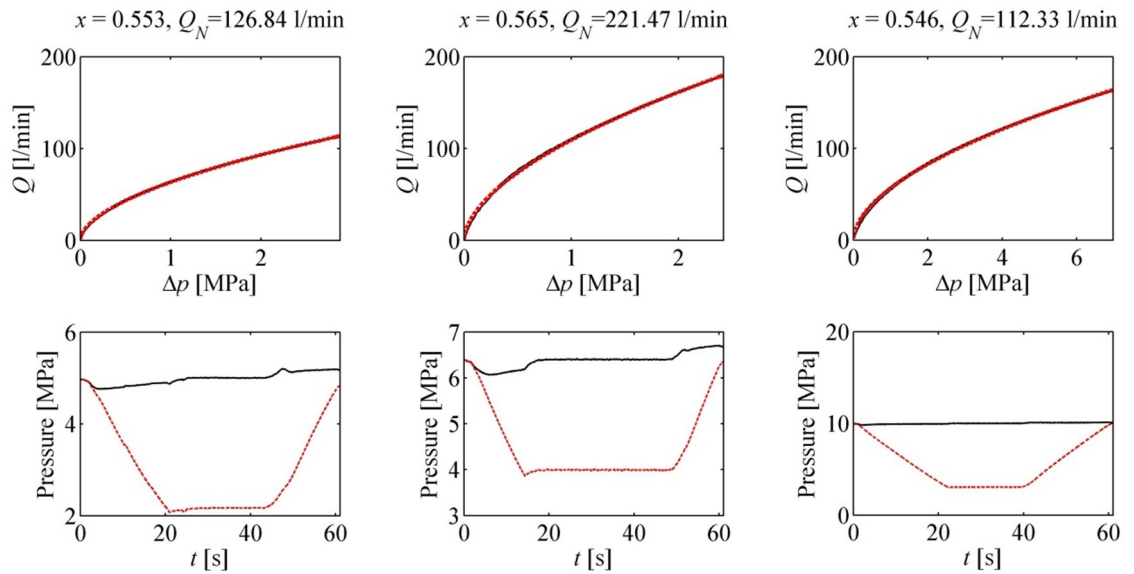


Figure 8. Constant inlet pressure measurements for three 4/2 spool type valves:  
 Screw-in cartridge valve Bosch Rexroth KDDE R 1EA/HN0V (left);  
 CETOP5 mounted valve Bosch Rexroth 4WE 10 EB3X/CG12N9K4 (middle);  
 Screw-in cartridge valve Parker DSH104 (right).  
 The oil temperature rises from 42 to 47 °C in the Parker measurement.

Figure 9 depicts the  $p$ - $Q$  curves for two seat type valves showing again good model fit. The flow geometries are also sketched in the figure. The first valve is Bosch Rexroth KSDER screw-in cartridge valve without orifice. The maximum allowed flow rate of the valve is 20 l/min and the valve starts to close spontaneously at 30 l/min, which explains the weird flow curve. The cavitation choking parameter is not known and it is assumed to be 0.3. The second valve is a miniature needle valve prototype [7]. Interesting feature of this measurement is sudden jump from normal flow curve to the cavitation choking curve. The increase in the flow rate is not caused by the armature movement but some other cavitation related and poorly understood phenomenon. The jump behaviour is not unique for this valve but has been detected with several valve-orifice combinations.

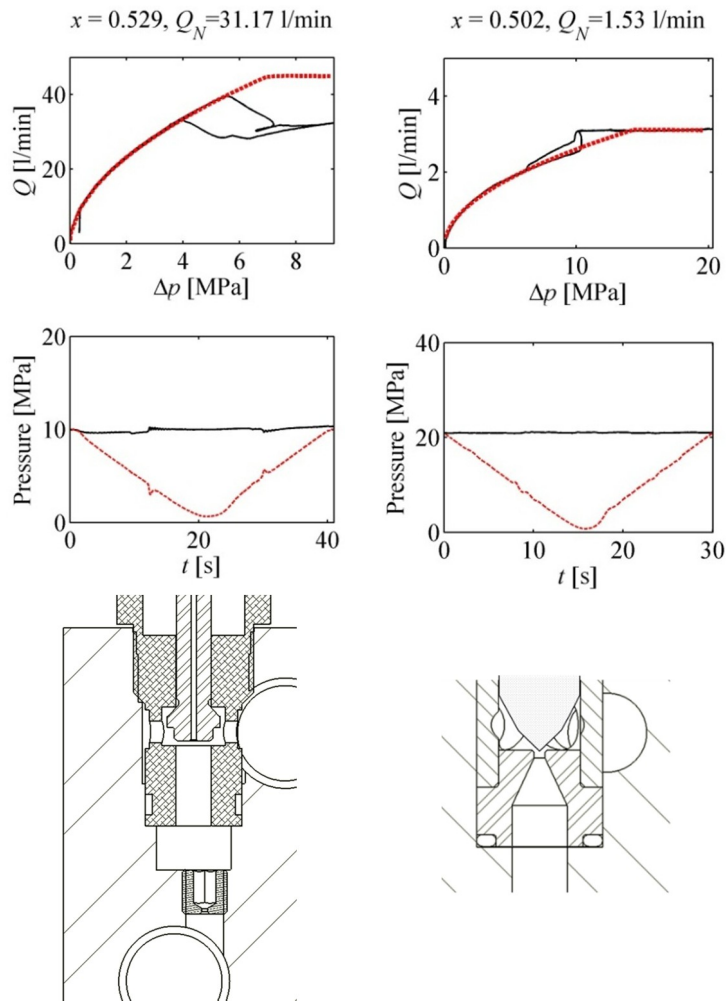


Figure 9. Constant inlet pressure measurements for Bosch Rexroth KSDER valve (left, nose-in) and miniature needle valve prototype (right, side-in). The cavitation choking parameter is assumed to be 0.3 for the KSDER valve. Suggestive drawings of the flow paths are also shown. The orifice shown in the drawing is not present in this KSDER measurement.

### 3.3. The effect of orifice

The most common implementation of the digital valve system is to use one type of valves and to adjust flow capacities by serial orifices. If both valve and orifice followed the square root flow equation, the effective flow coefficient would be:

$$K_{v,eff} = \frac{K_{v,valve} K_{v,orifice}}{\sqrt{K_{v,valve}^2 + K_{v,orifice}^2}}$$

If both the valve and orifice have the same flow coefficient, the effective flow coefficient is 71 % smaller. If the flow capacity of the orifice is 30 % of the flow capacity of the valve, the effective flow capacity is 28.7 % and it can be said that the valve has only a minor effect on the flow capacity. This 30 % is used as a limit when analysis is presented for orifices only.

Figure 10 shows  $p$ - $Q$  curves for the Bosch Rexroth KSDER valve combined with orifice. The orifice is commercial with M8 thread and it is located according to Figure 9. The oil viscosity is quite high, about 65 cSt, which may have an effect on the results. The 2.6 mm orifice has flow capacity comparable to the valve itself while the orifice is dominating in other cases. The exponent increases when orifice becomes smaller. Figure 11 presents the exponent as a function of orifice diameter for 55 valve measurements in which the orifice is dominating the flow. The trend is clear but dispersion is quite large. The exponent for 0.8 mm orifice can be from 0.51 to 0.63 depending on geometry and oil viscosity, for example.

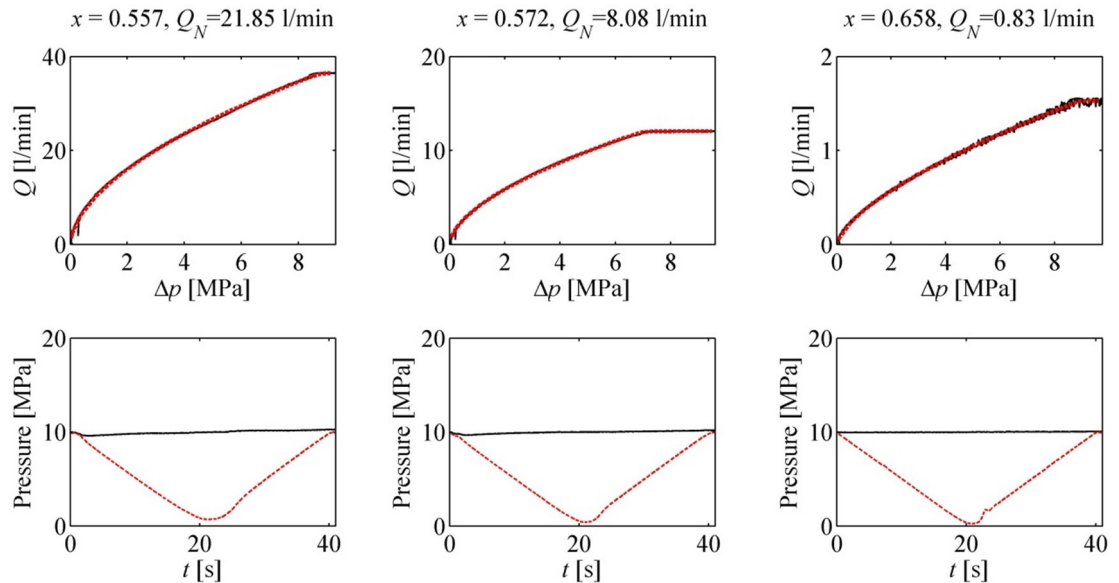


Figure 10. Measured  $p$ - $Q$  curves for Bosch Rexroth KSDER valve with different orifice sizes: 2.6 mm (left), 1.5 mm (middle) and 0.5 mm (right). Flow direction is Nose-In Side-Out. The oil temperature is 28-33 °C.

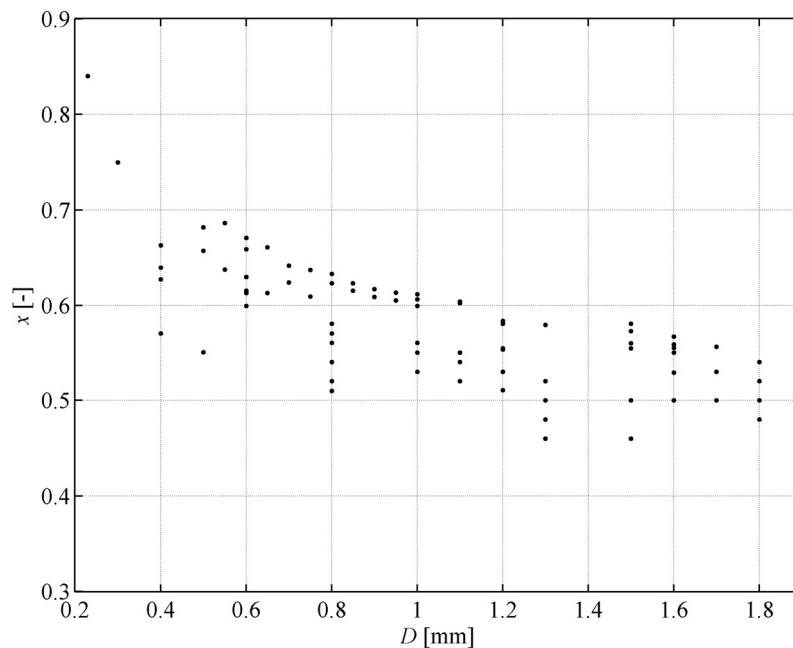


Figure 11. The effect of orifice diameter on the exponent of the flow model.

The exponent determines the shape of the flow curve. The nominal flow is another measure of the repeatability of flow curve. Figure 12 shows the ratio of flow rate at 3.5 MPa pressure differential and orifice area. The average value is 4.2 (l/min)/mm<sup>2</sup> and variation is below ±20 % in most cases. The relative flow rate starts to decrease when orifice size drops below 0.5 mm. One two measurements with 0.6 mm orifice show relative flow rate of 5.6 l/min. This may be caused by the bypass flow through the orifice thread. The  $p$ - $Q$  curves for the 0.6 mm case are shown in Figure 13. The valve with the biggest flow rate has increasing flow at the cavitation choking area, which supports the assumption of bypass flow.

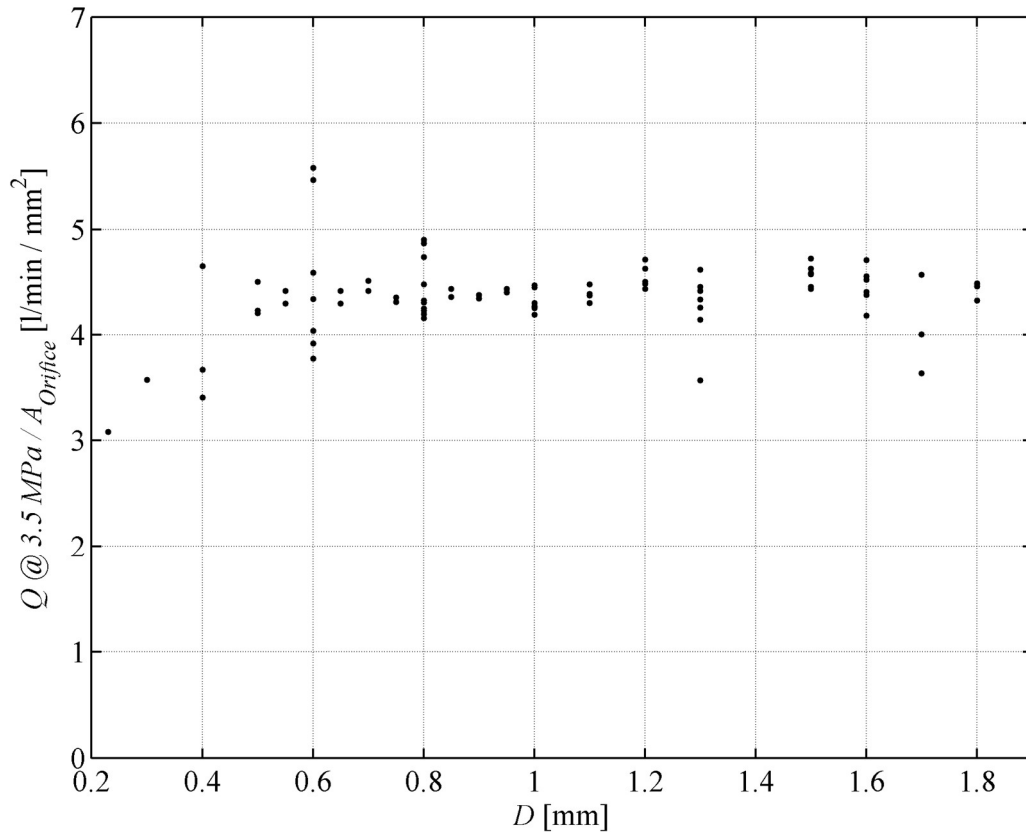


Figure 12. Relative flow capacity of different valve-orifice combinations in which orifice is dominating the flow.

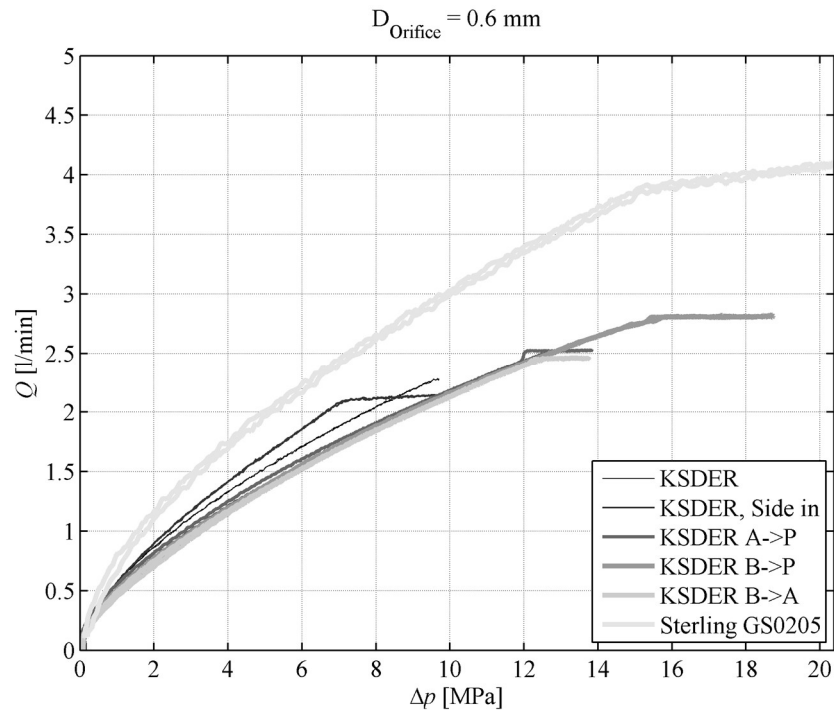


Figure 13. Measurements from different valves and manifolds with 0.6 mm orifices.

#### 4. DISCUSSION AND CONCLUSIONS

Results show that the generalized exponent model gives good approximation for the flow characteristics of different on/off valves and valve-orifice combinations. The model has three parameters: one for flow capacity (flow coefficient  $K_v$ ), one for shape of the curve (exponent  $x$ ) and one for cavitation choking (critical pressure ratio  $b$ ). The accuracy of the traditional square root model is poor and it is not recommended for the modeling, simulation or model-based control. The inaccuracy is clearly seen in Fig. 6a and the situation is even worse in most cases because exponent is usually in the range of 0.55-0.65.

Two calibration measurements have been used in order to find out parameter values. In general, the same parameter values do not give exact model fit for both measurements, which simply means that the model is not perfect. The constant inlet pressure measurement is recommended for valves, which are targeted to be used in the pressure side in the valve system. The zero outlet pressure measurement can be used in order to find out parameters for valves, which are located in the tank side control edges. The parameter values can be different in different flow directions.

The imperfections of the model come from several sources. The effect of viscosity on flow rate is not considered at all, which causes error especially with smaller orifices. The critical pressure ratio is assumed to be constant which is not true in practice [4]. The compressibility of the oil is also neglected and the fact that inflow and outflow side flow rates are different is not considered. The flow rates shown in this paper are pressure side flow rates. These topics could be addressed by taking Reynolds number as a parameter and by using mass flow model.



## ACKNOWLEDGEMENT

The research was supported by Academy of Finland (Grant No. 139540).

## REFERENCES

- 1 Linjama, M., Seppälä, J., Mattila, J. & Vilenius, M. 2008. **Comparison of Digital Hydraulic and Traditional Servo System in Demanding Water Hydraulic Tracking Control.** In: Johnston, D.N. & Plummer, A.R. (eds.) Fluid Power and Motion Control (FPMC 2008) Centre for Power Transmission and Motion Control University of Bath, UK, pp. 393-403.
- 2 Linjama, M., Hopponen, V., Ikonen, A., Rintamäki, P., Vilenius, M. & Pietola, M. 2009. **Design and implementation of digital hydraulic synchronization and force control system.** The 11th Scandinavian International Conference on Fluid Power SICFP'09, Linköping, Sweden, June 2-4 2009, 13 p.
- 3 Linjama, M. & Vilenius, M. 2005. **Improved digital hydraulic tracking control of water hydraulic cylinder drive.** International Journal of Fluid Power, Vol. 6, No. 1, pp. 29-39.
- 4 Koivula, T., Ellman A. & Vilenius, M. **Cavitation behaviour of hydraulic orifices and valves.** SAE 1998 Transactions, Journal of Commercial Vehicles, Section 2, Society of Automotive Engineers, Warrendale PA, USA, pp. 387-394.
- 5 Linjama, M., Tamminen, P., Andersson, B. & Vilenius, M. 2005. **Performance of the Valvistor with digital hydraulic pilot control.** The Ninth Scandinavian International Conference on Fluid Power, June 1.-3., Linköping, Sweden, 14 p. (CD-ROM)
- 6 Hyöty, I. 2012. **Commercial high flow on/off valves for digital hydraulics.** To be published in Proceedings of the 5<sup>th</sup> Workshop on Digital Fluid Power, Oct. 24-25, 2012, Tampere, Finland.
- 7 Puumala, V. 2012. **Nopea neulaventtiili digitaalihydrauliikkaan.** M. Sc. Thesis, Tampere University of Technology, Tampere, Finland. 71 p. (in Finnish)

## SIMULATIONS WITH FAULT-TOLERANT CONTROLLER SOFTWARE OF A DIGITAL VALVE

Mikko Huova, Miikka Ketonen, Petr Alexeev\*, Pontus Boström\*, Matti Linjama,  
Marina Waldén\*, Kaisa Sere\*

Tampere University of Technology  
Department of Intelligent Hydraulics and Automation  
P.O.Box 589, 33101 Tampere, Finland

E-mail: mikko.huova@tut.fi

\* Åbo Akademi University, Turku Centre for Computer Science  
Joukahaisenkatu 3-5, 20520, Turku, Finland

E-mail: alexeev.petr@abo.fi

### ABSTRACT

Model-based design approach is widely used to optimize controllers of distributed digital valve systems, leading to controllers simultaneously minimizing power consumption and tracking error. According to this approach an optimal controller (OC) is designed by comprehensive modelling of the relationship between parallel connected on/off-valves and the cylinder actuator in steady-state conditions. Unfortunately this relationship is highly non-linear. The design complexity of the OC is high. For this reason existing verification tools do not allow ensuring absence of design errors in this controller. These errors can cause incorrect valve control signal or result in absence of this signal leading to potentially hazardous physical processes in the hydraulic system. This requires designing the controller as a fault tolerant safety-critical hard real-time system. It is important to ensure that the system will work in a reasonable manner despite of possible design errors in the OC. This paper presents a method to resolve the problem by introducing an acceptance test (AT) to verify output signals of the OC. A safe controller (SC) – a simplified version of the OC for which the design can be verified is proposed. Control signal from SC is submitted to valves if AT detects incorrect output signals of OC. Simulation study shows that the SC gives good enough control performance even though the control resolution is not as good as with the OC.

**KEYWORDS:** Digital valve control, Real-time, Controller development, Safety critical control, Fault-tolerance, Preemptive scheduling

### 1. INTRODUCTION

Fault tolerant operation of digital valve system is studied by Siivonen et al. in [1] and [2]. However, the analysis of the fault-tolerance has been so far restricted to the valve faults. This paper concentrates on fault-tolerant architecture of the controller of a digital

valve. The goal is to develop methods which allow fault tolerant operation of the controller even if a runtime error occurs in the controller or it overruns its deadline. Fault-tolerance is achieved by having two redundant controllers and careful design of the real-time scheduling scheme of the controller software. The idea is to utilize an optimal controller and a separate safe controller. The optimal controller is complex and results in the best possible control accuracy, but may lead to erroneous functionality because of possible programming defects. The erroneous functionality might include hazardous valve command signals or even hang ups of the algorithm. The other controller is simple and considered safe. It should always lead to at least suboptimal valve command signals and its correct operation can be verified by utilizing formal methods.

### 1.1. Digital valve control

Figure 1 shows a typical distributed digital valve setup. It consists of four digital flow control units (DFCUs). A DFCU is comprised of several parallel connected on/off-valves, which are controlled to achieve a number of unique flow rates. There are different ways to control an actuator using the distributed digital valve. Following list presents examples of control methods that can be utilized:

1. Control of opening of the DFCUs proportional to the user input.
2. Control of flow rates of the DFCUs proportional to the required cylinder flow rates (calculated from velocity reference).
3. Control of steady-state velocity using model-based control (square root valve model and simultaneous opening of two DFCUs).
4. Control of steady-state velocity using model-based control (generalized valve model and simultaneous opening of 2-4 DFCUs).

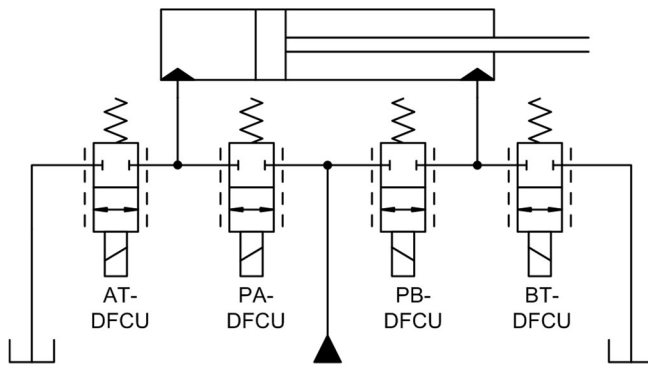


Figure 1. Distributed digital valve system

The first method is the most simplistic and does not allow for example active pressure compensation. Although simple, the method could be suited to some applications and still allows for example the pre-programming of the spool to match the area ratio of different cylinders.

The second control method allows software based pressure compensation by utilizing pressure measurement. Opening of the DFCUs are set according to the calculated flow demand of both cylinder chambers to achieve the desired velocity.

The control accuracy can be improved by calculating the resulting steady-state velocity for different DFCU opening combinations and by selecting the optimal one. The third

method relies on square root model of the on/off-valves to allow symbolic solution for the steady-state model of the system [3].

In order to improve the modelling accuracy, a generalized valve model may be utilized as in the fourth method. The generalized valve model allows the setting of the exponent (typically 0.4...0.6) according to measured pQ-data. As there is no symbolic solution to this valve-cylinder model, iterative methods are utilized to solve the steady-state velocity of the actuator for a number of different DFCU opening combinations. As all four DFCUs are under simultaneous control, the resolution is significantly improved against the three more simplistic methods [4], [5].

## 1.2. Issues in development of safety critical controllers

Controllers of digital hydraulics systems are implemented by software (firmware) of specialised computing devices, e.g., an embedded PC. Since the controller handles potentially dangerous physical processes in hydraulics, this controller has to be considered as safety-critical hard real-time system. For this reason and because of a high design complexity of a controller, modern design tools are used for the development of the controller's software. Unfortunately verification process of complex controllers used in digital hydraulics becomes very time consuming if it is even possible at all. State-of-the art verification tools can effectively be used to check correctness of small and relatively simple components and ensure their reliability and safety. In practice it is therefore more efficient to ensure safety of digital hydraulics systems by establishing fault-tolerance to possible design faults in their software.

Different software faults, specific for controllers and their influence on hydraulics, are described below.

### 1.2.1. *Incorrect execution results*

If the result of the termination of the control software is wrong, the result is said to be incorrect or inconsistent, in particularly:

- Plus/minus infinities and not-numbers (NaNs). These results cannot be converted into valid output values of DFCUs (on/off valves).
- Imprecise results are correct numbers of the correct type, but applying these results to actuators of the digital hydraulics system is unsafe. For example, imprecise results may go beyond the permitted range of output values.

### 1.2.2. *Deadline misses*

A deadline miss is the situation when the duration of the execution time of software module exceeds the specified time limit (deadline). The controller has to update output values of all DFCUs periodically with minimal timing jitter. Maximum allowed jitter can be defined in requirements by the deadline value. The behaviour of the hydraulics system can be unpredictable if controller will not keep this deadline.

### 1.2.3. Run-time exceptions

An exception is a run-time error (e.g., division by zero, overflow and underflow) that occurred during execution of software and forces its abnormal termination. The obvious consequence of an exception in controller is unavailability to update output signals of DFCUs.

## 2. SAFE ARCHITECTURE OF A MULTI-THREAD CONTROL ALGORITHM

### 2.1. Overall description of the architecture

A controller for digital hydraulic system can be considered as non-linear digital control system, which consists of: plant (hydraulics), sensors, actuators and computing device with software. A generalized architecture of the example of such control system used in this paper as a case study is presented in Figure 2.

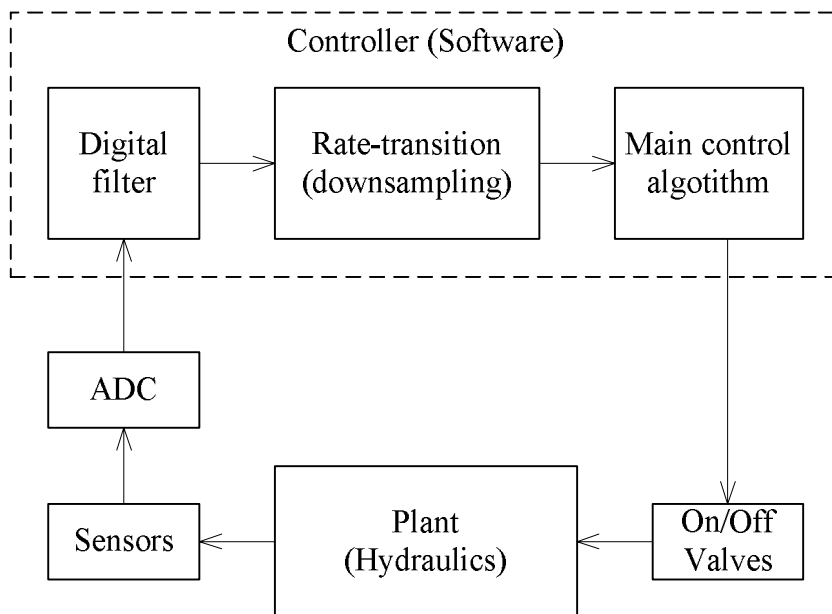


Figure 2. Generalized architecture of the proposed control system. The sampling frequency of ADC is higher than the sampling frequency of on/off valves (DFCUs) output.

## 2.2. The approach of the safe architecture

As mentioned in Subsection 1.2, the software of the optimal controller cannot be guaranteed to be completely reliable (error-free) because of its high complexity. In order to ensure safety of the system software design errors should be mitigated or masked. Effective way of masking such errors is a recovery blocks (RcB) structure [6, 7]. RcB provides fault-tolerance based on redundancy of software design. In the simplest form RcB consists of:

- *Primary* version of the software function which provides accurate results but can contain errors. For the case of digital hydraulics this primary version is represented by the *optimal controller* (OC) – an optimized but potentially unsafe version of the main control algorithm.
- One or more *alternative* versions of the same software function which provides results of the same purpose but may be with less accuracy. For the case of digital hydraulics this primary version is represented by the *safe controller* (SC) – a simplified version of OC.
- *Acceptance test* (AT) which allows analysing results of primary or alternative versions of software function to define if these results are correct. So, the output of AT is binary: “correct” and “not correct”.

The general algorithm of RcB for the case of just one SC is the following:

1. Execute OC and perform AT on its results  $u_{optimal}$ . Return  $u_{optimal}$  if the result of AT is “correct” otherwise proceed to the step 2.
2. Execute SC and perform AT on its results  $u_{safe}$ . Return  $u_{safe}$  if the result of AT is “correct” otherwise RcB fails.

For the case of digital hydraulics, the simplicity of SC allows ensuring its reliability confirmed it by various verification tools suitable for Simulink models, e.g. [9]. In particular, we can assume that no fault, described in Subsection 1.2, can occur during the execution of SC. For this reason there is no need to execute AT on results of SC. Note also that it is assumed that the RcB never fails in this approach.

The disadvantage of this structure is low precision of  $u_{safe}$  that sometimes cannot prevent unwanted processes in the hydraulics, e.g., cavitation. However,  $u_{safe}$  ensures safety of the system.

Execution results  $u_{safe}$  and  $u_{optimal}$  are comparable, so the basic algorithm for the AT can be constructed as a comparison with a threshold of the absolute value of the subtraction  $u_{safe}$  and  $u_{optimal}$ . The implementation of the RcB approach to the controller is presented in Figure 3. It is obvious that AT will require as input parameters both  $u_{safe}$  and  $u_{optimal}$ .

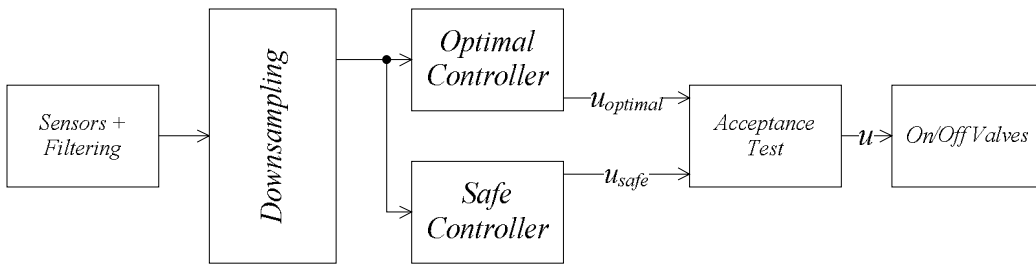


Figure 3. Implementation of the recovery blocks approach for the controller.

The algorithm of RCB requires OC to be executed, so the worst-case execution time (WCET) [8] of RCB strongly depends on WCET of OC. In practice a deadline miss of OC may force RCB to miss its deadline too. For this reason the approach of RCB should be adapted to meet real-time requirements.

Modern real-time software is implemented by utilising pre-emptive scheduling schemes: the whole software is decomposed into several tasks with different priorities. Each task execution is called *tasks instance* or *job*. The event of start of a job called *release*. If high-priority job is released during the execution of low-priority job, this low-priority job suspends while high-priority job starts and executes until its termination. The low-priority job can continue its execution afterwards. This process is called *pre-emption*. If priorities of tasks do not change during execution, this scheduling scheme called *static*. The scheduling scheme is called *feasible* if all tasks terminate before their deadlines.

The pre-emptive scheduling scheme can be applied for the RCB in order to prevent possible deadline misses of the OC. The task decomposition will be the following: low-priority task for OC and high-priority task for SC and AT. This approach allows pre-empting OC in case of its deadline miss by SC and AT. By this reason controller will be able to submit correct output data to valves without missing deadline even in case of fault of OC.

This tasks decomposition implies special precedence constraint: both OC and SC should be terminated before correspondent AT can be started. This constraint can be met by different solutions, for example by additional decomposition of high-priority task into the following two tasks: the first task for the SC and the second task for the AT. The second task needs to be released with some offset providing a time slot for SC and OC to ensure precedence constraint.

For periodical task set the offset for the second task is not required because this task can perform AT for execution results of OC and SC from the previous period. For tasks with the same period and deadline, e.g. AT, OC and SC, precedence constraints can be ensured by arranging priorities by the following rule: higher priority means earlier execution.

The proposed task decomposition is feasible for both periodical and non-periodical task sets. The controller has to acquire signals from sensors and to submit signals to valves periodically. This implies that its software should be decomposed into several periodical tasks with different but fixed priorities (static scheduling). In this case the whole software of the controller was modeled as multi-rate Simulink diagram where each rate corresponds to specific task.

There are different static scheduling schemes for periodical task sets. Most of these schemes do not take into account data transfers between tasks (define tasks as *independent*). Data transfers between tasks can be mitigated by using non-pre-emptive protocol (NPP) of data transfers. The detailed description of this protocol and its properties is presented in the Section 7.10 of [12].

Here two widely use scheduling schemes for periodical task sets are considered: (RM) [10] or deadline-monotonic (DM) [11]. The RM algorithm arranges priorities according the following rule: higher priorities are assigned to tasks with shortest periods. Let  $N$  be the total number of tasks,  $C_i$  and  $T_i$  be the WCET and period of task number  $i$  respectively. According to [10] RM scheduling is feasible if tasks deadlines are equal to their periods and the condition  $\sum_{i=1}^N \frac{C_i}{T_i} < N \left( 2^{\frac{1}{N}} - 1 \right)$  hold.

The DM algorithm is similar to RM, but higher priorities are assigned to tasks with shortest deadlines. This allows reducing periodical task release jitter by specifying a relative deadline less than the period for one or several tasks. The feasibility rule for DM requires using the algorithm presented in [11].

The scheduling scheme for the controller can be either RM or DM. But DM is more preferable because of possibility to reduce timing jitter for the output signal to on/off valves. This can be done by minimizing release time for the task of AT by establishing its deadline equal to WCET. The complete timing diagrams for both RM- and DM-based scheduling schemes are presented in Figure 4 and 5 respectively. Both proposed schemes presents feasible schedule and provide fault-tolerance to the OC.

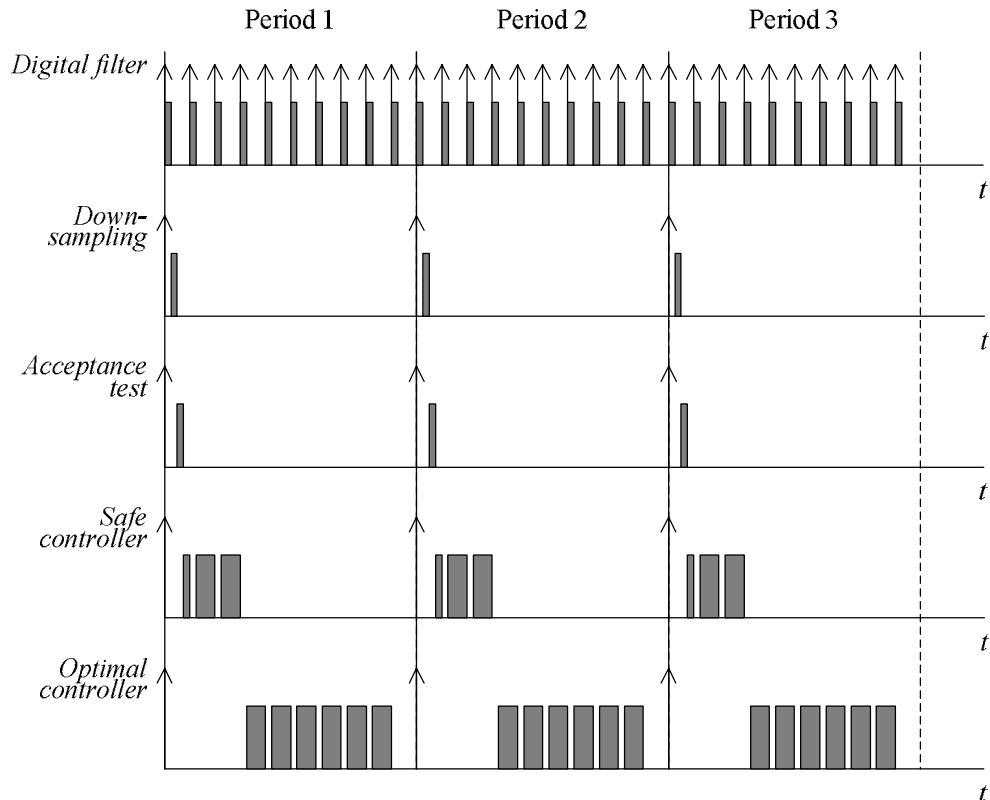


Figure 4. RM-based fault-tolerant scheduling scheme.



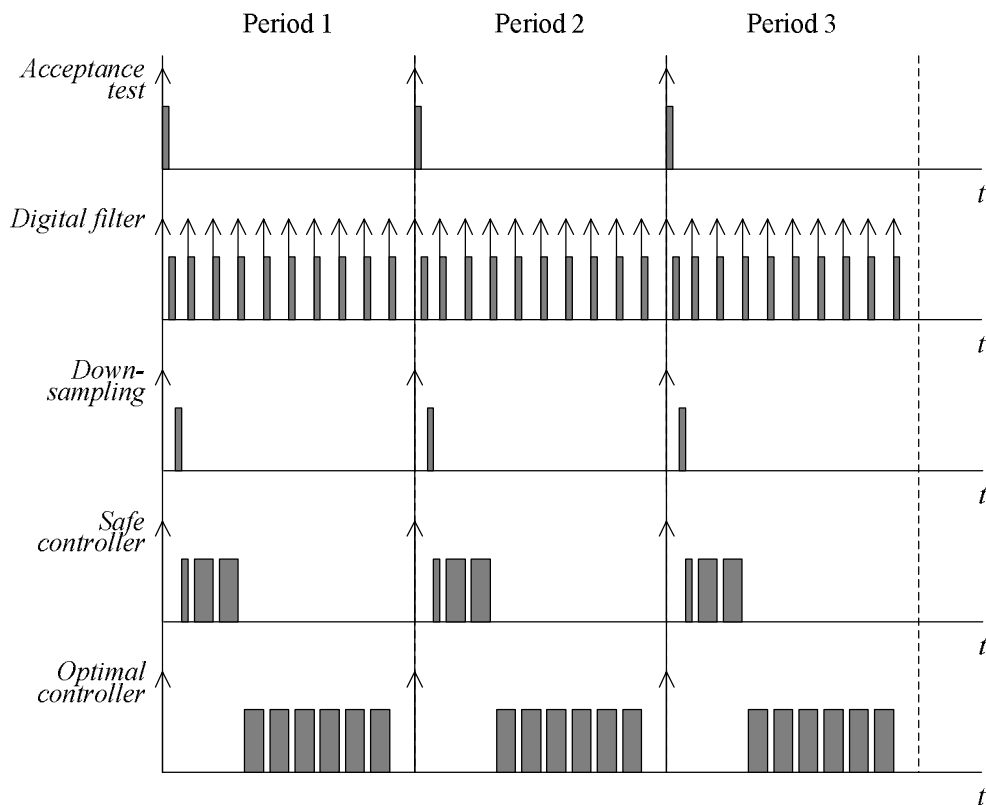


Figure 5. DM-based fault-tolerant scheduling scheme.

### 3. DESIGN OF FAULT-TOLERANT CONTROLLER FOR DIGITAL VALVE SYSTEM

#### 3.1. Model-based optimal controller

The model-based optimal controller (control method 4) is developed in [5] for energy efficient control of a four-DFCU valve setup. The controller is based on four different subsystems, presented below.

Control mode is selected according to measured load conditions and supply pressure. Possible control modes include inflow-outflow modes as well as differential control modes which enable the improvement of energy efficiency. Chamber pressure references are selected so that smooth switching between the control modes is possible. Search space selects a group of DFCU opening combination candidates which are promising based on current load force and velocity reference. Steady-state velocity and chamber pressures are solved for these candidates and a cost function based optimization scheme is utilized to find the best DFCU command signals.

### 3.2. Simplified safe controller

In order to simplify the safe controller (Figure 6) considerably when compared to the model-based controller, the flow control based algorithm is utilized (control method 2).

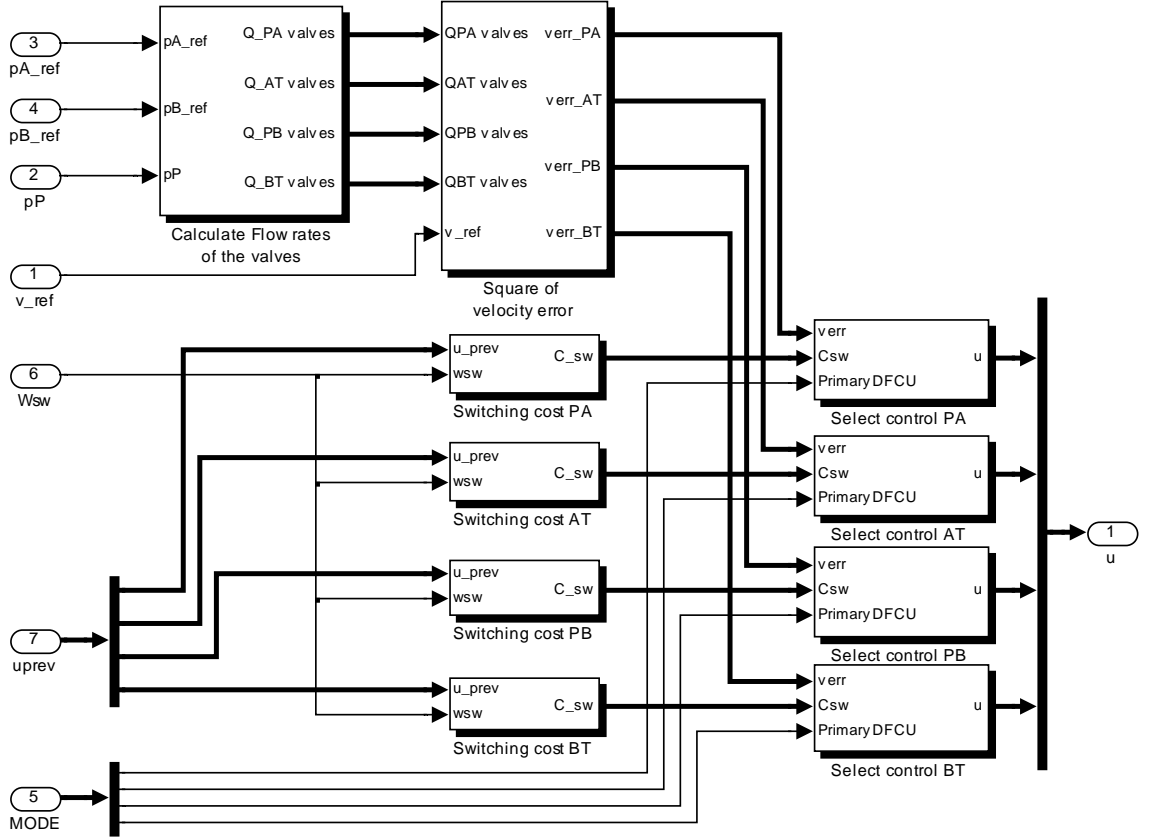


Figure 6. The Simulink implementation of the safe controller.

Measured and low pass filtered supply pressure and chamber pressure references are used in calculation of the flow rate of each valve. All unique, non-zero flow rates of the DFCUs are calculated simply utilizing matrix multiplication (1).

$$\mathbf{Q}_{PA} = \mathbf{Q}_{PA\_valves} \times \mathbf{ctrl\_mtrx} \quad (1)$$

The control matrix  $\mathbf{ctrl\_mtrx}$  is a  $[N_{valves}, 2 N_{valves}-1]$  sized matrix defining each unique opening combination of the DFCU. The calculated flow rate of each valve is defined by the row vector  $\mathbf{Q}_{PA\_valves}$ .

As the flow rates of the DFCU opening combinations are calculated it is straight forward to calculate corresponding velocity errors. Another aspect that should be minimized by the optimization scheme is the number of valve switchings. Cost term for switching is calculated for each DFCU opening combination. Equation 2 is utilized for calculation of the switching cost term:

$$\mathbf{C}_{sw} = w_{sw} \times \mathbf{Q}_N \times |\mathbf{u}_{prev} \times \mathbf{J}_{1,2N_{valves}-1} - \mathbf{ctrl\_mtrx}| \quad (2)$$

, where  $w_{sw}$  is the weight term,  $\mathbf{Q}_N$  is  $N_{valves}$  sized row vector defining the nominal flow rate of the valves,  $\mathbf{u}_{prev}$  is  $N_{valves}$  sized column vector defining the previous command

signal of a DFCU,  $J_{1,2Nvalves-1}$  is a row vector of ones required to expand the previous command signal for subtraction.

The selection of the control signal for each DFCU is trivial. Switching cost related to each possible control signal candidate is summed to the square of the velocity error and the control signal with smallest cost function value is fed to the valves. Mode information is utilized to set DFCU command signal to 0 for each DFCU that is not utilized by the mode.

### 3.3. Design of acceptance test for the controllers

An acceptance test is required for real time decision of whether the command signal of the model-based controller should be trusted and utilized as valve control signal. In case the command signal of the model-based controller cannot be trusted, the command signal of the safe controller is utilized instead.

The acceptance test can be designed in various ways and it is not trivial to select the best one. The design of the acceptance test can be started by looking for control signals that are hazardous at any times. E.g. the opening of solely tank side valves for both cylinder chambers does not make sense in typical velocity control with a zero-pressure tank line. For any operating condition there is a multitude of control signal candidates that are not feasible at all and finding these sets of control signals is difficult.

Another approach is to find a range of reasonable control signals and check whether the command signal of the model-based controller falls inside the range. One option is to compare the command signals of the safe controller and optimal controller and utilize the command signal of the model-based controller whenever the two command signals are similar enough. The command signals cannot be compared directly as the model-based controller can utilize crossflow while the safe controller cannot. However, the flow rates to the cylinder chambers should be similar and these can be calculated by utilizing the valve model. In order to improve the user interface and setting of the parameters, calculated velocities are compared instead of the flow rates. Figure 7 presents an upper level view on the algorithm.

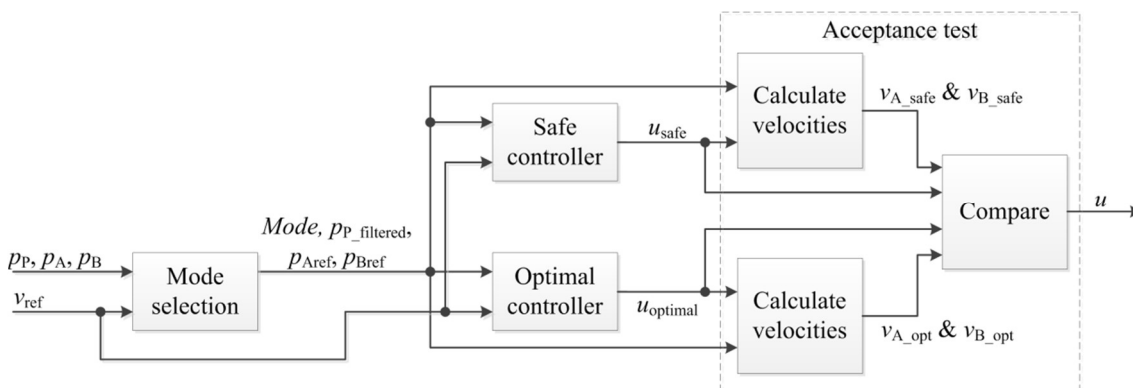


Figure 7. Upper level view on the controller architecture

Following comparison of the calculated velocities is carried out. The optimal controller is interpreted as faulty operating when at least one of the conditions hold:

1.  $\left| \frac{v_{A_{opt}} + v_{B_{opt}}}{2} - \frac{v_{A_{safe}} + v_{B_{safe}}}{2} \right| > v_{tres}$
2.  $\left| v_{A_{opt}} - v_{A_{safe}} \right| > 2 * v_{tres}$
3.  $\left| v_{B_{opt}} - v_{B_{safe}} \right| > 2 * v_{tres}$
4.  $v_{A_{safe}} = 0 \text{ AND } (v_{A_{opt}} \neq 0 \text{ OR } v_{B_{opt}} \neq 0)$
5.  $v_{A_{safe}} > 0 \text{ AND } \min(v_{A_{opt}}, v_{B_{opt}}) < -\frac{1}{2} * v_{tres}$
6.  $v_{A_{safe}} < 0 \text{ AND } \max(v_{A_{opt}}, v_{B_{opt}}) > \frac{1}{2} * v_{tres}$

The first condition is true if the average calculated velocities of the two cylinder sides differ more than the user-set threshold value. The second condition hold if the calculated velocity error of A-side differs more than two times the threshold value. Condition three is the same for B-side. Condition four holds if the safe controller outputs stop command while the optimal controller does not. Condition five holds if the output of the optimal controller results in significantly negative calculated velocity for either side while the safe controller results in positive velocity. Condition six equals condition five into opposite direction.

The first condition is the basis of the acceptance test. Conditions two and three take care of situations, where the average velocity of the optimal controller is correct while the calculated velocities of both cylinder sides are far from the correct value. Condition four takes care of situation, where the optimal controller would continue to drive the system with small velocity when the system should be stopped. Conditions five and six take care of situations, where the calculated velocity of the optimal controller has wrong direction. It is worth to note that small velocity to wrong direction is considered acceptable as this occurs from time to time close to zero velocity.

## 4. SIMULATION STUDY ON DIGITAL VALVE CONTROL

### 4.1. Simulation model

The system studied is presented in Figure 8. Simulation model is based on a boom mockup which is sized to model dynamics of a typical mobile boom. Big inertia of the system results in low natural frequency of 3-5 Hz when fully loaded.

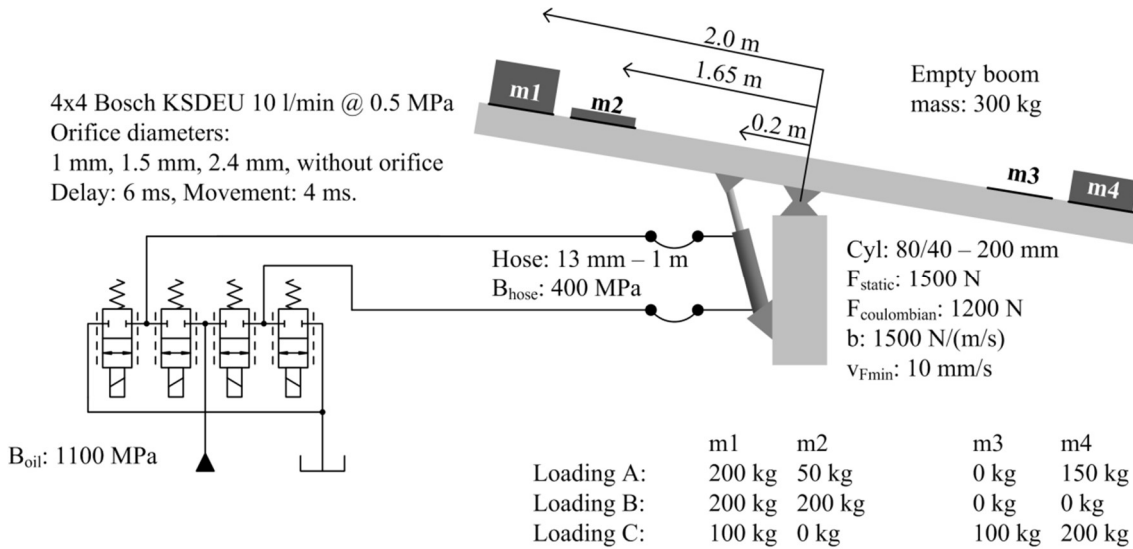


Figure 8. Simulated system and its parameters

### 4.2. Simulations with optimal controller

The optimal controller is presented thoroughly in [5] and it is utilized in this study with slightly altered controller parameters, which are listed in table 1.

Table 1. Controller parameters

Controller sample time	12 ms	Input filter sample time	2 ms
Position controller gain	3	Velocity feed forward gain	0.74
Start treshold	4 mm/s	Stop treshold	3 mm/s
Minimum pressure	3 MPa	Maximum pressure	20 MPa
Nominal pressure difference	1.5 MPa	Minimum pressure difference	0.5 MPa
Corner frequency of load force filter	8 rad/s	Corner frequency of supply pressure filter	40 rad/s
Force hysteresis	5 kN	Power treshold	100 W
Earn time	500 ms	Mode switching delay	120 ms
Supply pressure rate	50 MPa/s	Weight for pressure error	2e-16
Weight for switching	0.03	Weight for power loss	4e-7
Acceptance test velocity treshold	20 mm/s	Minimum time period of safe controller	200 ms

Most of the controller parameters remain the same as in [5]. The valve block simulated is different to the valve block utilized in [5]. Therefore some parameters have been altered to achieve optimal control performance. Controller sample time is set according to the valve response time. Start and stop thresholds are increased slightly to avoid

repetitive starting and stopping especially with the safe controller algorithm. Supply pressure rate is increased to match the rate of the current supply system in the actual boom mock up. Cost function weight for power loss is decreased to improve low velocity control resolution. The only parameter that is utilized by the safe controller (apart from the common mode selection parameters) is the weight term for switching, which is slightly reduced to achieve better control resolution. Judging by the simulations, the switching weight of the safe controller needs to be multiplied by a factor of four to reach similar activity of the valves as with the optimal controller.

The velocity threshold related to the acceptance test is set to 20 mm/s. It is defined as smallest value which does not result in discarding of the optimal controller output, when there is no actual fault in the operation. It is beneficial to require certain time period of correct operation of the optimal controller before the output of the optimal controller is utilized after a malfunction. In this case the parameter is set to 200 ms to avoid repetitive switching between the optimal and the safe controller.

Three different position trajectories are tested. The references include single extending movement and single retracting movement, which last 1.25 s each. The trajectory is a fifth order polynomial and the amplitudes of the movements are 12 mm, 30 mm and 70 mm, resulting in maximum velocity references of 18 mm/s, 45 mm/s and 105 mm/s.

#### *4.2.1. Control performance of the optimal and the safe controller*

Figures 9, 11 and 13 present simulated trajectories driven with the optimal controller. Medium size trajectory is presented, which maximum velocity is roughly half of the maximum velocity of the valve-cylinder system studied. The system is simulated with variable supply pressure and full mode selection logic. Therefore, the cylinder is driven in inflow-outflow mode to both moving directions: extending (IOe) and retracting (IOr) as well as in differential connection (De, Dr). Optimal controller utilizes crossflow in order to improve the control resolution, which can be seen as simultaneously active supply side and tank side DFCUs. Figures 10, 12 and 14 present the controllability utilizing the safe controller for comparison. Exactly same trajectory and loadings are driven as with the optimal controller.

Figures 9 and 10 present comparison of the performance of the two controllers driving the system with loading A. Most significant difference can be noted at slow velocities, where the control resolution of the optimal controller is considerably more accurate. The coarse resolution of the safe controller yields oscillations when the motion is stopped. Even though the control performance of the safe controller is not as good as the optimal controller, a lot of the functionality is still achieved by utilizing such simple control scheme: velocity tracking is acceptable and chamber pressure tracking is as good as with the optimal controller.

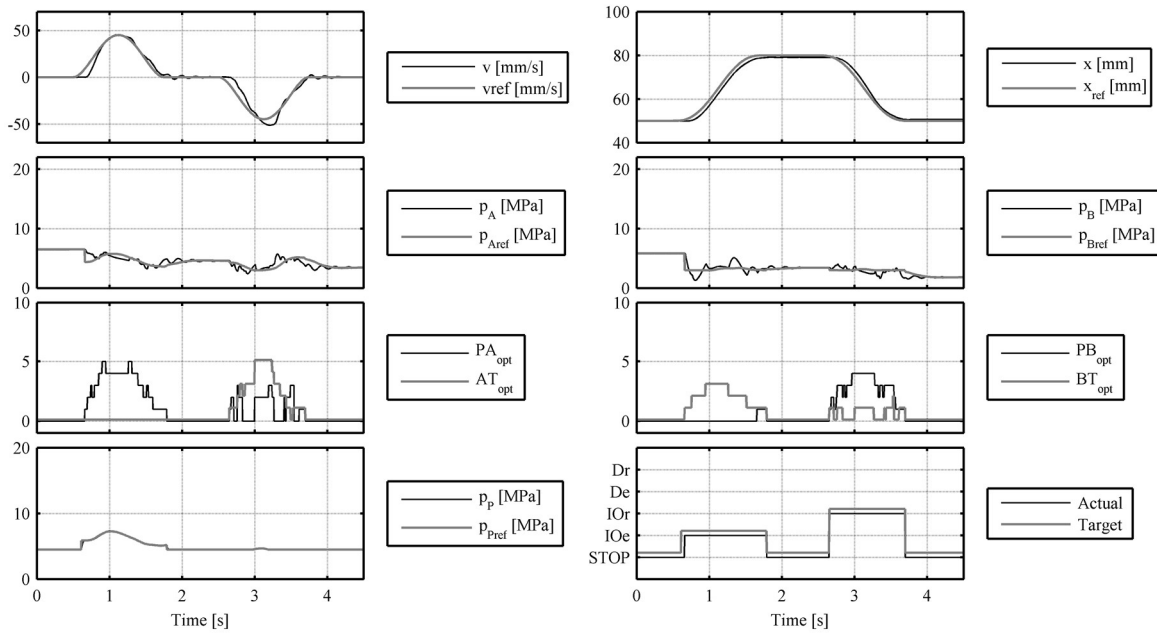


Figure 9. Optimal controller, medium size trajectory, loading A.

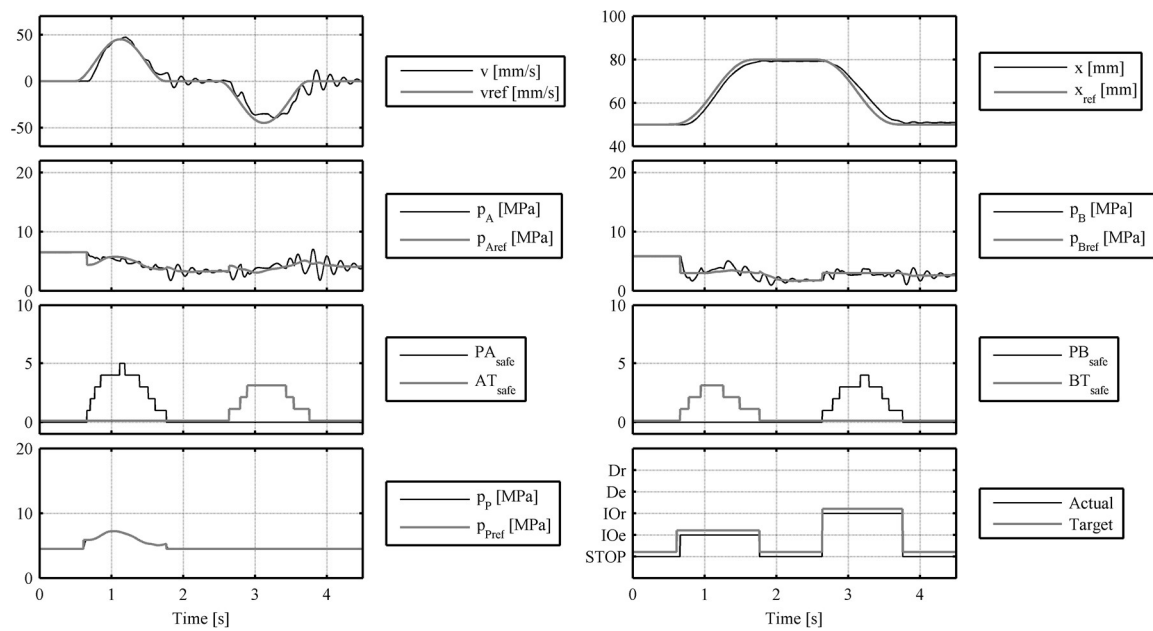


Figure 10. Safe controller, medium size trajectory, loading A

Figures 11 and 12 compare the two control schemes when driving restricting loading B. Although both controller algorithms generate small oscillations during stopping of the motion, the velocity control of the optimal controller is slightly smoother than the operation of the safe controller. The optimal controller utilizes cross flow for a short time period only, as the high supply pressure would lead to relatively big energy losses.

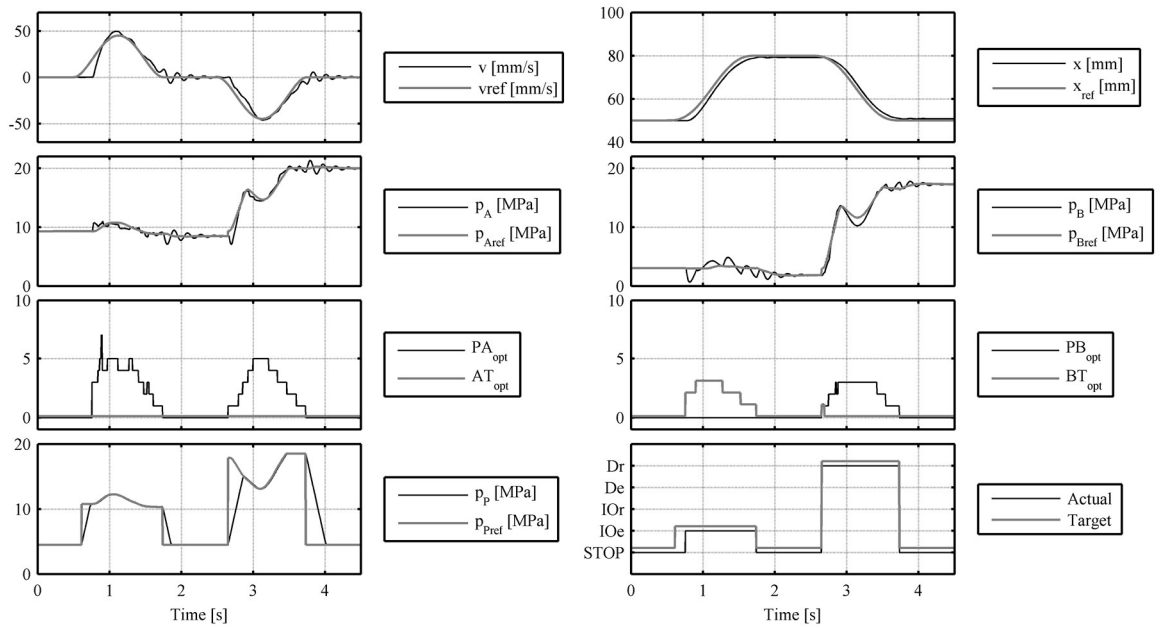


Figure 11. Optimal controller, medium size trajectory, loading B

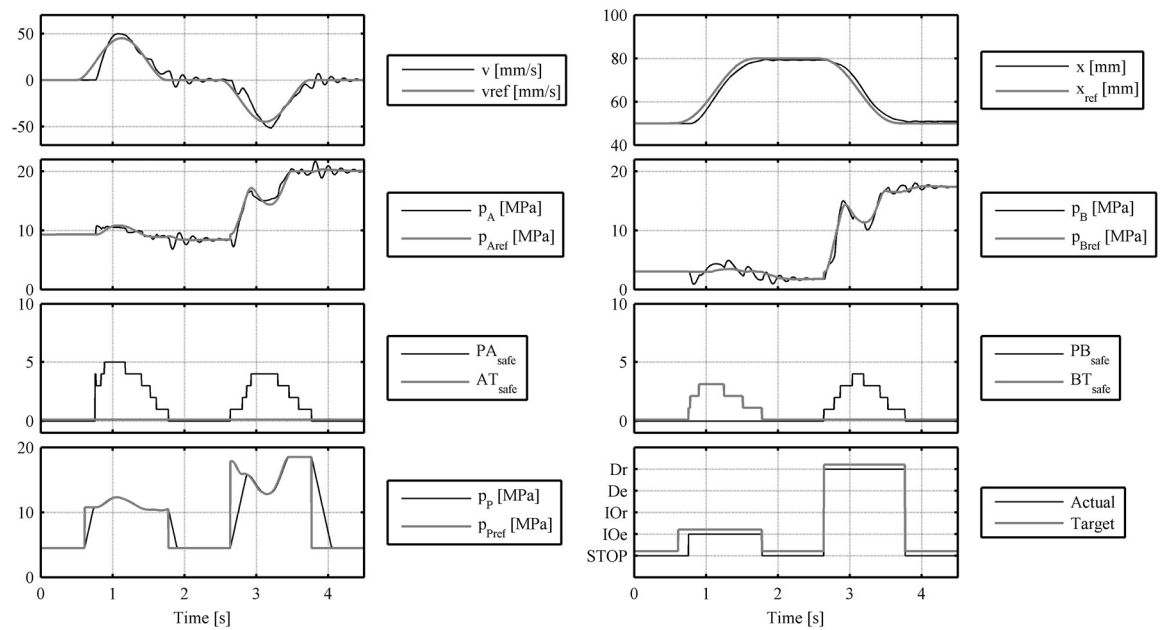


Figure 12. Safe controller, medium size trajectory, loading B

Figures 13 and 14 present the results with overrunning loading C. The difference between the performance of the two controllers is significant: the slow velocity resolution of the optimal controller is better because of crossflow and the velocity trajectory is also smoother resulting from the optimization of the steady-state velocity of the system.



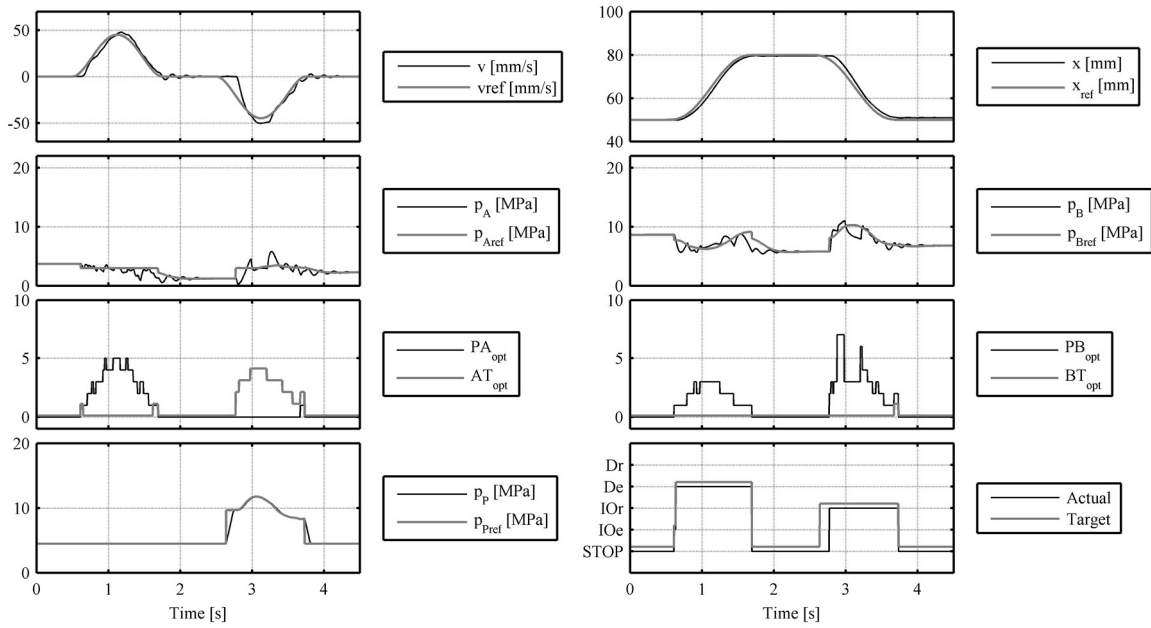


Figure 13. Optimal controller, medium size trajectory, loading C

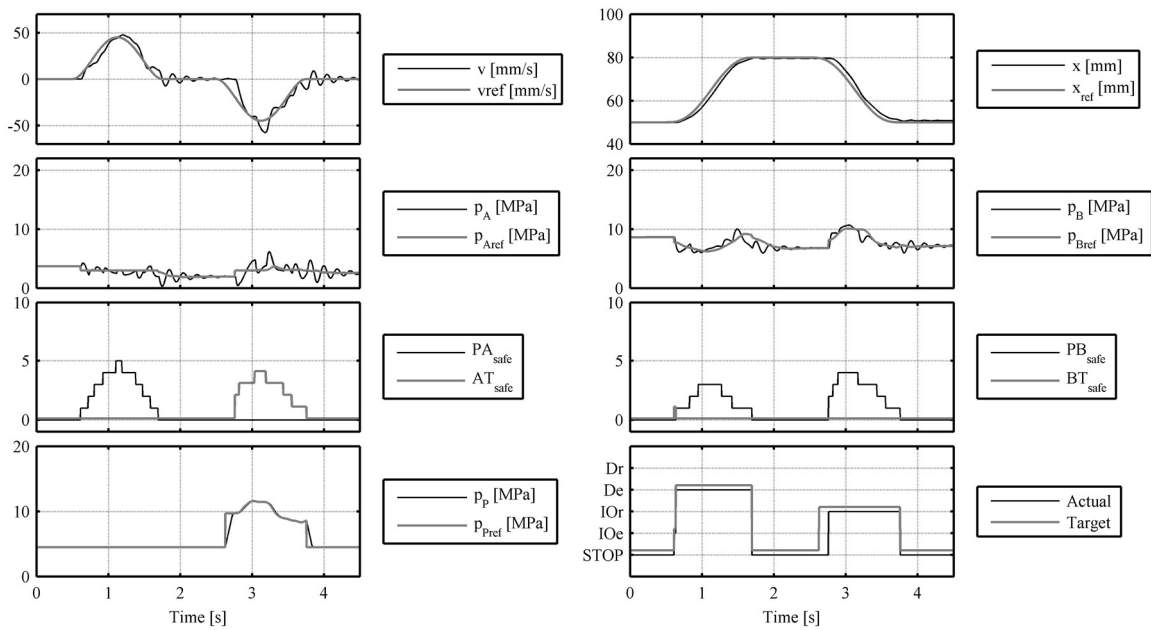


Figure 14. Safe controller, medium size trajectory, loading C

#### 4.2.2. Simulations with fault tolerant control architecture

Figure 15 presents a large trajectory driven with the optimal controller. Runtime error of the controller is simulated by virtually hanging up the operation of the controller at 1 s. The output of the controller is held from that point on. Both the output of the optimal controller and the output of the safe controller are presented. Fault detection is inactivated and the hazardous operation of the optimal controller results in fast extending motion until the cylinder end is reached.

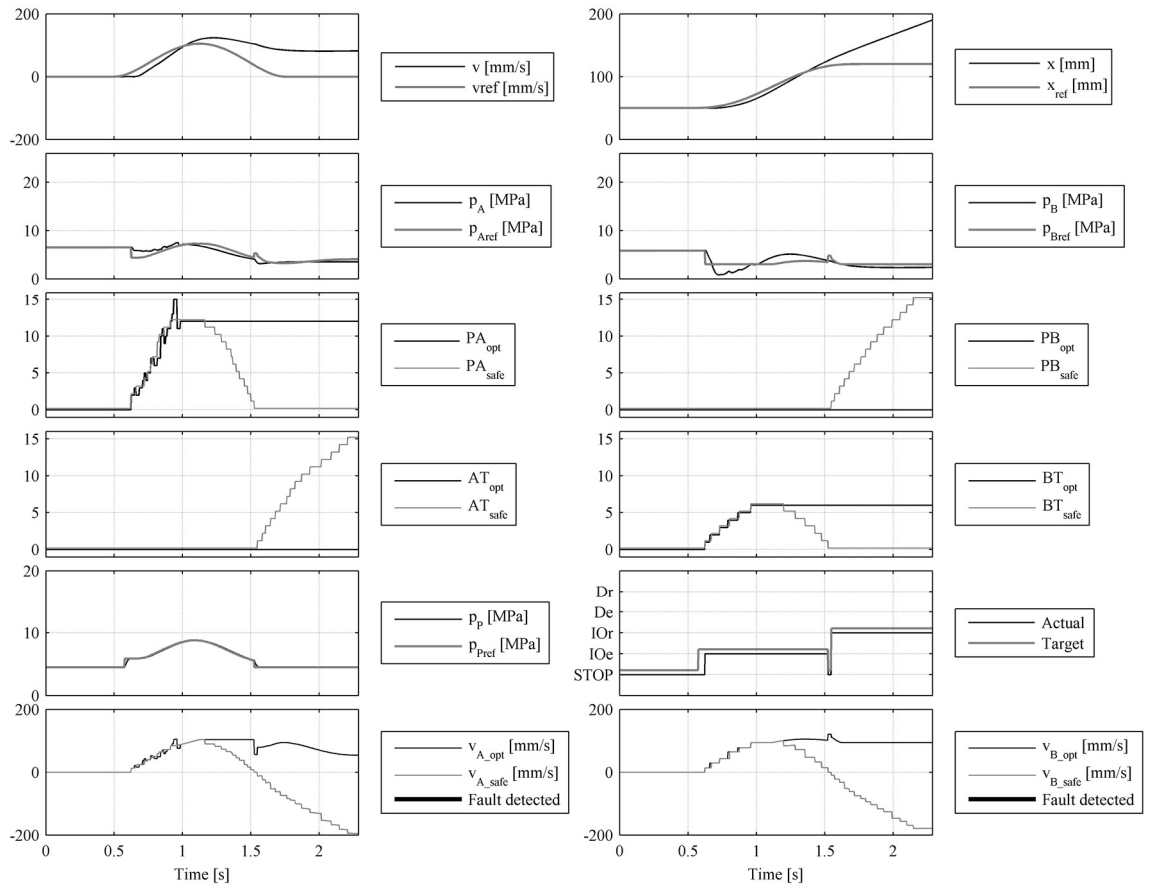


Figure 15. Large trajectory, loading A. Fault detection inactivated.

Figure 16 presents the same trajectory with the defect in the optimal controller. The operation of the optimal controller hangs up at 1 s and revives at 3 s. The output of the optimal controller is fed to the valves until the calculated velocity resulting from the outputs of the two controllers differ sufficiently, after which the output of the safe controller is fed to the valves. The calculated velocities of the two controllers are presented in the figure as well as the time period, when the faulty action of the optimal controller is detected and the output of the safe controller is utilized. As the operation of the optimal controller is again fully functioning at 3 s, the output of the safe controller is utilized until 3.2 s, which is because of the user set time period parameter.

Figure 17 presents the small trajectory with the identical fault. The fault is detected when the output of the safe controller is zero while the output of the optimal controller is nonzero. Even if the faulty action of the optimal controller is not detected before the stopping of the motion, there is no big position error or other hazardous action. The only deterioration of the control performance can be seen as more abrupt stopping of the motion. The optimal controller hangs up with DFCU state 2 for both cylinder sides and the motion is stopped stepwise by closing the DFCUs resulting in some oscillations.

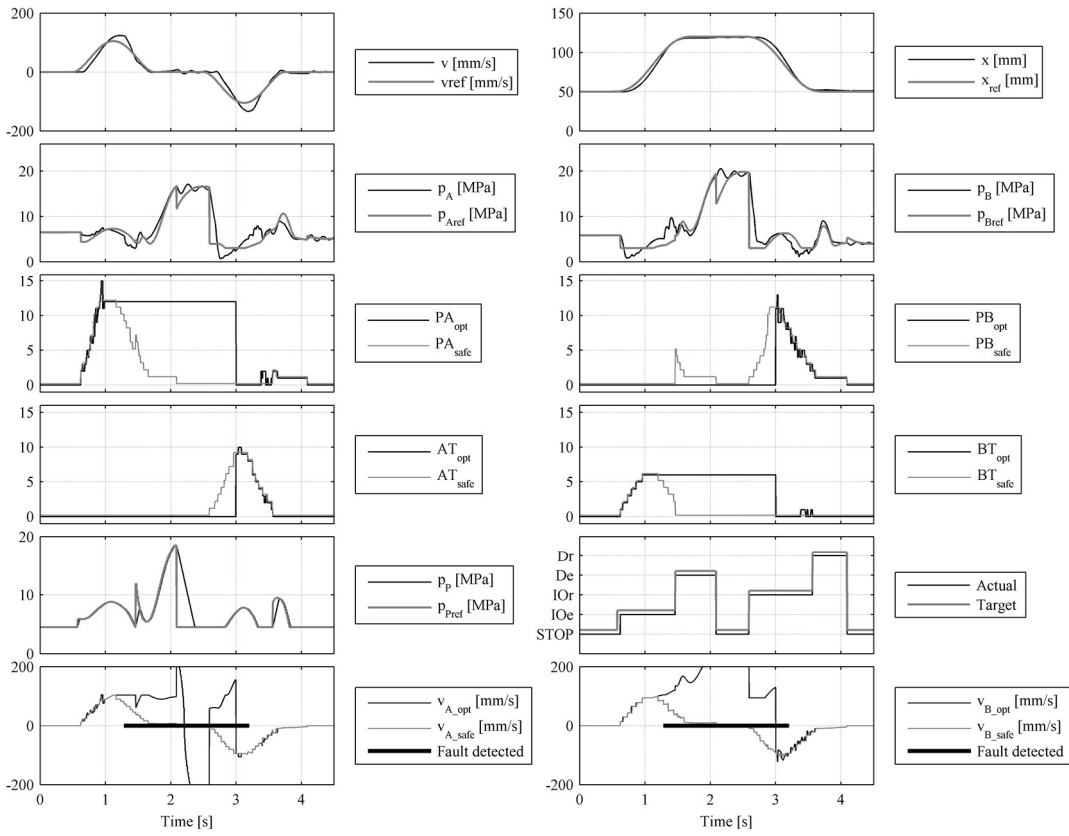


Figure 16. Large trajectory, loading A. Fault detection active.

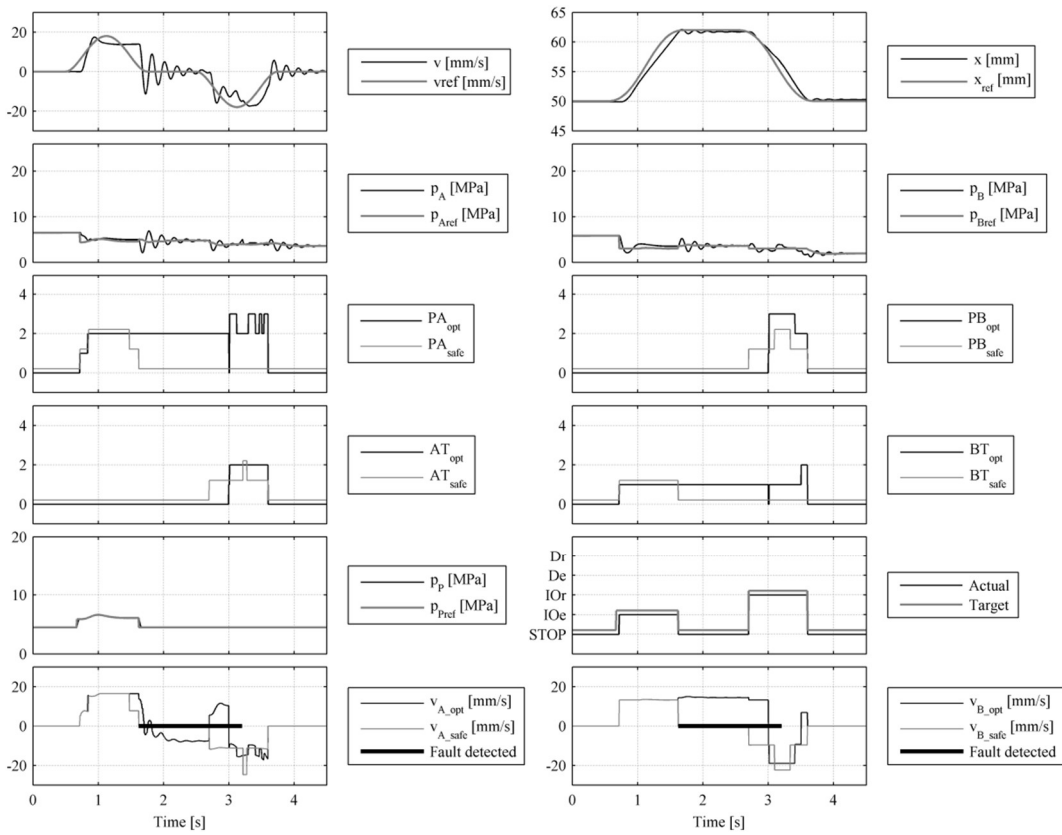


Figure 17. Small trajectory, loading A. Fault detection active.

## 5. CONCLUSION AND FUTURE WORK

The simulations of the safe controller show acceptable control performance. Thus the safe controller seems to enable relatively good controllability despite its simplicity. The biggest difference in comparison to the optimal controller can be seen in small velocity resolution.

The proposed architecture of the controller, based on the recovery blocks approach, leads to safe operation of the whole system despite of possible design faults in the model of optimal controller. The acceptance test is relatively simple, but ensures that the physical valves are always driven with an acceptable control signal. The proposed architecture can mask runtime errors, erroneous results and deadline misses of the optimal controller. It should be noted that on platforms, in which all tasks run in the same memory space, memory corruption in the optimal controller can affect the safe controller.

Switching between safe controller and optimal controller during motion does not result in big stepwise changes to the valve command signals. Therefore, the system performs smoothly even if the optimal controller misses its deadline or suggests a hazardous valve control signal.

The fault-tolerant control system presented will be tested on real experimental system.

## 6. ACKNOWLEDGEMENTS

This research is funded by the Academy of Finland (Grant No. 139540) and by the DIGIHYBRID-project which is part of EFFIMA-program of the Finnish Metals and Engineering Competence Cluster, FIMECC Ltd.

## REFERENCES

- [1] Siivonen, L., Linjama, M. & Vilenius, M. 2005. Analysis of Fault Tolerance of Digital Hydraulic Valve System. Bath Workshop on Power Transmission and Motion Control, September 7-9, Bath, UK, pp. 133-146
- [2] Siivonen, L., Linjama, M., Huova, M. & Vilenius, M. 2009. Jammed on/of valve fault compensation with distributed digital valve system. *International Journal of Fluid Power*, 2, pp. 73-82
- [3] Linjama, M., Koskinen, K.T. & Vilenius, M. 2003. Accurate trajectory tracking control of water hydraulic cylinder with non-ideal on/off valves. *International Journal of Fluid Power*, 1, pp. 7-16.
- [4] Linjama, M. & Vilenius, M 2005. Improved digital hydraulic tracking control of water hydraulic cylinder drive. *International Journal of Fluid Power* , 1, pp. 29-39.
- [5] Linjama, M., Huova, M., Boström, P., Laamanen, A., Siivonen, L., Morel, L., Walden, M. & Vilenius, M. 2007. Design and implementation of energy saving digital hydraulic control system. The Tenth Scandinavian International Conference on Fluid Power, May 21-23, Tampere, Finland, pp. 341-359.
- [6] K.H. Kim and H.O. Welch. Distributed execution of recovery blocks: an approach for uniform treatment of hardware and software faults in real-time applications. *IEEE Transactions on Computers*, 38(5):626 –636, may 1989.
- [7] Nguyen, D. and Dar-Biau Liu “Recovery blocks in real-time distributed systems” *Reliability and Maintainability Symposium*, 1998. Proceedings, pp.149-154, 19-22 Jan 1998.
- [8] Reinhard Wilhelm, Jakob Engblom, Andreas Ermedahl, Niklas Holsti, Stephan Thesing, David Whalley, Guillem Bernat, Christian Ferdinand, Reinhold Heckmann, Tulika Mitra, Frank Mueller, Isabelle Puaut, Peter Puschner, Jan Staschulat, and Per Stenström. The worst-case execution time problem - overview of methods and survey of tools. *ACM Trans. Embed. Comput. Syst.*, 7(3):36:1–36:53, May 2008.
- [9] Pontus Boström. Contract-based verification of Simulink models. In *Proceedings of the 13th international conference on Formal methods and software engineering, ICFEM’11*, pages 291–306, Berlin, Heidelberg, 2011. Springer-Verlag.
- [10] C. L. Liu and James W. Layland. Scheduling algorithms for multiprogramming in a hard-real-time environment. *J. ACM*, 20(1):46–61, January 1973.
- [11] N C Audsley, A Burns, M F Richardson, and A J Wellings. Hard real-time scheduling: The deadline-monotonic approach. *Proc IEEE Workshop on RealTime Operating Systems and Software*, pages 1–6, 1991.
- [12] Giorgio C. Buttazzo. *Hard Real-Time Computing Systems*. Springer US, 2011.

## DIGITAL CONTROL OF PRESSURE IN A VESSEL

P.I. Greshnyakov, A.F. Sinyakov, D.M. Stadnick, V.N. Ilyukhin, V.Y. Sverbilov  
Samara State Aerospace University (National Research University)  
34 Moskovskoye shosse, Samara 443086, Russia  
pavel.ssau@gmail.com, blues87@yandex.ru, v.sverbilov@mail.ru

### ABSTRACT

In the paper, software for digital control of gas pressure in a vessel is developed to increase process quality and accuracy. Operating principal is based on stepped variation of a throttle area at the vessel output (or/and input) using pulse code modulation. The control device is made as set of parallel on-off valves. Flow areas of the valves can be presented by binary dependencies of the smallest cross-section or by the Fibonacci series. The number of valves depends on control process accuracy.

During transient it often occurs that one group of valves is closing when the other is opening simultaneously. Such transients are accompanied with noise and high pressure fluctuations. To avoid such phenomena a control algorithm is developed to stabilize pressure by means of switching one or more additional valves. Simulation results show a good correlation with experimentally obtained data proving efficiency of the proposed control strategy to providing high accuracy and proper quality of transients

**KEYWORDS:** Digital fluid power, fuel tank, pressure control

### 1. INTRODUCTION

In fuel propulsion systems of power plants operating at different pressures of the environment, you need a boost of fuel tanks to ensure the strength of thin-walled design of the tank and reliable operation of fuel pumps. The main purpose of the system is to maintain the desired boost pressure in the tank with high accuracy throughout the flow range of the working environment for all operating conditions.

Traditionally, these systems use proportional control valves. Their disadvantage is the substantial dependence of the control pressure from the aerodynamic lift force acting on the valve poppet. At higher accuracy of such systems it is often occurred unstable behavior of the valve, oscillations of the spool, accompanied by impacts on the valve seat. This leads to wear of contacting surfaces and the loss of the valve tightness. The need for compensation of the lift force acting on the valve in a wide range of flow rates complicates the process of designing a controller.

The task is greatly simplified by using digital control system instead of analog technology [1, 2]. The main idea of the digital flow control is to sample stream through a parallel connection of 2/2 valves with different flow areas. Cross-sectional area of individual valves forms a numerical sequence of binary code {1, 2, 4, 8, 16...}. The required flow rate is given by the switching one or more parallel valves. In the digital controller it is possible to replace algorithmically the faulty valve by the other operational with the larger cross-sectional area (or an equivalent combination of open valves), which allows for continued operation of the system with impaired head flow response which has larger discretion.

Using the methods of digital instead of analog control can increase stability and improve the quality of regulation [3, 4]. The accuracy of the system determines by the number of valves and control algorithm [5], and its speed of operation – by the speed of their response [6].

## 2. DEVELOPING MATHEMATICAL MODEL OF THE PRESSURE CONTROLLER

Schematic diagram of the boost system is shown in Figure 1.

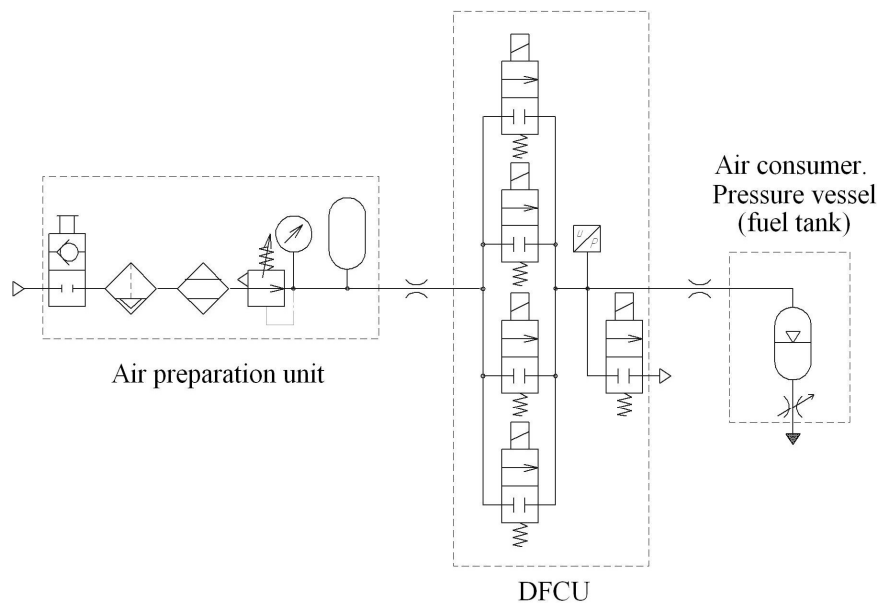


Figure 1. Schematic diagram of the digital pressure control system

High pressure gas from the input line enters the tank through the discrete flow control unit (DFCU). The process of pressure changing in the tank is determined by the quantities of gas flow rate and fuel consumption at a variable gas cushion volume. Information about the pressure coming from the sensor to the controller compares with the set value. The pressure difference is analyzed by controller, which defines the number of on-off valves opened for gas delivery to the tank or dumping excess pressure in the atmosphere.

The mathematical model of the described system is based on fundamental thermodynamic laws of conservation of mass and energy for the working fluid of variable mass. The model is implemented in Matlab Simulink software package and is presented in Figure 2.

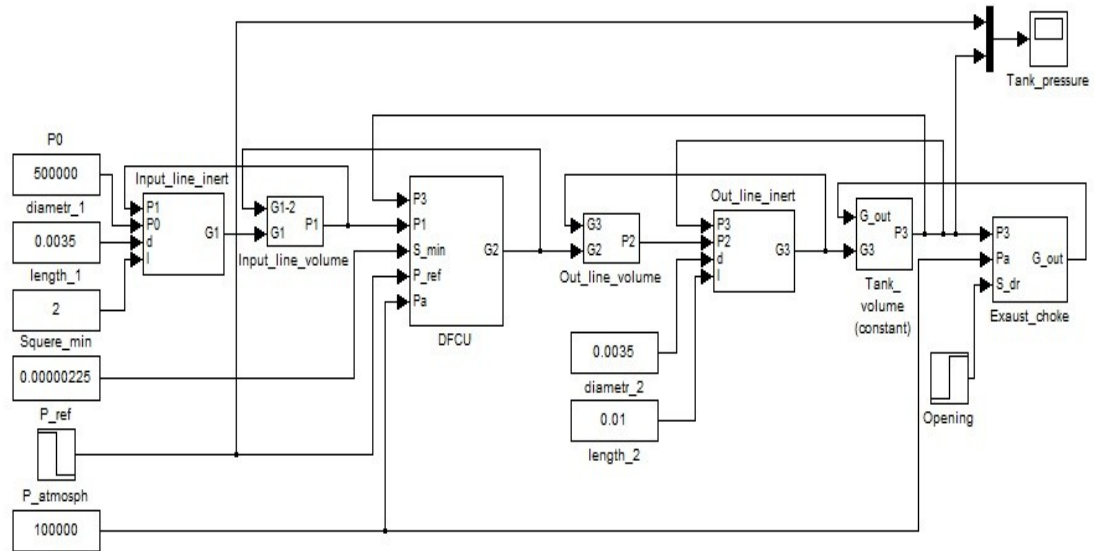


Figure 2. Simulink circuit of the pressure control system

The main parameters of the prototype system are: the boost tank pressure 4.5 bar abs., the error is  $\pm 0.2$  bar, operating flow range expenses from 0 to 2 kg/s.

In the model the dynamic characteristics of the proposed digital controller are investigated with a different number of on-off valves and various control algorithms. In addition, there are studied the effect of valve response time, diameter of the cross sections, the number of valves and the lengths of lines on the control accuracy.

Figure 3 shows the curves of the transients with a step change in fuel flow and pressure settings.

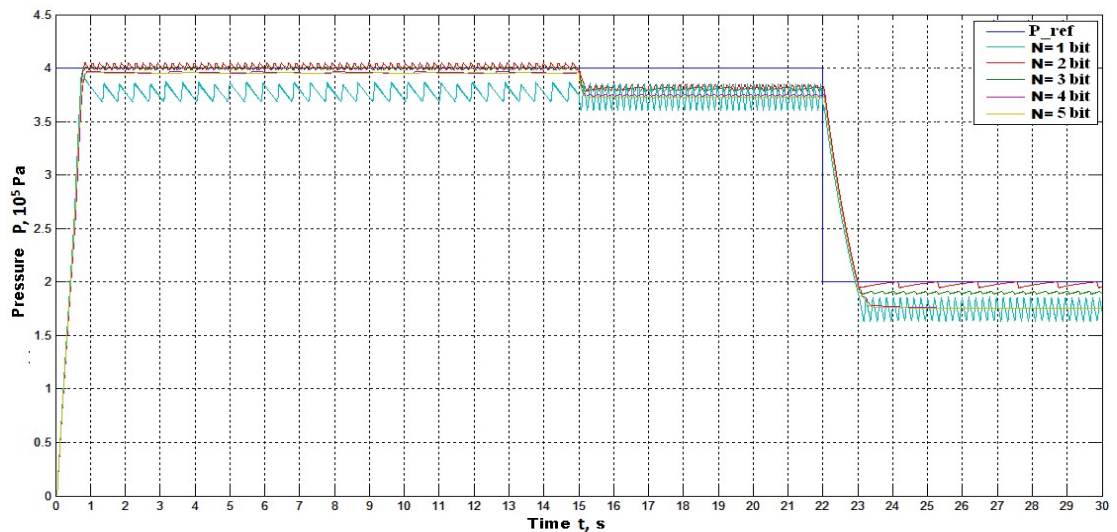


Figure 3. Simulation results for binary DFCU with different number of valves



Since starting up to 15 seconds, the system sets the minimum flow rate specified by section of the throttle at the outlet of the tank. At the 15 second, output flow rate increases to a maximum. Then, at the 22 seconds, the value of the control signal changes – the pressure set point is reduced from 4 to 2 bar.

As one can see, the control accuracy increases with increasing number of valves. The appearance of a static error to the perturbing effects is due to the usage of P - control. The usage of PI (PID) – control would allow to avoid static errors and to improve the accuracy of regulation.

### 3. EXPERIMENTAL RESEARCH

To verify the simulation results, a special stand simulating the control system of pressurized fuel tanks has been developed (Figure 4). A prototype digital air pressure controller was implemented on the basis of Camozzi A321-1C2 valves with nominal bore 1.5 mm. Main parameters of the valve are presented in Table 1. The different valve openings were achieved by tuning variable throttles connected in series with each valve. As the control object 10 liters tank was used. Features of the stand allowed changing the air flow at the outlet of the tank from 0 to 300 NI/min.

The algorithm and control software for the pressure control system was developed in LabVIEW 2010 package. Hardware of the control system was implemented on the basis of National Instrument units:

- Controller NI cRIO-9023;
- Chassis NI cRIO-9116;
- Analog Input Module NI cRIO 9215;
- Sourcing Digital Output Module NI cRIO 9474;
- Pressure sensor SMC PSE530-M5.

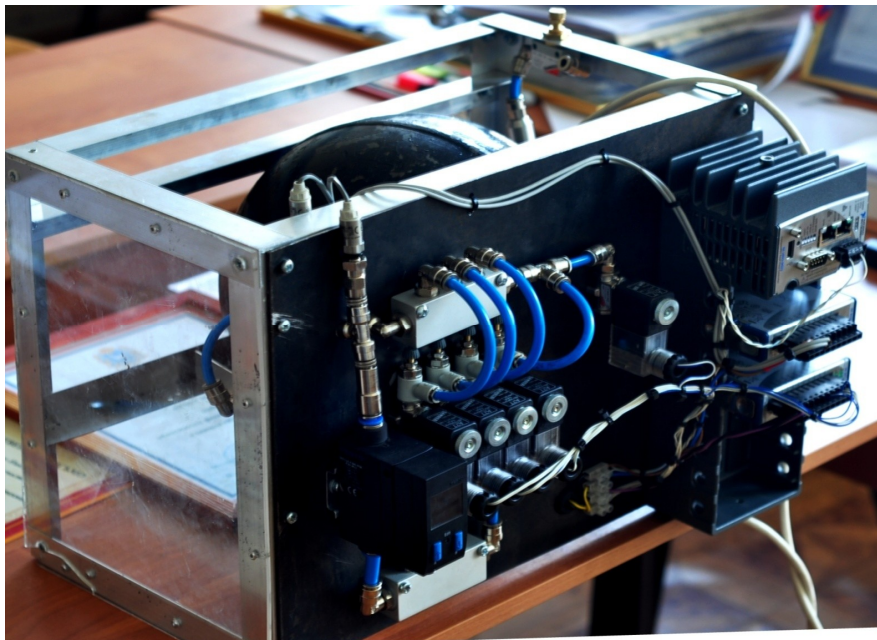


Figure 4. Digital pressure controller connected to tank

Table 1. Camozzi A321-1C2 valve characteristics

Parameters	Value
Solenoid voltage	24 V
Nominal diameter	1.5 mm
Connection	1/8 "
On consumption	57 NI/ min
Response time	15 ms
Nominal pressure	6 bar

In the experiments on the test rig transient responses of pressure in the gas tank with a step change of the control signal (pressure setting) and disturbance (gas flow at the tank outlet simulating fuel consumption) were obtained. Examples of transients are shown in Figure 5.

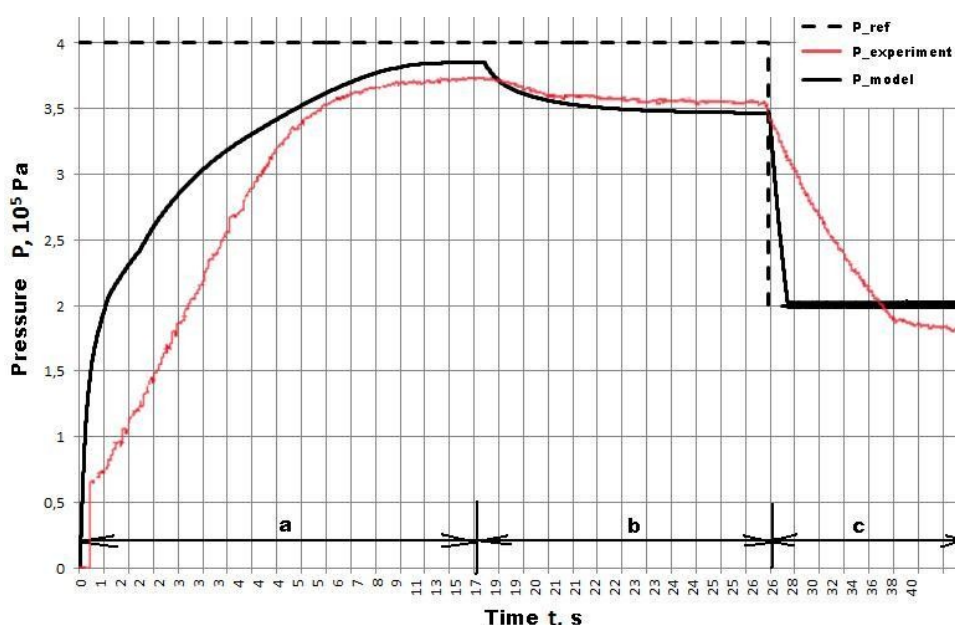


Figure 5. Transients obtained by simulation and experiment

The curve in the section "a" (the time interval from 0 to 17) presents the transient process to the pressure stabilization mode to maintain a given boost pressure of 4 bar for a given air flow at the tank outlet 150 NI/min. In the section "b" (from 17 to 26 seconds) there is a response to the step disturbance of the system - air flow at the tank outlet increases up to 300 NI/min. The last section "c" (from 26 to 40) - response of the system to a step change of the control signal - reducing the pressure setpoint from 4 to 2 bar.

A comparison of the transfer characteristics shows that the results of simulation and experiment agree qualitatively indicating the applicability of the digital controller with the adopted control algorithm and the adequacy of the computational model.

The reason for the discrepancies is that in the simulation, a number of assumptions were accepted, such as no heat exchange with the environment and the absence of inertial properties of the control loop. In addition, mathematical models of the lines were presented as lumped resistance.

#### 4. CONCLUSIONS

In the paper the possibility of application digital control technology to the fuel tank pressurization system was considered. It is shown that the proposed digital controller scheme based on parallel connection of 2/2 valves allows pressure stabilization at the required accuracy.

The algorithms and control circuit solutions using the P – control were developed. The accuracy and speed response of the controller can be improved by using larger number of valves and PI - or PID – algorithm.

An experimental setup for the study of the physical model of the tank pressurization system was created which allows for testing digital controller, debugging algorithm and control program.

The mathematical model of digital tank pressurization control system was developed. The adequacy of the mathematical model is confirmed by experiments. The model can be used when dimensioning the tank pressurization system.

#### ACKNOWLEDGEMENT

The authors are grateful to the Russian Federal Ministry of Education and Science for their support of this work (project 2010-1.3.1-207-003-031) in the frame of the federal program “Educational and scientific human resources of innovative Russia in 2009-2013.

#### REFERENCES

- [1] Linjama M., Vilenius M. 2007. Digital Hydraulics - Towards Perfect Valve Technology. In: Proc. of Tenth Scandinavian International Conference on Fluid Power (SICFP 2007), Tampere, Finland, Vol.2, pp.181-190.
- [2] Linjama, M. 2008. Digital Hydraulics Research at IHA. In: Linjama, M. & Laamanen, A. (eds.) Proceedings of the First Workshop on Digital Fluid Power 3rd October, 2008, Tampere, Finland, pp. 7-30.
- [3] Laamanen A., Linjama M. and Vilenius M. 2007. On The Pressure Peak Minimization In Digital Hydraulics. In: Proc. of Tenth Scandinavian International Conference on Fluid Power (SICFP 2007), Tampere, Finland, Vol.1, pp. 107-114.
- [4] Linjama, M., Huova, M. & Vilenius, M. 2007. On Stability and Dynamic Characteristics of Hydraulic Drives with Distributed Valves. In: Johnston, D.N. & Plummer, A.R. (eds.) Power Transmission and Motion Control (PTMC 2007), University of Bath, UK, Sept. 12–14, pp. 297–314.
- [5] Jyh-Chyang Renn, Yi-Hao Yang, Chin-Yi Cheng. 2009. Position control of a pneumatic rodless cylinder using full-digital nonlinear coding scheme. In:

Proceedings of the Seventh International Conference on Fluid Power Transmission and Control (ICFP 2009), Hangzhou, China, pp. 555-560.

- [6] Karvonen M., Ketonen M., Linjama M., Puumala V. 2011. Recent Advancements In Miniature Valve Development. In: Proc. of the Fourth Workshop on Digital Fluid Power, 21st – 22nd September, 2011, Linz, Austria, pp. 90-103.